VOLUME 7 ISSUE 1 FEBRUARY 2022

IJEG

International Journal of Engineering and Geosciences

e-ISSN 2548-0960

Assist. Prof. Dr. Yelda TURKAN
Oregon State University,
USA

Dr. G. Sanka N. PERERA
Sabaragamuwa University Faculty of Geomatics
Sri Lanka

Dr. Hsiu-Wen CHANG
National Cheng Kung University, Department of Geomatics
Taiwan

The International Journal of Engineering and Geosciences (IJEG)

The International Journal of Engineering and Geosciences (IJEG) is a tri-annually published journal. The journal includes a wide scope of information on scientific and technical advances in the geomatics sciences. The International Journal of Engineering and Geosciences aims to publish pure and applied research in geomatics engineering and technologies. IJEG is a double peer-reviewed (blind) OPEN ACCESS JOURNAL that publishes professional level research articles and subject reviews exclusively in English. It allows authors to submit articles online and track his or her progress via its web interface. All manuscripts will undergo a refereeing process; acceptance for publication is based on at least two positive reviews. The journal publishes research and review papers, professional communication, and technical notes. IJEG does not charge for any article submissions or for processing.

CORRESPONDENCE ADDRESS
Journal Contact: engineeringandgeoscience@gmail.com

CONTENTS

Volume 7 - Issue 1

RESEARCH ARTICLES

International Journal of Engineering and Geosciences

https://dergipark.org.tr/en/pub/ijeg

e-ISSN 2548-0960

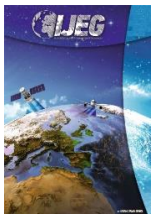

Investigating changes in land cover in high-density settlement areas by protected scenario

Ahmet Emir Yakup[*1], **İsmail Ercüment Ayazlı** [2]

[1]*Hitit University, Osmancik Vocational School, Department of Architecture and Urban Planning, Corum, Turkey*
[2]*Sivas Cumhuriyet University, Engineering Faculty, Department of Geomatics Engineering, Sivas, Turkey*

Keywords
GIS
Urban Growth
SLEUTH
Cellular Automata
Land Management

ABSTRACT

Uncontrolled urban growth is one of the most prominent problems in modern urbanism and planning. Rapid urbanization and population growth cause changes in land cover. In addition, determining the effects of these changes is essential in terms of sustainable urban management policies. Urban growth is a complex, dynamic structure that initiates changes in land cover. For this reason, simulation models are used extensively in planning studies. In this study, land cover simulation of the Sancaktepe district in Istanbul was carried out with the SLEUTH model based on cellular automata (CA). The study aims to identify the damage caused by uncontrolled urbanization. In this context, a scenario was created based on the assumption that forests will be protected based on the changes in land cover that occurred between 1961-2014. The data used in the model were generated from cadastral maps on a parcel basis. For this purpose, four-period data sets (1961-1992-2001-2014) were prepared between 1961-2014. According to the simulation results, 82% of agricultural land, 2% of forest land and 84% of open land will probably be converted into residential use. According to the results, it has been determined that almost all of the open and agricultural land in the towns of Pasakoy and Samandira in the district of Sancaktepe have been converted into residential areas. According to the prediction that the changes in current land cover will continue, no change is expected in forests, while it has been determined that the potential to transform agricultural land and open land into settlement areas is quite high.

1. INTRODUCTION

Population growth leads to urban growth, which leads to the expansion of cities and the destruction of agro-forest land. Therefore, it is becoming increasingly difficult to obtain the requirements for essential nutrients and clean air.

With the growth of cities, changes in land cover cause people to live in unhealthy conditions day by day. The growth in population, especially after 1950, witnessed the beginning of rural-urban migration and the urbanization movement across the world (Satterthwaite, 2005). The destruction of the environment has brought areas of unplanned land, settlement irregularity, and problems in planning and management. The transformation of forests and agricultural land into urban, residential areas results in excessive pressure on natural resources and poses challenges for environmental management (EEA, 2016). For this reason, controlling the process of urbanization is important for achieving the goals of policies of sustainable development.

Several models have been generated to understand urban systems and to control urban growth. The initial models were in a radial and linear form, therefore, they were insufficient for modelling the complex and dynamic structure of cities (Ayazli, 2019; Foot, 2017).

Today's advancements in computer technologies have made it possible to model the complex and dynamic structure of cities with simulation. Models estimate land cover changes based on historical data, economic data, physical constraints, or logical transition rules (Verburg, 2006). In urban modelling techniques, such as artificial neural networks (ANN), agent-based modelling (ABM) and cellular automata (CA) are the most suitable for modelling the complex and dynamic structure of cities (Batty, 2009; Grimm et al., 2005; Tobler, 1970).

One of the most widely used CA-based models in research is the SLEUTH urban growth model. SLEUTH is a model that simulates urban growth dynamics and land cover transformations. It is an open-source software

* **Corresponding Author**

*(emiryakup@hitit.edu.tr) ORCID ID 0000 – 0002 – 1789 – 4448
(eayazli@cumhuriyet.edu.tr) ORCID ID 0000 – 0003 – 0782 – 5366

Cite this article

Yakup A E & Ayazli I E (2022). Investigating changes in land cover in high-density settlement areas by protected scenario. International Journal of Engineering and Geosciences, 7(1), 01-08

Research Article / DOI: 10.26833/ijeg.850247

Received: 30/12/2020; Accepted: 09/03/2021

developed with the C programming language (Gigalopolis, 2020). The model consists of three processing stages: test, calibration and predict. The compliance of the input data with the model standards is checked during the test phase. The parameters of the growth rules in the model are calculated during the calibration phase. Finally, in the predict stage, land cover simulations of the area are created.

In studies conducted with SLEUTH, urban growth and land cover simulations of the world's leading cities have been successfully produced. The model was first applied in San Francisco (Clarke et al., 1997) and the Washington-Baltimore (Clarke & Gaydos, 1998) region. In the following period, a series of studies were carried out in Santa Barbara to determine the technical development of the urbanization process (Candau & Clarke, 2000; Goldstein et al., 2004; Herold et al., 2003). It was first implemented in Europe by Silva and Clarke (2005; 2002) for the Lisbon and Porto metropolitan areas of Portugal. On the other hand, SLEUTH has the highest number of applications in China. Simulations were produced under the ongoing conditions of the city or under alternative scenarios to evaluate the impact and extent of urbanization in rapidly growing cities such as Chongqing (Huanga et al., 2008), Beijing (Yi & He, 2009), Lanzhou (Xie et al., 2010) and Nanjing (Zhang et al., 2010). The model has also been extensively used in mapping and imaging urban growth and land cover changes in other countries, for example, Istanbul, Turkey (Ayazli et al., 2015), Cape Town, South Africa (Watkiss, 2008), Muscat, Oman (Al-Awadhi, 2007) and Hyderabad, India (Gandhi & Suresh, 2012).

Studies have shown that CA-based models are useful and reliable in obtaining information about the dynamics of place and time of a complex system such as a city (Bihamta et al., 2014; Chaudhuri & Clarke, 2013; Clarke & Gaydos, 1998; Dennunzio et al., 2012; Di Lena & Margara, 2008). For this reason, the SLEUTH model, which is a CA-based model that simulates urban growth and land cover using historical data, was chosen for the simulation model of Sancaktepe.

Simulation models produced in the literature often use low-resolution data (Akin et al., 2014; Bihamta et al., 2014; Jantz et al., 2004; Saadani et al., 2020; Sandamali et al., 2018). To improve model accuracy, high-resolution cadastral data were used in this study.

At the first stage of the model, data from 1961, 1992, 2001 and 2014 were obtained from The Land Registry and Cadaster IInd Regional Directorate, and growth dynamics were examined more accurately in the geographic information system (GIS) environment. According to the findings, a scenario was created with the prediction that trends of land cover change in the region will continue in the future. In previous studies of Sancaktepe, attention was drawn to the pressure of urbanization on forests (Ayazli et al., 2019; Ayazli & Baslik, 2016). In this study, a new scenario was created based on the transformation rate in forests according to temporal change analysis between 1961-2014. With the scenario created in this context, and by examining past behaviours in changes in land cover, it was determined that 87% of forests were protected. For this reason, considering that the forests in the study area will be protected, the zoning movements, natural protection zones and places with high agricultural potential in the region are arranged within the zoning data, while the possible effects of urban growth are investigated. Furthermore, to measure the success of the generated scenario, the predicted land cover image for 2020 was rectified and calculated using kappa statistics to determine its accuracy, by comparing actual high-resolution land cover images.

In this study, answers to the following questions were investigated:

- How do possible urban growth trends in Sancaktepe affect changes in land cover?
- How does the direction and speed of urban growth change according to the scenario produced?
- How will the land cover of the Sancaktepe region change in 2030, 2050 and 2070?

2. STUDY AREA

The district of Sancaktepe is located on the Anatolian side of Istanbul. The district of Cekmekoy is to the north of Sancaktepe. Kartal and Maltepe are located to the south, Sultanbeyli and Pendik to the east, and Umraniye and Atasehir to the west (Fig-1). It was formed with the merging of the towns of Samandira, Sarıgazi and Yenidogan following the law that came into force in 2008. Consisting of 19 neighbourhoods, the district of Sancaktepe has an area of 62.41 km^2 (Sancaktepe, 2020).

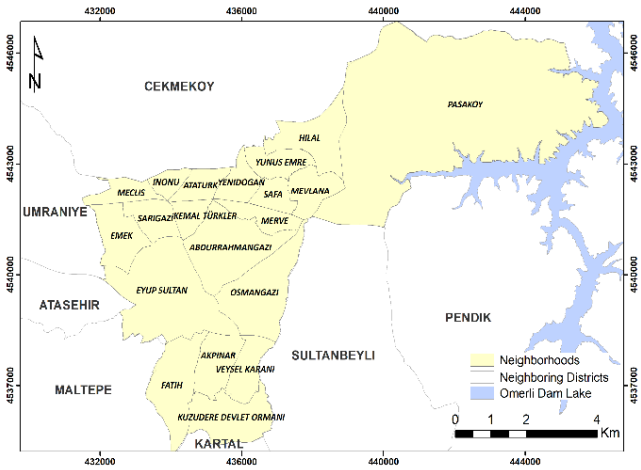

Figure 1. Sancaktepe's administrative borders.

According to data from the Turkish Statistical Institute, the population of Sancaktepe in 2008 was 229,093, growing to 329,788 in 2014, and 436,733 in 2019; an increase of 90% compared to 2008 (TUIK, 2020).

The importance of the region, which is an extremely sensitive residential area due to its basin nature, is increasing day by day due to transport opportunities. The Pasakoy region, which was specified as unsuitable for settlement throughout the region, is located within the short-range protection zone and in the absolute protection zone of the stream. However, as a result of rapid population growth and intense urbanization

activities, urbanization has almost reached the basin border (Aydin, 2010; Sancaktepe, 2010).

3. MATERIALS AND METHOD

3.1. Cellular Automata

The CA, one of the mathematical modelling methods, is used as an effective tool in the creation of complex place and temporal process models.

The CA concept consists of five basic components. These are lattice, state set, neighbourhood relationship (determined by the nearest neighbouring cells), transformation rules and time. Cells are the smallest units that are adjacent to each other. The cells come together to form the grid network. Every cell has a state. An infinite number of state types can be specified in the state set. But a cell can only take one state at a time. The situations can change according to the transformation rules determined by the neighbourhood function (Benenson & Torrens, 2004).

CA is a suitable method for simulating urban systems because it is directly compatible with Raster GIS and is dynamic; state transitions intuitively mimic the temporal dynamics of urban change (Clarke et al., 1997).

3.2. SLEUTH

SLEUTH is an open-source software developed by Keith Clarke, based on CA, simulating urban growth dynamics and land cover transformations. The name of the model is derived from the initials of the input data: **S**lope, **L**andcover, **E**xcluded, **U**rban, **T**ransportation, and **H**illshade.

The model has three processing stages i.e. test, calibration and prediction stages. During the test phase, the suitability of the input data is questioned. If it is successful, the calibration process is started. The calibration phase is particularly important in capturing the characteristics of urban growth and to successfully predict the model. The calibration phase itself consists of four steps. These steps are coarse, fine, final, and forecast calibration, respectively. In the calibration phase, the goal is to select the optimal growth coefficients that affect four different growth rules. For this, the Brute Force Calibration method is used. These values, which are initially in the range of 0-100, are narrowed after each calibration step and a single value is determined at the last step. Finally, the urban growth simulation is created in the prediction phase.

3.3. Data Acquisition and Processing

In Sancaktepe, the data belonging to previous years and needed by SLEUTH to create an urban growth simulation model are divided into time zones, taking into account the cadastral sheet production dates and zoning movements. As a result, four different time periods were determined: the years 1961, 1992, 2001 and 2014.

Cadastral data and land registry records were used as sources in the preparation of land cover, settlement, and transportation data. The slope and shaded relief data were produced with the digital elevation model (DEM) obtained from the General Directorate of Mapping.

The first facility of the regions within the boundaries of Sancaktepe started in the 1950s, and 36 maps were produced in different scales and coordinate systems in line with the possibilities of 1950-1980 (Ayazli & Baslik, 2016). The second period covers the years 1987-1993, and during this period 58 cadastral maps were prepared in the local coordinate system and in different scales. In the third period covering 1997-2003, a total of 83 cadastral maps were produced in the ED50 coordinate system (Yakup, 2018). In the fourth period, the current cadastral base map produced in the ED50 coordinate system of October 2014 was used in a digital environment.

In the study, more than 70,000 parcel data from archival studies from different years were organized in a GIS environment and attribute information was entered through land registry data.

The input data of the model must be produced to certain standards. The standards for all data types are 8-bit images in greyscale GIF format, they should be prepared in the common datum and coordinate system, in the same resolution and in accordance with the naming format. For the model to work, at least four periods of settlement, at least two periods of the transport network, two periods of land cover, and one period of slope, exclude, and shaded data are required (Gigalopolis, 2020). In this context, input data in the same coordinate system, the number of rows and columns was determined as 10 metres; 1184 rows, 1488 columns, 20 metres; 592 rows, 744 columns and 40 metres; 296 rows, 372 columns.

Land cover data were prepared for two periods: 1961 and 2014 (Figs. 2 and 3, Table 1).

Table 1. 1961-2014 Land Cover Classes.

Land Cover Class	1961		2014	
	Pixel Count	Rate (%)	Pixel Count	Rate (%)
Urban	2290	4	200,989	36.1
Agriculture	287,009	50	87,797	15.7
Forest	271,087	45.7	235.349	42.2
Open Land	15,774	0.3	33,379	6

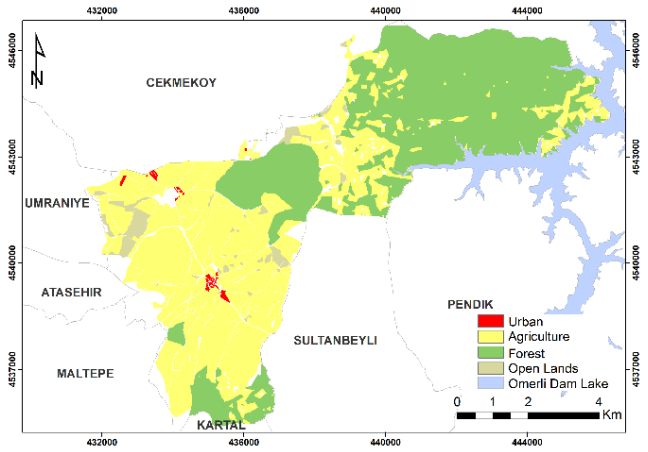

Figure 2. Sancaktepe land cover in 1961.

Settlement data was produced for 1961, 1992, 2001 and 2014. In this context, the urban mass expanded by approximately 36% from the starting year of 1961 until the last control year 2014 (Table 2 and Fig-4).

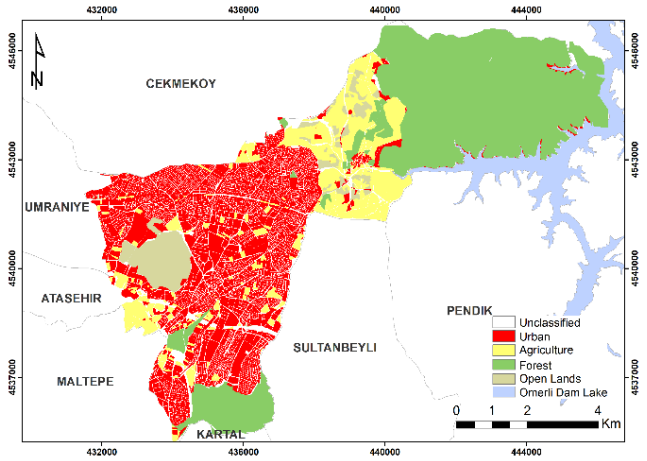

Figure 3. Sancaktepe land cover in 2014.

Specifying the parcel type as "land" in the land registry or cadaster records indicates that the parcel is a development parcel. Zoning parcels are formed as a result of land and plot arrangements. These parcels have been turned into forms suitable for construction and their intended use is in this direction. Parcels that do not have any construction are also included in the settlement data. In short, the construction criteria are not taken into account in the settlement data.

Transport network data from 1961, 1992, 2001, and 2013 are produced from cadastral sheets. In addition, road data for the year 2006 was obtained readily and included in the model. Transportation networks are weighted in four different classes according to the importance of roads.

The TEM highway, which divides Samandira into two, the Sile Highway, the dam road connecting Yenidogan and Sarıgazi, and the Pasakoy connection roads of the Northern Marmara Motorway Project have been determined as the first-degree transportation network because they are the most important of these roads, and carry much of the traffic of the district. Various boulevards and main streets in the region are specified as second-degree transportation networks. Third and fourth-degree networks represent side streets or village roads (Table 3).

Table 2. Settlement mass by years.

Year	Pixel Count	Rate (%)
1961	4,102	0.7
1992	35,576	6
2001	154,160	28
2014	201,320	36

Table 3. Total lengths of roads according to their levels and period.

Period	Level of Transportation Network			
	1(km)	2(km)	3(km)	4(km)
1961	6.08	-	29.71	85.71
1992	20.57	19.96	65.97	124.33
2001	28.29	107.77	95.10	114.65
2006	27.71	106.98	95.20	114.62
2013	35.58	215.26	446.13	-

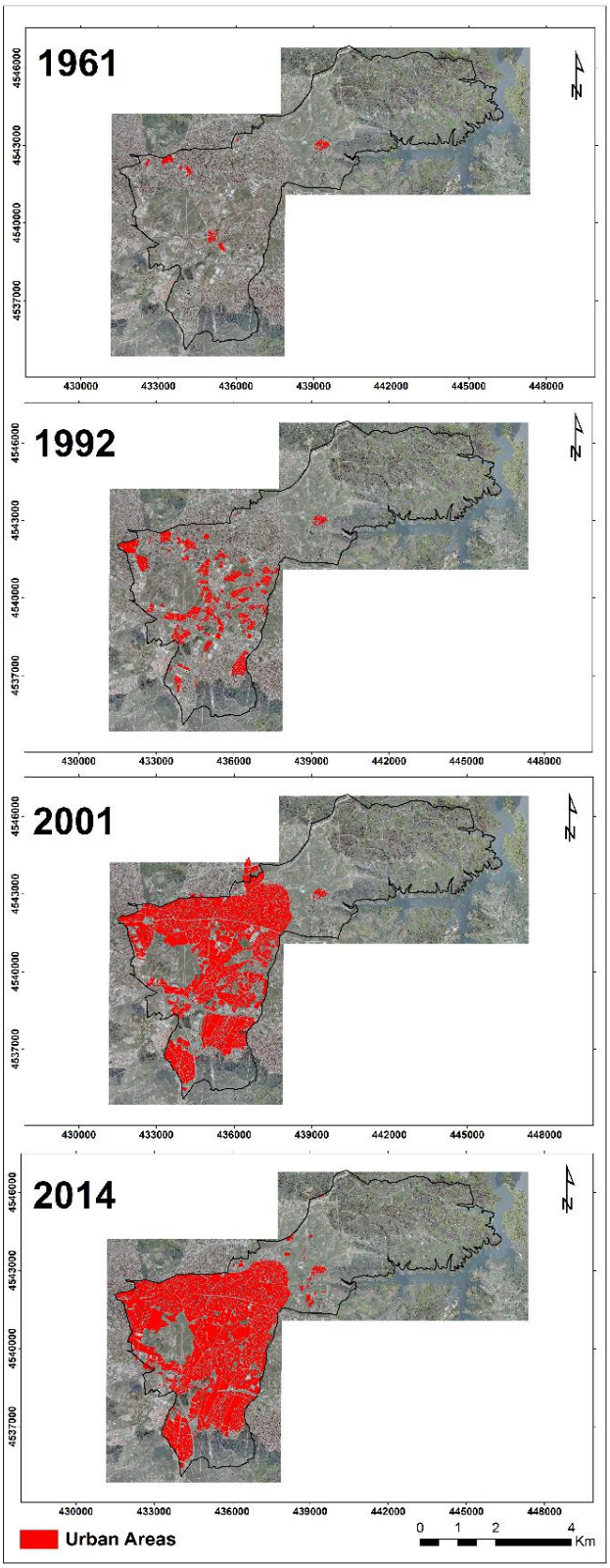

Figure 4. Urban areas by period.

Past behaviours in land cover changes, zoning movements in the region, natural protection zones, and places with high agricultural potential are organized within the excluded data. In the scenario created, it is assumed that the ongoing land cover trends will continue. In this direction, temporal change analysis was conducted between 1961-2014 and the transformation percentage of residential areas was determined as 13%. The transformation of forest areas is 13%. For this reason, assuming that forest areas are preserved at this rate, the complement of 13% was taken and pixel values of forests were weighted as 87% in the excluded data (Fig 5).

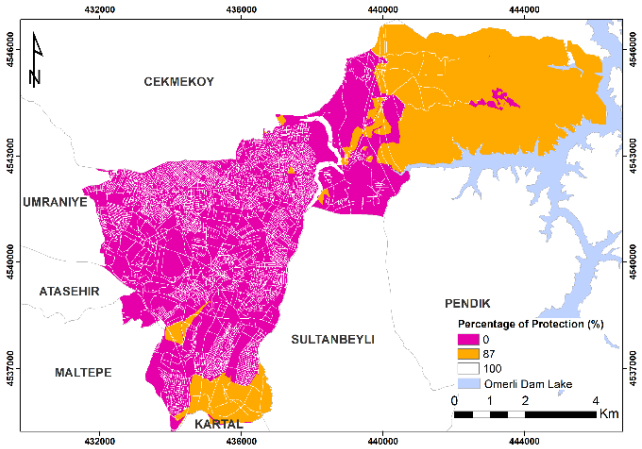

Figure 5. Excluded input data.

4. RESULTS

It was observed that all five coefficients were effective in the urban growth of Sancaktepe. The coefficient values obtained are shown in Table 4. Three different coefficient values are calculated as close to 100, which is the ceiling value. Among the coefficients, the highest values were the diffusion, spread and breed coefficients. High values of the coefficients indicate that the four growth rules are intensely effective. The diffusion coefficient indicates random growth, the breed coefficient indicates new propagation-centred growth, and the road gravity coefficient indicates that path-efficient growth is effective.

According to the results of the urban growth simulation, urban growth rates of 32% from 2014 to 2030, 25% from 2030 to 2050, and 1% between the years 2050-2070 have been determined. This means that in total there is an urban growth rate of 21%.

In this context, when the trend of growth rates is examined, the urban growth rate, which increased from 2014 to 2030, will accelerate further between 2030 and 2050. In the 2050-2070 interval, the growth rate begins to slow down.

The direction of growth was determined to be predominantly towards the northeast of the study area (Pasakoy). However, urban growth has also been observed in the Kuzudere state forest in the south and in the open land area in the inner part of Sarıgazi (Fig 7).

Amounts and rates of land cover changes in Sancaktepe were obtained by analysis of the changes. Accordingly, it was calculated that 82% of agricultural land, 2% of forest areas, and 84% of open land can be converted into residential areas (Fig 6).

As expected, due to the preserved percentages of forest areas, it is concluded that the forest is protected to a large extent by not experiencing much urbanization. However, the city, which has spread to the forest border of Pasakoy, has caused destruction to the forest periphery and the land cover function to change, as dispersed in the inner parts. This behaviour is valid not only for the area of Pasakoy but also for the Kuzudere state forest in the region of Samandira.

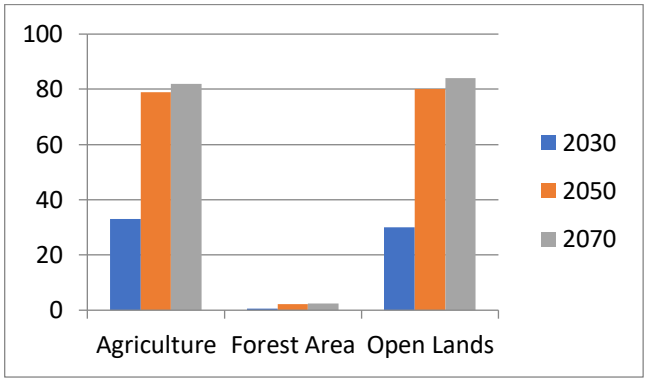

Figure 6. Percentage conversion of land cover classes to settlement

The kappa statistic was calculated for the predicted land cover image in 2020 in order to calculate the success of the scenario created. Fifty trial samples for each class of land cover were produced to determine the accuracy of the assessment by calculating the kappa statistic. The trial samples were compared with Google Earth images and the kappa value was estimated as 89%.

Table 4. Model Calibration Stages and Calculated Coefficients.

Coefficient Name	Coarse Calibration		Fine Calibration		Final Calibration		Calculated Coefficient Values
	Number of iterations = 8		Number of iterations = 10		Number of iterations= 10		
	Range	Step	Range	Step	Range	Step	
Dispersion	0-100	25	75-100	5	100-100	1	100
Breed	0-100	25	100-100	1	100-100	1	100
Spread	0-100	25	100-100	1	100-100	1	100
Slope	0-100	25	25-100	15	85-100	3	94
Road Gravity	0-100	25	25-100	15	25-100	15	85

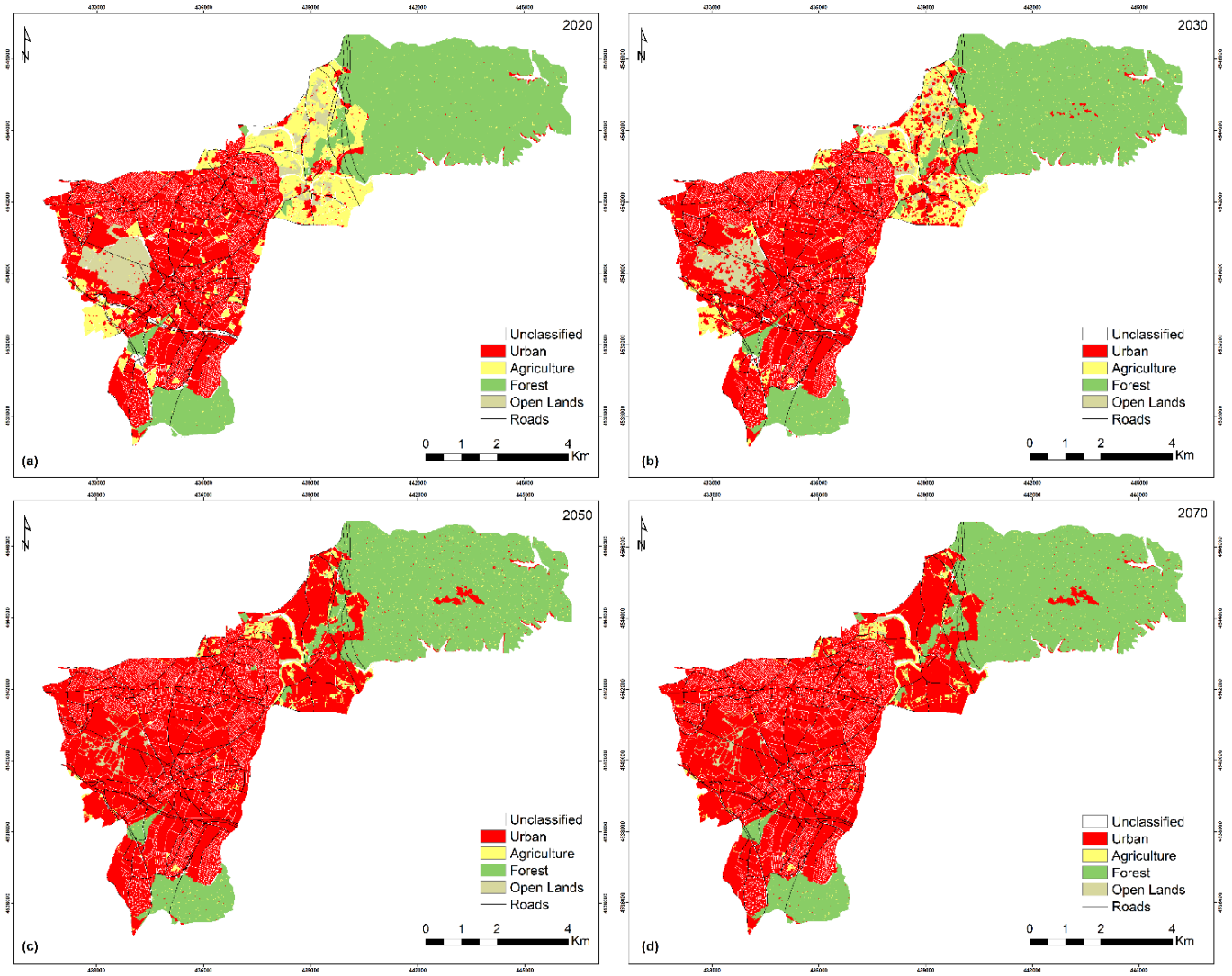

Figure 7. Land cover prediction maps (a for 2020, b for 2030, c for 2050, d for 2070)

5. CONCLUSION

Rapid population growth in Sancaktepe has caused urban growth. Therefore, an urban growth model that can describe land cover and assist local government decision-making is needed to evaluate the potential effects of growth policies. In this direction, the CA-based SLEUTH model has been preferred for modelling urban growth in Sancaktepe.

Very intense urbanization has been experienced in Sancaktepe between 1990 and 2000. In particular, the town of Yenidogan has taken its current urban form by dividing it into 6,456 parcels from a single 441-hectare special forest type parcel. Intensive urbanization in Yenidogan ensured the continuation of its rural character by protecting Pasakoy and forest areas. Due to its proximity to Yenidogan and the land stock in the area, this study focused specifically on Pasakoy and its surrounding areas.

When the parcels of Yenidogan, which is the neighbouring town of Pasakoy, are examined geometrically, it is observed that it has spread like an oil stain towards Pasakoy in a northeast direction. However, due to a stream crossing on the border of Pasakoy and Yenidogan, and a rehabilitation project belonging to this stream, urbanization in Pasakoy takes place centrally and in parts.

It has been determined that almost all of the agricultural land in the Pasakoy and Samandira regions can be converted into residential areas. Intense urban growth has not been observed in areas protected from urbanization such as the Omerli Basin Protection Zone and Kuzudere forest. A trend towards urban growth has been observed, particularly in Pasakoy. It has also been observed, to a lesser extent than Pasakoy, in the former military area in the Samandira and Sarigazi regions. Accordingly, changes in land cover triggered by urban growth took place in these regions. It has been concluded that open land and agricultural land can be largely urbanized.

The kappa value was estimated as 89% for the year 2020 and it can be said that the generated scenario is close to real. According to Figure 7a, urbanization influences created by motorways in the forest areas have been at a minimum level between 2014-2020. However, the trend towards urbanization may increase in Pasakoy after 2030 if further precautions are not taken.

ACKNOWLEDGEMENT

The data used in this paper were generated within the scope of the TUBITAK 112K469 numbered project.

Author contribution

Ahmet Emir Yakup: Data curation, Software, Writing-Original draft preparation, Visualization, Investigation, Writing-Reviewing and Editing. **İsmail Ercüment Ayazlı**: Conceptualization, Methodology, Validation, Writing-Reviewing and Editing.

Conflicts of interest

The authors declare no conflicts of interest.

REFERENCES

Akin A, Clarke K C & Berberoglu S (2014). The impact of historical exclusion on the calibration of the SLEUTH urban growth model. *International Journal of Applied Earth Observation and Geoinformation*, *27*(PARTB), 156–168. https://doi.org/10.1016/j.jag.2013.10.002

Al-Awadhi T (2007). *Monitoring and Modeling Urban Expansion Using GIS & RS: Case Study from Muscat, Oman*. https://doi.org/10.1109/URS.2007.371790

Ayazli I E (2019). An Empirical Study Investigating the Relationship between Land Prices and Urban Geometry. *ISPRS International Journal of Geo-Information*, *8*, 457. https://doi.org/10.3390/ijgi8100457

Ayazli I E & Baslik S (2016). *Creating Simulation Model of the Relationship between the Ownership Pattern and Urban Growth; Project Report*.

Ayazli I E, Gul F K, Baslik S, Yakup A E & Kotay D (2019). Extracting an Urban Growth Model's Land Cover Layer from Spatio-Temporal Cadastral Database and Simulation Application. *Polish Journal of Environmental Studies*, *28*(3), 1063–1069. https://doi.org/10.15244/pjoes/89506

Ayazli I E, Kilic F, Lauf S, Demir H & Kleinschmit B (2015). Simulating urban growth driven by transportation networks: A case study of the Istanbul third bridge. *Land Use Policy*, *49*, 332–340. https://doi.org/https://doi.org/10.1016/j.landusepol.2015.08.016

Aydin B (2010). *Identification of ecological criteria for the greenfield development and adaptation of these criteria within current city planning policies: Ömerli waterbasin-Sancaktepe case study*. Istanbul Technical University.

Batty M (2009). Urban Modeling. In *International Encyclopedia of Human Geography* (pp. 51–58). https://doi.org/10.1016/B978-008044910-4.01092-0

Benenson I & Torrens P (2004). *Geosimulation: Automata-based modeling of urban phenomena*. John Wiley & Sons.

Bihamta N, Soffianian A, Fakheran S & Gholamalifard M (2014). Using the SLEUTH Urban Growth Model to Simulate Future Urban Expansion of the Isfahan Metropolitan Area, Iran. *Journal of the Indian Society of Remote Sensing*, *43*. https://doi.org/10.1007/s12524-014-0402-8

Candau J & Clarke K C (2000). Probabilistic Land Cover Transition Modeling Using Deltatrons. *2000 URISA Annual Conference, Orlando*.

Chaudhuri G & Clarke K C (2013). The SLEUTH Land Use Change Model : A Review. *The International Journal of Environmental Resources Research*, *1*(1), 88–104.

Clarke K & Gaydos L (1998). Loose-coupling a cellular automaton model and GIS: long-term urban growth prediction for San Francisco and Washington/Baltimore. *International Journal of Geographical Information Science*, *12*(7), 699–714. https://doi.org/10.1080/136588198241617

Clarke K, Hoppen S & Gaydos L (1997). A Self-Modifying Cellular Automaton Model of Historical Urbanization in the San Francisco Bay Area. *Environment and Planning B: Planning and Design*, *24*(2), 247–261. https://doi.org/10.1068/b240247

Dennunzio A, Formenti E & Kurka P (2012). *Cellular Automata Dynamical Systems*.

Di Lena P & Margara L (2008). Computational complexity of dynamical systems: The case of cellular automata. *Inf. Comput.*, *206*, 1104–1116.

EEA (2016). *Urban Sprawl in Europe: Joint EEA-FOEN*.

Foot D (2017). *Linear urban models* (pp. 137–173). https://doi.org/10.4324/9781315105307-6

Gandhi S & Suresh V (2012). Prediction of Urban Sprawl in Hyderabad City using Spatial Model, Remote Sensing and GIS Techniques. *International Journal of Scientific Research*, *1*, 80–81. https://doi.org/10.15373/22778179/JUL2012/25

Gigalopolis (2020). *Project Gigalopolis Web Page*. USGS. http://www.ncgia.ucsb.edu/projects/gig/

Goldstein N C, Candau J T & Clarke K C (2004). Approaches to simulating the "March of Bricks and Mortar." *Computers, Environment and Urban Systems*, *28*(1), 125–147. https://doi.org/https://doi.org/10.1016/S0198-9715(02)00046-7

Grimm V, Revilla E, Berger U, Jeltsch F, Mooij W M, Railsback S F, Thulke H H, Weiner J, Wiegand T & DeAngelis D L (2005). Pattern-oriented modeling of agent-based complex systems: Lessons from ecology. In *Science*. https://doi.org/10.1126/science.1116681

Herold M, Goldstein N C & Clarke K C (2003). The spatiotemporal form of urban growth: measurement, analysis and modeling. *Remote Sensing of Environment*, *86*(3), 286–302. https://doi.org/https://doi.org/10.1016/S0034-4257(03)00075-0

Huanga J, Zhangb J & Luc X (2008). *Applying SLEUTH For Simulating and Assessing Urban Growth Scenario Based on Time Series TM Images : Referencing to a Case Study of Chongqing, China*.

Jantz C A, Goetz S J & Shelley M K (2004). Using the SLEUTH urban growth model to simulate the impacts of future policy scenarios on urban land use in the Baltimore-Washington metropolitan area. *Environment and Planning B: Planning and Design*, *31*(2), 251–271. https://doi.org/10.1068/b2983

Saadani S, Laajaj R, Maanan, M, Rhinane, H & Aaroud A (2020). Simulating spatial–temporal urban growth of a Moroccan metropolitan using CA–Markov model. *Spatial Information Research*. https://doi.org/10.1007/s41324-020-00322-0

Sancaktepe (2010). *1/1000 Scale Sancaktepe Implementary Development Plan Sancaktepe Municipality*.

Sancaktepe (2020). *Sancaktepe Municipality Web Page*. http://www.sancaktepe.bel.tr/tr/cografi-durumu

Sandamali S, Kantakumar L & Sivanantharajah S (2018). Remote Sensing Data and SLEUTH Urban Growth Model: As Decision Support Tools for Urban Planning. *Remote Sensing Data and SLEUTH Urban Growth Model*, *28*, 274–286. https://doi.org/10.1007/s11769-018-0946-6

Satterthwaite D (2005). *The Scale of Urban Change Worldwide 1950-2000 and Its Underpinnings*. International Institute for Environment and Development. https://books.google.com.tr/books?id=M47aajCtKr8C

Silva E A & Clarke K C (2005). Complexity, emergence and cellular urban models: lessons learned from applying SLEUTH to two Portuguese metropolitan areas. *European Planning Studies*, *13*(1), 93–115. https://doi.org/10.1080/0965431042000312424

Silva E & Clarke K (2002). Calibration of the SLEUTH urban growth model for Lisbon and Porto, Portugal. *Computers, Environment and Urban Systems*, *26*, 525–552. https://doi.org/10.1016/S0198-9715(01)00014-X

Tobler W R (1970). A Computer Movie Simulating Urban Growth in the Detroit Region. *Economic Geography*, *46*, 234–240. https://doi.org/10.2307/143141

TUIK (2020). *Turkish Statistical Institute Web Page*. Turkish Statistical Institute. https://biruni.tuik.gov.tr/medas/?kn=95&locale=tr

Verburg P H (2006). Simulating feedbacks in land use and land cover change models. *Landscape Ecology*, *21*(8), 1171–1183. https://doi.org/10.1007/s10980-006-0029-4

Watkiss B M (2008). *The SLEUTH urban growth model as forecasting and decision-making tool*. Stellenbosch University.

Xie Y, Ma A & Wang H (2010). Lanzhou urban growth prediction based on Cellular Automata. In *2010 18th International Conference on Geoinformatics, Geoinformatics 2010*. https://doi.org/10.1109/GEOINFORMATICS.2010.5567556

Yakup A E (2018). *Research the relationship between the ownership pattern and urban growth*. Sivas Cumhuriyet University.

Yi W & He B (2009). Applying SLEUTH for simulating urban expansion of Beijing. In *Proceedings - 2009 International Forum on Information Technology and Applications, IFITA 2009* (Vol. 2). https://doi.org/10.1109/IFITA.2009.543

Zhang Z, Jiang L, Peng R & Yin Y (2010). The spatiotemporal change of urban form in Nanjing, China: Based on SLEUTH and spatial metrics analysis. *2010 18th International Conference on Geoinformatics*, 1–5. https://doi.org/10.1109/GEOINFORMATICS.2010.5567753

International Journal of Engineering and Geosciences

https://dergipark.org.tr/en/pub/ijeg

e-ISSN 2548-0960

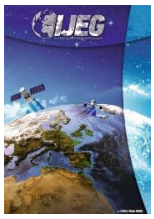

Estimating the seasonal relationship between land surface temperature and normalized difference bareness index using Landsat data series

Subhanil Guha*[1] , Himanshu Govil[1]

[1]*National Institute of Technology Raipur, Department of Applied Geology, Raipur, India*

Keywords
Landsat
LST
LULC
NDBaI
Raipur

ABSTRACT

The present study analyzes the seasonal variability of the relationship between the land surface temperature (LST) and normalized difference bareness index (NDBaI) on different land use/land cover (LULC) in Raipur City, India by using sixty-five Landsat images of four seasons (pre-monsoon, monsoon, post-monsoon, and winter) of 1991-1992, 1995-1996, 1999-2000, 2004-2005, 2009-2010, 2014-2015, and 2018-2019. The mono-window algorithm was used to retrieve LST and Pearson's correlation coefficient was used to generate the LST-NDBaI relationship. The post-monsoon season builds the best correlation (0.59) among the four seasons. The water bodies builds a moderate to strong positive correlation (>0.50) in all the four seasons. On green vegetation, this correlation is moderate to strong positive (>0.54) in the three seasons, except the pre-monsoon season. The built-up area and bare land generate a moderate positive correlation (>0.34) in all the four seasons. Among the four seasons, the post-monsoon season builds the best correlation for all LULC types, whereas the pre-monsoon season has the least correlation. This research work is useful for environmental planning of other citieswith similar climatic conditions.

1. INTRODUCTION

Land surface temperature (LST) is an indispensable parameter in analyzing the bio-geochemical functions of the earth surface features (Tomlinson et al. 2011; Hao et al. 2016; Guha et al. 2020a). Green plants, wetlands, and water bodies generate low LST, whereas human settlement, and bare land surface produce high LST in the summer season of tropical areas (Chen et al. 2006). Thus, LST and normalized difference spectral indices related studies are quite important in the ecological planning of the recent urban agglomerations (Sekertekin et al. 2016; Li et al. 2016; Guha et al. 2020b). Normalized difference bareness index (NDBaI) is one of the most popular indices for bare land extraction that is often used in LULC and LST related studies (Zhao and Chen 2005; Chen et al. 2006; Essa et al. 2012; Guha et al. 2017).

Several research articles presented the LST-NDBaI relationship in recent years. As-Syakur et al. (2012) investigates various bareness indices for bare land mapping in Denpasar of Bali, Indonesia. Ahmed et al. (2013) used NDBaI along with other LULC indices to simulate the land surface changes and their impact on LST in Dhaka, Bangladesh. Sharma et al. (2013) examined the relationship between LST and NDBaI in Surat City of India. Guo et al. (2014) estimated sub-pixel LST and built a relationship between LST and NDBaI in Guangzhou core urban area of China. Ali et al. (2017) compared the relationship of LST with NDBaI and other LULC indices in London and Baghdad cities. Macarof et al. (2017) investigated the relationship between LST and NDBaI in Iaşi Municipality Area of eastern Romania from 2013 to 2016 by using Landsat 8 data. Alibakshi et al. (2020) investigated the relationship between NDBaI and LST from 2001 to 2015 in Tehran and its satellite cities in Iran by the geographically weighted regression model using Landsat 7 data. Alexander (2020) evaluated the LST-NDBaI relationship in Aarhus City of Denmark by using Landsat 8 data. Jain et al. (2020) investigated the LST-NDBaI relationship in Nagpur City, India from 2000 to 2015 by using Landsat data.

The LST and NDBaI values vary due to the seasonal variation of various atmospheric components. Thus, to estimate the characteristics of seasonal variation of the LST-NDBaI relationship in Indian context, Raipur City ofChhattisgarh has been chosen. The main aim of the study is to estimate the seasonal variation of LST-NDBaI

*Corresponding Author

*(subhanilguha@gmail.com) ORCID ID 0000-0002-2967-7248
(himgeo@gmail.com) ORCID ID 0000-0002-3433-8355

Cite this article

Guha S & Govil H (2022). Estimating the seasonal relationship between land surface temperature and normalized difference bareness index using Landsat data series. International Journal of Engineering and Geosciences, 7(1), 09-16

Research Article / DOI: 10.26833/ijeg.833260

Received: 29/11/2020; Accepted: 21/01/2021

relationship on different categories of LULC. The study will be a beneficial one for ecological planning and management in an urban environment.

2. STUDY AREA AND DATA

Figure 1 shows the geographical location of Raipur city of India which extends from 21°11'22"N to 21°20'02"N and from 81°32'20"E to 81°41'50"E. The city covers an area of around 165 km^2. Figure 1(a) presents the outline map of India (URL-1). Figure 1(b) presents the outline map of Chhattisgarh State (URL-1). Figure 1(c) represents the false colour composite (FCC) image of Raipur City (URL-2) from recent Landsat 8 data of 07 November 2018(URL-3). Figure 1(d) shows the digital elevation map (DEM) of Raipur City produced by the ArcGIS software using the last available ASTER DEM data of 11 October 2011 (URL-3). The city is characterised by the tropical dry and wet type of climate (URL-4). The mean monthly temperature ranges from 12°C to 42°C. May presents the highest average temperature (35°C), while December presents the lowest average temperature (20°C). The highest average rainfall (327 mm) is observed in July. March, April, and May are considered as the summer or pre-monsoon months. June, July, August, and September are the monsoon months. The post-monsoon months are October and November, when the weather remains pleasant. The winter months are December, January, and February, when the temperature falls significantly.

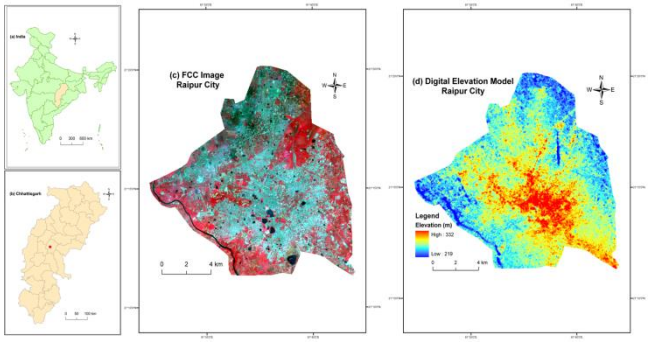

Figure 1. Location of the study area: (a) India highlighting Chhattisgarh; (b) Chhattisgarh highlighting Raipur City; (c) False colour composite image of Raipur; (d) Digital elevation model of Raipur.

Table 1 shows the specification of Landsat data of different sensors. The band 10 of Landsat 8 thermal infrared sensors (TIRS) dataset was used as the only TIR band in the present study due to a larger calibration certainty (Barsi et al. 2014). Landsat 5 thematic mapper (TM) data has only one TIR band (band 6) of 120 m resolution. Landsat 7 enhanced thematic mapper plus (ETM+) data has a TIR band (band 6) of 60 m resolution. The TIR bands of all the Landsat sensors were resampled to 30 m pixel size by the data provider (USGS) as the spatial resolution of visible to near-infrared (VNIR) and shortwave infrared (SWIR) bands of the three types of Landsat sensors is 30 m. All theraster calculations were processed in the environment of ArcGIS 9.3 and ERDAS IMAGINE 9.1 software.

Table 1. Specification of the used Landsat data

Date of acquisition	Time (UTC)	Cloud cover (%)	Resolution of TIR bands (m)
18-Mar-91	04:17:34	0	120
03-Apr-91	04:17:46	0	120
21-May-91	04:18:39	1	120
26-Sep-91	04:20:03	13	120
12-Oct-91	04:20:12	6	120
13-Nov-91	04:20:19	1	120
16-Jan-92	04:20:22	3	120
01-Feb-92	04:20:27	0	120
17-Feb-92	04:20:15	4	120
14-Apr-95	04:05:06	0	120
10-Dec-95	03:56:47	0	120
27-Jan-96	04:00:14	0	120
23-Sep-96	04:14:16	2	120
09-Oct-96	04:15:07	0	120
25-Oct-96	04:15:55	5	120
10-Nov-96	04:16:41	7	120
11-Nov-99	04:49:00	0	60
30-Jan-00	04:48:55	0	60
03-Apr-00	04:48:35	0	60
05-May-00	04:48:20	0	60
26-Sep-00	04:46:33	6	60
15-Dec-00	04:46:31	0	60
21-Mar-04	04:35:14	0	120
22-Apr-04	04:36:01	1	120
24-May-04	04:36:54	0	120
09-Jun-04	04:37:23	9	120
29-Sep-04	04:40:16	9	120
15-Oct-04	04:40:36	4	120
16-Nov-04	04:41:11	0	120
02-Dec-04	04:41:33	0	120
18-Dec-04	04:41:52	0	120
19-Jan-05	04:42:17	0	120
04-Feb-05	04:42:29	0	120
03-Mar-09	04:42:22	0	120
19-Mar-09	04:42:44	2	120
04-Apr-09	04:43:05	0	120
20-Apr-09	04:43:24	0	120
06-May-09	04:43:42	0	120
22-May-09	04:44:00	1	120
23-Jun-09	04:44:35	0	120
13-Oct-09	04:46:12	0	120
29-Oct-09	04:46:20	0	120
16-Dec-09	04:46:44	1	120
17-Jan-10	04:46:55	6	120
02-Feb-10	04:46:59	0	120
18-Feb-10	04:47:02	7	100
17-Mar-14	04:56:36	0	100
02-Apr-14	04:56:19	0	100
20-May-14	04:55:38	5	100
05-Jun-14	04:55:45	0	100
12-Nov-14	04:56:21	7	100
30-Dec-14	04:56:09	0	100
15-Jan-15	04:56:09	0	100
31-Jan-15	04:56:04	0	100
16-Feb-15	04:55:55	0	100
12-Mar-18	04:55:43	2	100
28-Mar-18	04:55:36	0	100
15-May-18	04:55:08	0	100
16-Jun-18	04:55:01	2	100
06-Oct-18	04:55:53	0	100
22-Oct-18	04:55:59	0	100
07-Nov-18	04:56:03	0	100
25-Dec-18	04:55:59	0	100
11-Feb-19	04:55:52	0	100
27-Feb-19	04:55:48	4	100

3. METHODOLOGY

3.1. Retrieving LST from Landsat Data

In this study, the mono-window algorithm was applied to retrieve LST from multi-temporal Landsat satellite sensors (Qin et al. 2001) where three necessary

parameters are ground emissivity, atmospheric transmittance, and effective mean atmospheric temperature. At first, the original TIR bands (100 m resolution for Landsat 8 OLI/TIRS data, 120 m resolution for Landsat 5 TM data, and 60 m resolution for Landsat 7 ETM+ data) were resampled into 30 m by USGS data centre for further application.

The TIR pixel values are firstly converted into radiance from digital number (DN) values (Markham & Barkar 1985). Radiance for TIR band of Landsat 5 TM data and Landsat 7 ETM+ data is obtained using Eq. (1) (URL-3):

$$L_\lambda = \left[\frac{L_{MAX\lambda} - L_{MIN\lambda}}{QCAL_{MAX} - QCAL_{MIN}}\right] * \left[Q_{CAL} - QCAL_{MIN}\right] + L_{MIN\lambda} \qquad (1)$$

where, L_λ = Top of Atmosphere (TOA) spectral radiance ($Wm^{-2}sr^{-1}mm^{-1}$), Q_{CAL} = quantized calibrated pixel value in DN, $L_{MIN\lambda}$ ($Wm^{-2}sr^{-1}mm^{-1}$) = spectral radiance scaled to $QCAL_{MIN}$, $L_{MAX\lambda}$ ($Wm^{-2}sr^{-1}mm^{-1}$) = spectral radiance scaled to $QCAL_{MAX}$, $QCAL_{MIN}$ = minimum quantized calibrated pixel value in DN and $QCAL_{MAX}$ = maximum quantized calibrated pixel value in DN. $L_{MIN\lambda}$, $L_{MAX\lambda}$, $QCAL_{MIN}$, and $QCAL_{MAX}$ values are obtained from the metadata file of Landsat TM and ETM+ data. Radiance for Landsat 8 TIR band is obtained from Eq. (2) (Zanter 2019):

$$L_\lambda = M_L.Q_{CAL} + A_L \qquad (2)$$

where, L_λ = TOA spectral radiance ($Wm^{-2}sr^{-1}mm^{-1}$), M_L = band-specific multiplicative rescaling factor from the metadata, A_L = band-specific additive rescaling factor from the metadata, Q_{CAL} = quantized and calibrated standard product pixel values (DN). All of these variables can be retrieved from the metadata file of Landsat 8 data.

For Landsat 5 and 7 data, the reflectance value is obtained from radiances using Eq. (3) (URL-3):

$$\rho_\lambda = \frac{\pi.L_\lambda.d^2}{ESUN_\lambda.\cos\theta_s} \qquad (3)$$

where, ρ_λ = unitless planetary reflectance, L_λ = TOA spectral radiance ($Wm^{-2}sr^{-1}\mu m^{-1}$), d = Earth-Sun distance in astronomical units, $ESUN_\lambda$ = mean solar exo-atmospheric spectral irradiances ($Wm^{-2}\mu m^{-1}$) and θ_s = solar zenith angle in degrees. $ESUN_\lambda$ values for each band of Landsat 5 and 7 can be obtained from the handbooks of the related mission. θ_s and d values can be attained from the metadata file (Coll et al. 2010).

For Landsat 8 data, reflectance conversion can be applied to DN values directly as in Eq. (4) (Zanter 2019):

$$\rho_\lambda = \frac{M_\rho.Q_{CAL} + A_\rho}{\sin\theta_{SE}} \qquad (4)$$

where, M_ρ = band-specific multiplicative rescaling factor from the metadata, A_ρ = band-specific additive rescaling factor from the metadata, Q_{CAL} = quantized and calibrated standard product pixel values (DN) and θ_{SE} = local sun elevation angle from metadata file.

Eq. (5) is used to convert the spectral radiance to at-sensor brightness temperature (Wukelic et al. 1989; Chen et al. 2006):

$$T_b = \frac{K_2}{\ln(\frac{K_1}{L_\lambda} + 1)} \qquad (5)$$

where, T_b = brightness temperature in Kelvin (K), L_λ = spectral radiance in $Wm^{-2}sr^{-1}mm^{-1}$; K_2 and K_1 =calibration constants. For Landsat 8 data, K_1 = 774.89, K_2 = 1321.08 ($Wm^{-2}sr^{-1}mm^{-1}$). For Landsat 7 data, K_1 = 666.09, K_2 = 1282.71 ($Wm^{-2}sr^{-1}mm^{-1}$). For Landsat 5 data, K_1 = 607.76, K_2 = 1260.56 ($Wm^{-2}sr^{-1}mm^{-1}$).

The land surface emissivity ε, is measured from Eq. (6) using the NDVI Thresholds Method (Sobrino et al. 2001, 2004; Vlassova et al. 2014).

$$\varepsilon = \varepsilon_v F_v + \varepsilon_s(1 - F_v) + d\varepsilon \qquad (6)$$

where, ε =land surface emissivity, ε_v = vegetation emissivity, ε_s = soil emissivity, F_v = fractional vegetation, $d\varepsilon$ = effect of the geometrical distribution of the natural surfaces and internal reflections that can be expressed by Eq. (7):

$$d\varepsilon = (1 - \varepsilon_s)(1 - F_v)F\varepsilon_v \qquad (7)$$

where, ε_v = vegetation emissivity, ε_s =soil emissivity, F_v = fractional vegetation, F = a shape factor whose mean is 0.55, the value of $d\varepsilon$ may be 2% for mixed land surfaces (Sobrino et al. 2004).

The fractional vegetation F_v, of each pixel, is estimated from the NDVI using Eq. (8) (Carlson & Ripley 1997):

$$F_v = \left(\frac{NDVI - NDVI_{min}}{NDVI_{max} - NDVI_{min}}\right)^2 \qquad (8)$$

where, $(a) NDVI < 0.2$ for bare soil; $(b) NDVI > 0.5$ for vegetation; $(c) 0.2 <= NDVI <= 0.5$ for mixed land with bare soil

and vegetation; $(d) NDVI < 0$ for water body (Sobrino et al. 2001, 2004; Vlassova et al. 2014).

Finally, the land surface emissivity ε can be expressed by Eq. (9):

$$\varepsilon = 0.004 * F_v + 0.986 \quad (9)$$

where, ε = land surface emissivity, F_v = fractional vegetation.

Water vapour content is calculated by Eq. (10) (Yang and Qie 1996; Li 2006):

$$w = 0.0981 * \left[10 * 0.6108 * \exp\left(\frac{17.27 * (T_0 - 273.15)}{237.3 + (T_0 - 273.15)} \right) * RH \right] + 0.1697 \quad (10)$$

where, w = water vapour content (g/cm^2), T_0 = near-surface air temperature in Kelvin (K), RH = relative humidity (%). These parameters of atmospheric profile are obtained from the Meteorological Centre, Raipur (http://www.imdraipur.gov.in). Atmospheric transmittance is estimated for Raipur City using Eq. (11) (Qin et al. 2001; Sun et al. 2010):

$$\tau = 1.031412 - 0.11536w \quad (11)$$

where, τ =total atmospheric transmittance, w = water vapour content (g/cm^2).

Raipur City is located in the tropical region. Thus, Eq. (12) is applied to calculate the effective mean atmospheric transmittance of Raipur (Qin et al. 2001; Sun et al. 2010):

$$T_a = 17.9769 + 0.91715T_0 \quad (12)$$

LST is retrieved from Landsat 5, Landsat 7, and Landsat 8 satellite data by using Eq. (13-15) (Qin et al. 2001):

$$T_s = \frac{\left[a(1 - C - D) + \left(b(1 - C - D) + C + D \right) T_b - DT_a \right]}{C} \quad (13)$$

$$C = \varepsilon\tau \quad (14)$$

$$D = (1 - \tau)\left[1 + (1 - \varepsilon)\tau \right] \quad (15)$$

where, ε = land surface emissivity, τ =total atmospheric transmittance, C and D = internal parameters based on atmospheric transmittance and land surface emissivity, T_b = at-sensor brightness temperature, T_a = mean atmospheric temperature, T_0 = near-surface air temperature, T_s = land surface temperature, $a = -67.355351$, $b = 0.458606$.

3.2. Retrieving Extraction of Different Types of LULC by Using NDBaI

The study emphasized NDBaI for determining the relationship with LST (Zhao and Chen 2005; Chen et al. 2006). NDBaI is determined by the SWIR and TIR bands. For, Landsat 5 and Landsat 7 data, band 5 and band 6 are used as the SWIR and TIR band, respectively. For Landsat 8 data, band 6 and band 10 are used as the SWIR and TIR bands, respectively (Table 2). The value of NDBaI ranges between −1 and +1. Generally, the positive value of NDBaI indicates the bare land. The bareness increases with the increase of the positive NDBaI. NDBaI value ranges between -0.2 to 0 shows the built-up area, NDBaI > 0 shows the bare land,NDBaI < -0.25 presents the vegetation, and NDBaI < -0.65 presents the water bodies (Chen et al. 2006). LULC maps have been generated using the aforesaid threshold limits of NDBaI and the results have been validated by the maximum likelihood classification. The average calculated values of the Kappa coefficient and overall accuracy for all the images are 0.91 and 92.19%, respectively.

Table 2. General description of NDBaI

Acronym	Description	Formulation	References
NDBaI	Normalized difference bareness index	$\frac{SWIR1 - TIR}{SWIR1 + TIR}$	Zhao and Chen 2005; Chen et al. 2006

3.3. LST-NDBaI relationship generation on different types of LULC

LST-NDBaI correlation develops on the following LULC categories, i.e., green plants, water bodies, human settlement, and bare lands. The study also evaluates the seasonal and temporal variability of the LST-NDBaI correlation.

4. RESULTS AND DISCUSSION

4.1. Extraction of LULC Types Using NDBaI

Figure 2 shows the classified LULC maps from the post-monsoon data,prepared by the threshold limits of NDBaI and these maps have been validated by applying the maximum likelihood classification method. In the earlier period, the built-up area and bare land were developedalong the middle portion of the city. The northwest part has been rapidly urbanized till 2004-05. Most of the vegetation covered areasof this area were converted into the built-up areas. However, in the last phase of the study period, most of the remaining vegetal covered partsweredecreased due to quick convertion into bare land and built-up area. This conversion was mainly by the anthropogenic activities, although some natural desertification process was also responsible in the semi-arid parts. Conversion of the water bodies is lesser than the vegetation. On the other hand, a high increasing rate was observed for the settlement and bare earth surface (approximately 3 km^2 area annually).

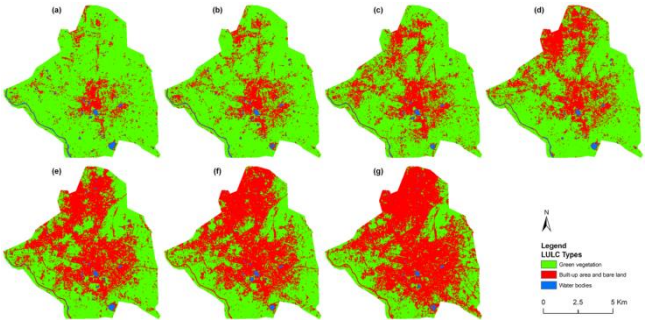

Figure 2. LULC maps of the study area: (a) 1991-1992; (b) 1995-1996; (c) 1999-2000; (d) 2004-2005; (e) 2009-2010; (f) 2014-2015; (g) 2018-2019.

4.2. Seasonal Distribution of LST and NDBaI

A prominent seasonal variation in the minimum, maximum, mean and standard deviation values of LST is noticed in Table 3. The average values of LST and the Pearson's correlation coefficient between LST-NDBaI relationship from 1991-92 to 2018-19 have been shown in italic font text inside Table 3.

Table 3. Seasonal variation of LST and LST-NDBaI relationship (0.05 level of significance).

Season	Year of acquisition	LST (°C)				Correlation coefficients for LST-NDBaI relationship
		Min.	Max.	Mean	Std.	
Pre-monsoon	1991-92	23.81	36.27	31.54	1.52	0.58
	1995-96	24.54	41.07	34.64	1.89	0.51
	1999-00	26.36	42.23	36.38	1.93	0.49
	2004-05	26.95	44.07	38.01	2.19	0.48
	2009-10	28.81	46.48	39.60	2.54	0.43
	2014-15	31.93	48.22	41.28	1.75	0.41
	2018-19	33.46	51.11	43.74	1.75	0.40
	Average	*27.98*	*44.21*	*37.88*	*1.94*	*0.47*
Monsoon	1991-92	19.87	30.83	25.74	1.41	0.66
	1995-96	21.21	33.01	26.50	1.33	0.54
	1999-00	22.76	35.91	27.81	1.34	0.53
	2004-05	24.17	36.20	31.32	1.33	0.54
	2009-10	25.94	38.38	33.06	2.40	0.56
	2014-15	27.74	40.15	34.87	1.68	0.50
	2018-19	30.59	41.98	37.30	1.13	0.55
	Average	*24.61*	*36.64*	*30.94*	*1.52*	*0.56*
Post-monsoon	1991-92	19.72	29.56	24.32	1.72	0.69
	1995-96	20.42	30.33	25.12	1.34	0.59
	1999-00	22.41	33.47	26.84	1.91	0.57
	2004-05	23.03	35.25	28.01	1.71	0.56
	2009-10	24.62	37.91	30.26	1.60	0.58
	2014-15	26.24	38.22	31.68	1.12	0.56
	2018-19	28.92	41.28	33.70	1.34	0.57
	Average	*23.62*	*35.15*	*28.56*	*1.53*	*0.59*
Winter	1991-92	18.22	28.33	23.29	1.22	0.53
	1995-96	20.08	28.68	24.40	1.04	0.48
	1999-00	20.44	32.80	25.21	1.81	0.46
	2004-05	21.08	33.21	26.47	1.25	0.44
	2009-10	22.06	34.36	27.98	1.23	0.42
	2014-15	22.80	36.21	28.90	1.39	0.41
	2018-19	24.31	38.36	30.46	1.37	0.37
	Average	*21.28*	*33.14*	*26.67*	*1.33*	*0.44*

The mean LST of the city was increased gradually. The pre-monsoon season always createshighmean LST values (31.54°C in 1991-92, 34.64°C in 1995-96, 36.38°C in 1999-00, 38.01°C in 2004-05, 39.60°C in 2009-10, 41.28°C in 2014-15, and 43.74°C in 2018-19) (Figure 3). In the urban heat island zones, the LST-NDBaI relationship is direct or high LST areas have high NDBaI values. Moreover, at the micro-level analysis, the high peaks of LST also presented the high peaks of NDBaI. The correlation coefficient values between the LST and NDBaI are positive throughout the span. In the post-monsoon season, the best mean correlation coefficient value (0.59) is found, followed by the monsoon (0.56), pre-monsoon (0.48), and winter (0.44) seasons. Hence, it can be concluded that wet weather produce a better LST-NDBaI relationship.

Figure 3 shows that in the summer season of 2018-19, the LST for most of the places (>90%) have>40°C. In winter, LST of the whole city is less than 40°C. A moderate LST values are noticed in the monsoon and post-monsoon seasons. The mean LST of the study area has been gradually increased between 1991-92 and 2018-19. The converted bare land and built-up area produce high LST value compared to the other LULC categories. The low LST value is found in the unchanged vegetation covered area. The moderate LST value is observed in the unchanged water bodie, wetland, orsettlement with hometaead orchard.

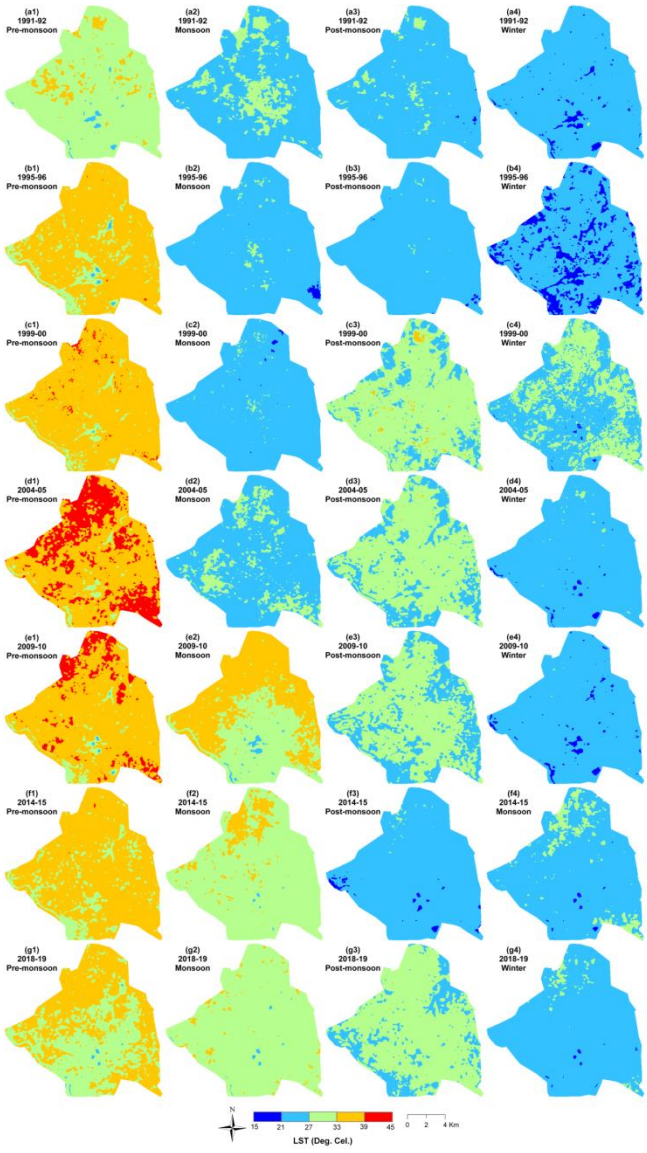

Figure 3. Seasonal distribution of LST: (a1,a2,a3a4) 1991-1992; (b1,b2,b3,b4) 1995-1996; (c1,c2,c3,c4) 1999-2000; (d1,d2,d3,d4) 2004-2005; (e1,e2,e3,e4) 2009-2010; (f1,f2,f3,f4) 2014-2015; (g1,g2,g3,g4) 2018-2019.

Figure 4 shows the seasonal change in the spatial distribution of NDBaI from 1991-92 to 2018-19. The high and low NDBaI regions were seasonally stable since the 1991-92 sessions. The change was observed

only in the values of the NDBaI, not in the distributional pattern. The central part and the periphery of the city show the reverse value of the NDBaI.

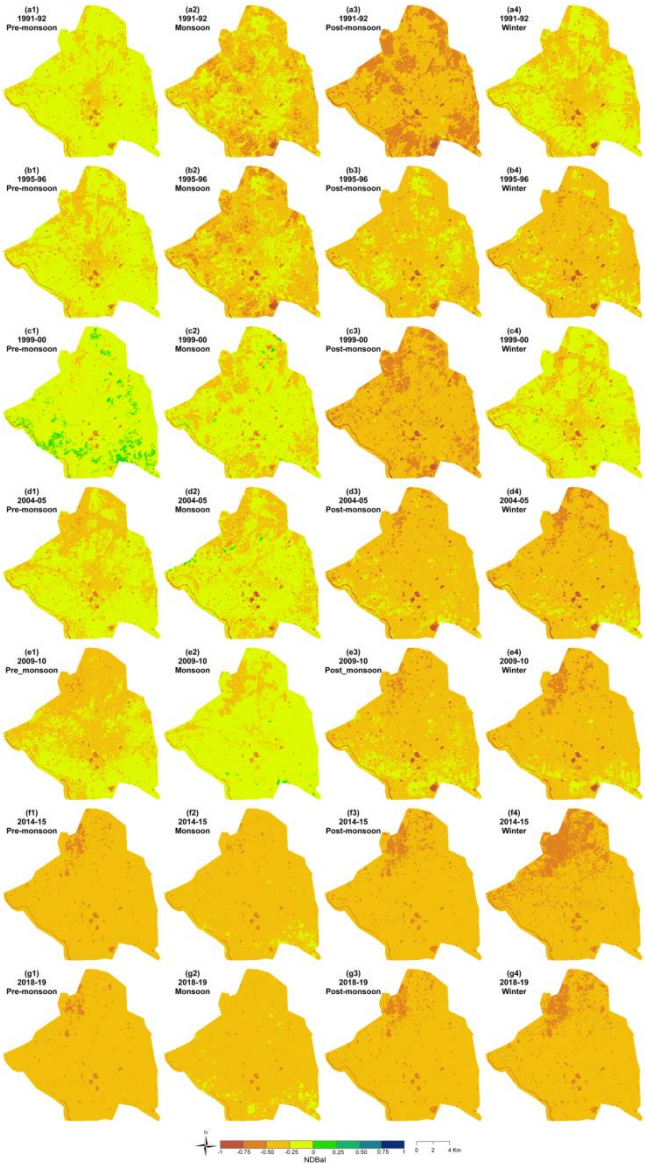

Figure 4. Seasonal distribution of NDBaI: (a1,a2,a3,a4) 1991-1992; (b1,b2,b3,b4) 1995-1996; (c1,c2,c3,c4) 1999-2000;(d1,d2,d3,d4) 2004-2005; (e1,e2,e3,e4) 2009-2010; (f1,f2,f3,f4) 2014-2015; (g1,g2,g3,g4) 2018-2019.

4.3. Seasonal Variation on LST-NDBaI Relationship

Figure 5 (a-d) shows the seasonal variation of LST-NDBaI relationships on different categories of LULC. This relationship is strongly positive on water bodies and wetland, strong to moderate positive on vegetation covered area, and moderate positive on the bare land/built-up area. The pre-monsoon season (Figure 5(a)) has a strong positive LST-NDBaI correlation on the water bodies (0.65) and a moderate positive correlation on green vegetation (0.37), bare land, and built-up area (0.35). In the monsoon season, the correlation is strongly positive on green vegetation (0.56) and water bodies (0.51), whereas it is moderate positive (0.43) on bare land and built-up area (Figure 5(b)). In the post-monsoon season,the best correlation has been built on green vegetation (0.62), followed by the water bodies (0.53), bare land and built-up area (0.48) (Figure 5(c)). In winter (Figure 5(d)), the LST-NDBaI correlation is strongly positive on water bodies (0.62) and green vegetation (0.54), whereasit is moderate positive (0.39) on the bare lands and built-up areas.

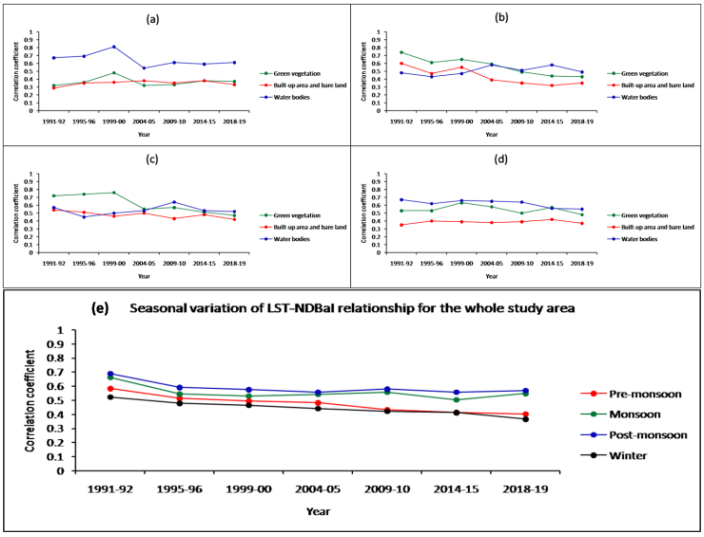

Figure 5. (a-d) Seasonal variation of the LST-NDBaI relationship on various categories of LULC: (a) Pre-monsoon; (b) Monsoon; (c) Post-monsoon; (d) Winter; (e) Seasonal variation of the LST-NDBaI relationship for the whole of the study area (0.05 level of significance).

Figure 5(e) represents the seasonal variation of LST-NDBaI relationships for the whole of the study area. The relationship is positive, for each season. The post-monsoon season presents the best correlation. The results also shows that the dry climate decreases the strength of the regression, while the moist climate increases the strength.

The study shows that LST builds a stable and strong to moderate positive correlation with NDBaI in Raipur City, India throughout the period. The result is comparable to the recently conducted other similar studies on the different urban agglomerations in the world. Essa et al. (2012) have shown that NDBaI generates a positive correlation (0.39) with LST in the Greater Dublin region, Ireland. A study conducted in Kunming of China shows that NDBaI and LST generate strong positive correlation (Chen and Zhang 2017). A weak positive correlation between LST and NDBaI has been presented in London (0.086) and Baghdad (0.469) by Ali et al. (2017). This relationship was also positive (0.458) in Kolkata Metropolitan Area, India (Nimish et al. 2020). The LST and NDBaI have built a weak negative correlation (-0.11) in Guangzhou, China (Guo et al. 2015). This correlation was weak positive (0.06) in Harare Metropolitan City, Zimbabwe (Mushore et al. 2017). Sharma and Joshi (2016) have shown the moderate positive nature of LSI-NDBaI correlation in the National Capital Region of India. The present study shows that the average correlation coefficient between LST and NDBaI of all the four seasons from 1991-92 to 2018-19 is moderate positive (0.052), which can be

considered as a very stable and authentic relationship between the two variables.

The present study is useful for the urban and environmental planning. The bare or fallow lands can be converted into road vegetation, park, wetland, or water bodies to resist the increasing rate of LST, at least to some extent.

5. CONCLUSION

The present study deals with the seasonal estimation of the relation between NDBaI and LST in Raipur City. It is seen that LST is directly correlated to NDBaI for all the seasons. This relationship varies in accordance with the variation of LULC. This correlation remains strong on the water bodies, irrespective of any season. On green vegetation, this correlation is moderate in pre-monsoon season and strong in the other three seasons. The barren land and settlement produce a moderate correlation for all the four seasons. Among the four seasons, the post-monsoon season builds the best LST-NDBaI correlation for all LULC types, whereas the pre-monsoon season has the least correlation. Among the various LULC categories, the water bodies present the best positive LST-NDBaI correlation, irrespective to any season. The high ratio of green plants and water surface can enhance the ecological health. Thus, this research work can be beneficial for the environmental planners. It is also suitable for the land use scientist and geographers. The study can be further expanded by the remote sensing scientist by apply the same methods on other satellite sensors and for different physical environment.

ACKNOWLEDGEMENT

The author is indebted to the United States Geological Survey (URL-3).

Author contributions

Subhanil Guha: Conceptualization, Methodology, Writing-Original draft preparation, Data curation, Validation, Software. **Himanshu Govil:** Visualization, Investigation, Writing-Reviewing and Editing.

Conflicts of interest

The authors declare no conflicts of interest.

REFERENCES

Ahmed B, Kamruzzaman M, Zhu X, Rahman M S & Choi K (2013). Simulating Land Cover Changes and Their Impacts on Land Surface Temperature in Dhaka, Bangladesh. Remote Sensing, 5(11), 5969-5998. https://doi.org/10.3390/rs5115969

Alexander C (2020). Normalised difference spectral indices and urban land cover as indicators of land surface temperature (LST). International Journal of Applied Earth Observation and Geoinformation, 86, 102013. https://doi.org/10.1016/j.jag.2019.102013

Alibakhshi Z, Ahmadi M& Farajzadeh Asl M (2020). Modeling Biophysical Variables and Land Surface Temperature Using the GWR Model: Case Study—Tehran and Its Satellite Cities. Journal of Indian Society of Remote Sensing,48, 59–70. https://doi.org/10.1007/s12524-019-01062-x

Ali J M, Marsh S H& Smith M J (2017). A comparison between London and Baghdad surface urban heat islands and possible engineering mitigation solutions. Sustainable Cities and Society, 29, 159-168. https://doi.org/10.1016/j.scs.2016.12.010

As-syakur A R, Adnyana I W S, Arthana I W & Nuarsa I W (2012). Enhanced Built-Up and Bareness Index (EBBI) for Mapping Built-Up and Bare Land in an Urban Area. Remote Sensing, 4(10), 2957-2970. https://doi.org/10.3390/rs4102957

Barsi J, Schott J, Hook S, Raqueno N, Markham B& Radocinski R (2014). Landsat-8 thermal infrared sensor (TIRS) vicarious radiometric calibration. Remote Sensing, 6(11), 11607-11626.

Carlson T N& Ripley D A (1997). On the Relation between NDVI, Fractional Vegetation Cover, and Leaf Area Index. Remote Sensing of Environment, 62, 241-252. https://doi.org/10.1016/S0034-4257(97)00104-1

Chen X L, Zhao H M, Li P X& Yi Z Y (2006). Remote sensing image-based analysis of the relationship between urban heat island and land use/cover changes. Remote Sensing of Environment, 104(2), 133–146. https://doi.org/10.1016/j.rse.2005.11.016

Chen X& Zhang Y (2017). Impacts of urban surface characteristics on spatiotemporal pattern of land surface temperature in Kunming of China. Sustainable Cities and Society, 32, 87-99. https://doi.org/10.1016/j.scs.2017.03.013

Essa W, Verbeiren B, Van der Kwast J, Van de Voorde T& Batelaan O (2012). Evaluation of the DisTrad thermal sharpening methodology for urban areas. International Journal of Applied Earth Observation and Geoinformation, 19, 163-172. https://doi.org/10.1016/j.jag.2012.05.010

Guha S, Govil H, Dey A & Gill N (2020a). A case study on the relationship between land surface temperature and land surface indices in Raipur City, India. Geografisk Tidsskrift-Danish Journal of Geography, 120(1), 35-50. https://doi.org/10.1080/00167223.2020.1752272

Guha S, Govil H, Gill N & Dey A (2020b). Analytical study on the relationship between land surface temperature and land use/land cover indices. Annals of GIS, 26(2), 201-216. https://doi.org/10.1080/19475683.2020.1754291

Guha S, Govil H & Mukherjee S (2017). Dynamic analysis and ecological evaluation of urban heat islands in Raipur city, India. Journal of Applied Remote Sensing, 11(3), 036020. https://doi:10.1117/1.JRS.11.036020

Guo G, Wu Z& Chen Y (2014). Estimation of subpixel land surface temperature using Landsat TM imagery: A case examination over a heterogeneous urban area. Third International Workshop on Earth Observation and Remote Sensing Applications (EORSA), Changsha, p. 304-308. https://doi.org/10.1109/EORSA.2014.6927900

Guo G, Wu Z, Xiao R, Chen Y, Liu X& Zhang X (2015). Impacts of urban biophysical composition on land surface temperature in urban heat island clusters. Landscape and Urban Planning, 135, 1-10. https://doi.org/10.1016/j.landurbplan.2014.11.007

Hao X, Li W& Deng H (2016). The oasis effect and summer temperature rise in arid regions-case study in Tarim Basin. Scientific Reports, 6, 35418. https://doi.org/10.1038/srep35418

Jain S, Sannigrahi S, Sen S, Bhatt S, Chakraborti S& Rahmat S (2020). Urban heat island intensity and its mitigation strategies in the fast-growing urban area. Journal of Urban Management, 9(1), 54-66. https://doi.org/10.1016/j.jum.2019.09.004

Li J (2006). Estimating land surface temperature from Landsat-5 TM. Remote Sensing Technology and Application, 21, 322-326.

Li Z N, Duan S B, Tang B H, Wu H, Ren H G& Yan G J (2016). Review of methods for land surface temperature derived from thermal infrared remotely sensed data. Journal of Remote Sensing, 20, 899–920.

Macarof P, Bîrlica I C& Stătescu F (2017). Investigating the relationship between land surface temperature and urban indices using landsat-8: a case study of Iaşi. Lucrările Seminarului Geografic Dimitrie Cantemir, 45, 81-88. https://doi.org/10.15551/lsgdc.v45i0.07

Mushore T D, Odindi J, Dube T& Mutanga O (2017). Prediction of future urban surface temperatures using medium resolution satellite data in Harare metropolitan city, Zimbabwe. Building and Environment, 122, 397-410. https://doi.org/10.1016/j.buildenv.2017.06.033

Nimish G, Bharath H A& Lalitha A (2020). Exploring temperature indices by deriving relationship between land surface temperature and urban landscape. Remote Sensing Application: Society and Environment, 18, 100299. https://doi.org/10.1016/j.rsase.2020.100299

Qin Z, Karnieli A& Barliner P (2001). A Mono-Window Algorithm for Retrieving Land Surface Temperature from Landsat TM Data and Its Application to the Israel-Egypt Border Region. International Journal of Remote Sensing, 22(18), 3719-3746. https://doi:10.1080/01431160010006971

Sekertekin A, Kutoglu SH & Kaya S (2016). Evaluation of spatio-temporal variability in Land Surface Temperature: A case study of Zonguldak, Turkey. Environmental Monitoring and Assessment, 188, 30. https://doi.org/10.1007/s10661-015-5032-2

Sharma R, Ghosh A& Joshi P K (2013). Mapping environmental impacts of rapid urbanization in the National Capital Region of India using remote sensing inputs. Geocarto International, 28(5), 420-438. https://doi.org/10.1080/10106049.2012.715208

Sharma R& Joshi P K (2016). Mapping environmental impacts of rapid urbanization in the National Capital Region of India using remote sensing inputs. Urban Climate, 15, 70-82. https://doi.org/10.1016/j.uclim.2016.01.004

Sobrino J A, Raissouni N& Li Z (2001). A comparative study of land surface emissivity retrieval from NOAA data. Remote Sensing of Environment,75(2), 256–266. https://doi.org/10.1016/S0034-4257(00)00171-1

Sobrino J A, Jimenez-Munoz J C & Paolini L (2004). Land surface temperature retrieval from Landsat TM5.Remote Sensing of Environment, 9, 434–440. https://doi:10.1016/j.rse.2004.02.003

Sun Q, Tan J & Xu Y (2010). An ERDAS image processing method for retrieving LST and describing urban heat evolution: A case study in the Pearl River Delta Region in South China. Environmental Earth Science, 59, 1047-1055.

Tomlinson C J, Chapman L, Trones J E& Baker C (2011). Remote sensing land surface temperature for meteorology and climatology: a review. Meteorological Application, 118, 296–306. https://doi.org/10.1002/met.287

URL-1: hthttp://www.surveyofindia.gov.in

URL-2: http://www.raipur.gov.in

URL-3: https://www.earthexplorer.usgs.gov

URL-4: http://www.imdraipur.gov.in

Vlassova L, Perez-Cabello F, Nieto H, Martín P, Riaño D, & De La Riva J (2014). Assessment of methods for land surface temperature retrieval from Landsat-5 TM images applicable to multiscale tree-grass ecosystem modeling. Remote Sensing, 6(5), 4345-4368.

Wukelic G E, Gibbons D E, Martucci L M&Foote H P (1989). Radiometric calibration of Landsat Thematic Mapper thermal band. Remote Sensing of Environment, 28, 339–347. https://doi.org/10.1016/0034-4257(89)90125-9

Yang J& Que J (1996). The empirical expressions of the relation between precipitable water and ground water vapor pressure for some areas in China.Scientia Atmospherica Sinica, 20, 620-626.

Zanter K (2019). Landsat 8 (L8) Data Users Handbook; EROS: Sioux Falls, SD, USA.

Zhao H M & Chen X L (2005). Use of normalized difference bareness index in quickly mapping bare areas from TM/ETM+. Geoscience and Remote Sensing Symposium. 3 (25–29), p.1666–1668. https://doi.org/10.1109/IGARSS.2005.1526319

International Journal of Engineering and Geosciences

https://dergipark.org.tr/en/pub/ijeg

e-ISSN 2548-0960

3D city model for monitoring flash flood risks in Salalah, Oman

Khalid Al Kalbani[*1], **Alias Abdul Rahman** [1]

[1]*Universiti Teknologi Malaysia, 3D GIS Research Lab, Faculty of Built Environment and Surveying, Johor Bahru, Malaysia*

Keywords
Flood risk management
3D city model
CityGML

ABSTRACT

This paper investigates the issues and challenges in using a 3D city model for monitoring flash flood risks in Salalah (Oman) designed using the City Geography Markup Language (CityGML) standards version 2.0. The investigation was made based on the fact that 2D and 2.5D GIS solutions cannot analyse flood complex problems inside the urban area. Hence, the study sought to reduce time and effort for the decision-makers by proposing a 3D city model for flood risk management. The study used geospatial tools and databases such as ArcGIS, Watershed Modelling System (WMS), FME, PostgreSQL-PostGIS, and 3D City Database (3DCityDB) to generate the 3D model and to test the capability of establishing a unified geospatial data structure including the 3D city objects, hydrological data, and geological data. The findings showed the importance of addressing flood risks data and arranging it in the 3D geodatabase. It was also revealed that establishing a 3D city model based on the CityGML standard requires homogenised definitions and standards for city objects (surface and subsurface) as well as hydrological data.

1. INTRODUCTION

Oman has coasts with a length of 3165 kilometres that facing towards the Indian Ocean, where tropical storms occur. Therefore, it experiences frequent climatic events such as tropical depression and cyclone (Al-Kalbani, 2011; Dube et al., 2020). In addition to that, the low parts of the coastal areas can be exposed to coastal floods caused by high waves that come along with the climactic event. These climatic events affect human lives and cause damage to city infrastructure, which costs millions of dollars. Salalah is one of the south Omani cities that has faced several climatic events such as cyclone Mekunu in 2018 and tropical depression from 27 May to 1 June 2020, as shown in Fig. 1.

The impact of these events has led to the importance of evaluating Salalah city infrastructure by using the 3D geospatial data approach to test the extent to which the Salalah city infrastructure matches with the hydrological system in that area. This study, thus, investigates the issues and challenges of implementing a 3D city model to monitor, evaluate and manage these dangers by developing a small-scale 3D city model using CityGML standard version 2.0.

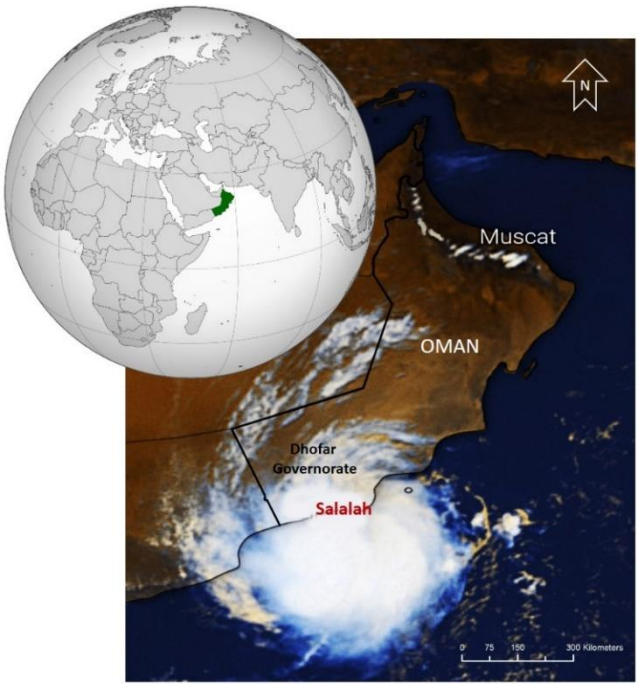

Figure 1. The tropical depression, 30 May 2020

* **Corresponding Author**
(asakkhalid2@graduate.utm.my) ORCID ID 0000-0002-3268-6831
(alias@utm.my) ORCID ID 0000-0001-5263-8266

Cite this study
Kalbani K A & Rahman A A (2022). 3D city model for monitoring flash flood risks in Salalah, Oman. International Journal of Engineering and Geosciences, 7(1); 17-23

Research Article / DOI: 10.26833/ijeg.857971

Received: 18/01/2021; Accepted: 25/03/2021

Monitoring and assessing flash floods and managing mitigation measures is a complex project that requires great effort and a relatively long period of time. The study seeks to reduce time and effort by employing a 3D city model, which mainly depends on the design of the 3D city model databases to manage the influence of the flood risk on the city infrastructure (surface and sub-surfaces spatial objects). Bee et al. (2008), Ruíz (2015) and Tymkow et al. (2016) demonstrated that a mechanism could be established to deal with flood risk data by linking geospatial data and identifying effective models, analysing appropriate simulation, estimation techniques, and designing a flood intensity scale. On the other hand, The Bureau for Crisis Prevention and Recovery (BCPR) in its 2004 international report indicated that more efforts should be made to collect disaster-related data. Also, it pointed out in its recommendations, the need to support the national risk management to produce the information needed for decision-making at a national level (UNDP, 2004).

Nowadays, the infrastructure such as multi-floor buildings and underground utilities, indoor and outdoor spatial objects in the urban areas is complicated as it requires using 3D geodata sets and 3D geospatial platforms with high performance. Additionally, employing the current geospatial solutions may not be useful to analyse and visualise complex problems, so there is an urgent need to develop 3D city model based on interoperability solutions (Biljecki et al., 2015b; Stoter et al., 2014, 2010). 3D geospatial platforms, 3D database and their related applications are considered as good initiatives to represent the 3D spatial objects and entire cities. The capability of these geospatial technologies offer some solutions in analysing complex data structure issues (Abdul Rahman et al., 2019; Siew and Kumar, 2019; Yao et al., 2018). Hence, efforts to make the 3D city model successful for flood risk management requires a homogenous and stable environment for all models and standards in terms of hydrology, meteorology, geomorphology, geology, and hydrogeology.

A number of countries around the world have applied the GIS for flood risk management, while other countries are working toward 3D GIS by using their standard, data format and database (Al-Kalbani, 2011; Ruíz, 2015). At this point, the 3D geospatial institutions and researchers have made an effort to develop a framework for flood modelling based on the use of OGC CityGML standard, CityJSON and others. Nevertheless, the pre-implementation has exposed several issues and challenges that need to be addressed during data processing, data integration, data modelling, data converting, and data visualising (Al Kalbani and Abdul Rahman, 2019; Kumar et al., 2018; Zlatanova et al., 2014). Part of the challenges is related to DEM sources efficiency in 3D flood modelling and complex hydraulic simulation. In this context, Bakuła et al. (2016) and Li and Wong (2010) investigated how hydraulic modelling and application can be influenced by the source of different elevation data. Meanwhile, Muhadi et al. (2020) discussed the use of Digital Elevation Model (DEM) extruded from LiDAR for flood applications.

Establishing a flood risk database within the 3D city model is a complex task at the national level. On the one hand, dealing with 3D city model requires new solutions to integrate the data structure for both the surface and subsurface spatial objects (Al Kalbani and Abdul Rahman, 2019). This is because most of the 3D geospatial initiatives focus on surface spatial objects data structure with less interest to model the subsurface spatial objects. On the other hand, there is a need to find an approach that bridges between different available 3D geospatial standards in terms of geometric and semantics information to supports the interoperability between Database Management Systems (DBMS), services, and stakeholders (Stoter et al., 2010).

This paper is arranged in nine sections, where Section 2 discusses the study area. Then, Section 3 reviews the CityGML standard. Section 4 reviews the current state of Oman geospatial data and Spatial Data Infrastructure (SDI), followed by the data and methods in Section 5. The Section 6 includes the discussion and outcomes of the study. Section 7 highlights the issues and challenges. The benefit of implementing a 3D city model for flood risk management is summarised in Section 8, and finally, Section 9 concludes the paper.

2. STUDY AREA

Salalah is one of the main cities in the Dhofar Governorate (southwest of the Sultanate of Oman) (Zerboni et al., 2020). The population of the governorate has reached 416,458 in December 2020 (NCSI, 2020), distributed between the coastal plain and mountainous and desert areas. The urban area in Salalah is spread on a narrow coastal plain, located between mountains, that are more than 1000 meters high (see Fig. 2), and a coastal line with a number of wadis and alluvial fans passing throughout the area.

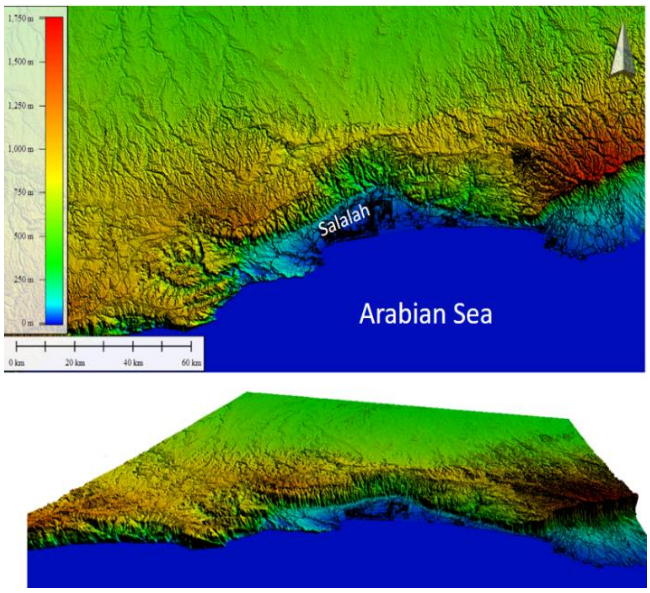

Figure 2. The digital elevation model (DEM) of Salalah

The coastal plain can reach 13 km in its maximum width. The mountain range in this area was formed by tectonic activity and uplift movement (Zerboni et al., 2020). Most of the rocky structure scattered in this region is dominated by solid limestone.

Dhofar is considered a semi-arid area with approximately 100–400 mm of rainfall per year (Zerboni et al., 2020). This area also has a monsoon from July to August, in which the weather becomes cloudy with little rain. This area can also be affected by cyclones and tropical depressions. One of the clime events Dhofar had experienced is the tropical depression (27 May to 1 June 2020) which caused heavy rains so much causing some of the Dhofar districts to receive more than 1000 mm of rains in 5 days. Salalah (study area) received 531 mm, causing flash floods and destroying some city infrastructure (Mrmwroman, 2020).

Rapid development in Salalah plays a role in the occurrence of natural phenomena such as floods. The accelerated pressure on urban spatial holdings contributed to the exploitation of flood-prone areas, and most exploitation was not accompanied by providing the infrastructure of water drainage (Al-Kalbani, 2011). The Crisis and Recovery Office has indicated in its global report to UNDP 2004 that "it does not necessarily mean that the urban transformation increases flood risk and can actually reduce it if it is well managed" (UNDP, 2004). However, the damage caused by floods cannot always be the main natural factor for exacerbating events. Instead, it is often the human factor that provides the right environment for these risks to develop into disasters.

The high cost for constructing and maintaining the flood protection infrastructure constrained the integration of flood risk measures into urban planning efforts effectively. In fact, establishing flood risk infrastructure at the government level can be affected by two elements, namely the economic feasibility and practical feasibility. Often, the economic factor is the dominant factor in addition to the amount of available budget (Al-Kalbani, 2011). In all scenarios, when planning deviates from the inclusion of flood risk as a priority, this uncontrolled planning may cause challenges in normal rainfall and make matters worse in the case of heavy rains.

3. CityGML STANDARD

CityGML is an open XML file format for exchanging, storing, and representing 3D objects. Its initiatives have been developed by the Special Interest Group 3D (SIG 3D). Now, it is organised by Open Geospatial Consortium (OGC). CityGML standard has been adopted as an international standard to exchange the format of 3D geospatial objects and the 3D city model based on the XML file format and the GML 3xx. Besides, CityGML version 2.0 includes 13 models to store the spatial objects and five levels of detail (LoD) (Biljecki, 2017; Biljecki et al., 2015b; Stouffs et al., 2018).

CityGML presents the most common natural and human spatial features that can be found in the cities and their surroundings by determining their geometric and semantic information (Arroyo Ohori et al., 2018; Biljecki, 2017; Biljecki et al., 2017, 2015a, 2015b; Kensek, 2014; Stoter et al., 2016). Furthermore, the structure of CityGML file format is developed based on the hierarchy structure for both geometric and semantic information. Now, there are various spatial applications for CityGML standard such as solar potential estimation, flood risk assessment and noise monitoring (Biljecki, 2017; Biljecki et al., 2015b; Preka and Doulamis, 2016; Soon et al., 2016; Yao et al., 2018).

4. THE CURRENT STATE OF OMAN GEOSPATIAL DATA AND SDI

Oman government established its National Spatial Data Infrastructure (NSDI) in 2014 to standardise the geospatial activities and business at the national level. Since then, the geospatial workflow of Oman NSDI and its partners (Oman GIS stakeholders) are limited to the 2D and 2.5D geospatial data (Al Kalbani et al., 2018; Das et al., 2017; NCSI, 2017a, 2017b). In fact, Oman is one of the developed countries which has a complex city infrastructure. As a result, using 2D and 2.5D geospatial data may not be efficient in analysing flood risk inside the big cities and complex structures. Hence, the decision-makers in Omani municipalities need GIS solutions based on utilising a 3D city model.

5. DATA AND METHODS

5.1. Data

The study created a small-scale 3D city model for Salalah district using CityGML version 2.0 and spatial data collected from the related geospatial agencies in Oman (2D, 2.5D geospatial data). Satellite images (Sentinel-2) with a resolution of 10 meters for the tropical depression from 1-3 June 2020 were obtained from https://eos.com/landviewer.

5.2. Method

The methodology in this study is given below.

5.2.1. Creating Surface and Subsurface Models at LoD1

A building model was created at CityGML LoD1 by extruding the building footprint using a high value from the file attributes. LoD1 was also used to create a terrain model. Geospatial tools such as FME engine was used to generate 3D spatial objects for surface and subsurface spatial objects based on CityGML standard version 2.0 and also for exchanging the file format from one model to the other. Since the CityGML 2.0 does not fully support the subsurface spatial objects and models, the study used the CityGML generic module to develop some of these subsurface models such as geological model and pipeline networks.

5.2.2. Creating Wadi Networks and Watershed

The study used ArcGIS (hydrology tools) and the Watershed Modelling System (WMS) to extract wadi (stream) networks and watershed using ASTER DEM with a resolution of 30 meters. Besides, WMS applications were used to produce flood spread layers based on digital terrain data and floodwater estimative elevation values between 1 – 3 meters.

5.2.3. Creating A unified 3D Database

The study carried out some experiments to investigate further the issues and challenges for constructing a unified 3D database. Related to this, databases PostgreSQL-PostGIS and 3DCityDB were used to register and store the 3D models for surface and subsurface objects in a relational database. It also, explored the data structure integration challenges between geological models, hydrological models and 3D city models.

5.2.4. Integration Between Satellite Images and 3D City Models

The study investigated how to integrate the benefits of satellite images and 3D city models for flood risk management. Satellite images (Sentinel-2) were analysed using change detection methods. The role of satellite images in this study is to draw a map of the flood spread in the study area by overlapping the 3D models (building and road) in the 3D city model with 2D satellite images that are classified using change detection. In addition, this step contributed to tracking and highlighting some of the flooding problems related to the failure of drainage networks along highways and inside cities.

5.2.5. Visualising

Since there is no professional 3D viewer to visualise both surface and subsurface spatial objects, the study used visualising tools such as FME Data Inspector, Google Earth, FZK viewer and Cesium.

6. RESULTS AND DISCUSSION

A small-scale 3D city model was created for most surface city spatial objects in LoD 1 (see Fig. 3). However, it faced a challenge to go higher to LoD 3 and LoD 4 due to missing rich data such as BIM/IFC. In addition, the study able to generate wadi (stream) networks and watershed using Salalah digital terrain data.

Figure 3. The small-scale 3D city model for Salalah

The real challenge in developing the 3D city model was how to create the subsurface spatial objects. This is because the CityGML version 2.0 does not provide a definition to support the subsurface objects except for the CityGML Application Domain Extension (ADE) for utility network. Thus, the study created some of the subsurface spatial objects in LoD1 using the CityGML generic module. However, there are some challenges related to semantic, geomatic and topology that need to be addressed to enhance 3D subsurface models. Other challenges are related to 3D spatial analysis and the process of creating a unified relational database for surface and subsurface spatial objects.

Since the CityGML version 2.0 does not include hydrological models and flooding simulation, this study used several applications separately and the outcomes were linked to one 3D city model. During this stage, the experiments showed that the 3D city model was able to determine the areas that might be subjected to water flooding by linking the 3D city model, terrain and flood layer exported from WMS, as shown in Fig. 4.

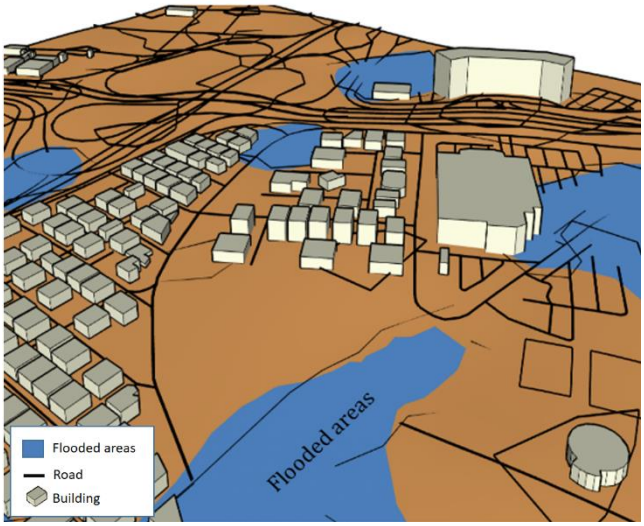

Figure 4. The areas subjected to flooding

Another advantage of managing flood data in 3D city model is providing the capability to determine the level to which floodwater can reach in each of the city buildings (see Fig. 5).

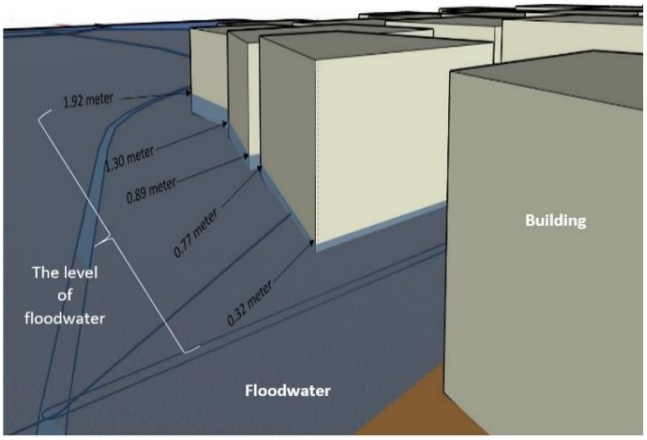

Figure 5. The level of floodwater in residential areas

Nevertheless, there is still a challenge in registering the value to which floodwater can reach automatically in

the database for each of the building faces and edges due to the complexity of CityGML data structure in terms of systematic and geometric information.

Moreover, the experiments demonstrated that there is a possibility to integrate the analysis of satellite images using change detection methods and 3D city models to map the distribution of internal floods in residential areas and to highlight some issues in the city infrastructure (see Fig. 6).

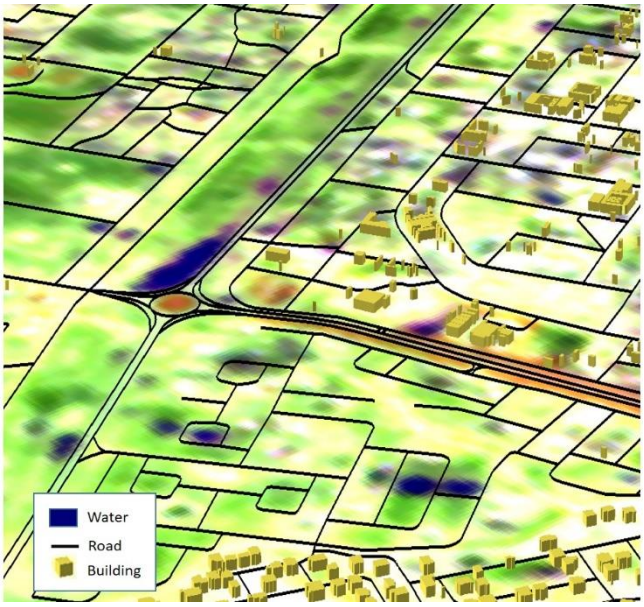

Figure 6. The integration between satellite images using the change detection method and 3D city models

Based on this approach, the results revealed that floodwater collects on the sides of highways and some modern bridges as well as residential areas. There are many reasons that can caused the phenomenon, but lack of water drainage networks, failure of drainage channels due to accumulation of impurities coming from the watershed, incompatibility of the engineering design of the drainage channels and the volume of water flow are the most important factors. Other challenges are due to the low level of the ground surface in some residential areas and weak water infiltration into the ground.

7. ISSUES AND CHALLENGES

The establishment of a 3D city model for flood risk monitoring based on the use of CityGML version 2 requires compatible solutions. Hence, this study was performed to address the issues and challenges listed as follows:

- Integrating the CityGML and the current mathematic hydrological models in a unified ADE, data structure and 3D geodatabase.
- Designing suitable equations to estimate the floods' peak considering Salalah environment, climate, the nature of urban patterns and characteristics of dams and their ability to drain water. Therefore, creating hydrodynamic modelling of flood flows using CityGML standard needs to determine the relation with other factors such as the surface of the wadi, slope, velocity, leakage rate to the underground, evaporation, and 3D objects resistance.
- Upgrading 3DCityDB data structure to import subsurface spatial objects.
- Developing homogenised definitions within CityGML standard to manage relationships between different subsurface spatial objects, geological models and hydrological models.
- Developing a new logarithm of hydrodynamic modelling of flood flows based on CityGML standard and 3D raster map (voxel).
- Calculating the water drainage that comes from the city's infrastructure, where the roofs of buildings and paved areas contribute to the gathering of rainwater in residential areas and low areas.
- Designing a mechanism to predict urban infrastructure behaviour during the flooding, where the failure of bridges, roads and drainage channels can shut down the natural paths of valleys and change the direction of their flow, causing internal flooding in residential areas.
- Integrating indoor and outdoor navigation and flood risk management.
- Updating the hydrology simulation results automatically into the databases at the level of CityGML schema(s) and LoD(s).
- Defining the water stream paths inside the city in the absence of Light Detection and Ranging (LiDAR) data, which is a restricted data in Oman and needs several official permissions.

Other challenges are related to CRS/SRID, quality of data structures, geomatics representation, the problem of semantic cording, creating the data structure in terms of schema(s) and LoD(s), integration with the DEM, the 3D object topology issues, flood topology issues, data retrieval, data size, data index, 3D spatial analysis, spatial operations and rendering over Cesium.

8. THE BENEFITS OF IMPLEMENTING A 3D CITY MODEL FOR FLOOD RISK MANAGEMENT

The expected benefits of using a 3D city model for flood risk management study are summarised as follows:

- A suitable environment for the modelling of floods and their impact on the urban areas in 3D
- The ability to test infrastructure projects before implementation on the ground
- A suitable environment for flood risk management and rescue operations

9. CONCLUSION

This study successfully investigated the use of a 3D city model to monitor flood risks in Salalah and determined the challenges faced during the investigation. This evidently showed that the issues and challenges are related to the efficiency of this standard for hydrological analysis and in managing surface and subsurface spatial objects in the unified data structure.

The results also demonstrated that the 3D geospatial data is more efficient in solving planning problems and defining the issues that may increase flood risks. This, in turn, helps to understand and assess the

nature of risks, and thus design a clear vision to manage rescue efforts. This research is still a work-in-progress and the authors believe that the initial outcomes of this paper can highlight the importance of including 3D geospatial solutions for flood risk management in Oman. In the future, based on the outcomes, we would like to examine the performance of the JavaScript Object Notation (JSON) and CityJSON data structure as alternative solutions to create a flood spatial data structure in the 3D city model.

ACKNOWLEDGEMENT

The authors would like to acknowledge the Ministry of Higher Education, Research, and Innovation (MoHERI) of the Sultanate of Oman for supporting the main project (3D SDI). The research leading to these results has received funding from MoHERI under the GRG program. Funding Agreement No: MoHERI/GRG/INT.S/09/2020.

Author contributions

Khalid Al kalbani: Conceptualization, Methodology, Software, Data curation, Writing-Original draft preparation, Validation, and Visualization. **Alias Abdul Rahman**: Conceptualization, Methodology, Reviewing and Editing.

Conflicts of interest

The authors declare no conflicts of interest.

REFERENCES

Abdul Rahman, A., Rashidan, H., Musliman, I.A., Buyuksalih, G., Bayburt, S., Baskaraca, P., 2019. 3D Geospatial Database Schema for Istanbul 3D City Model. ISPRS - Int. Arch. Photogramm. Remote Sens. Spat. Inf. Sci. XLII-4/W16, 11–16. https://doi.org/10.5194/isprs-archives-XLII-4-W16-11-2019

Al Kalbani, K., Abdul Rahman, A., 2019. Integration Between Surface and Subsurface Spatial Objects for Developing Oman 3D SDI Based on the CityGML Standard. Int. Arch. Photogramm. Remote Sens. Spat. Inf. Sci. XLII-4/W16, 79–84. https://doi.org/10.5194/isprs-archives-XLII-4-W16-79-2019

Al Kalbani, K., Abdul Rahman, A., Al Awadhi, T., Alshannaq, F., 2018. Development Of A Framework for Implementing 3D Spatial Data Infrastructure In Oman – Issues And Challenges. ISPRS - Int. Arch. Photogramm. Remote Sens. Spat. Inf. Sci. XLII-4/W9, 243–246. https://doi.org/10.5194/isprs-archives-XLII-4-W9-243-2018

Al-Kalbani, K., 2011. Monitoring and Assessing Flood Risks & Maintaining the Procedures to Limit their Danger using Geographical Information Systems, Remote Sensing and Hydrological Modeling (Case Study :Al-Seeb Willayat) ". Sultan Qaboos University.

Arroyo Ohori, K., Biljecki, F., Kumar, K., Ledoux, H., Stoter, J., 2018. Modeling Cities and Landscapes in 3D with CityGML, in: Building Information Modeling. Springer International Publishing, Cham, pp. 199–215. https://doi.org/10.1007/978-3-319-92862-3_11

Bakuła, K., StĘpnik, M., Kurczyński, Z., 2016. Influence of Elevation Data Source on 2D Hydraulic Modelling. Acta Geophys. 64, 1176–1192. https://doi.org/10.1515/acgeo-2016-0030

Bee, M., Benedetti, R., Espa, G., 2008. Spatial Models for Flood Risk Assessment. Environmetrics 19, 725–741. https://doi.org/10.1002/env.932

Biljecki, F., 2017. Level of Details in 3D City Models,Published PhD Thesis. Delft University of Technology. https://doi.org/10.4233/uuid:f12931b7-5113-47ef-bfd4-688aae3be248 Uzbekistan (Hz. Osman's Mushafi). International Congress on Cultural Heritage and Tourism (ICCHT), 115-123, Bishkek, Kyrgzstan.

Biljecki, F., Ledoux, H., Stoter, J., 2017. Generating 3D City Models Without Elevation Data. Comput. Environ. Urban Syst. 64, 1–18. https://doi.org/10.1016/j.compenvurbsys.2017.01.001

Biljecki, F., Ledoux, H., Stoter, J., 2015a. Improving the Consistency of Multi-LoD CityGML Datasets by Removing Redundancy. pp. 1–17. https://doi.org/10.1007/978-3-319-12181-9_1

Biljecki, F., Stoter, J., Ledoux, H., Zlatanova, S., Çöltekin, A., 2015b. Applications of 3D City Models: State of the Art Review. ISPRS Int. J. Geo-Information 4, 2842–2889. https://doi.org/10.3390/ijgi4042842

Das, A., Chandel, K., Narain, A., 2017. Value of Geospatial Technology in Boosting Omans Economy, in: Oman Geospatial Forum 2017. Oman National Survey Authority, Muscat, pp. 1–74.

Dube, A., Ashrit, R., Kumar, S., Mamgain, A., 2020. Improvements in Tropical Cyclone Forecasting through Ensemble Prediction System at NCMRWF in India. Trop. Cyclone Res. Rev. https://doi.org/10.1016/j.tcrr.2020.04.003

Kensek, K.M., 2014. Building Information Modeling. Build. Inf. Model. 1–285. https://doi.org/10.4324/9781315797076

Kumar, K., Ledoux, H., Stoter, J., 2018. Dynamic 3D Visualisation of Floods: Case of the Netherlands. ISPRS - Int. Arch. Photogramm. Remote Sens. Spat. Inf. Sci. XLII-4/W10, 83–87. https://doi.org/10.5194/isprs-archives-XLII-4-W10-83-2018

Li, J., Wong, D.W.S., 2010. Effects of DEM Sources on Hydrologic Applications. Comput. Environ. Urban Syst. 34, 251–261. https://doi.org/10.1016/j.compenvurbsys.2009.11.002

Mrmwroman, 2020. Precipitation Report from 27 May to 1 June, Mrmwroman Report.

Muhadi, N.A., Abdullah, A.F., Bejo, S.K., Mahadi, M.R., Mijic, A., 2020. The Use of LiDAR-Derived DEM in Flood Applications: A Review. Remote Sens. 12, 2308. https://doi.org/10.3390/rs12142308

NCSI, 2020. Monthly Statistical Bulletin, December 2020, Monthly Statistical Bulletin. https://doi.org/10.36548/jsws.2020.2

NCSI, 2017a. Oman National Spatial Data Infrastructure Strategy V5.0. National Center for Statistics and Information, Oman.

NCSI, 2017b. Oman National Spatial Data Infrastructure, 1st ed. National Center for Statistics and Information, Oman.

Preka, D., Doulamis, A., 2016. 3D Building Modeling in LoD2 Using the CityGML Standard. ISPRS - Int. Arch. Photogramm. Remote Sens. Spat. Inf. Sci. XLII-2/W2, 11–16. https://doi.org/10.5194/isprs-archives-XLII-2-W2-11-2016

Ruíz, A.A.B., 2015. An Urban Flooding Simulation Technique by Using 3D City Information Model 3, 54–67.

Siew, C., Kumar, P., 2019. CitySAC: A Query-Able CityGML Compression System. Smart Cities 2, 106–117. https://doi.org/10.3390/smartcities2010008

Soon, K.H., Tan, D., Khoo, V., Soon, K.H., Tan, D., Khoo, V., 2016. Initial Design to Develop a Cadastral System that Supports Digital Cadastre, 3D and Provenance for Singapore, in: 5th International Workshop on 3D Cadastres. pp. 419–432.

Stoter, J., Brink, L. Van Den, Vosselman, G., Goos, J., Verbree, E., Klooster, R., Berlo, L. Van, Vestjens, G., Reuvers, M., Thorn, S., 2010. A Generic Approach for 3D SDI in the Netherlands. Lect. Notes Comput. Sci. 1–22.

Stoter, J., Ploeger, H., Roes, R., Riet, E. Van Der, Biljecki, F., Stoter, J., Ploeger, H., Roes, R., Riet, E. Van Der, Biljecki, F., 2016. First 3D Cadastral Registration of Multi-level Ownerships Rights in the Netherlands, in: 5th International Workshop on 3D Cadastres. pp. 491–504.

Stoter, J., Vosselman, G., Dahmen, C., Oude Elberink, S., Ledoux, H., 2014. CityGML Implementation Specifications for a Countrywide 3D Data Set. Photogramm. Eng. Remote Sens. 80, 1069–1077. https://doi.org/10.14358/pers.80.11.1069

Stouffs, R., Tauscher, H., Biljecki, F., 2018. Achieving Complete and Near-Lossless Conversion from IFC to CityGML. ISPRS Int. J. Geo-Information 7, 355. https://doi.org/10.3390/ijgi7090355

Tymkow, P., Karpina, M., Borkowski, A., 2016. 3D GIS for Flood Modelling in River Valleys. ISPRS - Int. Arch. Photogramm. Remote Sens. Spat. Inf. Sci. XLI-B8, 175–178. https://doi.org/10.5194/isprsarchives-XLI-B8-175-2016

UNDP, 2004. Bureau for Crisis Prevention and Recovery (Bcpr) 2004 Report : Thematic Trust Fund for Crisis Prevention and Recovery United Nations Development Programme. Bur. Cris. Prev. Recover.

Yao, Z., Nagel, C., Kunde, F., Hudra, G., Willkomm, P., Donaubauer, A., Adolphi, T., Kolbe, T.H., 2018. 3DCityDB - a 3D Geodatabase Solution for the Management, Analysis, and Visualization of Semantic 3D City Models Based on CityGML. Open Geospatial Data, Softw. Stand. 3. https://doi.org/10.1186/s40965-018-0046-7

Zerboni, A., Perego, A., Mariani, G.S., Brandolini, F., Al Kindi, M., Regattieri, E., Zanchetta, G., Borgi, F., Charpentier, V., Cremaschi, M., 2020. Geomorphology of the Gebel Qara and Coastal Plain of Salalah (Dhofar, Southern Sultanate of Oman). J. Maps 16, 187–198. https://doi.org/10.1080/17445647.2019.1708488

Zlatanova, S., Ghawana, T., Kaur, A., Neuvel, J.M.M., 2014. Integrated Flood Disaster Management and Spatial Information: Case Studies of Netherlands and India. ISPRS - Int. Arch. Photogramm. Remote Sens. Spat. Inf. Sci. XL–8, 147–154. https://doi.org/10.5194/isprsarchives-XL-8-147-2014

International Journal of Engineering and Geosciences

https://dergipark.org.tr/en/pub/ijeg

e-ISSN 2548-0960

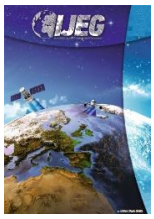

Classification comparison of Landsat-8 and Sentinel-2 data in Google Earth Engine, study case of the city of Kabul

Abdul Baqi Ahady[*1, 2], **Gordana Kaplan** [3]

[1]*Graduate School of Science, Eskisehir Technical University, Eskisehir, Turkey*
[2]*Kabul Polytechnic University, Kabul, Afghanistan*
[3]*Institute of Earth and Space Sciences Institute, Eskisehir Technical University, Eskisehir, Turkey*

Keywords
Classification
Landsat-8
Sentinel-2
Surface Water
Cropland
Urban and Bare land

ABSTRACT

In recent years, Kabul city's rapid urbanization has adversely affected the urban land cover, such as surface water bodies and croplands. Surface water resources are threatened due to overpopulation in the city either qualitatively or quantitatively, also croplands are being lost with the development of urbanization activities through the city. To monitor and assess surface changes accurately, we classified the city area using satellite images of both Landsat-8 and Sentinel-2 and compared both of their findings. The Support Vector Machine classifier was applied to multi-senor data to classify four different land categories using the same training sites and samples with the same period. All the procedures were conducted in Google Earth Engine (GEE) cloud platform. The surface reflectance bands of both satellites were used for classification. Confusion matrixes were created using the same reference points for Sentinel-2 and Landsat-8 classification to compare the results and determine the best approach for classification of land cover. Results show that overall accuracy was 94.26% for Sentinel-2 while it was 85.04% for Landsat-8, similarly, the Kappa coefficient was calculated 91.7% and 78.3% for Sentinel-2 and Landsat-8, respectively.

1. INTRODUCTION

Observation of land changes is an important factor for urban and environmental management. Automatically extracting land coverage and land use information from remote sensing images in a particular region, especially in a big urban area, is not an easy activity (Cai et al., 2019). Moreover, accurate information about the land cover of a region allows for the best possible management, planning and monitoring of natural resources. High temporal frequency Earth Observation (EO) satellites are vital tools to be used (Shang & Zhu, 2019). Land surface changes could be surface water dynamics, forest disturbance, vegetation anomaly, phenology changes and agricultural practice. There are some other satellites with high temporal frequency such as Moderate Resolution Imaging Spectroradiometer (MODIS) (Pagano & Durham, 1993), Medium Resolution Imaging Spectrometer (MERIS) (Verstraete, et al., 1999), and Visible Infrared Imaging Radiometer Suite (VIIRS), which has already been used for classification and land observations and it has been established that they are not suitable for identifying land surface changes that typically occur on a far smaller scale than their pixel sizes (Shang & Zhu, 2019).

On the contrary, moderate resolution satellites, such as Landsat and Sentinel can provide higher special resolution observations with 30 meter and 10-60 meter each respectively (USGS). Also, the temporal resolution for Landsat is lower than the Sentinel, which is not enough for near-real-time observations. For instance, it takes16 days to revisit the same location for Landsat satellite; even with both satellites of Landsat 7 and 8 we can observe the same location in each 8 days, while this period is decreased to 5 days with the new launched Sentinel-2A and 2B. However, the same observations can be made by both the Sentinel and Landsat satellites, varying in field of view, spectral bandwidth, spatial resolution, and spectral response function (Zhang et al., 2018), some corrections can be done using the Bidirectional Reflectance Distribution Function (BRDF)

* **Corresponding Author**

*(ab_ahady@eskisehir.edu.tr) ORCID ID: 0000-0001-5574-1859
(kaplangorde@gmail.com) ORCID ID: 0000-0001-7522-9924

Cite this article

Ahady A B & Kaplan G (2022). Classification comparison of Landsat-8 and Sentinel-2 data in Google Earth Engine, study case of the city of Kabul. International Journal of Engineering and Geosciences, 7(1), 24-31

Research Article / DOI: 10.26833/ijeg.860077

Received: 13/01/2021; Accepted: 01/04/2021

correction method to minimize and overcome this discrepancy (Shang & Zhu, 2019).

Finding access to cloud-free, high-quality and high-resolution images over a large region for land-changing observations and land classification has been challenging and resource-intensive. To some extent, these challenges have been overcome through a recent development in remote sensing data collection, management and processing. For example, managing large volumes of satellite data for analysis over a large region is a major challenge when implementing typical remote sensing methods that use commercial image processing software on PC-based workstation systems. No matter how strong and powerful these systems are, the procedure takes a lot of time and is cumbersome, slow, and tedious. Fortunately, these limitations have been overcome by a powerful geo data processing platform of Google Earth Engine (GEE) developed with planetary-scale geospatial analysis (Ghorbanian et al., 2020). GEE is an ideal data organization platform that enables geospatial processing over a large region and comprehensive resources and computational capabilities (Teluguntla et al., 2018). Having all these capabilities, using GEE can reduce most of the time-consuming procedures required for traditional remote sensing approaches. Recently, several studies have been carried out using the GEE platform for various research topics in remote sensing (Kaplan & Aghlmand, 2020; Mobariz & Kaplan 2020; Mutanga & Kumar, 2019; Pu et al., 2020; Stromann, et al., 2020; Xiong et al., 2017).

Thereby, this study's main goal is to classify the city of Kabul, one of the rapid development cities in the world, into four classes; Water, Cropland, Urban, and Bare land. using Landsat-8 and Sentinel-2 data and to compare the results. Kabul city is the capital of Afghanistan, the city with an upward trend in urbanization evolution during the recent years. Surface water is one of the important resources for tourism and urbanization, which is seriously affected by constructional activities and the indiscriminate use of water resources by the residents. Moreover, we intend to analyze and compare the results of the classification and accuracy of the Sentinel-2 and Landsat-8 moderate resolution satellites using the same training sites and samples with the same timeframe for each image. To do the accuracy assessment of each satellite image, overall validation accuracy and kappa statistic coefficients are calculated and compared. Similarly, the area covered by each class is calculated and compared.

2. DATA AND METHODS

2.1. STUDY AREA

This study is carried out over the city of Kabul; the capital city of Afghanistan, which ranges from longitude 68^0 57’ 00” E to 69^0 28’ 15’’ E and latitudes 34^0 16’ 15’’ N to 34^0 40’ 00’’ N (Figure 1). Kabul is not only one of the largest cities in Afghanistan in terms of population, but one of the largest in the world, ranking 64th. From the perspective of rapid urbanization, the city was ranked 5th in the world (The Guardian, 2014). Kabul city has the total area of 1023 square kilometers and 4.22 million population estimated in 2020 with population density of 4500 persons per square kilometer (World Population Review, 2020).

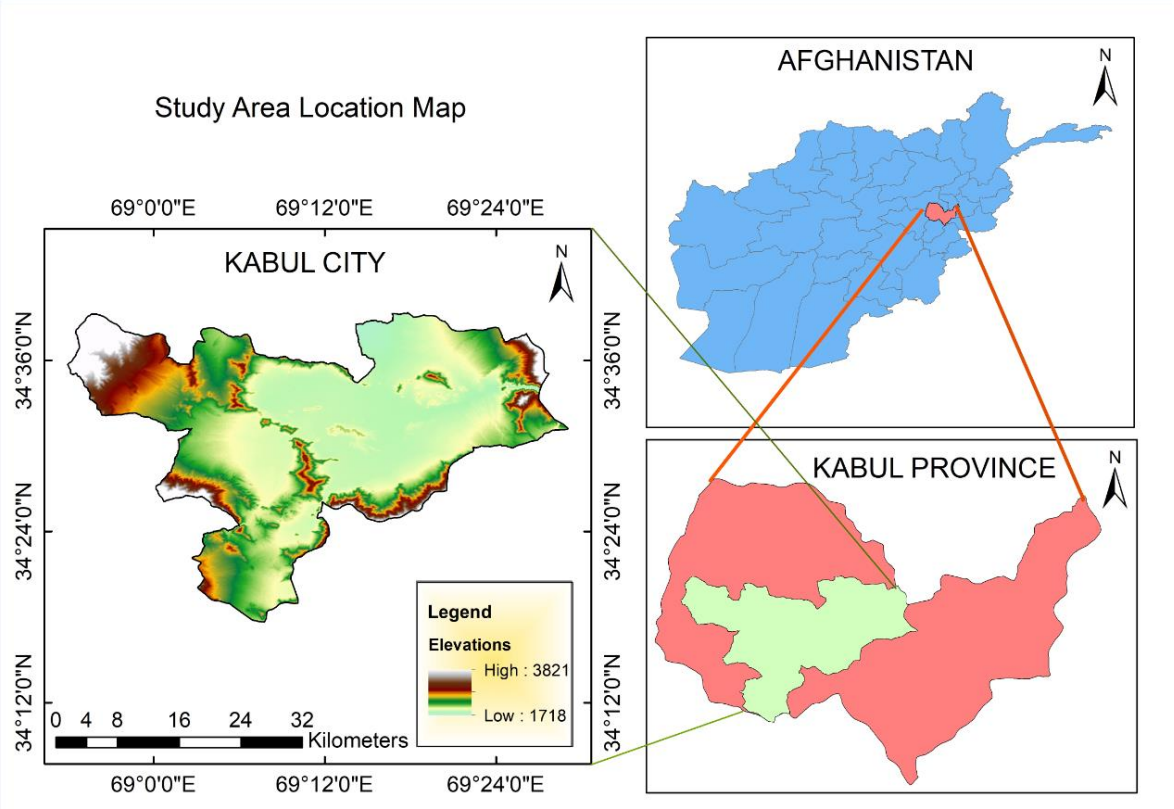

Figure 1. Location of study area, DEM of Kabul city

Kabul is a city with cold semi-arid climate, with precipitation concentrated in winter (almost exclusively falling as snow) (Köppen climate classification BSk) and spring months, with low humidity in summer. The lowest temperature is -6 ^{0}C in January and the highest is 33 ^{0}C in July through the year with the maximum 14.5 hours of sunshine in June (Figure 2). Kabul has an average of 312 mm of rainfall per year, or 26 mm on a monthly basis, where the maximum rainfall is 71.9 mm in April and the lowest rainfall is approximately 1 mm in June, as shown in (Figure 3) (World Climate & Temperature, 2017).

The study area contains of four major classes; water, cropland, urban and bare land. Available surface water in Kabul city consists of Kabul River flows from west to east through the city, a large lake and wetland Kol-e Hashmat Khan protected area located just to the southeast from the city where some rare species of birds have been spotted, and Qargha reservoir located in northwest of the city a major attractive place for locals and foreigners for tourism. The altitude ranges from 1718m to 3821m above mean sea level. From March to June, the Kabul River's water level is at its peak when the snow; from the Paghman snow-capped mountains in the west of Kabul, melts and joins the river.

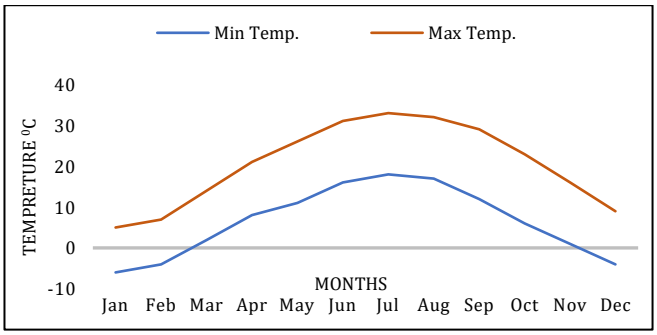

Figure 2. Temperature of Kabul city (Source: National Oceanic and Atmospheric Administration (NOAA)).

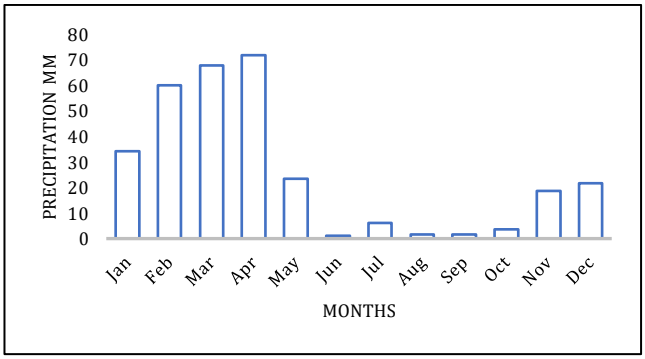

Figure 3. Precipitation in Kabul city (Source: (NOAA)).

2.2. Data

Image collections, a set of images from Sentinel-2 and Landsat-8 were used in this study. Furthermore, the image collection was combined into one image used for classification. The Sentinel-2 image collection was used to generate the satellite image of Sentinel-2 for Kabul city using GEE cloud platform (Figure 4). Sentinel-2 is a wide-swath, high-resolution, multi-spectral imaging mission funded by the European Union/ESA/Copernicus, supporting Copernicus Land Monitoring studies, covering vegetation, soil and water cover monitoring and observation of inland waterways and coastal areas. The data for Sentinel-2 L2 is downloaded from the scihub. The assets include 12 spectral bands of UINT16 that reflect SR scaled by 10000 (unlike in L1 data, there is no B10).

Figure 4. Sentinel-2 satellite image of Kabul city generated on Apr-June 2020.

The Landsat 8 satellite for the study area was also generated using the GEE cloud platform (Figure 5). This dataset is the atmospherically corrected surface reflectance from the Landsat 8 OLI/TIRS sensors provided by USGS since 2013-04-11. These satellite images have five visible and near-infrared (VNIR) bands, two short-wave infrared (SWIR) bands processed to orthorectified surface reflectance, with remaining two thermal infrared (TIR) bands processed to orthorectified brightness temperature. These data have been corrected atmospherically with Land Surface Reflectance Code (LaSRC) and contain a C code based on the Function of Mask (CFMASK) produced Cloud, shadow, water and snow mask and a per-pixel saturation mask. Strips of data collected are clustered in overlapping "scenes" measuring approximately 170 km x 183 km using a standardized reference grid.

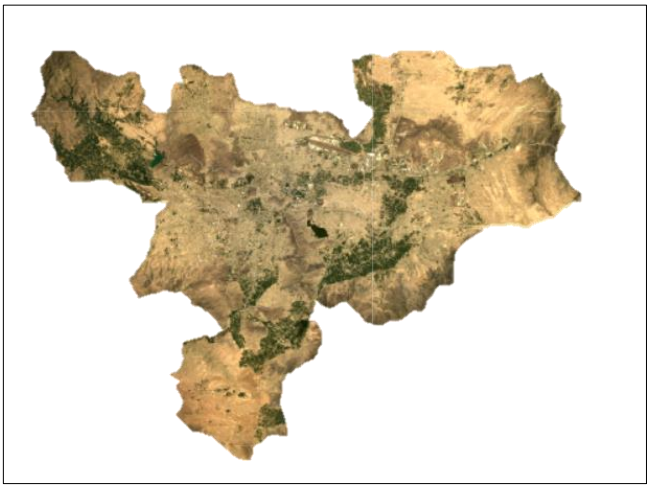

Figure 5. Landsat-8 satellite image of Kabul city generated on Apr-June 2020.

The main visible and near-infrared Sentinel-2A bands' spatial resolution is 10 meters, whilst the "red-

edge" (red and near-infrared bands) and two shortwave infrared bands have a spatial resolution of 20 meters. The spatial resolution of the coastal / aerosol, water vapor, and cirrus bands is 60 meters for Sentinel-2A.

The multispectral data recorded by each of the sensors has similar wavelength ranges (Table 1). The related characteristics of Sentinel-2 sensors to Landsat and shortened revisit time are now utilizing the combined multispectral observation capacity of three platforms observing the surface of the Earth at a resolution of 10-30 m, greatly expanding the ability to capture cloud-free observations at high latitudes (Runge & Grosse, 2019). In order to see the influence of the different spatial resolution of the images, no pan sharpening methods have been applied to the Landsat-8 imagery.

Table 1. Corresponding Landsat-8 and Sentinel-2 bands and characteristics

Landsat-8			Sentinel-2		
Bands	Pixel size (m)	Wavelength (µm)	Bands	Pixel size (m)	Wavelength (nm) (S2A)/ (S2B)
B1- Coastal	30	0.435-0.451	B1 - Coastal	60	443.9 / 442.3
B2 - Blue	30	0.452-0.512	B2 - Blue	10	496.6 / 492.1
B3 - Green	30	0.533-0.590	B3 - Green	10	560 / 559
B4 - Red	30	0.636-0.673	B4 - Red	10	664.5 / 665
B5 - NIR	30	0.851-0.879	B5 - Vegetation Red Edge	20	703.9 / 703.8
B6 - SWIR 1	30	1.566-1.651	B6 - Vegetation Red Edge	20	740.2 / 739.1
B7 - SWIR 2	30	2.107-2.294	B7 - Vegetation Red Edge	20	782.5 / 779.7
B8 - Pan	15		B8 - NIR	10	835.1 / 833
			B8A - Narrow NIR	20	864.8 / 864
B9 - Cirrus	30	10.60-11.19	B9 - Water Vapour	60	945 / 943.2
B10 - TIRS 1	30(100)		B10 - SWIR-Cirrus		
B11 - TIRS 2	30(100)	11.50-12.51	B11 - SWIR	20	1613.7 / 1610.4
			B12 - SWIR	20	2202.4 / 2185.7

Source: Earth Observing System (https://eos.com/sentinel-2/)

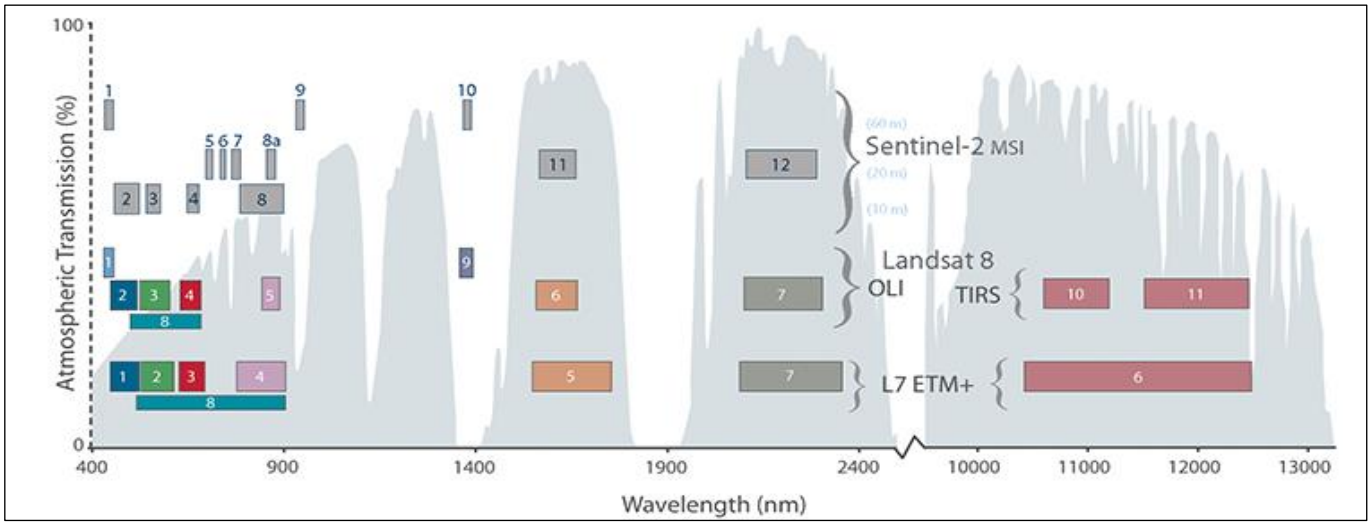

Figure 6. Comparison of Landsat 7 and 8 bands with Sentinel-2. (Source: USGS)

Spectral bands for both the images (Sentinel-2A and Landsat-8) are very similar except for Landsat 8's Thermal Infrared Sensor's thermal bands. According to Landsat 7 and 8 bands, the unique placement of Sentinel-2A bands can be seen in Figure 6 (USGS).

2.3. Methods

GEE is an on-scale cloud data analysis tool, powered by Google Cloud Platform to conduct geospatial data analysis. GEE offers an open forum for the development of geo-spatial algorithms, also GEE is designed to hold and process massive data sets (at petabyte-scale) for analysis and final decision making (Mutanga & Kumar, 2019). A user-friendly and easily accessible platform provides a convenient environment for the development of interactive data and algorithms.

The framework for mapping of Kabul city classification in this paper is shown in Figure 7. First, we extracted Sentinel-2 and Landsat-8 images in GEE platform. Then the images were filtered for boundaries, date and cloud, as a boundary filter we considered shapefile of Kabul city for clipping the images. The surface reflectance bands of both satellites were combined by Product stacking. After that, training site and sampling procedure was done. Afterwards, the LIBSVM (Library Supported Vector Machine) classifier method was used for classification of the study area. LIBSVM is an integrated software for support vector classification that supports multi-class classification. At the end, accuracy assessment was done and compared for both the images.

Sentinel-2 and Landsat-8 satellite images were imported in GEE platform for the study area and were clipped with Kabul city's shapefile. Both the images were

filtered by date from April to July 2020 and were used to classify the study area. To get the best result of the work, the imported images were then filtered to mask clouds' images. Masking clouds and cloud shadows in Sentinel-2 surface reflectance (SR) data was done using Earth Engine. The Sentinel-2 image was filter for clouds with the metaData CLOUD_PIXEL_PERCENTAGE, for cloud pixel percentage of 10%. In case of Landsat-8, the metadata CLOUD_COVER of 10% was applied to mask the clouds.

Eleven Sentinel-2 bands (Blue, Green, Red, Red-Edge 1, Red-Edge 2, Red-Edge 3, NIR, Red-Edge 4, Water vapor, SWIR 1, SWIR 2) and six Landsat bands (Blue, Green, Red, Near Infrared, ShorthWave Infrared-1, ShorthWave Infrared-2), were used for the classification.

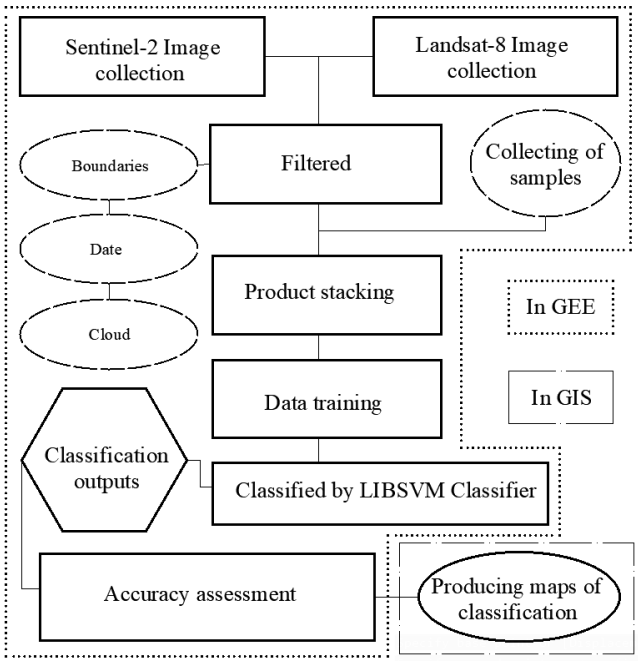

Figure 7. Flow chart of the overall procedure

In this paper, supervised classification for land cover classification was used. For both the images the same number of sample points with same position have been used which were collected for all four classes of (Water, Cropland, Urban and Bare land) Table 2. The sample training was done over the both the images with validation over high resolution imagery of satellite. The LIBSVM (Library Supported Vector Machine) _classifier was used for the classification. For both of the images, overall accuracy and kappa have been calculated.

Table 2. Training and sample points

Class	Sample points
Water	19
Cropland	83
Urban	70
Bare land	89

2.4. Accuracy Assessment

Accuracy assessment has been recognized one of the most important steps at classification process. The accuracy assessment aims to evaluate the effectiveness of sampling pixels in the right land cover groups (Rwanga & Ndambuki, 2017). Several methods have been used to assess the thematic accuracy of land cover classification. The confusion matrix helps us to measure the Overall Accuracy, User's accuracy, Producer's accuracy and Kappa coefficient. Overall accuracy shows the percentage of correctly mapped reference sites and is equal to number of correctly classified site per total number of reference sites. A statistical test is used to determine the accuracy of a classification to generate the Kappa Coefficient. Kappa basically examines how well the classification was carried out compared to just random assigning values (Humboldt State Geospatial Online, 2019).

3. Results and Discussion

The results obtained after running the Google Earth Engine platform code editor are shown in Figure 8 for Sentinel-2 and Figure 9 for Landsat-8. The results obtained from the classification of Kabul city on the Google Earth Engine platform clearly show that all four classes of water bodies, cropland, urban and bare land in the study area were successfully extracted, but it is also a fact that the system could not eliminate most of the misleading information in both Sentinel-2 and Landsat-8 cases. Some urban parts were misleadingly classified as water, possible building shadows, dark objects and asphalt with the Sentinel-2 image, and some parts of croplands appear to be classified as water with Sentinel-2 because the images were filtered by April to July dates; the time of irrigation of the croplands "Figure 10e".

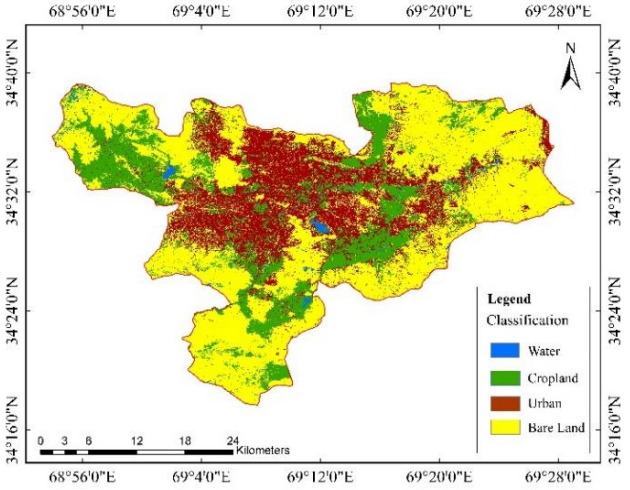

Figure 8. Sentinel-2 image classification Apr-July 2020

However, in the case of Landsat-8, there are some parts of the urban and cropland zone that are misleadingly classified as water bodies, but the number of such water bodies is less than that for Sentinel-2 Figure 10e and 10f. Some parts of Kabul River were missing and were not classified as water Figure 10f with Landsat-8, while those parts were purely classified as water with Sentinel-2 Figure 10e. The total area classified as water for Landsat-8, approximately 50 percent less than that of Sentinel-2.

In general, we can divide the water bodies into two categories in Kabul city, the water bodies which are permanently available such as Qargha Lake and Kabul River, and the temporarily available water bodies such as cropland irrigation areas.

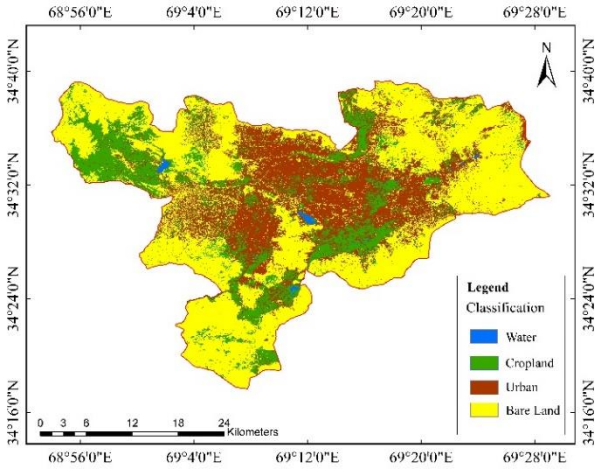

Figure 9. Landsat-8 image classification Apr-July 2020

Most of Kabul city's western and southern parts have been classified as cropland with both Sentinel-2 and Landsat-8 Figure 8 and 9, although there is less cropland in the northern and eastern parts of the city, the main reason is that high mountains occupy the area. For cropland region, both the cases could classify it well at all, but some misleading information were there with Landsat-8 image which could not classify the cropland and trees within the urban area Figure 10a and 10b, while it was well classified with Sentinel-2. This could be why the cropland area classified with Sentinel-2 is 233.5 square kilometers while it was 199.6 square kilometers in case of Landsat-8; approximately 15% less than that of Sentinal-2.

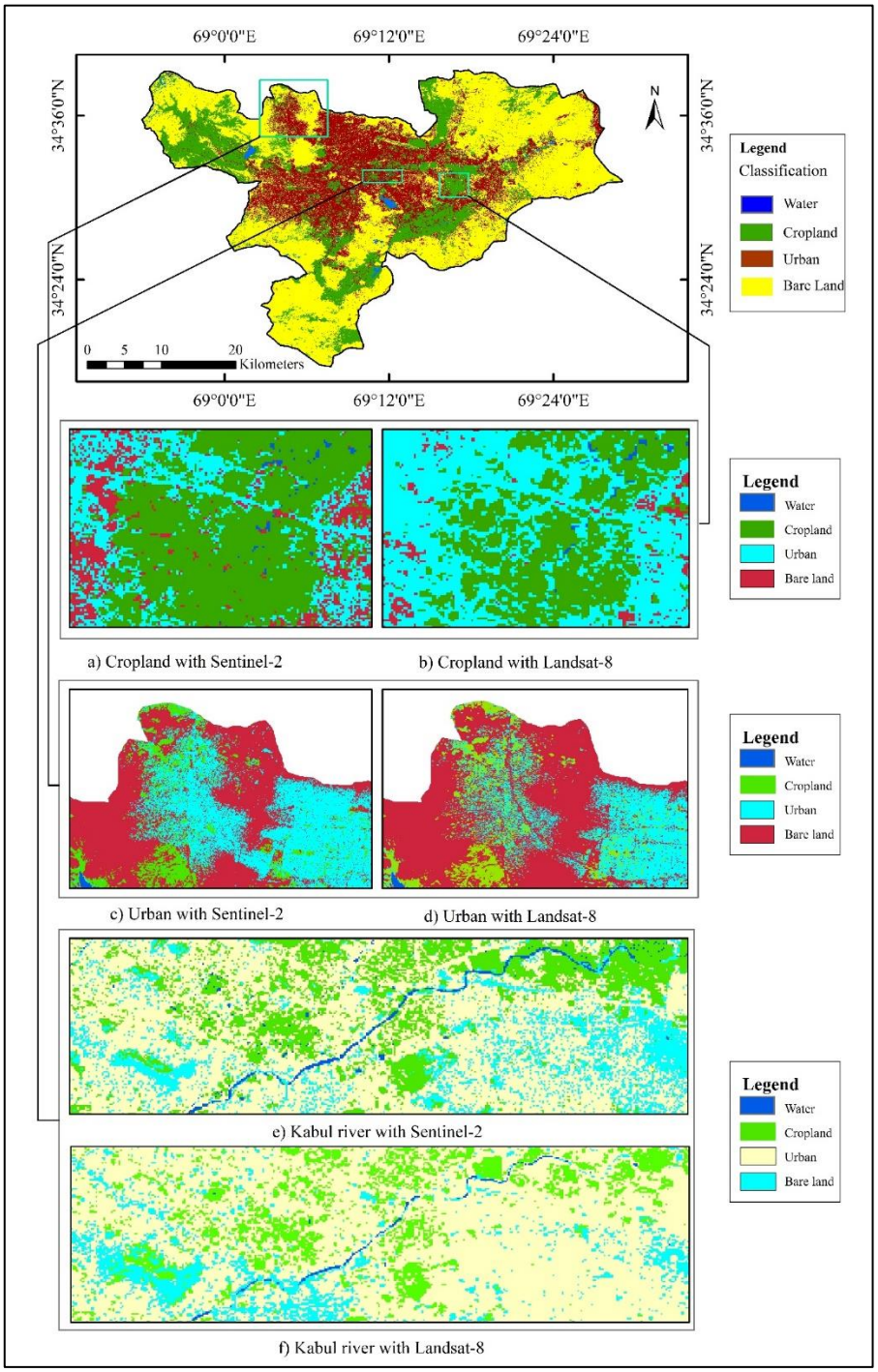

Figure 10. Detailed map of Classification of Kabul city

In case of urban region, the central and mostly flat part of the city is classified as urban area with both the images "Figure 8 and 9", and it is the second large class in terms of area in the city. Some parts of residential area were misleadingly classified as bare land with Landsat-8, while the results were most accurate with Sentinel-2 Figure 10c and 10d. The area classified as urban was 236.4 square kilometers for Sentinel-2 and it was 285.3 square kilometers for Landsat-8; higher by about 17% than that of Sentinel-2.

The bare land class in Kabul city is the largest class in terms of the area, containing deserts and mountainous areas surrounding the city's urban region. In bare land region, some parts of bare land were classified as urban in the eastern of the study area with both images. The bare land class area was calculated with a slight difference of 3.2 square kilometers, 550.7 square kilometers for Sentinel-2 and 547.5 square kilometers for Landsat-8, which show the best result for both images.

Classification outputs are compared only using the surface reflectance of spectral bands of Seninel-2 and Landsat-8 datasets and produce average validation overall accuracy of 93% and 85% respectively. The Classifier package with traditional ML algorithms in GEE platform was used to assess both the experiments' accuracy for classification of Kabul city with Sentinel-2 and Landsat-8. Based on the information from confusion matrix, the overall accuracy of the identification of all four classes with Sentinel-2 and Landsat-8 are 93.3% and 85% respectively, the Kappa coefficients are calculated 90% for Sentinel-2 and 78.3% for Landsat-8 Table 3.

Table 3. Confusion matric and accuracy evaluation for the classification of Kabul city map based on Sentinel-2 and Landsat-8

	Sentinel-2						Landsat-8					
Classes	Water	Cropland	Urban	Bare land	Total points	User accuracy (%)	Water	Cropland	Urban	Bare land	Total points	User accuracy (%)
Water	8	1	0	0	9	88.89	8	1	0	0	9	88.89
Cropland	0	37	0	1	38	97.37	1	33	4	2	40	82.5
Urban	0	0	26	4	30	86.67	0	2	21	3	26	80.77
Bare land	0	1	0	44	45	97.78	0	1	5	46	52	88.46
Validation overall accuracy						**94.26**	**Validation overall accuracy**					**85.04**
Kappa						**91.7**	**Kappa**					**78.3**

From the confusion matric shown above, water appears to have been classified with the same user accuracy of 88.9% with both Landsat-8 and Sentinel-2 images, while Sentinel-2 did better with 97.37% user accuracy in the case of cropland than Landsat-8 with 82.5%. In the same way, two remaining classes of urban and bare land were classified with higher user accuracy of each 86.67% and 97.78% respectively in Sentinel-2 image, while they were classified with lower accuracy of 80.77% for urban and 88.46% for bare land in case of Landsat-8 image. Similarly, for each urban and bare land classes with Seninel-2, the user accuracy was calculated 86.67% and 97.78% with a better result, whereas, urban was classified with 80.77% and bare land was classified with 88.46% in case of Landsat-8 image.

Similar studies also showed that Sentinel-2 preforms better than Landsat-8. Thus, Korhonen et al. (2017) compared the two sensors for estimation of boreal forest canopy cover and leaf area index. They have concluded that the better performance of Sentinel-2 may be related to the red-edge-vegetation bands, as their investigation of the mutual bands of the two sensors did not show any significant difference. On the other hand, in a comparison of the two sensors for assessing burn severity (García-Llamas et al., 2019), Sentinel-2 also showed better results, however, this performance was linked with the better spatial resolution of the sensor. Comparison for detection and mapping of soil salinity (Wang et al., 2020) also showed better results for Sentinel-2, where according to the authors, the higher temporal resolution of the sensor played curtail in the performance. Our study is another example of the better performance of Sentinel-2 in comparison with Landsat-8, using GEE.

4. CONCLUSION

Images from the Landsat-8 and sentinel-2 sensors were compared for classification of four classes each; Water, Cropland, Urban and Bare land in Kabul city to see which one present more accurate results. To compare the results, we considered the same interval of date, same training of samples, same number of points picked up for each class, and the same percentage of cloud masking for each image. Despite the overall good results gained from both of the sensors, there were slight differences between the results obtained from both images that can be linked to several parameters, including poor masking of the cloud, cloud shadow, and mixed pixels. The results earned from both the images were effective in their own area for instance, in water extraction maybe Sentinel-2 has some misleading information, but in urban area and agricultural part the Landsat was not good enough to classify it. The assessment was done based on the use of cloud platform of GEE; which could be the best option for future studies such extraction of a specific land cover class in the study area. Given that the results show that Sentinel-2 image with overall accuracy of 94.26% is more accurate than the Landsat-8 with an overall accuracy of 85.04% for classification of the study area, we

recommend the Sentinel-2 satellite image for conducting such kind of studies. Since our results were in line with the studies done before, we acknowledge that the GEE cloud platform is a useful and valuable tool for such comparison studies. For future studies, we recommend investigating the changes over a period of time and doing cross-comparison between Sentinel-2 and Landsat-8.

Author contributions

Abdul Baqi Ahady: Conceptualization, Methodology, Software, Data curation, Writing-Original draft preparation, Validation. **Gordana Kaplan:** Visualization, Investigation, Writing-Reviewing and Editing.

Conflicts of interest

The authors declare no conflicts of interest.

REFERENCES

Cai G, Ren H, Yang L, Zhang N, Du M & Wu C (2019). Detailed urban land use land cover classification at the metropolitan scale using a three-layer classification scheme. Sensors, 19(14), 3120.

García-Llamas P, Suárez-Seoane S, Fernández-Guisuraga J M, Fernández-García V, Fernández-Manso A, Quintano C, Calvo L (2019). Evaluation and comparison of Landsat 8, Sentinel-2 and Deimos-1 remote sensing indices for assessing burn severity in Mediterranean fire-prone ecosystems. International Journal of Applied Earth Observation and Geoinformation, 80, 137-144.

Ghorbanian A, Kakooei M, Amani M, Mahdavi S, Mohammadzadeh A & Hasanlou M (2020). Improved land cover map of Iran using Sentinel imagery within Google Earth Engine and a novel automatic workflow for land cover classification using migrated training samples. ISPRS Journal of Photogrammetry and Remote Sensing, 167, 276-288.

Humboldt State Geospatial Online. (2019). Accuracy Metrics Retrieved from http://gis.humboldt.edu/

Kaplan G & Aghlmand M (2020). Integration of Sentinel-1 and Sentinel-2 for Classification of Small Urban Areas in Rural Landscape aided by Google Earth Engine.

Korhonen L, Packalen P & Rautiainen M (2017). Comparison of Sentinel-2 and Landsat 8 in the estimation of boreal forest canopy cover and leaf area index. Remote sensing of Environment, 195, 259-274.

Mobariz M A & Kaplan G (2020) Monitoring Amu Darya River Channel Dynamics using Remote Sensing Data in Google Earth Engine.

Mutanga O & Kumar L (2019). Google Earth Engine Applications. In: Multidisciplinary Digital Publishing Institute.

Pagano T S & Durham R M (1993). Moderate resolution imaging spectroradiometer (MODIS). Paper presented at the Sensor Systems for the Early Earth Observing System Platforms.

Pu D, Sun J, Ding Q, Zheng Q, Li T & Niu X (2020). Mapping Urban Areas Using Dense Time Series of Landsat Images and Google Earth Engine. The International Archives of Photogrammetry, Remote Sensing and Spatial Information Sciences, 42, 403-409.

Runge A & Grosse G (2019). Comparing Spectral Characteristics of Landsat-8 and Sentinel-2 Same-Day Data for Arctic-Boreal Regions. Remote Sensing, 11(14), 1730.

Rwanga S S & Ndambuki J M (2017). Accuracy assessment of land use/land cover classification using remote sensing and GIS. International Journal of Geosciences, 8(04), 611.

Shang R & Zhu Z (2019). Harmonizing Landsat 8 and Sentinel-2: A time-series-based reflectance adjustment approach. Remote Sensing of Environment, 235, 111439.

Stromann O, Nascetti A, Yousif O & Ban Y (2020). Dimensionality Reduction and Feature Selection for Object-Based Land Cover Classification based on Sentinel-1 and Sentinel-2 Time Series Using Google Earth Engine. Remote Sensing, 12(1), 76.

Teluguntla P, Thenkabail P S, Oliphant A, Xiong J, Gumma M K, Congalton R G, . . . Huete A (2018). A 30-m landsat-derived cropland extent product of Australia and China using random forest machine learning algorithm on Google Earth Engine cloud computing platform. ISPRS Journal of Photogrammetry and Remote Sensing, 144, 325-340.

The Guardian. (2014). Kabul City Growth. Retrieved from https://www.theguardian.com/international

USGS. Comparison of Sentinel-2 and Landsat. Retrieved from https://www.usgs.gov/

Verstraete M M, Pinty B & Curran P J (1999). MERIS potential for land applications. International Journal of Remote Sensing, 20(9), 1747-1756.

World Climate & Temperature. (2017, 2021). Kabul Climate & Temperature. Retrieved from http://www.kabul.climatemps.com/

World Population Review. (2020). Kabul Population in 2020. Retrieved from https://worldpopulationreview.com/

Xiong J, Thenkabail P S, Tilton J C, Gumma M K, Teluguntla P, Oliphant A, . . . Gorelick N (2017). Nominal 30-m cropland extent map of continental Africa by integrating pixel-based and object-based algorithms using Sentinel-2 and Landsat-8 data on Google Earth Engine. Remote Sensing, 9(10), 1065.

Wang J, Ding J, Yu D, Teng D, He B, Chen X, . . . Yang X (2020). Machine learning-based detection of soil salinity in an arid desert region, Northwest China: A comparison between Landsat-8 OLI and Sentinel-2 MSI. Science of the Total Environment, 707, 136092.

Zhang H K, Roy D P, Yan L, Li Z, Huang H, Vermote E, . . . Roger J C (2018). Characterization of Sentinel-2A and Landsat-8 top of atmosphere, surface, and nadir BRDF adjusted reflectance and NDVI differences. Remote Sensing of Environment, 215, 482-494.

International Journal of Engineering and Geosciences

https://dergipark.org.tr/en/pub/ijeg

e-ISSN 2548-0960

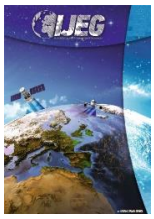

Multivariate statistical analysis application to determine factors affecting the parcel value to be used mass real estate valuation approaches

Sukran Yalpir*[1], Fatma Bunyan Unel[2]

[1]*Konya Technical University, Faculty of Engineering, Department of Geomatics Engineering, Konya, Turkey*
[2]*Mersin University, Engineering Faculty, Department of Geomatics Engineering, Mersin, Turkey*

Keywords
Criteria
Factor Analysis
Mass Appraisal
Parcel Value
Real Estate Valuation

ABSTRACT

Real estate is a form of immovable asset that enables individuals to exert their property rights and provides a form of material guarantee through its economic value. The economic value of real estate, which is reflected in the price, is an aspect that all countries emphasize today by identifying purchase and sale values in market conditions that are removed from large project rumors and speculations. The more the real estate market value is removed from reality, the more negative its effect will be on the cost-benefit of real estate management. This study aimed to identify the main criteria that affect parcel value, which constitutes a basis for real estate, narrow them down to the optimum level using questionnaires and standardize them. A total of 559 experts working in real estate valuation and 1,915 members of the public that play a role in real estate purchases and sales were contacted in Ankara, Konya and Kayseri, all of which are located in the Central Anatolia Region of Turkey. The factor analysis method was applied to the survey data. Grouping was carried out with 10 factors and the results were interpreted.

1. INTRODUCTION

Real estate valuation is important for both countries and people as it can change the economic course. Cities around the world are growing in accordance with their increasing population and requirements, making the knowledge regarding real estate management even more important. In order to effectively use real estate and carry out planning, project designing and investment decisions properly, the value of real estate should be covered in real estate management. A stable economy is only possible if real estate values are distributed normally and transparently, without giving rise to any kind of unearned income or speculation. Real estate can only provide a large contribution to national economies under these conditions. When identified correctly and truthfully real estate values can transparently contribute to the economy taxation, expropriation, privatization, assurance, land registry and cadastre fees, land readjustment and urban transformation.

Real estate valuation is the independent, impartial and objective projection of a real estate, the rights related to real estate and the responsibilities and restraints as described on its valuation day. The calculation of monetary reserves under real estate valuation is a difficult and complicated task (Açlar and Çağdaş, 2008).

Traditional methods such as comparison with equals, income and cost method, are sufficient for the calculation of a property's value. However, such methods are insufficient when valuing more than one property, also known as mass valuation. In implementations such as the taxing of real estate where mass valuation is in question, advanced methods including fuzzy logic, artificial intelligence, specialized systems, genetic algorithm, artificial neural nets and regression, hedonic and statistical methods, must be implemented in order to create mathematic model(s). Economic models in real estate often explicitly consider the effect of location (Pace et al., 1998). Thus, in order to obtain a mathematic model, criteria affecting the real estate value must be known. As the criteria are high in number and vary according to the regions in which people live in and their lifestyles they affect the model that is created for mass valuation. In other words, there are no standard optimum criteria to create a mathematic model. It is important to use the criteria and the most suitable methods in the most successful way and at an optimum level to obtain mass valuation.

* **Corresponding Author**

*(syalpir@ktun.edu.tr) ORCID ID 0000 – 0001 – 9366 – 5770
(fatmabunel@mersin.edu.tr) ORCID ID 0000 – 0002 – 9949 – 640X

Research Article / DOI: 10.26833/ijeg.862563

Cite this article

Yalpir Ş & Unel F B (2022). Multivariate statistical analysis application to determine factors affecting the parcel value to be used mass real estate valuation approaches. International Journal of Engineering and Geosciences, 7(1), 32-42

Received: 16/01/2021; Accepted: 09/03/2021

The aim of this study was to identify the minimum optimum criteria that affect plot value/parcel value by considering improved parcel that have been prepared for the construction of housing as a result of the implementation of a zoning plan, as the real estate types. As a result of the literature review, all criteria were listed, the legal, physical, locational, and neighbourhood features were grouped as the main topics and questionnaires were prepared. Data was collected from Ankara, Konya, and Kayseri, all of which are located in Central Anatolia, according to sample numbers by using face-to-face questionnaires.

1.1. Real estate

Real estate is a group of assets that is positionally stable. The subjects under real estate property can be listed as land, independent sections, and independent and constant rights. Independent and constant rights (right of building, right of fund) are servitudes that can be applied to the deed for 30 years (Turkish Civil Code, No 4721, Article 704). Independent sections are real estate that independent property rights can be applied to in a deed, can be used separately, and by themselves in sections such as a floor, apartment, employment department, shop, store and warehouse of a completed building (Property Ownership Law, No 634, Article 1). In order to construct these buildings, plots, whose cadastral parcels have been regulated in accordance with the zoning law, zoning plan and legislation principles, are required (Zoning Law No 3194, Article 5).

Land is defined as the terrain that is under the effects of soil, climate, topography, main material, hydrology, and all living creatures at varying rates and usually includes agricultural real estate such as, fields, vineyards and gardens (Law on Soil Protection and Land, No 5403, Article 3/ç). Furthermore, empty real estate that is in or near a city, has not undergone any zoning readjustment and has not been used can also be defined as land. The major difference between plot and land, both of which have different economic values, is that a plot has undergone zoning readjustments, while land has not. The subject of this study, was plots brought in compliance with home construction in accordance with zoning plans. Plots are a type of real estate that are the building blocks of a city and are created by local management, away from speculations regarding plot value, in order to meet demands and find their economic equivalent under normal conditions.

1.2. Literature review and problem description

The criteria that affect plot value have been identified, evaluated and listed in scientific, institutional, and organizational studies. Scientific studies consist of academic theses, projects and articles conducted at universities. National survey studies on real estate valuation are studies that are carried out with the aim of weighting criteria (Tiryakioğlu and Erdoğan, 2006; Yalpır, 2007; Timur, 2009) and collecting data regarding the house for value estimation (Üçdoğruk, 2001). In addition, model construction and method development processes have also been performed in such studies. In the survey study conducted by Yıldız (2014), the valuation commission was inquired regarding the criteria taken into consideration in real estate tax.

In various studies conducted on a national level criteria were cut down for specific regions using the survey method (Yomralıoğlu, 1993; Nişancı, 2005; Çakır and Sesli, 2013; Unel, 2017) in a way of listing the most important criteria. The employed criteria were generally similar, but differed in order of importance. According to the results of the studies in which the survey method was used, the most important common criteria were determined as basic municipality services, number of licensed floors, view, exit to the street, environment, location of plot in the block, frontage, available space, and the distance to the city center. In addition, it was determined that because the lands were purchased as real estate, the subject of "optimum criteria affecting the plot value" was not handled on a national basis.

Bender et al. (2000) conducted an international survey study on homeowners in Geneva, Zurich and Lugano with eight criteria regarding the environmental quality. They determined that the most important criteria for Zurich and Lugano were distance to the city and quality of view, whereas in Geneva, distance to nature (forest, outdoors, lake, etc.) and level of quietness (lack of traffic, railroads, or airport noises) were the leading criteria. Kryvobokov (2005) conducted a survey study based on 10 location features in Donetsk, Ukraine. A total of 20 people, including valuators, real estate agents, land managers and urban planners were interviewed and the most important criteria which were work place, a popular area, a disturbing location, and the nearest secondary center were determined. In the survey part of the study of Shimizu et al. (2016), house prices were identified by sending questionnaires to those who had purchased a house and evaluations were carried out with housing values in different phases of buyer/seller operations, floor area, age, distance to the nearest station, and travel time to the terminal station criteria.

Institutional studies cover legislation on national and international levels and projects that are carried out by institutions. National legislations cover applications subjects such as taxation, expropriation, privatization, and sales of public lands. The criteria in national legislations were taken into consideration for application. The Real Estate Valuation Pilot Implementation Preparation Survey Study was conducted within the scope of the General Directorate of Land Registry and Cadastre Modernization Project (TKMP, 2008). In the project, 96 criteria were identified as initial list and 37 of them were used for model (Yilmazer and Kocaman, 2020). On an international level, the International Valuation Standards (IVS, 2017), the Uniform Standards of Professional Appraisal Practice (USPAP, 2017), Standards on Mass Appraisal of Real Property (IAAO, 2017), and Guidance on International Mass Appraisal and Related Tax Policy (IAAO, 2014) were reviewed. In addition to the criteria for the legal use of real estate's there are also locational and economic criteria. However, there is no standardization regarding the number of these criteria or their structure.

The criteria used in a valuation project in Bosnia-Herzegovina, consisted of 22 locations, 27 main buildings (field, seismic zone, street width and noise/air pollution),

and 10 independent sections (USAID, 2006). The United Nations Economic Commission for Europe Working Party on Land Administration (UNECE WPLA) conducted surveys in various countries under the name of Land (Real Estate) Mass Valuation Systems for Taxation Purposes between 2000-2001 and Land Administration Systems in 2011 (UNECE WPLA, 2001; 2014). The questionnaires applied within the scope of these studies were about the real estate registration system in particular. There were no questions on the criteria that affected real estate value.

It was reduced to 30 criteria with method of Principal Component Analysis for mass appraisal criteria (Unel and Yalpir, 2017). Criteria of plots were weighted by using AHP method (Unel and Yalpir, 2019a; Bozdağ and Ertunç, 2020); criteria of housing and apartments were employed to prioritize and rank real estate alternatives by methods of the Decision-Making Trial and Evaluation Laboratory (DEMATEL) model and the Grey Relational Analysis (GRA) (Nguyen et al., 2020). Correlation between the dependent variable and the independent variables was measured (Zyga, 2020). It was modelled production and sharing standards and made mass valuation process by developing Geographic Data Infrastructure of non-geographical and geographical criteria (Aydinoglu et al., 2020). In addition, data and maps were disseminated by using open source geospatial software (Mete and Yomralioglu, 2021), updated by valuation method (Miotti and Loch, 2021), reflected location value (Cellmer and Trojanek, 2020).

Organizational studies include reports of appraiser and expert witnesses. The appraiser reports have been prepared for mortgages and credit facilities in loans from banks. The expert witnesses' reports have been regulated expropriation, partition, and inheritance that have been brought to trial. The criteria within the reports were examined, and criteria that were not included, such as servitude, population features and human relations, were added in this study.

Considering the studies in the literature it can be said that there are no optimum level criteria in Turkey or developed countries. It has not been mentioned criteria that have been determined in accordance with the commonly-held and real estate types, standardized and clearly defined. Optimum criteria are main parameters needed for all plot in national. There are many criteria affecting plot value, but which and how many of them to use for mass valuation are not known. Therefore, the study is based on determining the criteria that affect the plot value at the optimum level suitable for use in mass valuation.

The fact that there are not enough studies to create a mass valuation system causes a deficiency and brings about the need to find a solution. According to the literature review, it can be said that studies have mainly been conducted on housing and land and those conducted on plots are very few. However, as there are areas suitable for plots and most of the residential criteria originate from the features and location of these areas it is more suitable if the plot value is determined first.

2. MATERIALS AND METHODS

2.1. Participants and Procedure

As real estate valuation is used in the many areas of social and economic life and is related to many disciplines in respect to implementation, it is of a particular concern to various occupational groups. Therefore, support was received from individuals in occupational groups that work closely with real estate valuation and experienced individuals working in the related public institutions, professional organizations and private sector. The survey questions used in the present study were addressed to valuation experts holding a license granted by the Capital Market Board, people who are assigned as expert witnesses in cases regarding expropriation and elimination of joint ownership, the occupational groups mentioned in the literature (geomatics engineering, real estate and asset valuation, urban and regional planning, agricultural engineering, civil engineering, architecture, economics and administrative sciences, and law) (Erdem, 2018; Ertaş, 2019; Unel and Yalpır, 2019b), as well as contractors and real estate agents. In the survey conducted for citizens, people older than 18 years (Unel, et al., 2017) were preferred among those who applied to the Directorate of Land Registry and Cadastre for real estate purchase and sale.

In April and May 2015, the survey was carried out where experts work. For citizens, it was also made especially in the Directorate of Land Registry and Cadastre where citizens actualize title deed transactions. The survey was applied by asking one by one questions and marking the answers.

There were no standard questionnaires regarding the criteria affecting plot value was. Thus, the criteria used in academic studies, institutional studies, international valuation standards, large scoped projects, and implementations were put in to create a questionnaire. The questionnaires were copied and printed, and the survey application phase took place in two simultaneous stages, as the participants consisted of experts and members of the public. Face-to-face interviews were conducted with the experts in the first stage and with the members of the public in the second stage, with the help of pollsters. The questionnaires took approximately 20 minutes to complete per participant and the entire data consolidation stage was completed within three months. After gathering the survey data, the necessary arrangements were made and the analysis phase was initiated (Figure 1).

2.2. Sample Size

When determining sample size, areas in which groundmass will be measured and their size should be particularly identified. In this study, which was carried out in the Central Anatolia Region of Turkey, features such as density (person/km^2), number of electors, population increase rate, net immigration rate, sales in the certificates of ownership, housing mortgages and zoning implementations were taken into consideration

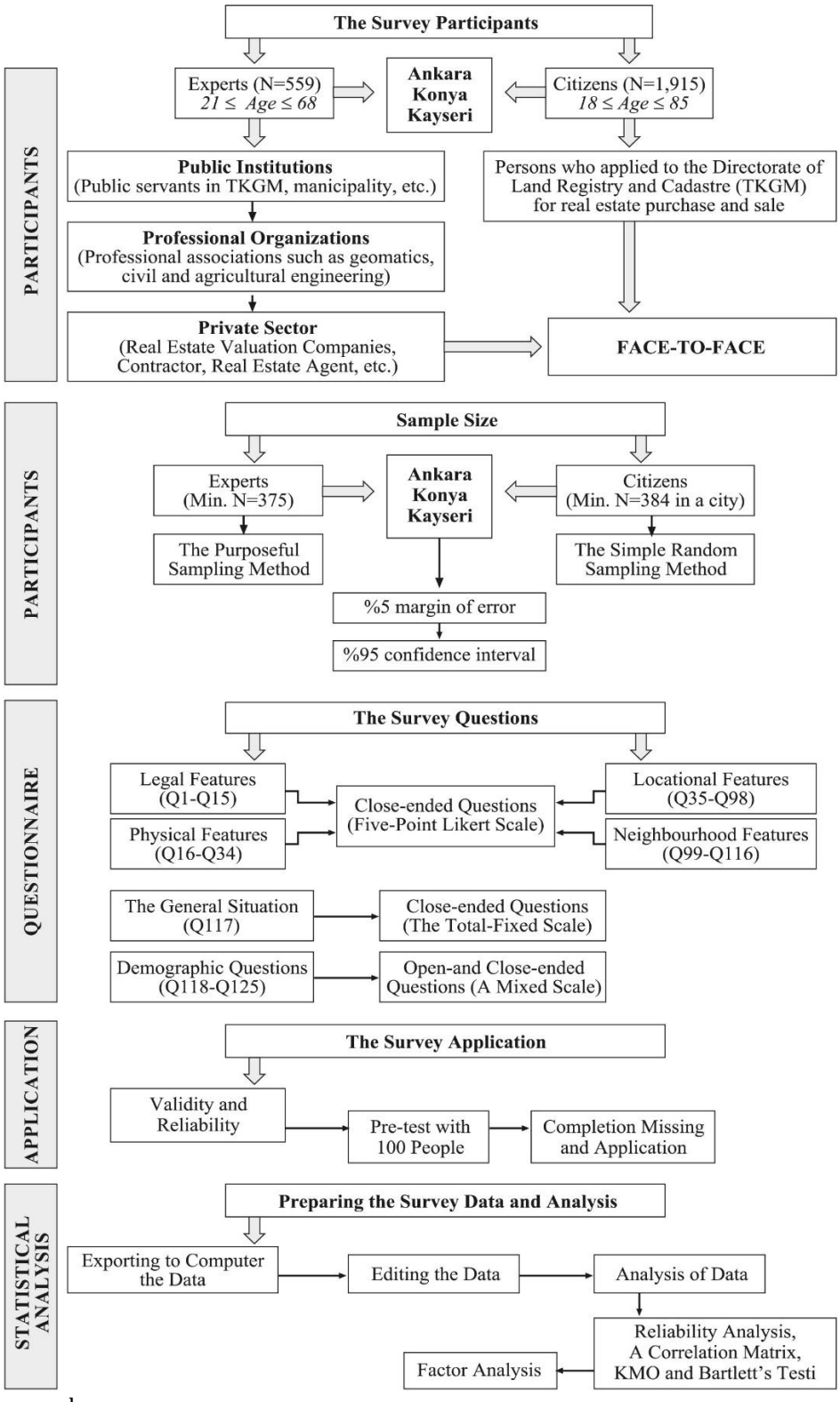

Figure 1. The study procedure

when choosing the cities to represent the region for this study. As a result, Ankara, Konya and Kayseri were determined as the cities to be sampled.

In terms of the sample size, a margin of error of 5% and a 95% confidence interval were identified. Additionally, in terms of the two main participant groups a total of 375 experts and 384 members of the public were determined. The purposeful sampling method was used for the experts, while the simple random sampling method was used for the members of the public. In case of incomplete questionnaires and answers given in the same order, the sampling amounts were planned to be 500 for the experts and 2,000 for the members of the public. As a result, 559 experts and 1,915 members of the public were reached.

2.3. Criteria Affecting Plot Value

Valuation is a technical matter that is affected by many criteria. Although these criteria include the technical data regarding the real estate, social perspective and thoughts of people are also important.

First and foremost, the technical data determines a real estate's value. The point where a buyer's emotions, thoughts, and perspectives are in balance with supply and demand is the value estimation point. Under these conditions and in accordance with objective criteria, the plot value should not be determined according to price, but instead the price should be determined according to the plot value.

Table 1. The survey questions (the subheadings are written in bold and italic) (Yalpir and Unel, 2017).

Ques. NO	Questions	Ques. NO	Questions	Ques. NO	Questions
NO	**A. LEGAL FEATURES**	Q42	Proximity to courses	Q86	Proximity to underdeveloped areas
Q1	***Property Conditions***	***Q43***	***Proximity to Public Institutions***	Q87	Proximity to marsh areas
Q2	Full Ownership	Q44	Proximity to governorships	Q88	Proximity to natural disaster areas
Q3	Shared Ownership	Q45	Proximity to Municipalities	Q89	Proximity to not improved river areas
Q4	***Zoning Status***	Q46	Proximity to Courthouses	***Q90***	***Proximity to Industrial Zones***
Q5	The Gross Floor Area	Q47	Proximity to Jailhouses	***Q91***	***Proximity to Graveyards***
Q6	Total Construction Area	***Q48***	***Proximity to Security Units***	***Q92***	***Proximity to Worship Places***
Q7	The number of floors≥10	Q49	Proximity to Police Stations	***Q93***	***Proximity to Business Centers***
Q8	The number of floors<10	Q50	Proximity to Military Zones	***Q94***	***Proximity to Parking Areas***
Q9	Detached Building	Q51	Proximity to Fire Departments/ 112 Emergency	***Q95***	***The View from the Plot***
Q10	Attached Buildings	***Q52***	***Proximity to Attraction Centers***	Q96	Mountain, valley, etc. views
Q11	***Legal Restraints***	***Q53***	***Proximity to Shopping Centers***	Q97	Lake, river, stream, etc. view
Q12	Right of Mortgage	Q54	Proximity to Hypermarkets	Q98	City view
Q13	Easement	Q55	Proximity to mini-markets	**NO**	**D. NEIGHBOURHOOD FEATURES**
Q14	Annotation of Lease	Q56	Proximity to open/closed bazaars	***Q99***	***Population density***
Q15	***Plot Area***	Q57	Proximity to commercial enterprises	Q100	Education Level
NO	**B. PHYSICAL FEATURES**	***Q58***	***Proximity to Cultural Centers***	Q101	Level of income
Q16	***Location of the plot***	Q59	Proximity to cinemas/theaters	Q102	Immigrant receiving level
Q17	Corner parcel	Q60	Proximity to historical sites and touristic attractions	Q103	Crime Rate
Q18	Intermediate parcel	***Q61***	***Proximity to Entertainment Centers***	Q104	Neighborliness Relations
Q19	***Geometric Structure***	Q62	Proximity to fairs, concert areas, etc.	Q105	Homeowner/tenant
Q20	Length of the Frontage	Q63	Proximity to sport facilities	***Q106***	***The Surrounding Environment***
Q21	Number of the frontage	Q64	Proximity to stadiums/hippodromes	Q107	A popular neighbourhood
Q22	Geometric shape	Q65	Proximity to entertainment venues	Q108	Residential Density
Q23	***Technical Infrastructure Services***	***Q66***	***Proximity to Green Areas***	Q109	Development potential
Q24	Water supply	Q67	Proximity to forest/copses	Q110	Purchasing and selling mobility of real estate
Q25	Electricity, sewer, natural gas, and telephone	Q68	Proximity to recreation areas	***Q111***	***Underground, soil, and aboveground features***
Q26	Solid waste collection service	Q69	Proximity to parks	Q112	Slope of the neighbourhood
Q27	Storm drainage	Q70	Proximity to playgrounds	Q113	Geological conditions
Q28	Unpaved road	***Q71***	***Proximity to Public Transportation Points***	Q114	Climate Conditions
Q29	Asphalt road	Q72	Proximity to airports	Q115	Air Pollution
Q30	***Road Conditions***	Q73	Proximity to railway stations	Q116	Noise Pollution
Q31	The Periphery Road	Q74	Proximity to coach station	**NO**	**E. THE GENERAL SITUATION**
Q32	Road width≥10 m	Q75	Proximity to tramway, subway and metrobus stations	Q117	Scoring features of legal, physical, locational and neighbourhood
Q33	Road width<10 m	Q76	Proximity to bus stops	**NO**	**F. DEMOGRAPHIC QUESTIONS**
Q34	***Slope of the Plot***	Q77	Proximity to shared taxi routes	Q118	Which city do you live in?
NO	**C. LOCATIONAL FEATURES**	Q78	Proximity to underpass/ overpass	Q119	Age

Q35	***Proximity to Health Facilities***	***Q79***	***Proximity to Unsanitary Areas***	Q120	Gender
Q36	Proximity to health center, village clinic, etc.	Q80	Proximity to was disposal areas	Q121	Level of education
Q37	Proximity to State/Private Hospitals	Q81	Proximity to treatment facilities	Q122	Occupation
Q38	***Proximity to Educational Institutions***	Q82	Proximity to natural gas and tube filling facilities	Q123	Your position in the field of real estate valuation
Q39	Proximity to Pre-schools	Q83	Proximity to petrol stations	Q124	How long have you been working in the field of real estate valuation?
Q40	Proximity to High Schools	Q84	Proximity to base stations	Q125	Any other criterion you wish to add
Q41	Proximity to Higher Education Institutions	Q85	Proximity to energy transmission lines		

In this study, all the criteria affecting plot value were listed with the help of the literature by taking the group headings into consideration (Unel, 2017; Unel and Yalpır, 2019b). As a result, an excessive number of criteria was obtained. The criteria changing the value in the economic market were not taken into consideration to simplify and organize the criteria. Similar criteria were reduced to one and unnecessarily detailed criteria were generalized, and in some cases, grouped. Then, the criteria were turned into survey questions using a language that all the participants, experts and members of the public could easily understand. The survey questions were prepared to determine the criteria that was important to participants when valuating plots. The survey questions consist of six sections (A-F) and have the criteria (A-D), the general situation which was total of main headings (E) and demographic questions (F) (Table 1).

The criteria were divided into four categories, namely legal, physical, locational and neighbourhood features, and the survey questions were prepared under these categories. The questions (Q1-Q116) were designed in five-point Likert scale format. The participants were asked to answer the questions as not important at all (1), somewhat important (2), reasonably important (3), important (4) and very important (5). Considering the fact that the criteria either decreased or increased the value, the participants were asked if the criteria had a positive (+) or negative (-) effect on the value. The criteria that made up the survey questions and the other questions are given in Table 1 with the question numbers (Q1, Q2, Q3, …, Q123, Q124 and Q125).

After completing the survey research and preparing the questions, a pre-test was applied to 100 people who were in the sampling group in order to test validity and reliability. The necessary corrections were made according to the results of the pre-test and validity was ensured. The most commonly used reliability test, also known as the reliability analysis (Cronbach), was carried out (Kalaycı, 2010; Altunışık et al., 2010; Baş, 2010; Arıkan, 2013) and an alpha factor of 0.918, which was concluded as reliable, was obtained.

2.4. Statistical Analysis

Factor analysis, which is a multivariate statistical method, enables the categorization and understanding of many variations as limited, significant and independent factors (Biçen, 2010). In an effective factor analysis, the desired property is to have a solution that represents the total data set in the best way, but that also consists of a low number of factors. A good factor analysis result is preferred to be simple and easy to interpret (Altunışık et al., 2010; Biçen, 2010).

Three methods, namely creating a correlation matrix, Bartlett's test, and Kaiser-Mayer-Olkin (KMO) tests, are used to assess whether the data set is suitable for a factor analysis or not (Kalaycı, 2010; Biçen, 2010). After identifying the suitability of the data for factor analysis, the following stages are carried out (Kalaycı, 2010; Altunışık et al., 2010; Alpar, 2013):

(1) Researching data suitability
(2) Mathematical model for factor analysis
(3) Identifying factor amount
(4) Rotating the factors (rotating axis)
(5) Interpreting the factors.

In order to carry out processes with a covariance matrix in the factor analysis, variables with the same units of measure and similar variances are required. However, in the correlation matrix, the variations' units of measure and variances are different. Additionally, unless a unit is not specified, solutions are achieved with the correlation matrix, which is used more frequently in statistical software (Özdamar, 2002; Alpar, 2013).

3. RESULTS

According to the results of the study, out of the 559 expert participants 208 were from Ankara (37.2%), 221 were from Konya (39.5%) and 130 were from Kayseri (23.3%). Fifteen percent of the participants were female, while 85% were male. The minimum age of the participants was 21, the maximum age was 68, and 72.1% of them had a bachelor's degree.

Of the 1,915 members of the public that participated in the study, 546 were from Ankara (28.5%), 942 were from Konya (49.2%) and 427 were from Kayseri (22.3%). Twenty five percent of the participants were female, while 75% were male. The minimum age of the participants was 18, the maximum age was 85, and 48.9% had a bachelor's degree.

3.1. Factor Analysis

The survey data in this study consisted of degrees and had no unit. Thus, the correlation matrix was used for the factor analysis. Before the factor analysis, the correlation matrix was scrutinized and the process was conducted by taking the coefficients that showed the relationship between the criteria into consideration.

Reliability Analysis

Exactly 99.7% of the total 2,474 questionnaires completed by the experts and citizens were determined to be eligible within the scope of the study. Data regarding 116 questions were collected with the questionnaires. In the reliability analysis, it was observed that the survey was highly reliable in accordance with the result of the 0.918 alpha coefficients (Table 2).

Table 2. Case processing summary and reliability statistics

Case Processing Summary

		N	%
Cases	Valid	2,466	99.7
	Excluded[a]	8	.3
	Total	2,474	100.0

a. Listwise deletion based on all variables in the procedure.

Reliability Statistics

Cronbach's Alpha	N of Items
.918	116

Research on Data Suitability

The suitability of 96 questions, excluding the 20 subheadings (Q1, Q4, Q11, Q16, Q19, Q23, Q30, Q35, Q38, Q43, Q48, Q53, Q58, Q61, Q66, Q71, Q79, Q95, Q106, and Q111), were investigated to determine their suitability for the factor analysis. Therefore, the correlation matrix, KMO, and Bartlett tests were examined. Whether the relationships between the criteria were less than 30% was determined by forming a correlation matrix. Five criteria, including Q7, Q28, Q31, Q102, and Q105, which were under 30% in the correlation matrix, were eliminated and were optimized for the factor analysis of the data set.

The KMO test result of 0.937 (Table 3) indicated "perfect" range and that the number of sampling was very good. According to the Bartlett's test, the "significance" value ($p<.05$) indicates that there is a high correlation between the criteria. Accordingly, the factor analysis was carried out according to the results of the KMO and Bartlett tests.

Table 3. KMO and Bartlett's tests

Tests		Result
Kaiser-Meyer-Olkin Measure of Sampling Adequacy.		.937
Bartlett's Test of Sphericity	Approx. Chi-Square	112494.580
	df	4095
	Sig.	.000

a. Based on correlations

Identification of factor amount

The percentage rates of the eigenvalues and variances of 91 factors were scrutinized. The rate of total variance explained for the 20th factor, whose eigenvalues were 1 and higher, was 62.478%. Thus, the number of factors according to the total variance explained rate was determined as 20. The number of factors equal to approximately 50% of the total variance explained rate was determined as 15. As can be seen in Figure 2, which was drawn with the number of factors of eigenvalues, the curved line starts to become parallel to the horizontal axis after the 10th factor. When this graph is taken into consideration, the number of factors can be observed as 10.

As can be understood from the results stated above, there were three different factors. The lowest number was selected as the aim of this study was to reduce the criteria. In other words, the number of factors was determined as 10 according to the eigenvalue-factor graph (Scree Plot) and the analysis was repeated in accordance with the 10 factors.

Rotation of the Factors

In order to easily interpret the factors, the rotation process (upright rotating) was applied using the most common method, namely varimax. When examining the rotating factor matrix, the factor loads were taken into consideration. Within this study, factor loads less than 40% were not taken into consideration and were excluded from the analysis as these loads equal low loads in the resources (Büyüköztürk, 2002; Alpar, 2013).

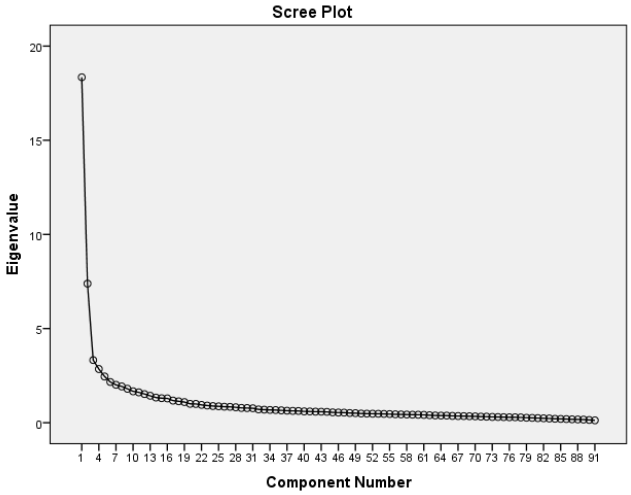

Figure 2. Scree Plot

There were criteria (Q18, Q32, Q33, Q34, Q47, Q52, Q54, Q55, Q56, Q57, Q90, Q91, Q92, Q93, Q94, Q99, Q104, Q108, Q112, Q113, and Q114) that had factor loads under 0.40 in the rotated factor matrix and cyclical criteria (Q36). The cyclical criteria was the criteria that had less than a 10% difference between the factor loads of the prominent one in two factors. If there is a difference more than 10% between the factor loads, it is not a cyclical factor and the largest factor load is taken into consideration. The criteria, which were cyclical and below 40%, were subject to repetitive analyses on an individual basis. This process continued until the conditions that were determined by scrutinizing the rotated matrix as a result of every analysis were met. After all these processes were complete, 22 criteria covering Q18, Q32, Q33, Q34, Q36, Q47, Q52, Q54, Q55, Q56, Q57, Q90, Q91, Q92, Q93, Q94, Q99, Q104, Q108, Q112, Q113 and Q114, were eliminated. The transactions were recorded following the final outcome.

Interpretation of the factors

Ten factors were denominated according to the general characteristics of the criteria in each of the factors (Table 4). When these criteria were scrutinized, it was mainly in accord with the previous grouping. For

example, the first factor (Unsanitary Areas), fourth factor (Technical Infrastructure Services), sixth factor (Entertainment and Cultural Areas), seventh factor (Public Transportation), eighth factor (Green Areas) and ninth factor (Legal Restrictions) were in conformity with the previous grouping. A total of 10 factors were determined among the four main headings. The Locational Features (5 factors) had to most factors and was followed by Legal Features (3 factors) and Neighbourhood (1 factor) and Physical Features (1 factor). The total variance explained ratio of these 10 factors was found to be 55.072 % (Table 4).

Table 4. Classification of the factors

Factor	Name of Factor	The Number of Question	The Question Numbers of Criteria	Main Title (Features)	Reliability	Variance %
1	Unsanitary Areas	13	Q82, Q85, Q87, Q84, Q88, Q81, Q86, Q80, Q89, Q83, Q116, Q115, and Q103.	Locational	.939	11.866
2	Public Institutions	11	Q44, Q45, Q41, Q46, Q40, Q42, Q50, Q37, Q49, Q39, and Q51.	Locational	.865	7.216
3	Popular Neighbourhood Information	8	Q97, Q96, Q98, Q107, Q101, Q109, Q100, and Q110.	Neighbour-hood	.822	5.568
4	Technical Infrastructure Services	5	Q26, Q25, Q24, Q27, and Q29.	Physical	.830	5.206
5	Zoning Status	8	Q20, Q21, Q5, Q6, Q22, Q15, Q17, and Q2.	Legal	.765	5.009
6	Entertainment and Cultural Areas	6	Q62, Q64, Q65, Q63, Q59, and Q60.	Locational	.831	4.796
7	Public Transportation	7	Q73, Q76, Q74, Q77, Q75, Q78, and Q72.	Locational	.781	4.389
8	Green Areas	4	Q69, Q67, Q68, and Q70.	Locational	.840	4.115
9	Legal Restraints	4	Q13, Q12, Q14, and Q3.	Legal	.757	3.518
10	Structuring Conditions	3	Q10, Q9, and Q8.	Legal	.799	3.389
N 2,474	**General Reliability**	**69**			**.876**	**55.072**

3.2. Criteria Mitigation Scenarios According to the Results of the Factor Analysis

Factors

The number of criteria in the factor analysis was 96 at the beginning and 69 after eliminating those under 40% and the cyclical ones. In fact, the 69 criteria were reduced to 10. However, these reduced factor headings were generalized names that were not information that had an exact equivalency in terms of plots (Table 4). For example, the Zoning Status factor contained a lot of information regarding plots, such as the length of the frontage, the number of plot frontage, the gross floor area, total construction area, geometric shape, plot area, the location of the plot (corner parcel) and the ownership status.

Assessment of the factors following the re-grading

The sequences in nine different sampling groups, namely general, all experts, all citizens, the experts in Ankara, Konya, and Kayseri, and the citizens in Ankara, Konya and Kayseri, were separately applied the factor analysis. The results of them were revaluated. The one of mass valuation aims is to estimation the value with the least criteria. It is brought out the most prominent of them accordance with responds of the experts and citizens because they are the actors of the real estate market. Scores were calculated by giving 10 points to the factor in first place and 1 point to the last one. The points of each factor were calculated and are presented in Table 5. The first five factors that received the highest points were Zoning Status (89), Technical Infrastructure Services (82), Unsanitary Areas (72), Structuring Conditions (57), and Popular Neighbourhood Information (55), respectively.

Table 5. Total points of the factors arranged in order according to the factor analysis (**Point Scoring in Factor Analysis**)

Factor	Name of Factor	Scoring in Factor Analysis
1	**Unsanitary Areas**	**72**
2	Public Institutions	30
3	**Popular Neighbourhood Information**	**55**
4	**Technical Infrastructure Services**	**82**
5	**Zoning Status**	**89**
6	Entertainment and Cultural Areas	13
7	Public Transportation	35
8	Green Areas	48
9	Legal Restraints	14
10	**Structuring Conditions**	**57**

Discrimination and generalization of the factors

It is not possible to collect all of the factors as information regarding the plots. In such cases, some should be separated and generalized. It may not be possible for all of the criteria in factors of Unsanitary Areas, Public Institutions, Technical Infrastructure Services, Entertainment and Cultural Areas, Green Areas, and Legal Restrictions to be close to a plot or found

within a plot together. For this reason, there is no need to separate these factors. However, the Zoning Status had to be separated, the Public Transportation factor had to be generalize according to transportation status and the Structuring Conditions factor had to be separated and generalized.

The Zoning Status factor included the criteria of length of the frontage, the number of plot frontage, the gross floor area, total construction area, geometric shape, plot area, the location of the plot (on the corner parcel) and the ownership status when modularized. The Public Transportation factor was generalized as proximity to intercity public transportation points, proximity to tramway, subway, and metrobus stations, and proximity to bus, shared taxi, etc. stops. In the Structuring Conditions factor, detached or attached building was generalized as building design and the number of floors was dissociated as a separate criterion. As a result, 20 criteria that affected plot value were achieved (Table 6).

Three scenarios were produced by both factor analysis, re-scoring of nine different results and generalization-decomposition. The criteria in the last scenario conformed to the definition. Although optimum criteria for the Central Anatolia Region were determined in form a sufficient number of and the most appropriate, it can be adapted for all plot in Turkey by adding/extracting some criteria. However, it should be given final decision after it is validated with market sampling.

4. CONCLUSION

Real estate values, which are very important in real estate management, are directly related to the criteria used in mass valuation. As a result, the need to reduce some criteria due to effort, time and cost may arise. There are many criteria that affect real estate value, which vary from region-to-region and person-to-person. In this study, working only on plots did not decrease the number of criteria. As gathering the entire criteria to determine the material value of more than one plot in mass valuation was not possible, the target was to decrease the criteria. A decreased number of criteria will make a significant contribution to both data collection on plots during operations such as taxation, expropriation, assurance, fees, land, plot arrangements, urban transformation, etc. and to the country's economy as revenue receipt. With the diminished number of criteria for plot values and their correct, trustworthy, and transparent calculation, people will gain ground in commerce and investment.

Table 6. Discrimination of some of the factors

Discriminated Factors		Non-Discriminated Factors		Generalized Factors	
No	**Factors**	**No**	**Zoning Status Factor**	**No**	**Structuring Conditions**
1	Unsanitary Areas	**1**	Length of frontage,	**1**	Building Design (Detached/Attached Building)
2	Public Institutions	**2**	The number of frontage	**2**	The number of floors
3	Popular Neighbourhood Information	**3**	The gross floor area		
4	Technical Infrastructure Services	**4**	Total construction area	**No**	**Public Transportation**
5	Entertainment and Cultural Areas	**5**	Geometrical shape	**1**	Proximity to intercity public transportation points
6	Green Areas	**6**	Plot Area	**2**	Proximity to tramway, subway and metrobus stations
7	Legal Restraints	**7**	The location of the plot (corner parcel)	**3**	Proximity to bus, shared taxis etc. stops
		8	Ownership Status-Full		***Total=20 Criteria***

In this study, a survey was used to gather the data and factor analysis was used to obtain a decreased number of criteria. The answers the experts and citizens gave were collected and organized to prepare for analysis. Then, factor analysis was implemented and the decreased number criteria were identified. According to the factor analysis results, 10 factors came to the fore: Unsanitary Areas, Public Institutions, Popular Neighbourhood Information, Technical Infrastructure Services, Zoning Status, Entertainment and Cultural Areas, Public Transportation, Green Areas, Legal Restrictions, and Structuring Conditions.

According to the factor analysis results, the criteria with the most effect on market value in Central Anatolia were determined. The answers given to the question "where?" regarding the building of a house covered most of the criteria determined in this study. In other words, it was concluded that Proximity to **Unsanitary Areas, Public Institutions, Entertainment and Cultural Areas, Public Transportation Points,** and **Green Areas** should be taken into consideration. As a result of the analysis the **Popular Neighbourhood Information** included the demographic and social characteristics of people living in the neighbourhood. In addition it was determined as an important group for the experts and citizens as a result of their answers to the survey questions. **Technical Infrastructure Services** was determined as another important criteria group and was one of the features that should be in a plot. However, as the insufficiencies were found to not end until most of the structuring was complete, they were included in the questionnaire and became one of the most important criteria groups. **Legal Restrictions** mean servitudes that are officially registered in the deed registry record for the plot and restrict its use, and constituted an important criteria group. **Zoning Status** and **Structuring Conditions** were some other criteria groups that had an effect on plot value. They contain very important data such as the gross floor area, total construction area, the number of floors, and building design related to the house to be built. While the criteria groups regarding locational features and the variation of Popular

Neighbourhood Information and Technical Infrastructure Services on a regional basis could be identified on micro scale maps, Zoning Status and Structuring Conditions needed to be examined in parcels with large scale maps. As a result, after the unbundling and generalizing of 10 factors, 20 criteria were obtained.

When scored according to all of the samples, the results of the factor analysis showed that the 10 factors decreased to five factors, namely Zoning Status, Technical Infrastructure Services, Unsanitary Areas, Structuring Conditions, and Popular Neighbourhood Information. In case of the decomposition of Technical Infrastructure Services, Unsanitary Areas, and Popular Neighbourhood Information as neighbourhood-based and Zoning Status and Structuring Conditions as parcel-based, they could be decreased to 13 criteria as Technical Infrastructure Services, Unsanitary Areas, Popular Neighbourhood Information, length of frontage, the number of plot frontage, the gross floor area, total construction area, geometric shape, plot area, the location of the plot (on the corner parcel), the ownership status, building design and the number of floors.

The validity of decreased number of criteria was not only region based. It was considered that the criteria could be used throughout the country. In case of extreme conditions, additions could be made to these optimum criteria in line with expert contributions. The results of the survey work are important for the construction of artificial intelligence or machine learning methods that can make automatic valuation in the establishment of the mass real estate appraisal system. The results of this study, which is applied very comprehensively and includes all objective variables that can be used in the estimation of the land value, are available in applications that require many value estimates, regardless of which value estimation method is preferred.

ACKNOWLEDGEMENT

The survey questions applied in this study had not negative effects on the health, feelings or thoughts of the participants. In addition, the necessary permission required for the survey questions was obtained from the Ethics Committee of Selcuk University in 2015.

The authors would like to thank the pollsters for their effort and the participants who patiently completed the questionnaire in the data collection phase of the survey. This study was supported by the Scientific and Technological Research Council of Turkey (TÜBİTAK) (project No. 115Y769).

Author contributions

Sukran Yalpir: Conceptualization, Methodology, Data Curation, Writing-Reviewing and Editing, Validation. **Fatma Bunyan Unel:** Investigation, Making the Survey, Analyzing, Writing-Original Draft Preparation.

Conflicts of interest

The authors declare no conflicts of interest.

REFERENCES

Açlar A & Çağdaş V (2008). Taşınmaz (Gayrimenkul) Değerlemesi (2. Baskı). Ankara, Türkiye: TMMO, HKMO.

Alpar R (2013). Çok Değişkenli İstatistiksel Yöntemler (Uygulamalı) (4. Baskı). Ankara, Türkiye: Detay Yayıncılık.

Altunışık R, Çoşkun R, Bayraktaroğlu S & Yıldırım E (2010). Sosyal Bilimlerde Araştırma Yöntemleri SPSS Uygulamalı. Sakarya, Türkiye: Sakarya Yayıncılık.

Arıkan R (2013). Anketler ve Anket Soruları. Ankara, Türkiye: Nobel Akademik Yayıncılık.

Aydinoglu A C, Bovkir R & Colkesen I (2020). Implementing a mass valuation application on interoperable land valuation data model designed as an extension of the national GDI, *Survey Review*, 1771967.

Baş T (2010). Anket (6. Baskı). Ankara, Türkiye: Seçkin Yayıncılık.

Bender A, Din A, Hoesli M & Brocher S (2000). Environmental preferences of homeowners, Further evidence using the AHP method. Journal of Property Investment&Finance, 18(4), 445–455.

Biçen S (2010). Uluslararası Sermaye Yatırımlarının Gelişmekte Olan Ülkelerin Bankacılık Sektörüne Etkisi, Türkiye Örneği. Doktora tezi, Kadir Has Üniversitesi, İstanbul, Türkiye.

Bozdağ A & Ertunç E (2020). Real Property Valuation in the Sample of the City of Niğde through GIS and AHP Method, Journal of Geomatics, 5(3), 228–240.

Büyüköztürk Ş (2002). Faktör Analizi: Temel Kavramlar ve Ölçek Geliştirmede Kullanımı. Kuram ve Uygulamada Eğitim Yönetimi, 32, 470–483.

Cellmer R & Trojanek R (2020). Towards Increasing Residential Market Transparency: Mapping Local Housing Prices and Dynamics, *ISPRS International Journal of Geo-Information*, 9(2), 9010002.

Çakır P & Sesli F A (2013). Arsa Vasıflı Taşınmazların Değerine Etki Eden Faktörlerin ve Bu Faktörlerin Önem Sıralarının Belirlenmesi. Harita Teknolojileri Elektronik Dergisi, 5(3), 1–16.

Erdem N (2018). The Content Analysis on Graduate Theses in the Field of Real Estate Valuation in Turkey, *APJES*, 6(1), 112–126.

Ertaş M (2019). Education for Real Estate Valuation in Turkey, *International Journal of Engineering and Geosciences (IJEG)*, 4(1), 008–015.

IAAO (2014). Guidance on International Mass Appraisal and Related Tax Policy 2014. The International Association of Assessing Officers (IAAO), the United States of America.

IAAO (2017). Standard on Mass Appraisal of Real Property 2017. The International Association of Assessing Officers (IAAO), the United States of America.

IVS (2017). International Valuation Standards (IVS). International Valuation Standards Council, United Kingdom.

Kalaycı Ş (Ed.). (2010). SPSS Uygulamalı Çok Değişkenli İstatistik Teknikleri. Ankara, Türkiye: Asil Yayın.

Kryvobokov M (2005). Estimating the weights of location attributes with the Analytic Hierarchy Process in

Donetsk, Ukraine. Nordic Journal of Surveying and Real Estate Research, 2(2), 5–29.

Law on Soil Protection and Land, No 5403. (5403 Sayılı Toprak Koruma ve Arazi Kullanımı Kanunu). Kanun Kabul Tarihi: 03.07.2005, Resmi Gazete Tarihi: 19.07.2005, Resmi Gazete Sayısı: 25880.

Mete M O & Yomralioglu T (2021). Implementation of serverless cloud GIS platform for land valuation, *International Journal of Digital Earth*, 1889056.

Miotti L A & Loch C (2021). Property value map updating by mass appraisal method a case in the city of Pato branco, state Paraná, *Acta Scientiarum*, Technology, 43, e48912.

Nguyen P H, Tsai J F, Nguyen T T, Nguyen T G & Vu D D (2020). A Grey MCDM Based on DEMATEL Model for Real Estate Evaluation and Selection Problems: A Numerical Example, Journal of Asian Finance, Economics and Business, 7(11), 549–556.

Nişancı R (2005). CBS ile Nominal Değerleme Yöntemine Dayalı Piksel Tabanlı Kentsel Taşınmaz Değer Haritalarının Üretilmesi. Doktora tezi, Karadeniz Teknik Üniversitesi, Trabzon, Türkiye.

Özdamar K (2002). Paket Programlar ile İstatistiksel Veri Analizi-1 (SPSS-MINITAB). Eskişehir, Türkiye: ETAM Kaan Kitabevi.

Pace R K, Barry R & Sirmans C F (1998). Spatial Statistics and Real Estate. Journal of Real Estate Finance and Economics, 17(1), 5–13.

Property Ownership Law, No 634. (634 Sayılı Kat Mülkiyeti Kanunu), Kabul Tarihi: 23.6.1965, Yayımlandığı Resmi Gazete Tarihi: 2.7.1965 Resmi Gazete Sayısı: 12038.

Shimizu C, Nishimura K G & Watanabe T (2016). House Prices at Different Stages of the Buying/Selling Process. Regional Science and Urban Economics, 59, 37–53.

Timur S (2009). CBS Destekli Taşınmaz Mal Değer Haritalarının Oluşturulması: İstanbul İli, Şişli İlçesi Örneği. Yüksek Lisans tezi, İstanbul Teknik Üniversitesi, İstanbul, Türkiye.

Tiryakioğlu İ & Erdoğan S (2006). Coğrafi Bilgi Sistemleri Destekli Taşınmaz Değerlemesi: Afyonkarahisar Örneği. 4. Coğrafi Bilgi Sistemleri Bilişim Günleri, İstanbul, Türkiye.

TKMP (2008). Tapu Kadastro Modernizasyon Projesi (TKMP). 4. Bileşen Gayrimenkul Değerleme, ÇŞB, TKGM, Kadastro Dairesi Başkanlığı, Ankara.

Turkish Civil Code, No 4721. (4721 Sayılı Türk Medeni Kanunu), Kabul Tarihi: 22.11.2001, Yayımlandığı Resmi Gazete Tarihi: 08.12.2001, Resmi Gazete Sayısı: 24607.

UNECE WPLA (2001). Land (Real Estate) Mass Valuation Systems for Taxation Purposes in Europe. The Federal Land Cadastre Service of Russia on behalf of the UN ECE Working Party on Land Administration, Moscow, Russian Federation.

UNECE WPLA (2014). Survey on Land Administration Systems. New York and Geneva.

Unel F B (2017). Development of Geography Data Model For Criteria of Real Estate Valuation, Ph.D. Thesis, Selcuk University, Konya, Turkey.

Unel F B & Yalpir Ş (2017). Reduction of Mass Appraisal Criteria with Principal Component Analysis and Integration to GIS, *International Journal of Engineering and Geosciences (IJEG)*, 4(3), 094-105.

Unel F B & Yalpir Ş (2019a). Valuations of Building Plots Using the AHP Method, *International Journal of Strategic Property Management*, 23(3), 197–212.

Unel F B & Yalpir Ş (2019b) Approach to Criteria Affecting Value of Real Properties in Turkey, *Journal of Geomatics*, 4(2), 112-133.

Unel F B, Yalpir S & Gulnar B (2017). Preference Changes Depending on Age Groups of Criteria Affecting the Real Estate Value, *International Journal of Engineering and Geosciences (IJEG)*, 2(2), 41–51.

USAID (2006). Tax Modernization in Bosnia and Herzegovina, USAID Assistance in Fiscal Reform, Bosnia and Herzegovina.

USPAP (2017). The Uniform Standards of Professional Appraisal Practice (USPAP) (2020-2021). The Appraisal Standards Board, the Appraisal Foundation, the United States of America.

Üçdoğruk Ş (2001). İzmir İlinde Emlak Fiyatlarına Etki Eden Faktörler-Hedonik Yaklaşım, Dokuz Eylül Üniversitesi, İİBF Dergisi, 16(2), 149-161.

Yalpır Ş (2007). Bulanık Mantık Metodolojisi ile Taşınmaz Değerleme Modelinin Geliştirilmesi ve Uygulaması: Konya Örneği. Doktora tezi, Selçuk Üniversitesi, Konya, Türkiye.

Yalpir S & Unel F B (2017). Use of Spatial Analysis Methods in Land Appraisal; Konya Example. In 5th International Symposium on Innovative Technologies in Engineering and Science (ISITES2017), Baku, Azerbaijan.

Yıldız Ü (2014). Gayrimenkul Bilimlerinde Kitlesel Değerleme Uygulamaları ve Türkiye için Model Önerisi. Yüksek Lisans tezi, Ankara Üniversitesi, Ankara, Türkiye.

Yilmazer S & Kocaman S (2020). A mass appraisal assessment study using machine learning based on multiple regression and random forest, *Land Use Policy*, 99, 104889.

Yomralıoğlu T (1993). A Nominal Asset Value-Based Approach for Land Readjustment and Its implementation Using Geographical Information Systems. PhD, University of Newcastle upon Tyne, UK.

Zoning Law No 3194. (3194 Sayılı İmar Kanunu). Kabul Tarihi: 3.5.1985, Yayımlandığı Resmi Gazete Tarihi: 9.5.1985, Resmi Gazete Sayısı: 18749.

Zyga J (2020). The influence analysis of criteria of comparables' selection on the accuracy of the property value estimation, *Reports on Geodesy and Geoinformatics*, 109, 9–15.

International Journal of Engineering and Geosciences

https://dergipark.org.tr/en/pub/ijeg

e-ISSN 2548-0960

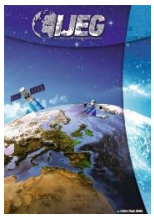

Clutter removal in millimeter wave GB-SAR images using OTSU's thresholding method

Enes Yigit[*1], **Şevket Demirci** [2], **Caner Özdemir** [2]

[1]*Bursa Uludağ University, Engineering Faculty, Department of Electrical Electronics Engineering, Bursa, Turkey*
[2]*Mersin University, Engineering Faculty, Department of Electrical Electronics Engineering, Mersin, Turkey*

Keywords
Synthetic Aperture Radar
OTSU
Back projection Algorithm
Clutter Cancellation

ABSTRACT

In this study, a filtering method based on the threshold value of normalized synthetic aperture radar (SAR) data is proposed to eliminate clutter in millimeter wave ground based synthetic aperture radar (GB-SAR) images. In the proposed method, first, stepped frequency continuous wave SAR data are reconstructed by using the back-projection algorithm and focused complex SAR data are obtained. Then, the amplitude values of the complex SAR data are normalized and the best threshold values to distinguish the target from clutter is determined by the OTSU's thresholding method. Next, a filter mask is created that cancels all data below the computed threshold values. The mask matrix is finally multiplied with the resulted GB-SAR data to eliminate all clutter from the image. With the proposed technique, the best threshold value is determined automatically by directly processing the raw data without converting the SAR data into any RGB images. The proposed technique is validated through real GB-SAR experiments that were carried out in the frequency band of 78-81 GHz. In the experiments, challenging GB-SAR data are obtained using high cluttered background materials, and very successful filtering operations are performed with the proposed technique.

1. INTRODUCTION

Synthetic aperture radar (SAR) is a highly effective remote sensing tool in producing high resolution images of moving and fixed land targets. While traditional SAR systems have been typically installed on satellites and aircrafts, they also have been applied to near-surface unmanned aerial vehicles and terrestrial vehicles in recent years. Compared to air-based SAR, ground-based (GB) SAR systems offer very cheap and practical implementations and thus find applications in many fields such as through the wall imaging (Engin et al., 2007), agricultural applications (Gomez et al., 2006), observing unstable slopes (Pieraccini et al., 2006), foreign object debris detection (Yigit et al., 2012; Beasley et al., 2004) and concealed object detection (Jaeger et al., 2007; Demirci et al., 2012). Among these, millimeter wave (MMW) SAR (Yigit et al., 2012; Jaeger et al., 2007; Demirci et al., 2012) applications, as providing very high resolution images, have become very popular in recent years. However, removal of clutter echoes in both traditional SAR images and millimeter wave (MMW) GB-SAR images are one of the most important problems encountered in target detection. This problem becomes more intense in high frequency and broadband MMW SAR images. Many studies have been carried on to eliminate different types of unwanted clutter from focused SAR images of various Earth regions (Freitas et al., 2005; Conte et al., 1991). Although the popular methods based on statistical modeling and Constant False Alarm Rate (CFAR) [Demirci et al., 2008] are frequently used for clutter removal, clutter has not been completely eliminated due to the tradeoff encountered in setting the CFAR window (Toktas et al.2017). When the large CFAR window is selected, much information about the target remains in the image, while there are still clutter residues in the background. When the window is selected small, the background is mostly cleared, but there is a loss of target information. However, advanced image processing techniques can be used effectively to overcome this trade-off problem. In this study, the OTSU method, which is highly effective in gray level filtering, has been proposed to eliminate unwanted clutter in MMW SAR images. Although OTSU method is an effective method in image processing, it is mostly used in Hough-Saturation-Value (HSV) regions of (Red, Green, and Blue) RGB images (Sabancı et al.2018). In many radar imaging applications where the OTSU method was used, the

* **Corresponding Author**

*(enesyigit@uludag.edu.tr) ORCID ID 0000-0002-0960-5335
(sdemirci@mersin.edu.tr) ORCID ID 0000-0002-3020-7067
(cozdemir@mersin.edu.tr) ORCID ID 0000-0003-2615-4203

Cite this article

Yigit E, Demirci S & Ozdemir C (2022). Clutter removal in millimeter wave GB-SAR images using OTSU's thresholding method. International Journal of Engineering and Geosciences, 7(1), 43-48

Research Article / DOI: 10.26833/ijeg.867467

Received: 24/01/2021; Accepted: 01/03/2021

operations were executed through the RGB image files (Işıker and Özdemir, 2019; Işıker et al., 2018; Işıker et al., 2015; Khoukhi et al.2019; Lu and Hu 2012). However, converting SAR data into image files and then filtering these files again with image processing causes high computation time and data loss. Thanks to the method proposed in this study, a practical but effective method for filtering raw SAR data is presented. With the proposed method, images with a low signal-to-clutter ratio, such as MMW-SAR data, were precisely cleaned. To assessment the success and performance of the technique, 2 different measurements were performed at MMW frequencies (in the range of 78-81 GHz) and visual comparisons were made by focusing on each GB-SAR data with the back projection algorithm (BPA) (Yigit et al., 2013; Yigit et al., 2020) in order to comprehend only the filter performance.

The main sections of the study are as follows: In the second part, the SAR imaging and focusing method is briefly presented, while the proposed filtering method is given in detail. The experimental organization and the outcomes of the measurements are given in the third section. In the last section, the results of the study are evaluated and the study is summarized.

2. METHOD: SAR IMAGE RECONSTRUCTION AND OTSU METHOD

2.1. GB-SAR IMAGE RECONSTRUCTION

Fig. 1 shows the setup of a simple GB-SAR scanning system. In a 2 dimensional (2D) imaging geometry, the reflection function of the targets in the scanning region is defined as $\rho(x,y)$ and the positions of the antennas are expressed in Cartesian coordinates as $(x,y) = (D_p sin\beta, D_p cos\beta)$where, D_p and β are the distance and angle between antennas and origin of the scene, respectively. Assuming that there are a total of P point scatterers in the scanned region, the backscatter signal obtained by the radar can be expressed as follows.

$$S_\beta(k) = \sum_{p=1}^{P} \rho_p e^{-jkD_p(\beta)} \quad (1)$$

where, $k = 4\pi f / c$ is a (two way) wave number, f and c are ferquency and speed of the light, respectively.

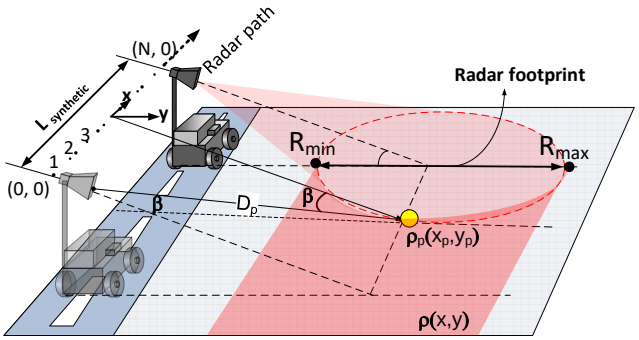

Figure 1. GB-SAR data acquisition geometry

The instantaneous distance between the antennas and targets,

$$D_p(\beta) = \sqrt{(x - x_p)^2 + (y - y_p)^2} \quad (2)$$

where, (x_p, y_p) and (x, y) correspond to coordinate of the p th scatterer and antennas, respectively.

As seen in the Fig. 1, the SAR platform collects back scatter data at a total of N different points along the L synthetic aperture and obtains 2D GB-SAR data (Yigit et al., 2013; Yigit et al., 2020). Then, in order to transform the obtained raw SAR data into a meaningful image, focused complex SAR data $\rho(x,y)$ is obtained using any reconstruction algorithm such as BPA (Yigit et al., 2013).

2.2. OTSU BASED FILTERING ALGORITHM

OTSU is an effective method especially used in automatic filtering of gray level images (Otsu, N., 1979). This method is mostly preferred for picture data in RGB format. For this reason, focused SAR data must first be converted into RGB image format and then processed into a suitable format such as HSV for OTSU filtering by additional processing (Işıker and Özdemir, 2019). However, this process adds additional cost and the success of the filter depends on the resolution of the SAR image. This is also a disadvantage for the filtering process. In this study, a filtering method based directly on focused raw SAR data rather than using any image format is proposed. The normalized filter method first starts with obtaining the amplitude $|\rho|$ of the complex $\rho(x,y)$ matrix.

Using Eq. 3, the values of the $|\rho|$ data are normalized to be between 0 and 1.

$$\rho_n = \frac{|\rho| - min|\rho|}{max|\rho| - min|\rho|} \quad (3)$$

In the ρ_n data, the values of target region are mostly close to 1, while the values in the non-target regions are close to 0. In order to clean the background clutter precisely, the mean value is subtracted from ρ_n data.

$$\rho_m = \rho_n - mean(\rho_n) \quad (4)$$

The values of the data obtained by Eq. 4 which are less than zero are equalized to 0 and ρ_m, data is obtained. This data is then normalized as follows.

$$\rho_{n'} = \frac{\rho_{m'} - min\rho_{m'}}{max\rho_{m'} - min\rho_{m'}} \quad (5)$$

The most appropriate threshold value of $\rho_{n'}$ is then determined by the OTSU (Otsu, N., 1979) method and the ρ_{mask} mask is created so that the values above the threshold value of the $\rho_{n'}$ matrix are marked as 1 and the values below it are 0. Finally, all clutter are removed by multiplying the original image with the mask as given below.

$$Fil_{SAR} = \rho_{mask} . |\rho| \quad (6)$$

3. RESULTS: MMW GB-SAR MEASUREMENTS

In order to conduct MMW GB-SAR imaging experiments, the measurement system given in Fig. 2a was constructed in the International Laboratory for High

Technology (ILHT) in the TUBITAK Marmara Research Center. The system consists of two MMW horn antennas (WR-10), a Vector network analyzer (VNA E8362B) and computer to control the mobile platform. Measurements were carried out in the frequency range of 75 - 110 GHz. Half-power beam width of the antennas was measured as 24^0 at 100 GHz. The dimensions of the materials used as target are given in Fig. 2b. Since the main purpose of this study was to eliminate unwanted clutter in GB-SAR images, the targets in both experiments were placed on the back side of the Electromagnetic (EM) absorber material. Since the back surface of the EM absorber material has a very high reflectivity, an artificial clutter was created and the performance of the proposed filter could be better observed.

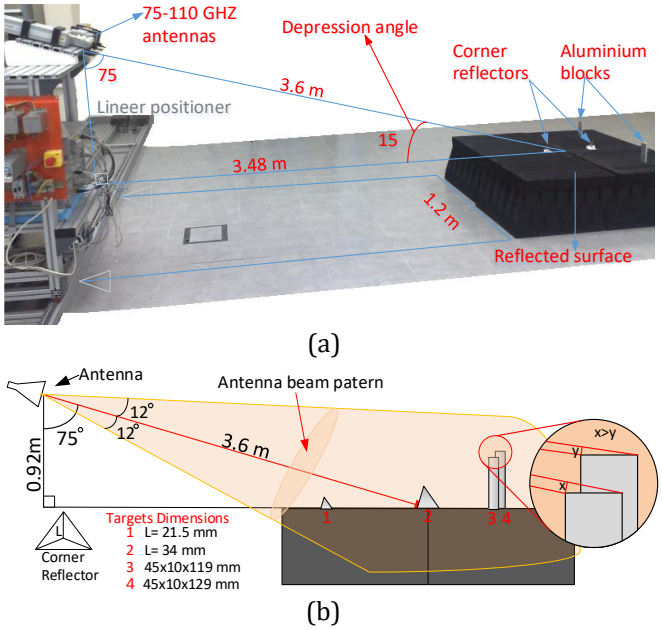

Figure 2. MMW GB-SAR imaging experimental setup; a) Linear positioner, antennas and an image of the targets, b) dimensions of the targets and geometry of the experimental setup

In the experiments, the VNA mounted on the mobile platform gathered backscatter data at a total of 301 points along a 1.2 m synthetic aperture. At each data collection point, the frequency of the VNA was altered between 75 GHz and 81 GHz in 201 steps. Thus, each GB-SAR data had been expressed as a 301x201 matrix. The distance of the reflective surface where the targets are deployed to the platform was determined as 3 m, and the altitude of the antennas was set as 0.92 m as shown in Fig. 2b.

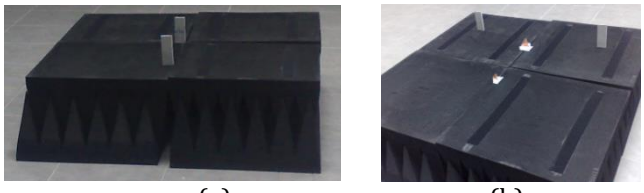

(a) (b)

Figure 3. Targets used in measurements; a) 1st Measurement, b) 2nd Measurement

3.1. Experiment 1

In the first measurement, 2 aluminum blocks shown in Fig. 3a were used as targets. The first block was located 3 m from the antennas, while the second block was located 3.8 m from the antennas. Then, scanning was performed with the given measurement parameters. As it can be seen in Fig. 4, it is impossible to make any inferences about targets from the raw GB-SAR image.

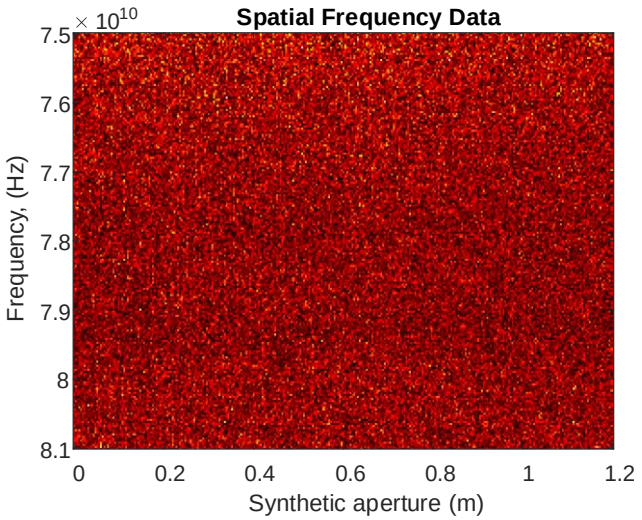

Figure 4. Raw GB-SAR data obtained from 2 aluminum blocks.

Since a highly reflective material was used as the background, the gathered row SAR image contains very high clutter. To apply the recommended filtering method, the image in Fig. 4 is primarily reconstructed with BPA and the amplitude of the complex SAR image is shown in Fig. 5.

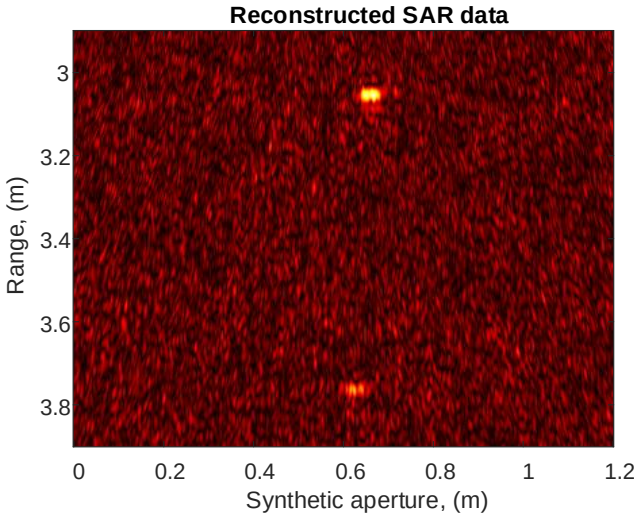

Figure 5. The SAR image of Experiment 1 reconstructed with BPA

As seen in the Fig. 5, the metal block at 3 m can be distinguished after reconstruction, while the second block at 3.8 m has almost disappeared among the background clutter. In order to clean the clutter in the image, the recommended process steps in the second section are applied and ρ_n, is showed in Fig. 6.

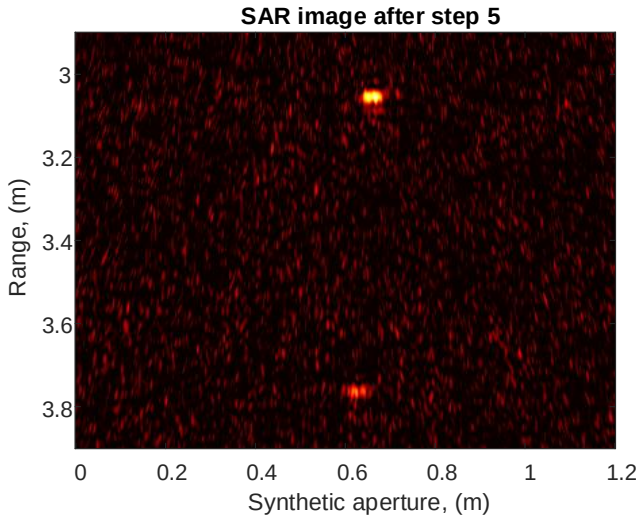

Figure 6. The image obtained after application of Eq. 5.

As can be seen in Fig. 6, the contrast in the SAR data has been increased and the target at 3.8 m has become a little more visible. To find the most appropriate threshold value, the OTSU method is applied to ρ_n, and the threshold value is found as 0.0941. A mask image (see Fig. 7) is then created where all items below the threshold value are 0 and items above the threshold are 1.

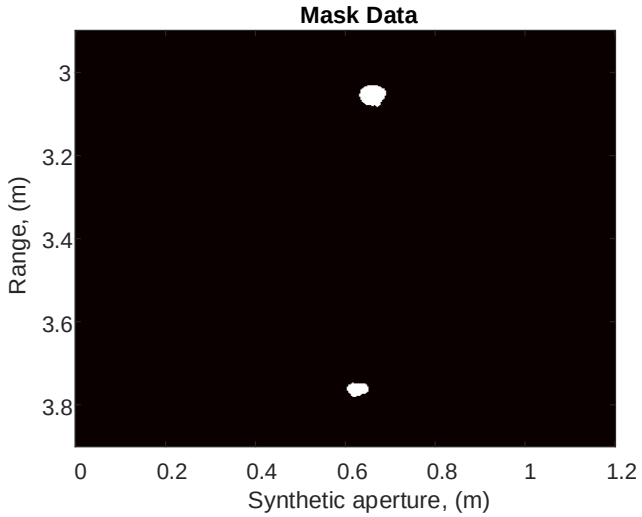

Figure 7. Mask image after application of the optimal thresholds found by OTSU's method.

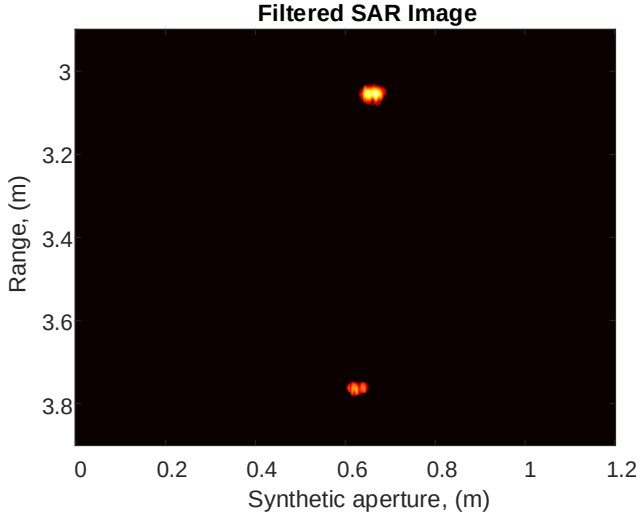

Figure 8. OTSU based filtered GB-SAR image

Then, the filtered image is obtained by multiplying the mask data given in Fig. 7 with the reconstructed raw GB-SAR data. The result is seen in Fig. 8, and reveals that with the proposed technique, almost all clutter is completely removed and only the scattering signatures of the targets of interest are remained in the image. Thanks to the success of the proposed method, the target at 3.8 m is clearly displayed without any loss of information.

3.2. Experiment 2

In the second measurement, 4 targets are tried to be detected by adding 2 corner reflectors given in Fig. 3b. In this measurement, since the first corner reflector shown in Fig. 1 has very small dimensions, it is almost not seen in the reconstructed image in Figure 9.

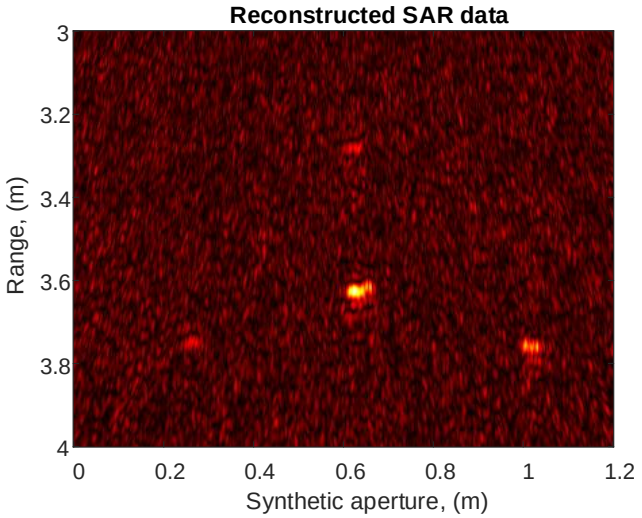

Figure 9. GB-SAR image, obtained from 2 aluminum blocks and 2 corner reflectors

The mask matrix obtained after applying the recommended filtering to the image in Figure 9 is shown in Fig. 10. In this measurement, the threshold value obtained with OTSU is found as 0.1020.

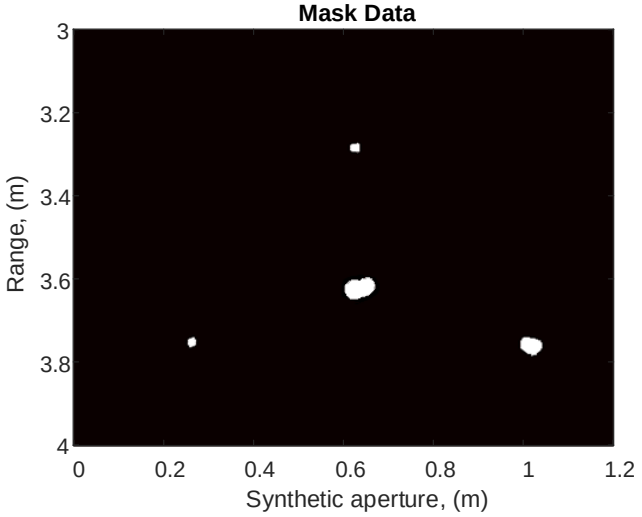

Figure 10. The created Mask image after thresholding found by OTSU method

When the data reconstructed with BPA is multiplied with the mask matrix shown in Fig. 10, the filtered GB-SAR image is given in Fig. 11.

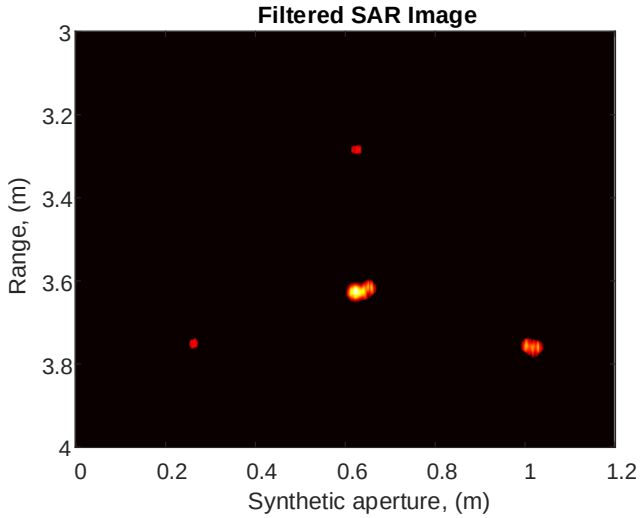

Figure 11. OTSU based filtered GB-SAR image of 4 targets

As seen in Fig. 11, owing to the suggested method, all the clutter is removed and the objects are obviously identified in their exact locations. Thanks to the filtering technique based on the OTSU method, since the targets are cleaned from clutter, there is no dynamic reduction in the filtered image. When Fig. 9 is examined, the small corner reflector and metal block are almost not visible. However, thanks to the applied technique, targets that could not be detected visually are clearly identified and no false target detection is realized. These results clearly demonstrate the performance of the presented technique in filtering highly dispersed data and are promising for further studies. When the results of both measurements are evaluated, it is seen that the threshold value of the first measurement is smaller than the second measurement. Since metal blocks with high reflectivity are closer to the SAR path in the first measurement, the signal to clutter value is higher than the second measurement. Therefore, with a lower threshold value compared to the second measurement, the clutter was completely cleaned. These results clearly demonstrate that the OTSU method can be effectively applied to raw SAR data other than RGB images.

4. CONCLUSION

In this study, an effective clutter removal method that can be applied in all kinds of SAR images is proposed. The most suitable threshold values are determined by using the OTSU method, which can be applied directly to raw data without converting the GB-SAR data into any RGB image. According to the found threshold value, clear GB-SAR images are obtained by masking processes. Thanks to the proposed technique, all targets are successfully detected without any loss of data regarding the target images. These results obtained in MMW measurements with very high clutter show that the proposed technique can be applied effectively to further SAR data. Since the clutter is mostly eliminated with the proposed technique, the performance of target detection algorithms such as machine learning-based SAR, ISAR or GPR [Ozkaya, 2020; Ozkaya and Seyfi, 2018] can be increased.

ACKNOWLEDMENT

The authors would like to thank Mr. Atilla Unal and Mr. Mustafa Tekbas for their assistance during the experiments. The authors also thank the ILHT for providing measurement facilities.

Author contributions

Enes Yigit: Developing the technique, Execution of experiments, Writing-Original draft preparation; **Şevket Demirci:** Execution of experiments, Writing-reviewing, and editing; **Caner Özdemir:** Conceptualization, Evaluation and presentation of results, reviewing and editing of the manuscript.

Conflicts of interest

The authors declare no conflicts of interest.

REFERENCES

Beasley P, Binns G, Hodges R & Badley R (2004). A Millimetre Wave Radar for Airport Runway Debris Detection. First Europen Radar Conference, Amsterdam, Nerherlands, 261-264.

Conte E, Longo M, Lops M & Ullo S L (1991). Radar detection of signals with unknown parameters in K-distributed clutter. IEE Proc F Radar Signal Process 138, 131–138.

Demirci S, Cetinkaya H, Yigit E, Ozdemir C & Vertiy A A (2012). A Study on Millimeter-Wave Imaging of Concealed Objects: Application Using Back-Projection Algorithm. Progress In Electromagnetics Research, 128, 457-477.

Demirci S, Ozdemir C, Akdagli A & Yigit E (2008). Clutter Reduction In Synthetic Aperture Radar Images With Statistical Modeling: An Application To Mstar Data. Microwave And Optical Technology Letters.50 (6).

Engin E, Çiftçioğlu B, Özcan M & Tekin İ (2007). High Resolution Ultrawideband Wall Penetrating Radar. Microwave and optical technology letters, 49(2), 320-325.

Freitas C C, Frery A C & Correia A (2005). The polarimetric G distribution for SAR data analysis. Environmetrics 16, 13–31.

Gomez-Dans J L, Quegan S & Bennett J C (2006). Indoor C-Band Polarimetric Interferometry Observations of a Mature Wheat Canopy. IEEE transactions on geoscience and remote sensing, 44(4), 768-777.

Işıker H & Özdemir C (2019). A Multi-Thresholding Method Based on Otsu's Algorithm for the Detection of Concealed Threats in Passive Millimeter-Wave Images. Frequenz, 73, issue 5-6, 179-187.

Işıker H, Özdemir C, Unal İ (2015). Millimeter-Wave Band Radiometric Imaging Experiments for the Detection of Concealed Objects. IEEE Radar Conference, Johannesburg, South Africa, 27-30 October.

Işıker H, Ünal İ, Tekbaş M, Özdemir C (2018). An Auto-Classification Procedure for Concealed Weapon Detection in Millimeter-Wave Radiometric Imaging Systems. Microwave Opt. Tech. Letters, 60(3), 583–594.

Jaeger I, Zhang L, Stiens J, Sahli H & Vounckx R (2007). Millimeter Wave Inspection of Concealed Objects. Microwave and optical technology letters, 49(11), 2733-2737.

Khoukhi H, Filali Y, Yahyaouy A, Sabri M A, Aarab A (2019). A hardware Implementation of OTSU Thresholding Method for Skin Cancer Image Segmentation. 2019 International Conference on Wireless Technologies, Embedded and Intelligent Systems (WITS),

Lu J & Hu R (2012). A new image segmentation method based on Otsu method and ant colony algorithm," 2012 International Conference on Computer Science and Information Processing (CSIP), Xi'an, China, 2012, pp. 767-769, doi: 10.1109/CSIP.2012.6308966.

Otsu N (1979). A Threshold Selection Method from Gray-Level Histograms. IEEE transactions on systems, man, and cybernetics, 9(1), 62-66

Ozkaya U (2020). Automatic Target Recognition (ATR) from SAR Imaginary by Using Machine Learning Techniques, European Journal of Science and Technology, 165-169

Ozkaya U, Seyfi L (2018). Deep dictionary learning application in GPR B-scan images. Signal, Image and Video Processing, 12, 1567–1575

Pieraccini M, Luzi G, Mecatti D, Noferini L & Atzeni C (2006). Ground-Based Sar for Short and Long Term Monitoring of Unstable Slopes. 3rd Europen Radar Conference, Manchester, United Kindgom, 92-95.

Sabanci K, Yigit E, Toktas A, Kayabasi A (2018). A Hue-domain filtering technique for enhancing spatial sampled compressed sensing-based SAR images. IET Radar, Sonar&Navigation, 13(3), 357-367.

Toktas A, Yigit E, Sabanci K, Kayabasi A. (2017). CFAR based morphological filter design to remove clutter from GB-SAR images: An application to real data. Microw Opt Technol Lett. 59, 2685 –2692.

Yigit E, Demirci S, Ozdemir C, Tekbas M (2013). Short-range ground-based synthetic aperture radar imaging: performance comparison between frequency-wavenumber migration and back-projection algorithms. J. Appl. Rem. Sens. 7(1).

Yigit E, Demirci S, Unal A, Ozdemir C & Vertiy A (2012). Millimeter-Wave Ground-Based Synthetic Aperture Radar Imaging for Foreign Object Debris Detection: Experimental Studies at Short Ranges. Journal of Infrared, Millimeter, and Terahertz Waves, 33(12), 1227-1238.

Yigit E, Ozkaya U, Ozturk S (2020). Enhancement of Near Field GB-SAR Image Quality Using Beamwidth Filter. European Journal of Science and Technology Special Issue, 480-487.

International Journal of Engineering and Geosciences
https://dergipark.org.tr/en/pub/ijeg
e-ISSN 2548-0960

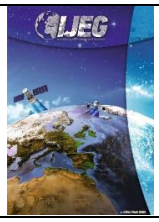

Assessment of the completion of the forest cadastre considering the legal grounds, collaboration, and the use of technology: The case of Turkey

Orhan Ercan[*1], **Nur Kemalettin Toker** [2]

[1]*International Federation of Surveyors (FIG), Ankara, Turkey*
[2]*General Directorate of Land Registry and Cadastre, Ankara, Turkey*

Keywords
Forest
Forest Cadastre
Forest Delimitation
Private Sector Involvement
Sustainable Development Goals

ABSTRACT

The forests are among the natural resources that have important economic, environmental, and cultural functions. However, global problems, which have been increasing each passing day, such as industrialization, increasing urban population, global climate change, and destruction of biodiversity also threaten forests. The first condition for the protection of forests and carrying out forestry activities is the demarcation of forest boundaries and the registration of the forests. The forest cadastre has remained a major issue on Turkey's agenda for years. In this article, the process beginning with the demarcation of the forest boundaries until their registration in the land registry system was reviewed and assessed considering the institutional and legal frameworks and amendments, technology use, the collaboration between institutions, and the participation of the private sector. As a result of this collaboration, the General Directorate of Land Registry and Cadastre and the General Directorate of Forestry together with the participation of the private sector completed the forest cadastre of 6,246,845 hectares in eight years between 2010 and 2017. Moreover, the registration of 82.52% of these lands was completed. Besides, solutions were proposed for other countries experiencing the same problem within the framework of the United Nations Sustainable Development Goals.

1. INTRODUCTION

The latest data covering the forest assets in Turkey was published in 2015. The area of the forest lands was stated to be 21,537,091 hectares in 2010. This figure was stated as 22,342,935 hectares in 2015 (TFA 2019). According to the forest cadastre works completed in 2017, the area of the forest lands was found to be about 24,000,000 hectares.

According to the General Directorate of Forestry (GDF) Strategic Plan 2010-2014, the ownership of 99% of the forests in Turkey belongs to the state. The forest lands, which cover 27.6% of the area of Turkey, have important economic, environmental, and cultural functions. About 10% of the population of Turkey lives in forest villages or the villages in the vicinity of the forests, where forest resources provide a vital contribution to the livelihood of the villagers. Urban dwellers have a growing interest in forests, particularly due to their biodiversity and environmental and social functions. (FAO 2015).

Within the framework of Goal 15 of the United Nations' 2030 Agenda for Sustainable Development Goals, several studies have been carried out to provide sufficient incentives for the protection, restoration, and promoting sustainable use of forests, sustainable management of all forest types, stopping deforestation, restoring degraded forests by rehabilitation by 2030. Moreover, the proposed solutions for the forest-related issues were brought to the agenda of the international community.

The primary condition for the proper execution of the forest regime in line with modern forestry principles is the demarcation of the boundaries of the lands considered forests and their cadastre (Çağlar 2004). Forests are subject to registration in accordance with Article 11 of Forest Law No. 6831. The land is registered with the attribute of "forest" in the name of the Treasury. The registration can only be made after the completion of the forest cadastre. Forest cadastre covers the demarcation of the boundaries of the forests, the

* **Orhan Ercan**

*(drorhanercan@yahoo.com) ORCID ID 0000-0001-5231-8692
(nktoker@tkgm.gov.tr) ORCID ID 0000-0002-7823-1269

Research Article / DOI: 10.26833/ijeg.927502

Cite this article

Ercan O & Toker N K (2022). Assessment of the completion of the forest cadastre considering the legal grounds, collaboration, and the use of technology: The case of Turkey. International Journal of Engineering and Geosciences, 7(1), 49-58

Received: 25/04/2021; Accepted: 17/05/2021

application works for the previous forest demarcation or cadastral operations following the new legislation, and registration of the lands whose boundaries are determined by the implementation of Article 2 of the Forest Law to the land registry system. The lands where the forest cadastre works and the application works were recently completed should be registered to the land registry system after solving the problems arising from the registration legislation of the General Directorate of Land Registry and Cadastre (GDLRC) and those arising from the private registered properties within the forest boundaries (GDF Strategic Plan 2013-2017).

In Turkey, the modern forest cadastre works started in 1937, when Forest Law No. 3116 entered into force. It was observed that forest demarcation and forest cadastre works were addressed in separate articles in the relevant Law. Article 10 of the Law stipulated that the forest demarcation works should be completed within five years. while Article 21 of the same Law stipulated that the cadastral works should be completed within 10 years. However, the forest cadastre works could not be completed until today due to various problems encountered in the implementation of this Law and its related regulations (Gençay 2012; GDF Strategic Plan 2010-2014).

The fact that the forest cadastre and ownership problems have not been resolved yet were based on the following reasons: property cadastre and forest cadastre works being carried out by different authorities (Ayanoğlu 1992; Anbar 2004; Gençay 2012); rural cadastre works being carried out faster than forest cadastre works due to these difficulties in forest demarcation (Ayanoğlu 1992); the relations between the administration and the local people negatively affected due to ownership disputes in many places; carrying out forestry activities in areas whose boundaries have not yet been demarcated; intensive political and social pressures; frequent amendments in legislation; insufficient number of staff; lack of expert staff; deficiencies in technology transfer and applications; that the economic, social, and educational status of the forest villagers are lower; that the forestry activities are open to nature; that the administration traditionally has centralized and instruction-oriented approaches; that the forest villagers constitute the economically poorest part of Turkey and they are generally forest-dependent for their livelihoods, etc. (GDF 2006).

On the other hand, the following solutions were proposed to ensure the protection and the safety of the forest assets: demarcation of the forests and registering them to the land registry system as soon as possible; facilitating the registration of the previous forest cadastre, which could not be registered to the land registry system, by cadastral renewal and update works (Köktürk 2004; Anbar 2004) carrying out property cadastre and forest cadastre works by a single administration (Anbar 2004); establishment of Forest Cadastre Information System (Köktürk 2004), and using modern technologies (Yalçın 2012; Livia et al. 2012).

The completion of the forest cadastre has become a corporate policy of the GDF. Also, this policy was included as a strategic goal in the annual reports and strategic plans of the institution. Annual Report 2011 states that it was aimed to complete the demarcation and cadastral procedures of all forest lands by the end of 2014, as well as, to complete the land registry procedures of the forest lands whose cadastre was completed and finalized. Moreover, it was stated that completing the forest cadastre procedures and registration of these lands to the land registry system was set as the ultimate goal in the Annual Report 2015 and Annual Report 2017 of the institution. On the other hand, in the GDF Strategic Plan 2010-2014, the goal was stated as completing the forest cadastre by the end of 2014. The issue was addressed in the GDF Strategic Plan 2010-2014 as the completion of the demarcation and cadastral procedures of the forest lands, as well as, the completion of the land registration procedures of the forest lands whose cadastre was completed and finalized. It was also stated that significant legal and technical infrastructure works had been completed. The GDF Strategic Plan 2010-2014 stated the strategic goal as the complete elimination of the forest cadastre issue together with GDLRC by using state-of-the-art technologies at the end of the plan period. Moreover, the establishment of a "Forest Cadastre Information System", where all digital and textual data about the permits granted for the lands considered forest and not forest were kept together, was also included in the goals of the GDF.

In a study on the factors that delayed the forest cadastre works and the solution of forest cadastre issue, Gençay (2012) stated that lack of coordination between institutions, insufficient attention paid by the administration, shortage of trained personnel and equipment were the most significant factors among others. However, the most significant conclusion of this study was that the problem could be solved by facilitating the collaboration of the institutions.

The present study evaluates the organizational structures, legal infrastructures, the uses of technology of GDLRC and GDF in terms of collaboration within the scope of the solution of the forest cadastre issue, examines the solution methodology, reveals the results of the implementation of the method, offers suggestions for the joint projects between institutions.

2. INSTITUTIONS AND THEIR DUTIES

2.1. The General Directorate of Forestry

The first initiatives in the forestry sector in Turkey started in 1839. In 1924, the Ministry of Agriculture was established and the GDF was affiliated. Forestry activities were carried out by GDF, which was affiliated with various ministries until today. GDF was affiliated with the Ministry of Agriculture and Forestry as per the Presidential Decree No. 4 dated 2018.

GDF carries out the forest cadastre activities through the Department of Forest Cadastre and Ownership. The major duties of the Department of Forest Cadastre and Ownership can be listed as follows: performing forest cadastre procedures; carrying out works and procedures regarding the determination and evaluation of the areas taken out of forest boundaries; settlement of various disputes regarding state forests; carrying out works and procedures regarding the inspection and control of

forests belonging to parties other than the state; carrying out works for granting permission, usufruct, and easement for forest areas; following up and finalizing the land registry procedures of the lands for which the forest cadastre works are completed, etc.

2.2. General Directorate of Land Registry and Cadastre

The First Land Registry Organization was established in 1847, and it served under various names until 1923 when the Turkish Republic was declared. In 1924, the "General Directorate of Land Registry" was established, and the cadastre branch was added in 1925. GDLRC, which attained its current organizational structure in 1936, was affiliated with the Ministry of Finance, then it was affiliated with the Ministry of Justice in 1939. GDLRC had been affiliated with the Prime Ministry in 1951 and served 51 years in this organization until it was affiliated with the Ministry of Public Works and Settlement in 2002. Finally, it was affiliated with the Ministry of Environment and Urbanization in 2011 and has been providing service under this Ministry.

The Presidential Decree No. 4 dated 2018, defined the following tasks for GDLRC:

i. Carrying out cadastre procedures in Turkey and to follow up the changes,
ii. Ensuring renewal and updating of the cadastre plans and performing the related control and auditing services;
iii. Ensuring the reliability of land registries, which is under the responsibility of the state, regularly,
iv. Performing all kinds of contractual and non-contractual registration transactions related to real estates,
v. Following up and controlling the changes on the registers,
vi. Ensuring the protection of records and documents by archiving,
vii. Establishing a geodetic network, spatial information system infrastructure, and map production monitoring centre for the production of large-scale cadastral and topographic maps.

3. LAWS AND REGULATIONS ON FORESTRY

3.1. Laws and Regulations on the Forestry Procedures

Land Law dated 1858, which was the first regulation on forests, stated that forests were public property and could not be subject to private property. On the other hand, Article 24 of the Forest Regulations dated 1870 prohibited the acquisition of the state-owned forests and forests specific to villages and towns through prescription.

The regulations on the forests are inspired by the principles of protection of forests and ensuring their sustainability, governance, and execution of the forest regime by the State, and demarcation of the forest boundaries within this framework. During the Republic period, forestry regulations were made after the Civil Code, which entered into force in 1926. The first comprehensive regulation on forestry was Forest Law No. 3116 dated 1937. This Law aimed to demarcate the boundaries of the State forests, to survey the forest lands and register them to the land registry system, and to complete these procedures within 5 years. The task of demarcation and mapping of the forests was assigned to the Forest Cadastre Commissions affiliated with the GDF. The "Regulation on the Demarcation and Registration of Forests" entered into force as the technical principles for the demarcation of the forests. The demarcation of the state-owned forests could not be completed in 5 years due to several challenges in terms of surveying, etc. According to the provisions of Law No. 4785, which entered into force in 1945, all forests belonging to real or legal persons were expropriated.

Law No.5653 and Law No. 5658, which were entered into force in 1950, amended the regulations. According to these laws, the forest lands that were subjected to private ownership in the forest demarcation/cadastre works carried out until 1945, were taken out of forest boundaries. With Law No. 6831 dated 1956, the term “forest” was defined, the lands that could not be considered forest were determined, and forests were classified in terms of their ownership and management.
The prerequisite for the sustainability of the forest regime is the demarcation of the forest boundaries, performing the cadastral works, and securing it by registering it to the land registry system. With the Constitution of 1961, the principle that the ownership and management/operation of the forests would be carried out by the Government has become the basic principles of the Forest Law for the protection and sustainability of the forests. Article 131 of the Turkish Constitution of 1961 ruled that the areas that scientifically and technically lost their forest character before 15 October 1961 should be taken out of forest boundaries.

Turkish Constitution of 1982 assigned the duty of protecting forests and expanding forest lands to public institutions. The Constitution ensured that the ownership of forests belonging to the state could not be transferred. However, the following areas were allowed to be taken out of forest boundaries:

i. The lands on which preservation of forest would be of no scientific and technical benefit, even converting them into agricultural lands would provide certain benefits,
ii. The lands that scientifically and technically lost their forest character before 31 December 1981, and determined to be suitable for various agricultural purposes such as farmland, vineyard, garden, orchard, olive grove, or livestock purposes,
iii. The residential areas where city, town, or village buildings exist together.

As can be understood from Article 169 and Articles 170 of the Turkish Constitution of 1982, the forests that are guaranteed by the Constitution and the shrinkage of which are prohibited are subject to registration.

Forest demarcation is the delimitation works carried out within the scope of Forest Law No. 3116 dated

08.02.1937. The Forest Cadastre means the determination of all real estates in the forests and adjacent to forests, and the common boundaries of the forests, as well as, the registration of these forest lands with the ownership of the Treasury (the works carried out within the scope of Forest Law No. 3116, Forest Law No. 6831, and Article 4 and Additional Article 5 of the Cadastre Law No. 3402). Taking out the areas that scientifically and technically lost their forest character in the name of Treasury (i.e. execution of Article 2/B) is also a part of forest cadastre.

With Forest Law No. 3116 dated 01.07.937, the works for demarcation (delimitation) and mapping of the forest lands were started by GDF (via the Forest Cadastre Commissions). Forest Law No. 3116 was repealed, and Forest Law No. 6831 dated 08.09.1956. With the new law, Forest Cadastre Commissions continued to the forest cadastre works for the forest lands belonging to the state, the forests that had been previously demarcated as forest but taken out of forest boundaries during the last demarcation even though it was forest land, the forests belonging to the public institutions with a legal personality, the private forests, as well as, determination of the common boundaries of all real estates in the forests and adjacent to forests.

On the other hand, with the "Law No. 1744 on the Amendment of Some Articles of the Forest Law No. 6831 and Adding a Provisional Article to this Law", which entered into force on 04.07.1973, the lands that scientifically and technically lost their forest character before 15 October 1961 began to be taken out of forest boundaries as stipulated by Article 131 of the Turkish Constitution of 1961.

With Law No. 2896 dated 23.09.1983 which amended Forest Law No. 6831, the lands that scientifically and technically lost their forest character before 31 December 1981 were continued to be taken out of forest boundaries for the settlement of all or part of the inhabitants of the villages located in the forest lands or allocation for these purposes after reclamation works carried out by the Government as stipulated by Article 169 and Article 170 of the Turkish Constitution of 1982.

With Law No. 3302 dated 05.06.1986, which also amended Forest Law No. 6831, the procedures of taking an area out of forest boundaries were carried out together with the demarcation works for the first time in forest cadastre.

The Forest Laws stipulated that technical works such as surveying and mapping during forest demarcation/cadastre would be carried out by the Forest Cadastre Commissions. However, there was no "survey engineer" in these commissions. Therefore, the forest maps prepared during the demarcation/cadastre works following Forest Laws were not produced under the responsibility of a survey engineer until 2003. Most of the forest maps produced until this year could not be registered to the land registry system due to the lack of technical quality. The forest maps that were registered directly to the land book without undergoing technical control by the cadastre directorates, also posed problems as they contained technical deficiencies.

Due to the need for legal regulations in this context, the following provisions have been introduced with the "Law on Amending the Forest Law" No. 4999 dated 18.11.2003:

i. Technical errors detected in the lands whose cadastre procedure has been finalized shall be corrected by the Forest Cadastre Commissions,
ii. Taking aerial imagery and map production works required for cadastre and other forestry services shall be carried out by GDF,
iii. For the lands where forest demarcation or cadastre works are completed and finalized by the announcement, in case of an issue detected in terms of the acreage and technical errors arising from surveying, drawings, and calculations, except for the change of classification and ownership, these errors shall be corrected by Forest Cadastre Commissions under the notice and supervision of GDF,
iv. The correction shall be announced following Article 10 of the Law, in case of no lawsuit is filed with the civil court of peace within thirty days from the date of the announcement, the correction shall be finalized.
v. The lapse of time stipulated in Article 11 shall not be applied to the corrections,
vi. Survey and cadastre engineers shall be responsible for surveying, calculating, drawing, and application work in the preparation of the maps of forests whose cadastre is completed, and these maps, which are produced following the cadastral technical standards, shall be approved by the head of the commission after the control by the survey and cadastre engineers.

With Law No. 6292 dated 19.04.2012, an additional paragraph was added to Article 10 of Law No. 6831. This paragraph states that “Surveying, calculation, drawing, and application works for the preparation of maps of forests whose cadastre works are completed or ongoing shall be carried out by survey and cadastre engineers or technicians; the responsibility shall belong to the survey and cadastre engineers; a control engineer shall be assigned by the local directorate of GDLRC to ensure that the surveying and mapping procedures conducted in the field are carried out duly and to control and approve these works; the maps, which are produced following the cadastral technical standards, shall be approved by the head of the commission after the control approval of the survey and cadastre engineers”.

Law No. 7139 dated 19.04.2018 also amended the Forest Law No. 6831. This amendment states that the Forest Cadastre Commissions shall be organized with a head of a forest engineer appointed by GDF and three members including a forest engineer, or a forest technician in case of their absence, an agricultural engineer, or an agricultural technician in case of their absence, and a representative to be notified by the municipal committee in the towns and by the village head (mukhtar) in the neighbourhoods and villages. Also, Article 10 of Law No. 7139 amended the seventh clause of Paragraph 7 of Article 9 of the Forest Law No. 6831. This amendment stipulates that the correction shall be finalized in case of no lawsuit is filed to the cadastral

courts or courts responsible for the cadastral cases where there are no cadastral courts for the cancellation of the correction within thirty days from the date of the announcement.

3.2. Laws and Regulations on Land Registry and Cadastre Procedures

GDLRC, which is affiliated with the Ministry of Environment and Urbanization, has been carrying property cadastre procedures since 1925 until today as per the following laws: Cadastre Law No. 658 dated 1925, Cadastre and Land Registration Law No. 2613 dated 1937, Land Registration Law No. 5602 dated 1950, Land Registration Law No. 509 dated 1964, Law No. 766 dated 1966, and Cadastre Law No. 3402 dated 21.07.1987; however, Law No. 2613 and Law No. 766 were repealed upon need.

As per Law No. 2613 dated 1934, demarcation of the forest lands and their cadastre were excluded from the scope of the cadastral procedure of the real estates located in the central municipalities of the provinces and districts.

The Land Registration Law No. 5602 dated 1950, and the Land Registration Law No. 766, which entered into force in 1966 and was in force until 10 October 1987, were introduced to establish the land registration stipulated in the Civil Code. These laws stated that they could not be applied in forest lands. Article 2 of the Land Registry Law No. 766 stipulates that " Unclaimed lands that are not suitable for agriculture and unclaimed rocks, hills, mountains with the same character, and the lands deemed forests under the Forest Law shall not be subject to registration". Therefore, the forests that have not yet been subjected to forest cadastre by GDF were excluded from the scope of the cadastral finalization works carried out by GDLRC until Law No. 3402 dated 1987.

However, because the boundaries of the forest lands were not certain, several objections were made about the finalization of those lands, the works dragged on; as a result, the required efficiency could not be achieved. Therefore, a meeting was held with the participation of the representatives of the State Planning Organization (SPO), GDF, and GDLRC to overcome the problems in the demarcation of the forest boundary and ownership of real estates in these lands, to accelerate the work by taking joint administrative and technical measures, and to improve the work efficiency. As a result of this meeting, a protocol was signed between GDLRC and GDF on 18.03.1965. Then, GDLRC published the circular numbered 4-1-1-7.1391 and dated 09.07.1965. In this circular, the works to be carried out and the measures to be taken by both institutions regarding the forest lands in the villages to be subjected to the rural cadastre were explained.

The Cadastre Law No. 3402 was introduced in 1987 to complete cadastral works quickly and without interruption and to prevent unnecessary financial losses and waste of labour by causing duplicate works with different practices carried out by various institutions. Article 4 of Law No. 3402 stipulated the following provisions:

i. In case of forest land that is not demarcated or subjected to forest cadastre in the cadastral area, the situation shall be reported to GDF two months before starting the cadastral work,
ii. The procedures of forest demarcation and taking areas out of forest boundaries shall be carried out by forest cadastre commissions as per Forest Law No. 6831. Forest cadastre commissions shall finalize the procedures and mark them on the map and deliver them together with their records to the cadastral teams.
iii. Cadastre teams shall complete surveying and mapping works of these lands based on the above-mentioned boundaries,
iv. In case the forest boundaries cannot be demarcated by the forest cadastre commissions within two months, the boundaries of the cadastral area shall be determined by the cadastral teams,
v. In the places finalized and announced by the cadastral teams in this way, the forest cadastre procedures shall be deemed to have been completed, these boundaries shall be strictly observed in places where the forest cadastre is finalized.

This practice continued until 2005 when a new regulation was introduced on this issue. In 2005, with the amendment made in Article 4 of the Cadastre Law No. 3402, the following provisions were stipulated:

i. In case there is forest land in the cadastre project area and the forest cadastre per Forest Law No. 6831 has not been started, the cadastral team shall carry out the forest cadastre and determine the common boundaries of all kinds of real estates in these forests and adjacent to these forests and finalize them.
ii. In these works, at least one forest engineer to be assigned by the provincial organization of the GDF and an agricultural engineer to be assigned by the Agricultural Directorates shall participate in the cadastral team within seven days from the notification.
iii. In case the village head (mukhtar) and expert witness do not participate in these works, the works shall be continued ex officio,
iv. In the examination of the objections made about the forest, a forest engineer to be assigned by the provincial organization of the GDF and an agricultural engineer to be assigned by the Agricultural Directorate, who have not taken part in the finalization work subject to objection, shall participate in the cadastral commission,
v. The demarcation of the forests in the cadastre project area and their finalization shall be made by this team, and it shall be partly announced for thirty days.
vi. The forest cadastre in these places shall be deemed to have been made, and these boundaries shall be followed exactly where the forest cadastre is finalized.

The additional Article 5 added to the Cadastre Law No. 3402 in 2013 stipulated that the forests that were not demarcated or did not undergo forest cadastre within the project areas where cadastre or rural cadastre works were completed should be subject to cadastre within the framework of the principles stated in Articles 4 and 39.

The following provisions were introduced with the paragraphs added to Article 4 of the Cadastral Law No. 3402 in 2018:

i. In case of detection of incompatibility between records, sheet, and ground requiring correction in forest maps that are finalized after forest demarcation or cadastre, regardless of whether it is registered to the land registry system or not, the cadastre team to be formed with the participation of at least one forest engineer to be assigned by the related forestry directorate and a control engineer or engineer to be assigned by the cadastre directorate as per Article 3 of this Law shall apply the boundary points and lines of the forest to the ground based on the forest cadastre records,
ii. The detected incompatibility shall be corrected following the technical regulations by the abovementioned cadastral team organized; at the end of the work, a report shall be prepared, and this report shall be signed together by the team members and the forest and cadastre engineers.
iii. The correction procedure shall be finalized following the announcement to be made as per Article 11 of this Law,
iv. Provided that GDLRC obtain the approval of the Ministry with which it is affiliated and the costs of such works are paid by GDF to the account of GDLRC Revolving Fund, GDLRC may also have some or all of the technical parts of such works done by natural or legal persons by way of tenders, and these tenders shall allow making commitments for the next years.

4. USE OF TECHNOLOGY

In the forest cadastre works, compass tacheometry method (1937-1964), photogrammetric method (1965-1982), terrestrial surveying methods (1982), and GPS method (1998) were used from past to present (Döner and Özdemir 2016).

As per Law No. 6831, theodolites were started to be used in the forest cadastre works after 1960 (Tüdeş and Bıyık 1997). In the survey method, the starting point was selected from certain points; however, the sequential boundaries of the forests, instead of the district boundaries, were taken this time. To complete the surveying of the boundaries of the forest more quickly, the angles were measured using a theodolite in grades, and distances were measured using a levelling rod in the traverse surveying according to those days' technology. The polygonal chains obtained were not connected to the national triangulation network. A specific point of the village or town, such as a mosque or a school, was taken as a reference, and the boundaries were ditched in the field; however, they disappeared over time. The collapse or displacement of buildings, which were deemed fixed and stationary points, did not often allow the demarcation map correctly to the ground (Ayanaoğlu 1992). This method was abandoned after using aerial photographs in mapping.

Then, the Photogrammetry Method, which is defined as "Photo interpretation and manual marking of forest lands into aerial photographs with 60% overlapping under stereoscopic view", was used. The aerial photographs marked in this way were evaluated using photogrammetry devices and transferred to 10K-scale maps obtained from 25K-scale standard topographic maps by using photomechanical methods. Later, this method, which aimed to demarcate the boundaries of forests quickly, brought about the issue of producing maps without technical quality.

The above-mentioned method was also used in the "Forest Cadastre" works within the scope of Law No. 1744. In addition to this method, the forest cadastre works were carried out using the images of 5K-scale Standard Topographic Maps and Standard Topographic Cadastral Maps showing integrity with the land in places where these maps were already produced. Also, the forest cadastre works were carried out by marking the parcels surveyed using the terrestrial surveying method on 10K- and 5K-scale maps.

All of the above-mentioned methods were abandoned as of 1983. Moreover, the principle of performing forest cadastre works using the terrestrial surveying method has been adopted since then. In case the forest cadastre or forest demarcation was to be re-marked (application) on the ground, it was suggested as the main principle that the work would be renewed by using the same technique and tools that had been used in the previous work.

The Technical Circular on the Forest Cadastre, which entered into force in 1997, aimed to ensure unity and solidarity in the forest cadastre works and procedure, implementation of Article 2/B of the Forest Law No. 6831, and implementation of Article 4 of the Cadastral Law No. 3402. In this framework, the terrestrial surveying method was used as the main surveying method to demarcate the borders of the forests. However, the use of aerial photographs was permitted if they complied with the principles specified in the Regulation on the Production of Large-Scale Maps. Moreover, the Circular dated 2014 allowed the use of the GPS method in surveys. Now, the Regulation on the Production of Large-Scale Maps and Map Information and the current "Technical Circular on the Forest Cadastre" are followed in the forest cadastre works.

5. SOLUTION METHODOLOGY

5.1. Collaboration

GDLRC has started the initial cadastre works in 1925, and GDF has started the forest cadastre works in 1934. However, the performance of the cadastre works by two institutions has brought about several problems since then.

Several problems were faced in the registration of the forest maps produced by the Forest Cadastre Commissions since they did not employ a survey engineer and these maps did not comply with the

technical standards. Therefore, some of the forest cadastre works could not be registered by GDLRC. Another problem was that the technical errors could not be corrected by GDF without a judicial decision (as well as the lack of a legal regulation on this issue).

Another issue was that the number and the organization of the teams and the cadastral activities (initial cadastre and forest cadastre activities) of both institutions were different. Therefore, the works could not be carried out synchronously, which caused duplications.

Two actions were taken to eliminate these problems. Firstly, employing a survey engineer to the forest cadastre commissions was decided to eliminate the technical errors in the forest maps under the responsibility of the survey engineer. However, the number of forest cadastre commissions was another issue even they were supported by employing a survey engineer. Therefore, the second effective formula was decided to increase the number of forest cadastre commissions to facilitate completing the forest cadastre works throughout the country. The best formula to solve this problem was the combination of the resources of GDF, as an expert institution in forestry, and GDLRC, as an expert institution in mapping. It was concluded that the collaboration environment should be provided for both institutions to carry out this work together.

Thus, carrying out the works with an understanding of 'collaboration' by mutual transfer of resources and staff (assignment) was decided to be an effective solution. Therefore, several fundamental and radical amendments were made in both Forest Law No. 6831 and the Cadastre Law No. 3402 in 2003, 2005, 2013, and 2018. These amendments could be considered reforms required for the needs of the time.

5.2. Establishment of the Legal Infrastructure

Until 2003, the Forest Laws stipulated that technical works such as surveying and mapping in the forest demarcation/cadastre should be carried out by the Forest Cadastre Commissions. Since these commissions had no "survey engineer" within their organizations, the forest maps were prepared according to forest demarcation/cadastre, which was not carried out under the responsibility of a survey engineer. Moreover, since most of these maps lacked technical accuracy, several challenges were faced in the registration. Law No. 4999 on the Amendment of the Forest Law dated 18.11.2003, stipulated that the correction of the technical errors detected in the finalized cadastre should be carried out by the Forest Cadastre Commissions for the solution of this problematic issue (for the lands where forest demarcation or cadastre works are completed and finalized by the announcement, in case of an issue detected in terms of the acreage and technical errors arising from surveying, drawings, and calculations, except for the change of classification and ownership).

After the first step was taken for correcting the technical mistakes in forest maps, a further step was taken in 'collaboration'. This time, Article 3 of Law No. 5831 dated 15.01.2009 stipulated the following provisions: "In the places where cadastre works started as per Cadastre Law No. 3402, in case of acreage errors arising from the calculations is detected during the control of the previously finalized forest maps, these errors shall be corrected by the cadastral team formed as per Article 4 of the Law No. 3402. In case of other issues in terms of the acreage and technical errors arising from surveying, drawings, and calculations, except for the change of classification and ownership, the Cadastral Directorate shall report the issue to the local forest directorate. A forest cadastre commission shall be assigned within 15 days from the date of notification and the correction shall be announced".

Then, Paragraph 10 of Article 11 of Law No. 6292 dated 19.04.2012 was repealed by Article 54 of Law No. 7139 dated 19.04.2018. Also, as per Article 35 of this Law, Paragraph 13 and Paragraph 14 were added to Article 4 of Law No. 3402. These paragraphs stipulated the following provisions:

i. "In case of detection of incompatibility between records, sheet, and ground requiring correction in forest maps that are finalized after forest demarcation or cadastre, regardless of whether it is registered to the land registry system or not, the cadastre team to be formed with the participation of at least one forest engineer to be assigned by the related forestry directorate and a control engineer or engineer to be assigned by the cadastre directorate following Article 3 of this Law shall apply the boundary points and lines of the forest to the ground based on forest cadastre records,
ii. The detected incompatibility shall be corrected following the technical regulations by the above-mentioned cadastre team to be organized; at the end of the work, a report shall be prepared, and this report shall be signed together by the team members and the forest and cadastre engineers. The correction procedure shall be finalized following the announcement to be made as per Article 11 of this Law,
iii. Provided that GDLRC obtain the approval of the Ministry with which it is affiliated and the costs of such works are paid by GDF to the account of GDLRC Revolving Fund, GDLRC may also have some or all of the technical parts of such works done by natural or legal persons by way of tenders, and these tenders shall allow making commitments for the next years.

Thus, the technical errors in forest maps could be corrected by the forest cadastre commissions, as well as, by the cadastre team to be formed by GDLRC with the participation of a forest engineer from the GDF and a control engineer from the cadastre directorate.

An additional paragraph was added to Article 10 of Law No. 6831 as per Article 13 of Law No. 6292 dated 19.04.2012. This additional paragraph states that "Surveying, calculation, drawing, and survey applications for the preparation of maps of forests whose cadastre works are completed or ongoing shall be carried out by survey and cadastre engineers or technicians; the responsibility shall belong to the survey and cadastral engineers; a control engineer shall be assigned by the

provincial directorate of GDLRC to ensure that the surveying and mapping procedures conducted in the field are carried out duly and to control and approve these works; the maps, which are produced following the cadastral technical standards, shall be approved by the head of the commission after the control approval of the survey and cadastre engineers".

Moreover, an additional paragraph was added to Article 10 of Law No. 6831 as per Article 13 of Law No. 6292. This additional paragraph stipulated that "Surveying, calculation, drawing, and application works for the preparation of maps of forests whose cadastre works are completed or ongoing shall be carried out by survey and cadastre engineers or technicians; the responsibility shall belong to the survey and cadastre engineers; a control engineer shall be assigned by the local directorate of GDLRC to ensure that the surveying and mapping procedures conducted in the field are carried out duly and to control and approve these works; the maps, which are produced following the cadastral technical standards, shall be approved by the head of the commission after the control approval of the survey and cadastre engineers".

Collaboration between the two institutions can be achieved in two ways. In the first option, in case the technical errors in forest maps are corrected by forest cadastre commissions, a control engineer from GDLRC may involve in the correction procedure. In the second option, in the forest cadastre works to be carried out by forest cadastre commissions, the surveying, calculation, drawing, and application work for the preparation of forest maps are carried out by the survey engineers or technicians to be assigned by the related cadastre directorate.

GDLRC has been carrying out forest cadastre during the initial cadastre works since 2005 (Article 4 of Law No. 3402). Moreover, GDLRC has been carrying out forest cadastre for the forest lands that were not finalized during the initial cadastre works completed in the villages or quarters since 2013 (Additional Article 5 of Law No. 3402). In these works, a forest engineer from GDF and an agricultural engineer from the agricultural directorate participated in the cadastre team.

5.3. Use of Technology

The amendments made to the laws in 2004 and 2005 introduced radical changes in both forest cadastre and general cadastral activities carried out by GDLRC. With these changes, the task of demarcating the forest boundaries in places that did not undergo cadastre was assigned to the GDLRC cadastre teams. It was stipulated that at least one forest engineer from the GDF and an agricultural engineer from the agricultural directorate should be assigned to these teams. Thus, GDF personnel participated in the cadastral works carried out by GDLRC in 3,000 villages since 2006 as per Law No. 3402.

GDF established GPS Teams in 8 Regional Directorates of Forestry for supporting all Forest Cadastre Commissions, densification of the triangulation network, and digitization of forest cadastral maps. Also, a control system based on a database was developed and put into practice. Moreover, a geographic information system-based map server was also put into service for the first time on a portal on the official website of GDF. Technical Circular on Forest Cadastre was prepared again to harmonize sub-regulations in line with the amendments in the laws considering the current techniques and technologies specified in the amended Regulation on the Production of Large-Scale Maps and Map Information in 2005.

As of 2014, great progress has been achieved by adopting the following approach in the Technical Specification for the Production of Forest Maps: "All kinds of coordinates shall be produced based on the latest version of Turkish National Fundamental GNSS Network (TUTGA), and 1/5000 scale digital photogrammetric vector maps and orthophotos shall be georeferenced with the Universal Transverse Mercator (UTM) projection with 3-degree zones using GRS80 ellipsoid and ITRF96 Datum. The digital data to be produced shall meet the standards specified in the relevant articles of the Regulation on the Production of Large-Scale Maps and the draft Regulation on the Production of Large-Scale Maps and Map Information.

On the other hand, GDLRC used the Regulation on the Production of Large-Scale Maps and the circulars published by the institution on the GNSS (Global Navigation Satellite System) surveying, calculation, and control, which are not addressed in the regulation.

With the widespread use of the CORS-TR (Continuously Operating Reference Stations) project, both institutions began to use it in 2009. Since CORS-TR has become the national fundamental infrastructure in geospatial projects, it has been widely used by all institutions and organizations. Also, geographical information systems applications have been widely used for creating the spatial data infrastructure in both institutions. With these technological developments, both GDLRC and GDF began to produce and share digital geospatial data.

6. RESULTS

Several significant factors caused the problems experienced for years in forest cadastre. The first factor was that the cadastre was classified as forest cadastre and property cadastre, and they were carried out by different institutions. The second factor was the technologies used in the cadastre works; although they were widely used in those days, they were obsolete today. Another factor was the complex structure of regulations due to frequent amendments due to needs.

The solution to the problem was achieved by giving priority to the completion of the property cadastre for meeting the investment priorities for the development of the country and the evolving needs with the conditions of the day, as well as, to solve the ongoing problems about forest lands and other property problems that arose in the following years due to these problems (such as ownership, acquisition, possession/occupation, real estate boundaries belonging to real persons, as well as, disputes about the property boundaries, zoning, settlement, land consolidation, energy projects, dam construction, infrastructure, agriculture, pasture, Article

2/B applications, renewal, technical error correction, etc.).

Forest cadastre was carried out by cadastre teams following Article 4 of the Cadastre Law No. 3402 during the initial cadastre, which was carried out following this Law. Then, it was carried out by forest cadastre commissions following Forest Law No. 6831.

As per Law No. 6495, Additional Article 5 was added to Law No. 3402. With this amendment, cadastre teams (with the participation of a forest engineer and an agricultural engineer as stipulated by Article 4 of Law No. 3402) have begun to carry out all forest cadastre works.

The collaboration between institutions was achieved based on the idea to eventually register the forest cadastre, and the required regulation amendments were made. Within the scope of the solution methodology, the approach of the participation of the private sector in forest cadastre works was adopted for digital and quick cadastre.

Therefore, the technical parts of the cadastre works were given out by contracts to the private sector by GDLRC under the coordination of both institutions. This outsourcing approach accelerated the projects through the use of modern technology.

Table 1 shows the distribution of forest cadastre and registration completed in recent years (TFA 2019). The history of the forest cadastre in Turkey started with Law No. 3116 in 1937. By 1973, only 4,558,000 hectares of the forests could undergo cadastre procedure. Between 1937 and 2004, only 51.8% of the forests could undergo cadastre procedure, and only 19.38% of the forests could be registered. However, thanks to the collaboration between the institutions and the use of the private sector, the forest cadastre of the remaining 48.2% and the registration of 60.2% were completed between 2010 and 2017. As of 2018, the forest cadastre of 24,000,000 hectares of forest has been completed, and 19,806,000 hectares of forest were registered. Registration works continue for forests that have not been registered yet.

Table 1. Forest lands that underwent forest cadastre and were registered

Year	Acreage of the forest lands that underwent forest cadastre		Acreage of the Forest lands that were registered	
	Cumulative acreage (ha)	Increase (ha)	Cumulative acreage (ha)	Increase (ha)
1973	4,558,000	-	3,055,079	-
2004	12,446,407	7,888,407	4,653,000	1,597,921
2010	17,573,155	5,126,748	11,824,130	7,171,130
2011	17,746,416	173,261	12,188,834	364,704
2012	19,073,052	1,326,636	16,230,739	4,041,905
2013	19,175,273	102,221	16,749,736	518,997
2014	20,774,691	1,599,418	16,950,000	200,264
2015	21,240,530	465,839	17,799,940	849,940
2016	23,450,000	2,209,470	18,860,000	1,060,060
2017	24,000,000	550,000	19,500,000	640,000
2018	-	-	19,806,000	3,506*

*The data for 2018 are taken from the GDF official website.

As can be seen from Table 2, within the scope of forest cadastre studies, 538.005 hectares of land were removed from the forest and registered in the land registry according to the article 2-B of the Forest Law Number 6831 as of the end of 2018 (TFA 2019). According to the 2020 report of the National Property General Directorate, 581,000 of the registered parcels were taken out of the forest and sold to their users (NREB'20).

Table 2. Forest lands that the areas taken out of forest boundaries

Year	Acreage of the areas taken out of forest boundaries	
	Cumulative acreage (ha)	Increase (ha)
1973	-	-
2004	341.521	341.521
2010	411.843	70.322
2011	432.397	20.554
2012	439.473	7.076
2013	450.461	10.988
2014	473.081	22.620
2015	483.155	10.074
2016	502.000	18.845
2017	535.598	33.598
2018	538.005	2.407

7. CONCLUSION

Cadastre Law No. 3402 aims to determine the legal status of real estates by marking their boundaries on the ground and map according to the national coordinate system and based on the cadastral maps or topographic cadastral maps. Thus, the land registry shall be established as stipulated by the Turkish Civil Code No. 4721, and the spatial information system infrastructure shall be established. Cadastre Law No. 3402 does not classify the cadastre of the real estates as property cadastre, forest cadastre, pasture cadastre, agricultural cadastre, etc. In other words, this law aims to determine the technical and legal status of real estates through cadastre and to establish their land registry accordingly.

Collaboration was achieved between the two institutions engaged in property cadastre and forest cadastre by establishing legal and technical infrastructures within the framework of the definition of Cadastre.

Thanks to the participation of the private sector, the forest cadastre was completed in digital format and in a very short time between 2010 and 2017 at the end of the project. Moreover, the registration of 82.52% of these lands was completed. Effective and efficient use of public resources has been through collaboration. However, a major social problem was solved by making cadastre of the areas taken out from the forest and these parcels were sold to the users.

In addition to these achievements, a model compatible with the UN Agenda 2030, Digital Transformation, Sustainable Development Goals has been created. This model sets an example for other countries experiencing similar problems within the framework of Goal 15.

Author Contributions:

Orhan Ercan: Conceived the original idea, made a significant contribution to the concept and took the lead in writing the manuscript. **Kemalettin Toker**: Helped

shape the research, analysis and manuscript, discussed the results and contributed to the final manuscript.

Conflicts of interest

The authors declare no conflicts of interest.

REFERENCES

Anbar Ö A, (2004). Orman Tahdit Haritaları Doğrultusunda Tapu ve Kadastro İşlemleri (Land Registry and Cadastre Procedures in Line with Forest Delimitation Maps), HKMO Orman Kadastrosu ve 2/B Sorunu Sempozyumu, 17-18 Eylül 2004

Ayanoğlu S (1992). Genel Kadastro-Orman Kadastrosu İlişkileri Üzerinde İncelemeler (Eng: Studies on General Cadastre-Forest Cadastre Relations), Journal of the Faculty of Forestry, Istanbul University, Seri B, Cilt: 42, Sayı: 3- 4, 1992

Cadastre and Land Registration Law No. 2613 dated 1937,

Cadastre Law No. 3402 dated 21.07.1987

Cadastre Law No. 658 dated 1925,

Çağlar Y (2004). 2B Olgusunun Tarihsel ve Nesnel Boyutları (Historical and Objective Dimensions of the 2B Fact), HKMO Orman Kadastrosu ve 2/B Sorunu Sempozyumu, 17-18 Eylül 2004

Döner F & Özdemir F (2016). Orman Kadastrosu Çalışmalarında Ölçme İşleri (Surveying Works in Forest Cadastre Studies), HKMO-Mühendislik Ölçmeleri STB Komisyonu 8. Ulusal Mühendislik Ölçmeleri Sempozyumu 19-21 Ekim 2016, Yıldız Teknik Üniversitesi, İstanbul

FAO (2015), Global Forest Resources Assessment 2015, Country Report

Forest Law No. 3116 and Laws No. 4785, 5653 and 5658 Amending this Law

Forest Law No. 6831

Gençay G (2012). Orman Kadastrosunun Güncel Sorunları Üzerinde Hukuksal İncelemeler (Legal Reviews on Current Problems of Forest Cadastre), Journal of the Faculty of Forestry, Istanbul University 2012, 62 (2): 173-195

Köktürk E (2004). Orman Kadastrosu (Forest Cadastre), Jeodezi, Jeoinformasyon ve Arazi Yönetimi Dergisi, 2004/91

Land Registration Law No. 509 dated 1964,

Land Registration Law No. 5602 dated 1950,

Livia B L, Costel B, Gabriel E, Nicoleta C (2010). Implementing the Forest Cadastre by Applying the Property Law in Order to Register A Forest Plot, FORMEC 2010 Forest Engineering: Meeting the Needs of the Society and the Environment July 11 – 14, 2010, Padova – Italy

Milli Emlak Bülteni '20 (2021), Çevre ve Şehircilik Bakanlığı, Ankara, 2021 (NREB'21, Ministry of Environment and Urbanization, National Property Bulletin '20, Ankara 2021)

Orman Genel Müdürlüğü 2006 Yılı Faaliyet Raporu (General Directorate of Forestry 2006 Annual Report)

Orman Genel Müdürlüğü 2011 Yılı Faaliyet Raporu (General Directorate of Forestry 2011 Annual Report)

Orman Genel Müdürlüğü 2015 Yılı Faaliyet Raporu (General Directorate of Forestry 2015 Annual Report)

Orman Genel Müdürlüğü 2017 Yılı Faaliyet Raporu (General Directorate of Forestry 2017 Annual Report)

Orman Genel Müdürlüğü Stratejik Plan 2010 – 2014 (General Directorate of Forestry Strategic Plan 2010 – 2014)

Orman Genel Müdürlüğü Stratejik Plan 2013 – 2017 (General Directorate of Forestry Strategic Plan 2013 – 2017)

Orman Kadastrosu Teknik İzahnamesi, 2014 (General Directorate of Forestry, Forest Cadastre Technical Prospectus, 2014)

Rural Cadastre Law No. 766 dated 1966,

Tüdeş T & Bıyık C (1997). Kadastro Bilgisi (Cadastre), Karadeniz Teknik Üniversitesi Basımevi, İkinci Baskı, Trabzon

Türkiye Ormancılar Derneği-TOD, Türkiye Ormancılığı 2019 (The Foresters' Association of Turkey, TFA, Turkey Forestry 2019): Ankara, 2019, ISBN:978-975-93478-4-0 Publication No: 47

UN (2016) Transforming our world: the 2030 Agenda for Sustainable Development, Goal 15, https://sdgs.un.org/goals/goal15

Yalçın G (2012). Forest and Cadastre in Turkey and Sustainable Development, FIG Working Week 2012, Knowing to manage the territory, protect the environment, evaluate the cultural heritage Rome, Italy, 6-10 May 2012

International Journal of Engineering and Geosciences
https://dergipark.org.tr/en/pub/ijeg
e-ISSN 2548-0960

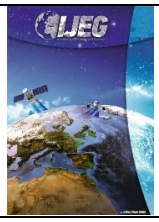

Determining the buried concrete amount using GPR/GPS combination method

Celalettin Uçar [*1], **Füsun Balık Şanlı** [2]

[1]*Turkish Airlines, Yesilkoy, Istanbul, Turkey*
[2]*Yıldız Technical University, Civil Engineering Faculty, Geodesy and Photogrammetry Department, Istanbul, Turkey*

Keywords
Concrete
GPR
NDT
EM Wave Field
GPS

ABSTRACT

This paper investigates the possibility of describing location based NDT (Non-Destructive Testing) samples for an officially finalized project of a buried concrete layer beneath the İstanbul-Millet Street, by the combination of high frequency GPR and CORS-GPS. For this purpose, field works and laboratory studies were performed. First, data acquisition was carried out over the asphalt surface along the construction route of the street. Reflected/scattered electromagnetic wave fields was studied over the processed radargram of the concrete layer. Hence, the upper and lower boundaries of buried concrete layer were determined as a value of depth and coordinate based on spatial dataset, where there was no information about the current amount of constructed concrete. According to the measurement results, the marked location of reflected/scattered wave field on the processed radargrams defined the newly constructed concrete layer. The vertical distance between upper and lower boundaries of the layer defines the thickness of concrete layer. All types of buried layers such as C-25 road concrete, plaster or asphalt have been extracted from the entire data using the amplitude differences.

1. INTRODUCTION

GPR (Ground Penetrating Radar) is a geophysics method, which is used in searching objects in shallow depth of Earth layers. In the light of the developments in the field of electronic engineering, during the last three decades, it is now more affordable, fast, and precision measure the speed of light, which was expensive and troublesome earlier. These developments not only provided to have precise measurements of the speed of light, but also provided researchers to be able to measure all the signals that are closely moving as fast as the speed of light underground in a detail of nanometre, and made it possible to reach accurate results in shallow geophysics. These studies and improvements lead to the GPR applications. GPR was first developed to measure the thickness of the ice. By the help of seismic data acquisition techniques, data that had been measured in natural ground conditions reached to the depth of 10-20 metres. Today, GPR method is widely used in researches of shallow ground and archaeometry. GPR, which was started to be used in mining and geologic studies in the beginning of 70's, was used to investigate shallow depths in 80's giving better resolutions with the 500 MHz -1GHz antennas. In the beginning of 1990s, low (10, 20 and 50 MHz) and high (2.5-3 GHz) frequency antennas were used in the working area (Millet Street). Finally, GPR was started to be used in the fields of studies related with the mining, stratigraphy, inspection of road covering, structures, constructions and water detection etc (Alp et al. 2003).

GPR method is based on the propagation of electromagnetic waves into the ground and recording the signals of those reflected waves that are back to the radar antenna as a function of time. As the signal of the radar propagates deeper, every chemical or physical change results in a different reflection of the energy back to the surface. This procedure goes on until the energy is attenuated. Reflections that are caused by variations in the ground layers occur according to the differences of electrical and magnetic features of all the reflective layers such as rocks, sediments, soil, and various mixtures of those, and change in rocks or stratigraphic differences in intensiveness in between layers. Radar reflections are produced while radar energies are getting through all the archaeological structures and layers surrounding them. Because all the structures; cemeteries, tunnels, burials and pipes, that the radar

* **Corresponding Author**
*(ucar_c@hotmail.com) ORCID ID 0000-0002-1742-4796
(fbalik@yildiz.edu.tr) ORCID ID 0000-0003-1243-8299

Cite this article
Ucar C & Sanlı F B (2022). Determining the buried concrete amount using GPR/GPS combination method. International Journal of Engineering and Geosciences, 7(1), 59-66

Research Article / DOI: 10.26833/ijeg.876310
Received: 07/02/2021; Accepted: 05/04/2021

came across, result in changes in the spreading of the radar waves, they produce significant radar reflections. Lots of wave forms that are overlapping each other are recorded as they were one serial in the same location of different depths. That is called the radar reflection trace of that location (Van Dam and Schlager, 2000).

While the resistivity of the underground structures increase, which means a decrease in conductivity, the quality of GPR images increase as well. The area of the target implementation area of GPR should be as dry as possible. Electromagnetic waves get into a fairly more conductive area when they reach to the level of underground water level. Relative di-electric permittivity contrast occurs at this specific humid level. It also occurs a decrease in dilatation of electromagnetic waves based on the absorption in high frequency content because of the sudden increase in the conductivity of the electricity (Alp et al. 2003).

Nowadays, GPR technology is used in various fields for different purposes such as;

Geographic studies, road condition inspection, remote detection from planes or satellites, pipe and tube inspection, ground research (road, airport, dam, water canal, settlement area research), tunnel research (railways, roads, tubes, mining gallery research), structure research (ceiling, ground and wall research, restoration research), archaeological research (antic city, temples, cemeteries, walls, base, galleries, and for finding similar historic remnants), industrial waste, leakage, and environmental pollution research (finding old or off record industrial waste areas, determining leakage in factories, gas stations, and water paths; waste discharge areas), searching old or off record city underground structures (finding old sewages, water paths, tunnels, tubes, shelters, electric and phone lines), mining research in ground and galleries (searching for mining in close to ground layers and improving reserves, coal search via exiling galleries, search targeted first aid in collapsed and mining diggings). (MTA Natural Resources Economy Bulletin, 2012)

There are several studies in the literature for each topic mentioned above that uses GPR technology such as; determining stratigraphic order close to the ground (Davis and Annan, 1989), determining geological units close to the ground (Koralay et al. 2007), mapping discontinuities as geological faults and fractures (Grandjean and Goury,1999; Green et al. 2003; Kadıoğlu et al. 2008), determining carstic emptiness (Kadıoğlu and Kadıoğlu 2006), determining underwater levels (Harrari 1996; Dannowski and Yaramancı 1999; Aspiron and Aigner 1999), researching liquid hydrocarbon close to the ground (Changryol et al. 2000). Besides these; in archaeological studies, finding temples, cemeteries, walls, base, and as such historical remnants (Sambuelli, et al. 1999; Daniels 2000; Hammon et al. 2000; Kadıoğlu et al. 2008), metallic item search, determining buried tubes underground, pipe lines, water or gasoline tanks and areas of old industrial waste (Kadıoğlu and Daniels, 2008), determining robustness of roads, railways, water tunnels, tubes, wall facades in mining galleries, searching degradations of areas and ores in galleries, to determine gallery headway directions, (Cardelli et al. 2003), searching archaeological sites and contexts from investigations into Roman era burial tombs in Egypt (Shaaban et al. 2009), detecting clandestine burials (Unterberger 1992; Mellett 1992; Miller 1996; Nobes 2000; Davenport 2001; Ruffell and McKinley 2005; Morgan and Bull 2007; Schultz 2007; Schultz andDupras 2008; Billinger 2009; Novo et al. 2011; Pringle et al. 2008), determination of the influence of soil parameters and sample density (Linck and Fassbinder 2013), near surface soil water content (Moghadas et al. 2014).

The purpose of this study is to determine buried concrete level under New-Jersey* productions which is bordering Bağcılar-Kabataş Light Metro Lines in Istanbul metropolitan city. This project went out to tender as a restoration of pavement for 1.803.797,25 USD to the contractor company by İstanbul Metropolitan Municipality under the law of tender on 7/12/2011, 540 number of the ruling of the court. As production is continuous for 24 hours per day, considering the traffic jam in the specific area, there seems unsatisfactory information about night productions. Therefore, it was decided in the beginning to search the level of the concrete by providing with destructive testing samples, however, the price of the authorized company of BIMTAS was 13.135,857 USD for destructive test at intended interval.

However, the amount of the payment to the company through model profile is 16.091,426 USD. Because the certain meterage of the production is not known, paying complete through model profile is considered to be a crime of public injustice, on the other hand paying deficient or any cut will also be a crime of misconduct and prejudice the company intentionally. Therefore, by preferring Non-destructive Testing Method, GPR-GPS combination measurements were done along the 5277 m at the pavement level in the path of New-Jersey. Then the data was analysed and 511 Non-destructive Testing samples acquired for the path. By the help of this method, the real thickness of the concrete construction was determined at a very short time period compared to the destructive testing method.

The difference of this study from others is, instead of destructive testing, by using Non-destructive Testing technique with GPR-GPS combination composed of CORS-GPS integration which has ± 0,02meter precision and GPR of 1200/1600 MHz central frequency system Mala Pro-Ex Series; to uncover the truth that a public law problem could be resolved at a much shorter time (5 days) and at a much lower cost (3.251,125 USD).

1.1 Preliminary Research

The main problem of research was distinguishing the new concrete construction part from non-concrete area, and determining the amount of concrete construction. Before surveying, model profile of the project was examined in order to decide for an appropriate location of profile line for the GPR surveying design. As a result of the preliminary works, it is understood that the New-Jersey borders are situated on the left and right sight of the Bağcılar-Kabataş Light Metro route as a double row. As can be seen in Figure 1, there are three different buried layers under the New-Jersey borders as asphalt (0,08m), plaster (0,07m) and concrete (0,10m). It is seen

that the layer of buried C-16 class concrete layer is situated under the New-Jersey-asphalt and plaster (Figure 2). It was constructed on top of the C-25 class road concrete layer that already exists. So it has a variable thickness because of keeping the elevation on the road surface. When model profile of the project was studied, it is understood that concrete layer was produced as 60 cm wide, which is 15 cm wider than the New Jersey (45.5 cm wide) blocks.

As can be seen in Figure 2, it was understood that C-16 class concrete with an approximately 10 cm width is lying under the intersection line of the asphalt boundary and New Jersey border. Furthermore, the bottom depth of C-16 concrete layer is approximately 0,4 m under the surface. Because of this shallow depth, it was decided that the frequency of GPR system must be chosen as high as possible. Thus, it is aimed to differentiate C-16 concrete road layer from C-25 concrete by using the amplitude differences. After deciding on the spatial location of GPR profile, it was time to solve the second problem of the project, which was differentiation of concrete and non-concrete locations with the location based Non Destructive Testing (NDT) samples by using GPR-GPS combination methodology.

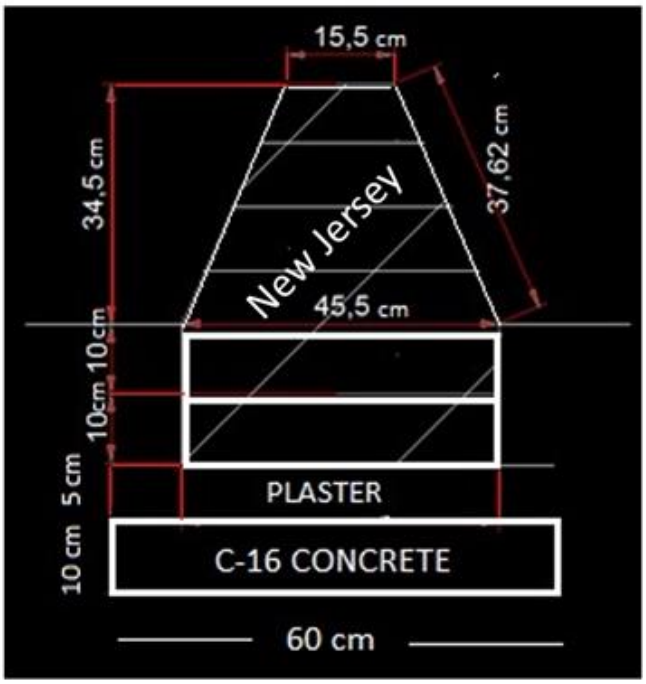

Figure 1. Model Profile of the construction project (Unit of length in centimetres)

Figure 2. New-Jersey borders and their boundaries, which used as a profile line

2. METHOD

Surveying was carried out on the Millet Street, which situated in Fatih region of İstanbul (Figure 3). The New Jersey border stone flooring construction, constructed on the boundaries of Bagcilar-Kabatas Light Metro, which was awarded and controlled by İstanbul Metropolitan Municipality with the responsibility of contractor company. According to the model profile of New-Jersey; the thickness of buried concrete layer must be 10 cm. The concrete layer was overlapped on the C-25 road concrete, to prepare a smooth surface for the flooring of New-Jersey borders. Despite the width of concrete construction is stable, the thickness of concrete could not be constructed as 10 cm that is stated in a project standard due to the variations of the elevation of C-25 road concrete layer. Since, it was a 24 hours' nonstop work, it was impossible to follow night time production by classic surveying methods such as geometric levelling, trigonometric levelling, or any other optic based surveying methods. So, the real volumetric amount of concrete construction could not be calculated.

The primary objective of the study is to detect the concrete construction whether it exists or not, and to

determine the value of concrete thickness with spatial location of detected concrete layer. In order to reach this goal, GPR/GPS combination technique was used for determining the amount of concrete and defining the coordinates of the non-destructive testing samples' position. Mala-ProEX series GPR system with a compatible 1200/1600 MHz antenna unit was integrated with Trimble R-8 series CORS-GPS system for achieving the synchronized data acquisition. Using this combined system, previously defined 36 GPR profiles are precisely positioned on the map (Figure 3).

As a result of velocity analysis, the electromagnetic wave velocity of field was measured at 0,0995 m/ns. The radargrams of the sample profiles indicating the concrete layer is depicted in Figure 4 and Figure 5.

Figure 3. Profile lines on left and right sight of the Millet Street - Fatih region of İstanbul

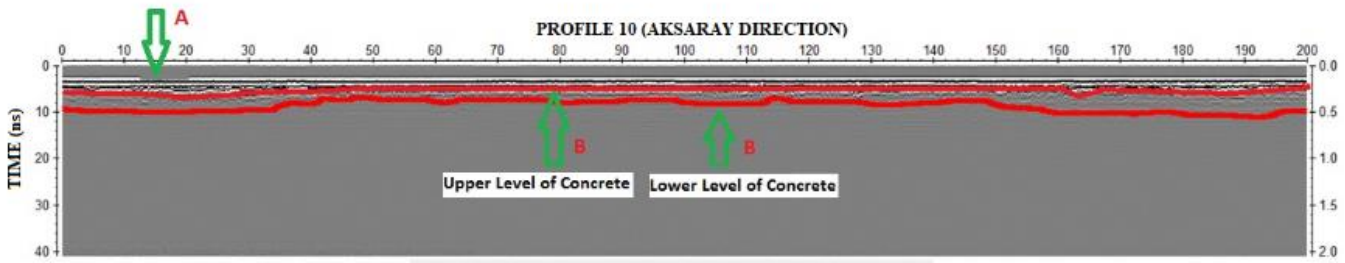

Figure 4. New concrete construction was detected on entire radargram of profile 10 - Upper and lower boundaries of the concrete layer – Amplitude Scale - Direct Propagating Wave Field (A) – Reflected/Scattered Wave Field (B)

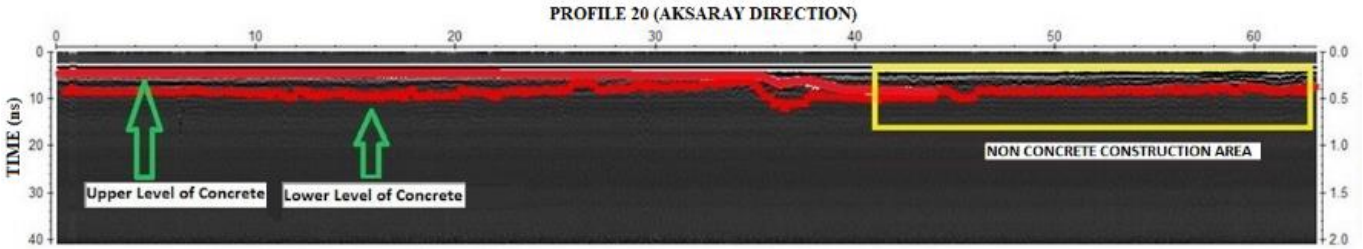

Figure 5. Boundaries of new concrete construction and non-concrete construction area shown on the radargram of profile 20

2.1. Data Processing

Reflex-Win v.3.5 (Sandmeier 2004) software was used for the collected data processing.

The order of applied data processing steps are;
1) Time Zero Correction,
2) Dewow,
3) Substracting Average,
4) Gain,
5) Frequency Band Pass,

Formations of the field generates artificial reflection anomaly deep down the surface, which has different contrast of formation. These effects were eliminated from the collected data using a special logarithmic negative amplitude functions. In this way, shadow effect of metal plumbings and equipment elements could have been removed. In final step of the data processing,

migration filter used for determining the boundaries of concrete layer. CORS-GPS unit integrated with the GPR and the GPR/GPS combination model was used for data collection Horizontal positioning error measured as ±2 cm for CORS-TR referenced GPS system. Reflex-Win software used for the data integration between GPR and GPS. As a result of velocity analysis, the electromagnetic wave velocity of concrete layer was calculated as 0,0995 m/ns.

Electromagnetic wave velocity of hyperbola was verified with super positioning with another hyperbola anomaly, which has a known velocity as mathematically.

Radargram's velocity and time period data was used to calculate the depth information as;

$$d = (v \times t)/2 \quad (1)$$

d: Distance; v: Velocity; t: Time

On the processed 2D radargrams, horizontal axis direction and vertical axis direction correspond to the distance and the roundtrip time period of the signal, respectively (Figure 4). Since the working area is one of the busiest streets in İstanbul, surveying was started at 00:30 am in 25.04.2015 assuming that the traffic density would be relatively less in the night. The surveying was delayed on 26.04.2015 for avoiding the negative effects of heavy rain on measurement result. It was started again on 27.04.2015 at 00:30 am and completed in the same day. A flashing vehicle was used as a security precaution to ensure the safety of surveying team during the period from 25.04.2015 to 27.04.2015 (Figure 6). In this study the location, size and variety information of buried layers/objects were determined from radargrams gathered using GPR and GPS data (Figure 7).

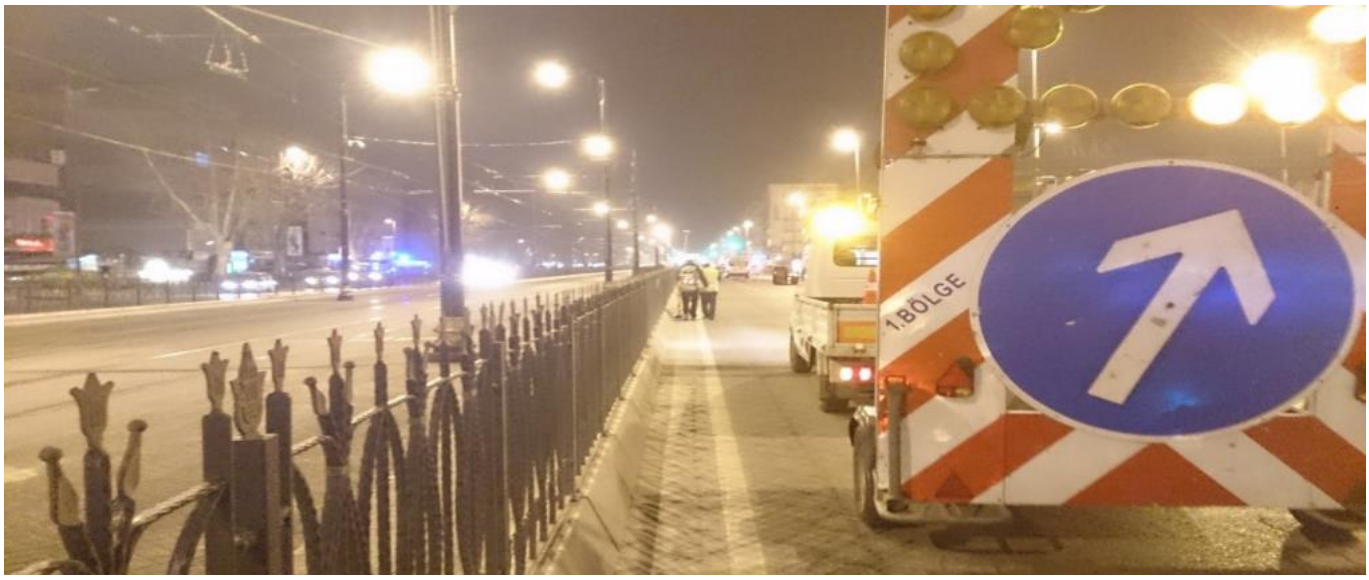

Figure 6. Flashing vehicle was used as a security precaution during the study

3. RESULTS

GPR and GPS data are used together for determination of radargrams, which obtained as a result of the study (Figure 7).

The average distance between upper and lower boundaries of concrete layer is measured on radargrams using the same amplitude value of radar trace to determine the varying thickness of concrete layer of radargrams in the processing step. The main goal of the study is determining the vertical average thickness of target object point on the concrete layer picked on the radargram. The measurements have a horizontal position error caused by the distance between transmitter and receiver antennas as theorically, however, this horizontal error in decimetre level is ignored in this study.

On the other hand, there is no vertical geometric deviation in the depth of concrete layers in different profiles i.e., same depth values were measured on the consecutive profiles on the intersection lines. Amplitude and polarity research are the most effective method ever for classifying the buried layers. If amplitude/reflected wave is positive, the polarity will be positive. If the first value of amplitude is negative, the polarity will be negative. First, electromagnetic wave's polarity must be determined to get the polarity of field (A), which shown in Figure 4. If the amplitude value of direct propagating wave field is positive at zero time, the polarity will be positive. If it is negative on the scale of amplitude, the polarity will be negative. So that, the polarity of direct propagating wave was determined positive as result of the laboratory analysis of our study. Next step of the study is defining the polarity of electromagnetic waves reflected/scattered from buried objects. The value of amplitude was found on amplitude scale table. If the polarity of direct propagating wave is same with reflected/scattered wave polarity, the polarity will not change. On the other hand, if the polarity of direct propagating wave is different from the polarity of reflected/scattered wave, the polarity will change. Searching the amplitude constant of the wave reflected from concrete layer, is the easiest way to explain why the polarity is the same or not.

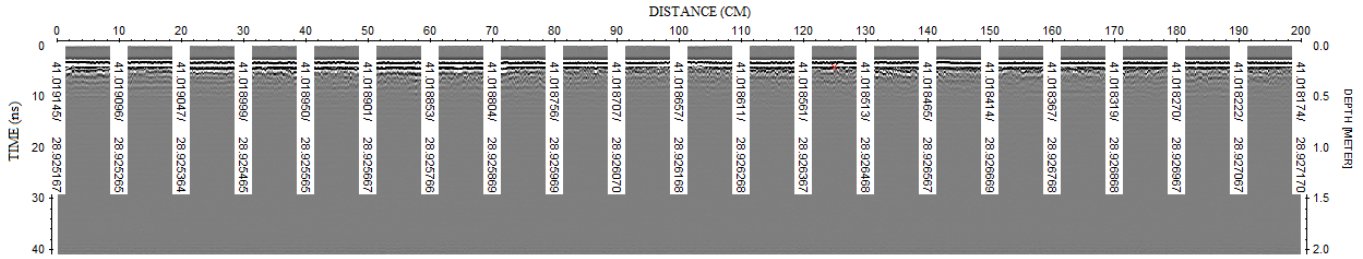

Figure 7. Radargram sample of a GPR/GPS combination

Reflection constant for a direct wave is defined with equations given below (Annan 2000).

$$R = \frac{V2-V1}{V2+V1} = \frac{\sqrt{\mathcal{E}}1-\sqrt{\mathcal{E}}2}{\sqrt{\mathcal{E}}1+\sqrt{\mathcal{E}}2} \quad (2)$$

V1 and $\mathcal{E}1$ represent the velocity and the di-electric constant of the electromagnetic wave of field, respectively. V2 and $\mathcal{E}2$ represent the velocity and the di-electric constant of electromagnetic wave for concrete layer, respectively.

As soon as the propagating waves hit the concrete layer, the wave is scattered/reflected back with an amplitude calculated as the multiplication of propagating wave's amplitude and the reflection constant, and then recorded for all receiver points as a function of arriving time. These scattered/reflected waves are also called as electromagnetic wave fields. If the velocity of electromagnetic wave in concrete layer is higher than the velocity of wave in field, the reflection constant will be positive. In this case, there will be no change on the polarity of reflecting/scattering wave, and then it will be the same as the polarity of direct propagating wave. On the contrary, if the velocity of electromagnetic wave in field higher than the velocity of concrete layer (V1>V2), then polarity of reflected/scattered wave will change to negative values. Defining the amplitude values and polarity of reflected/scattered wave field is the most effective method for the classification of buried layer. Electromagnetic wave in fields is usually less than the velocity of electromagnetic wave within the concrete. It is known that, the wavelength of an electromagnetic wave of 1000 MHz is 0.122 m in the concrete layer with the RDP value of 6 (Conyers L B 2004). Since the concrete has a higher velocity then the velocity of other layers (such as dry sand and asphalt) in the field, theoretically a polarity change in the concrete layer is expected. Hence, the overlapped concrete layer in the field, which was 0,26-0,45 m deeper from the surface, has a higher amplitude and a contrast (-) polarity as compared to the other layers. In this study, for distinguishing the concrete layer from different type of layers, amplitude and polarity differences were also used.

In this study, for the purpose of NDT the spatial location based radargram samples were generated for the buried concrete layer. Radargrams were determined asa result of multiplying the amplitude by reflection constant, hence the amount of reflected/scattered energy could be determined for the arriving time of direct propagating wave to the concrete layer, which was recorded as a time function, and position based radargram samples. Although there is no negative interactive field such as decomposition zone or electromagnetic wave absorber, it was also detected too many buried installations, which was affecting the condition of measurement under the ground surveying. Such irrelevant elements or objects, which are out of focus, were removed from the results of radargram analysis in the processing steps, and focused only on to the research of the concrete layer. The average depth could be measured as 1.6 m at the end of the data processing steps by applying the filters to the radargrams, elevation correction and eliminating the exterior effects from the measurement.

Upper level of concrete layer on the 2D radargrams, which continued in a row, was picked using manual and automatic phase fallow method to check the contract layers' depth and geometry on successive radargrams.

As the result of GPR analysis; C-16 concrete layer was detected through the area, which situated under the New-Jersey borders and the layer has a variable thickness between 0,07 to 0,15 meter.

Another high amplitude layer was detected between the depth of 0,3 – 0,4 meter, which is overlapping with some part of the C-16 concrete layer, and it has the same amplitude value and polarity. It is interpreted as an old road concrete layer belonging to the C-25 concrete class. According to the model profile of the project C-16 concrete, layer takes place between the depths of 0.15-0.25 m. As the concrete layers with irrelevant depth related with the old C-25 concrete layer, it was removed from the results.

Buried concrete layer of 4900 m was detected/mapped along the 5277,56 m surveying profile. This means, no concrete layer was detected on 377,2 (5277,2-4900= 377,2) meter part of the total surveying profile. However, the 735 (15%) meter part of this 4900 meter concrete layer detected in the depth of 0,5 meter was belonging to the C-25 road concrete, which was constructed in the past as defined previously. So, there is no new concrete construction in the 735 meter part of the profile.

As a result, the length of new concrete construction in the effective research depth (0,4 m) on Millet Street was calculated as (4900-735) = 4165 meter. Average thickness of concrete layer was calculated as 13,47 cm with using the 511 Non-destructive Testing samples that were generated on the profile line with 10 meter intervals (Figure 8).

Figure 8. NDT samples on the GPR surveying line

GPR/GPS combination method helps to improve accuracy of locations of all NDT samples, ±2 cm horizontal positioning error in UTM coordinates.Due to having same amplitude value and relative di-electric permittivity (RDP) of C-25 and C-16 concrete layers, the average thickness of new concrete construction (C-16) could be measured with ±3 cm vertical precision. Since the average thickness of concrete layer is calculated as 13,47 cm, ±3 cm vertical measurement precision, the thickness of concrete is varying between 10,47 cm and 16,47 cm. Thus, the minimum value (10,47) is enough to verify the existence of the new concrete construction. Because the concrete layer is defined as 10 cm on the approved model profile of construction project. Instead of minimum concrete thickness (10,47 cm) calculated from radargram analysis, the controller engineering group of Istanbul Metropolitan Municipality calculated the amount of the payment to the construction company based on the model profile as 10 cm, for the use of public interest. The aim of the C-16 concrete construction was preparing a smooth area for flooring the New-Jersey borders. So the width of construction on the model profile is 0,6 meter. Finally, all the parameters are ready for calculating the volume of concrete construction as;

4165 m (Length) x 0,6 m (Width) x 0,10 m (Thickness) = 249,9 m^3

In this study; the amount of buried concrete construction, which could not be measured by classical surveying methods in the construction duration, is determined by this research. The result of the calculation is used for defining the amount of payment to the company. Furthermore, profile lines and Non-destructive Testing samples were attached an official document to the project folder for the first time.

4. CONCLUSION

The results of this study help to improve calculation accuracy for the amount of buried concrete construction using Non-destructive Testing technique (GPR) combined with CORS-GPS. By the help of this study, the certain level of the concrete construction was determined in a very short time efficiently and economically compared to the destructive testing method. Thus, it was prevented the unlawful profit or the loss of contractor in the judicial process according to the public law. Additionally, a public law problem could be resolved at a much shorter time i.e. in 5 workdays instead of 20 workdays, and at a much lower cost i.e. 3.251,125 USD instead of 13.004,500 USD comparing with destructive testing method. Since the actual concrete distance was found, the payment was done for 4165 m instead of 5277.56 m for buried concrete layer.

As a case study, location-based NDT samples generated for the first time for determining the volume of buried concrete layers using GPR-GPS combination methodology in Istanbul Metropolitan Municipality.

Author contribution

Celalettin UÇAR: Supervisor, Conceptualization, Methodology, Software. **Fusun BALIK SANLI**: Data curation, Writing-Original draft preparation, Validation.

Conflicts of interest

The authors declare no conflicts of interest.

REFERENCES

Alp K, Gelişli K, Yılmaz A O, Kaya R & Çavuşoğlu (2003). Mermer İşletmeciliğinde Yer Radarı Uygulamaları, MRSEM, Türkiye IV. Mermer Semposyumu. Bildiriler Kitabı, 37-48.

Annan A P (2000). Ground Penetrating radar workshop notes, Sensors and Software Inc., Canada.

Aspiron U & Aigner T (1999). Towards realistic aquifer models: Three dimensional georadar surveys of Quaternary gravel deltas (Singen Basin, SW Germany), Sedimentary Geology, 129, 281-297.

Billinger M S (2009). Utilizing ground penetrating radar for the location of a potential human burial under concrete, J of Forensic Sciences, 42(3), 200-209.

Cardelli E, Maronne C & Orlando L (2003). Evaluation of tunnel stability using integrated geophysical methods, Journal of Applied Geophysics, 52, 93-102.

Changryol K, Daniels J J, Guy E, Radzevicius S J & Holt J (2000). Residual hydrocarbons in a water-saturated medium: A detection strategy using ground penetrating radar, Environmental Geosciences, 7(4), 169-176.

Conyers L B (2004). Ground Penetrating Radar for Archaeology-Altamira Press-ISBN 0-7591-0772, 23-55.

Daniels J J (2000). Ground penetrating radar for imaging archeological objects in the subsurface, Proceedings of the New Millennium International Forum on Consideration of Cultural Property, Kongju, Korea, 247-265.

Dannowski G & Yaramancı U (1999). Estimation of water content ant porosity using combined radar and geoelectric measurements, European Journal of Environmental and Engineering Geophysics, 4, 71-85.

Davenport G C (2001). Remote sensing applications in forensic investigations, Historical Archaeology, 35(1), 87-100.

Davis J L & Annan A P (1989). Ground Penetrating Radar for high resolution mapping of soil and rock stratigraphy,Geophysical Prospecting, 37, 531-551.

Grandjean G & Gourry J C (1999). GPR data processing for 3D fracturemapping in a marble quarry (Thassos, Greece), Journal of Applied Geophysics, 36, 19-30.

Green A, Gross R, Holliger K, Horstmeyer H & Baldwin J (2003). Results of 3-D georadar surveying and trenching the San Andreas Fault near its northern landward limit,Tectonophysics, 368, 7-23.

Hammon W S, McMechan G A & Zeng X, Forensic (2000). GPR: finite-difference simulations of responses from buried human remains,Journal of Applied Geophysics, 45(3), 171-186.

Harrari Z (1996). Ground penetrating radar (GPR) for imaging stratigraphic features and groundwater in sand dunes, Journal of Applied Geophysics, 36, 43-52.

Kadıoğlu S & Daniels J J (2008). 3D visualization of integrated ground penetrating radar data and EM-61 data to determine buried objects and their characteristics,Journal of Geophysics and Engineering, 5, 448-456.

Kadıoğlu S & Kadıoğlu Y K (2006). Yer radarı yöntemi ile bir mermer sahasındaki kırıkların, sağlam ve bozuk alanların belirlenmesi, Selçuk Üniversitesi, Mühendislik Mimarlık Fakültesi Dergisi, 2(1-2), 127-135.

Kadıoğlu S, Kadıoğlu Y K & Akyol A A (2008). Geoarchaeological research of the mid-Age Ilyasbey Complex buildings with ground penetrating radar in Miletus, Aydın, Western Anatolia, Turkey. Donald Harrington Symposium on the Geology of the Aegean, IOP Conference Series: Earth and Environmental Science, 2, published online.

Koralay T, Kadıoğlu S & Kadıoğlu Y K (2007). A new approximation in determination of zonation boundaries of ignimbrite by ground penetrating radar: Kayseri, Central Anatolia, Turkey, Environmental Geology, 52(7), 1387-1397.

Linck R & Fassbinder J W E (2013). Determination of the influence of soil parameters and sample density on ground-penetrating radar: a case study of a Roman picket in Lower Bavaria, ArchaeolAnthropol, 6, 93-106.

Mellett J S (1992). Location of human remains with ground penetrating radar, Fourth international conference on ground penetrating radar. Geological Survey of Finland Special Papers, 16, 359-365.

Miller P S (1996). Disturbances in the soil: Finding buried bodies and other evidence using ground penetrating radar, Journal of Forensic Sciences, 41(4), 648-652.

Moghadas D, Jadoon K Z, Vanderborght J, Lambot S, Vereecken H (2014). Estimation of the near surface soil water content during evaporation using air-launched ground-penetrating radar, Near Surface Geophysics, 12, 623-633.

Morgan R M & Bull P A (2007). Forensic geoscience and crime detection: Identification, interpretation and presentation in forensic geosciences, Minerva Medicolegale, 127, 73-89

MTA Doğal Kaynaklar ve Ekonomi Bülteni (2012).

Nobes D C (2000). The search for "Yvonne": A case example of the delineation of a grave using near-surface geophysical methods, Journal of Forensic Sciences, 45(3), 715-721.

Novo A, Lorenzo H, Rial F I & Solla M (2011). 3D GPR in forensics: Finding a clandestine grave in a mountainous environment, Forensic Science International, 204(1-3), 134-138.

Pringle J K, Jervis J, Cassella J P & Cassidy N J (2008). Time-lapse geophysical investigations over a simulated urban clandestine grave, J of Forensic Sciences, 53(6), 1405-1416.

Ruffell A & McKinley J (2005). Forensic geoscience: Applications of geology, geomorphology and geophysicst criminal investigations, Earth-Science Reviews, 69. 235-247.

Sambuelli L, Socco L V & Brecciaroli L (1999). Acquisition and processing of electric, magnetic and GPR data on a Roman site (Victimulae, Salussola, and Biella), Journal Applied Geophysics, 41, 189-204.

Sandmeier K J (2004) Scientific Software, REFLEXW ver.3.5 program for processing and interpretation of reflection and transmission data.

Schultz J J & Dupras T L (2008). The contribution of forensic archaeology to homicide investigations, Homicide Studies, 12(4), 399-413.

Schultz J J (2007). Using ground-penetrating radar to locate clandestine graves of homicide victims, Homicide Studies, 11(1), 15-29.

Shaaban F A, Abbas A M, Atya M A & Hafez M A (2009). Ground-penetrating radar exploration for ancient monuments at the Valley of Mummies -Kilo 6, Bahariya Oasis, Egypt, Journal of Applied Geophysics, 2, 194-202.

Unterberger R R (1992). Ground penetrating radar finds disturbed earth over burials, Fourth international conference on ground penetrating radar, Geological Survey of Finland Special Papers, 16, 341-357.

Van Dam R I & Schlager W (2000). Identifying causes of ground-penetrating radar reflections using time-domain reflectometry and sedimentological analysis, Sedimentology, 47, 435-449.

International Journal of Engineering and Geosciences
https://dergipark.org.tr/en/pub/ijeg
e-ISSN 2548-0960

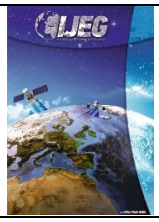

Comparative analysis of the performance of Multi-GNSS RTK: A case study in Turkey

Omer Faruk Atiz*[1], Ceren Konukseven [1], Sermet Ogutcu [1], Salih Alcay [1]

[1]*Necmettin Erbakan University, Engineering and Architecture Faculty, Geomatics Engineering Department, Turkey*

Keywords
CORS
GAMIT/GLOBK
Multi-GNSS
RTK
ZTD

ABSTRACT

The Real Time Kinematic (RTK) method is widely used in the land surveying. Whereas RTK method has the advantage of practical use, positioning accuracy depends mostly on the baseline length due to the atmospheric errors. In general, RTK measurements are made by using GPS and GLONASS satellite systems. For this reason, the positioning performance of the technique is adversely affected under restricted satellite geometry conditions such as urban canyons. At present, most receivers on the market have the ability to track signals of Galileo and BeiDou satellites. Therefore, in this study, the positioning performance of RTK with different satellite combinations (GPS-only, GPS+GLONASS, GPS+GLONASS+GALILEO+BeiDou) was examined with a comparative approach. A field test was carried out considering approximately 20, 40, 60, and 80 km length of baselines. Three different cut off elevation angles – namely, 10°, 20°, and 30° – were chosen for the field test. The results were investigated in terms of accuracy and precision. Also, the ground truth coordinates of the rovers were obtained by post-processing relative method using GAMIT/GLOBK software. The results showed that multi-GNSS combinations provided better repeatability at the 10° cut off angle option. The accuracy of GPS-only solutions varied between 0.63/2.17 cm and 2.40/4.94 cm for horizontal and vertical components, respectively. However, the multi-GNSS combinations did not have a remarkable superiority in terms of position accuracy even at high satellite cut off angle (30°) compared to the GPS-only RTK.

1. INTRODUCTION

In recent years, Global Navigation Satellite Systems (GNSS) have been used by relative or absolute methods for millimeter to centimeter level positioning. One of the relative methods, Real Time Kinematic (RTK) method which eliminates many errors by double differencing (DD) technique is extensively used in many geospatial studies (Odijk et al. 2012; Yu et al. 2016; El-Mowafy and Kubo 2017; Erenoglu 2017; Dabove 2019; Li et al. 2019; Ogutcu 2019). The accuracy in RTK mostly depends on the distance between reference station and rover so-called -baseline length- due to the orbital errors and the changing atmospheric conditions. Apart from the error sources, the distance limitations of radio modems' due to wave propagation were another obstacle for longer baseline lengths in RTK measurements. Thanks to the Networked Transport of RTCM via Internet Protocol (NTRIP), this issue became no longer a problem (Weber et al. 2005). In present, with the development of Continuously Operating Reference Stations (CORS), the necessity of establishing a reference station is eliminated on the user side. The main purpose of CORS networks is to provide predicted RTK corrections to users using stations around the rover. These corrections can be estimated with several approaches that differ in the calculation of rover errors i.e., VRS (Virtual Reference Station), FKP (Flate Plane Correction Parameter), MAC (Master Auxiliary Concept) (Ogutcu and Kalayci 2018). However, the performance of the system still highly depends on the nearest reference station. Since the CORS offers RTK correction via Internet (GSM) protocols, it can be used for long distance RTK using a single CORS station (Wielgosz et al. 2005; Kim and Langley 2008; Odolinski et al. 2015a; Shu et al. 2018; Baybura et al. 2019; Bramanto et al. 2019). As the baseline distance becomes longer, the correlation between the reference station and rover decreases due to troposphere-ionosphere errors.

Generally, GPS and GLONASS satellite systems are used for the majority of RTK measurements as they were the first global constellations reached the Full Operational Capability (FOC). In recent years, the coverage of GNSS has been expanded with Galileo and BeiDou global satellite systems as well. With this

* **Corresponding Author**

*(oatiz@erbakan.edu.tr) ORCID ID 0000–0001–6180–7121
(cerenkonk@gmail.com) ORCID ID 0000-0001-6598-9479
(sermetogutcu@erbakan.edu.tr) ORCID ID 0000-0002-2680-1856
(salcay@erbakan.edu.tr) ORCID ID 0000–0001–5669–7247

Cite this article

Atiz O F, Konukseven C, Ogutcu S & Alcay S (2022). Comparative analysis of the performance of Multi-GNSS RTK: A case study in Turkey. International Journal of Engineering and Geosciences, 7(1); 67-80

Research Article / DOI: 10.26833/ijeg.878236

Received: 10/02/2021; Accepted: 19/03/2021

development, many studies have been carried out on multi-GNSS RTK (Odolinski et al. 2015b; Li et al. 2017a; Paziewski and Wielgosz 2017; Dabove and Di Pietra 2019; Mi et al. 2019; Tian et al. 2019; Castro-Arvizu et al. 2020; Luo et al. 2020; Zhang et al. 2020). Accordingly, the additional satellites can provide a better satellite geometry and improve the positioning performance of RTK by increasing ambiguity fixing ratio.

Although many studies have been conducted referring to multi-GNSS RTK, it is still a hot topic of research. Thus, in this study, the contribution of multi-GNSS to single base RTK is examined regarding different baseline distances. For this purpose, a field experiment was performed considering different satellite combinations such as GPS-only, GPS+GLONASS, and GPS+GLONASS+Galileo+BeiDou in Konya, Turkey. Also, different elevation cut-off angles (10°,20°,30°) were chosen to represent open sky and urban canyon conditions. The results were analyzed in terms of accuracy and precision. The condition of the ionosphere and troposphere were also investigated since they have a key role in the performance of real-time positioning.

2. DATA AND METHODOLOGY

In general, two types of positioning methods, relative and absolute, can be used for real-time precise positioning with GNSS. The Precise Point Positioning (PPP) method is one of the absolute positioning techniques which presents centimeter level positioning accuracy using precise satellite ephemeris and clock products (Zumberge et al. 1997; Kouba and Héroux 2001). Although PPP is a powerful technique, it requires a long convergence time. However, Real-Time PPP (RT-PPP) method provides an accuracy of decimeter level (Alcay and Atiz 2021). On the other hand, the relative method has been used for decades and its reliability has been proven. The RTK method is based on double differencing (DD) of carrier phase measurements. For multi-GNSS integration in RTK positioning, loose and tight combined approaches can be employed (Paziewski and Wielgosz 2017). If overlapping frequencies from GNSS satellites are used to create double-differences, the tight combined approach needs to be employed. In this model, a single reference satellite is used as a pivot satellite for creating double difference observations from the all GNSS systems. As a result, "inter-system" double differencing biases, originated from the receivers, need to be established (Odijk and Teunissen 2013). Despite the tight combined model, observations from GNSS satellites with different frequencies can be integrated easily using the loose combined method. In this method, pivot satellites need to be defined separately for each GNSS system to create double-difference observations. Thus, double-differenced observations are created uniquely for each GNSS system. As a result, number of double-differenced observables decreases compared with the tight combined approach. At the same time, number of the estimated parameters also decreases due to absence of the "inter-system" double differencing biases parameter in the loose combined approach (Li et al. 2017b). In this study, loose combined model was used for multi-GNSS RTK positioning. In this way, all visible satellites at each test point were used for RTK positioning. The functional model of loose combined method can be expressed as follow:

$$\begin{aligned} \rho_{kl}^{mn} &= \lambda_{f_1}\varphi_{kl,f_1}^{mn} - \lambda_{f_1}N_{kl,f_1}^{mn} \\ \rho_{kl}^{mn} &= P_{kl,f_1}^{mn} \\ \rho_{kl}^{mn} &= \lambda_{f_2}\varphi_{kl,f_2}^{mn} - \lambda_{f_2}N_{kl,f_2}^{mn} \\ \rho_{kl}^{mn} &= P_{kl,f_2}^{mn} \end{aligned} \quad (1)$$

where $k\ and\ l$ denote receivers, $m\ and\ n$ denote GNSS satellite, $f1 and f2$ denote first and second frequencies, λ is the wavelength of the associated signal, φ denotes carrier phase data, P is the pseudorange data, and ρ is the geometric range. Ionospheric and tropospheric terms were neglected for simplicity. The above double-difference phase and pseudorange equations are formed separately for each GNSS system in the loose combined method. Receivers' coordinates in the geometric range and double-differenced integer phase ambiguities are the estimated parameters.

In order to investigate the contribution of multi-GNSS to single base RTK, a field experiment was conducted in Konya, Turkey between 3-6 July 2020. The NEU-CORS station, installed on the roof of the Necmettin Erbakan University Faculty of Engineering building, was used as a reference station. NEU-CORS is capable of tracking GPS, GLONASS, BeiDou and Galileo satellites with 220 channels. However, it has a GSM modem and can provide real-time data stream (Atiz et al. 2020). As rovers, three CHC i50 geodetic GNSS receivers were used. These receivers can also track GPS, GLONASS, BeiDou and Galileo satellites. In addition, rovers used in this study, have the same firmware version to avoid any systematic biases between the rovers. Simultaneous measurements have conducted using GPS-only (G), GPS+GLONASS (GR), and GPS+GLONASS+Galileo+BeiDou (GREC) satellite combinations. Four different test sites were selected for the measurements, considering the varying length of base length. The location of the sites is given in Figure 1.

A, C, and D test sites have an open sky and far from buildings which could cause multipath. In contrast, site B is closer to the highway and is a more challenging test point. The details on the baselines are provided in Table 1.

Table 1. The details of baselines

Name	Latitude	Longitude	Height (m)	Distance
Base	37.8662	32.4192	1210.72	-
Site-A	37.9845	32.5902	1041.85	20.0 km
Site-B	38.1093	32.7336	1058.94	38.6 km
Site-C	38.3373	32.7796	1002.50	61.1 km
Site-D	38.4861	32.8378	982.16	78.0 km

Traditionally in RTK method, it is assumed that rover and base stations are at similar heights. The height difference between base and rover can decrease the troposphere correlation (Edwards et al. 2010). For this case study, the height differences are between ~170 m and ~230 m. The RTK coordinates were obtained approximately for 9 hours at each test site with G, GR, and GREC satellite configurations, in three phases. These

three phases consist of measurements at 10°, 20° and 30° elevation cut-off angles. However, for the purpose of post-process relative positioning, the first phase was extended to 5-hours by including static data recording. The other phases were continued for 2-hours with only RTK surveying. Due to the disconnection caused by the GSM operator, the first phase could only last for 3 hours on July 4th. A special apparatus was used to place three receivers on the tripod. Hence, the rovers had the same multipath and atmospheric conditions for each test site. Figure 2 shows the instruments during the measurements. Furthermore, each rover is connected to a power supply in the box at the bottom. Thanks to these power supplies, there was no battery blackout during measurements.

As a preliminary analysis, the mean visible satellites were examined. For each session and satellite combination, the average of visible satellites is given in Table 2.

Table 2. Average of visible satellites

Sites	Cut-off	G	GR	GREC
A	10°	9	15	34
	20°	7	13	28
	30°	6	10	22
B	10°	8	15	40
	20°	7	13	29
	30°	7	10	24
C	10°	8	15	34
	20°	7	13	26
	30°	6	10	18
D	10°	8	15	35
	20°	7	13	28
	30°	6	9	21

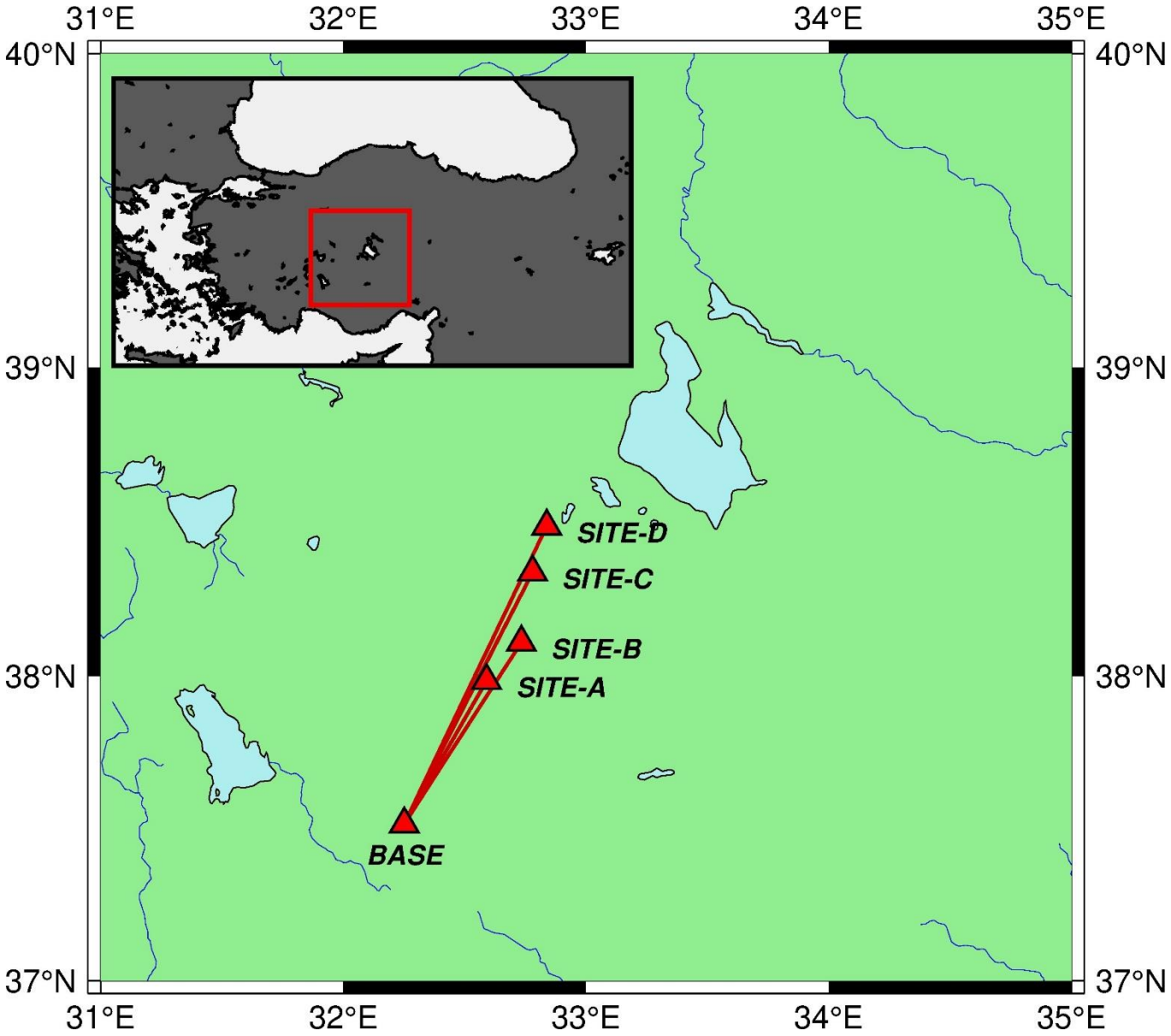

Figure 1. The locations of field tests (Created by GMT software, Wessel et al. 2019)

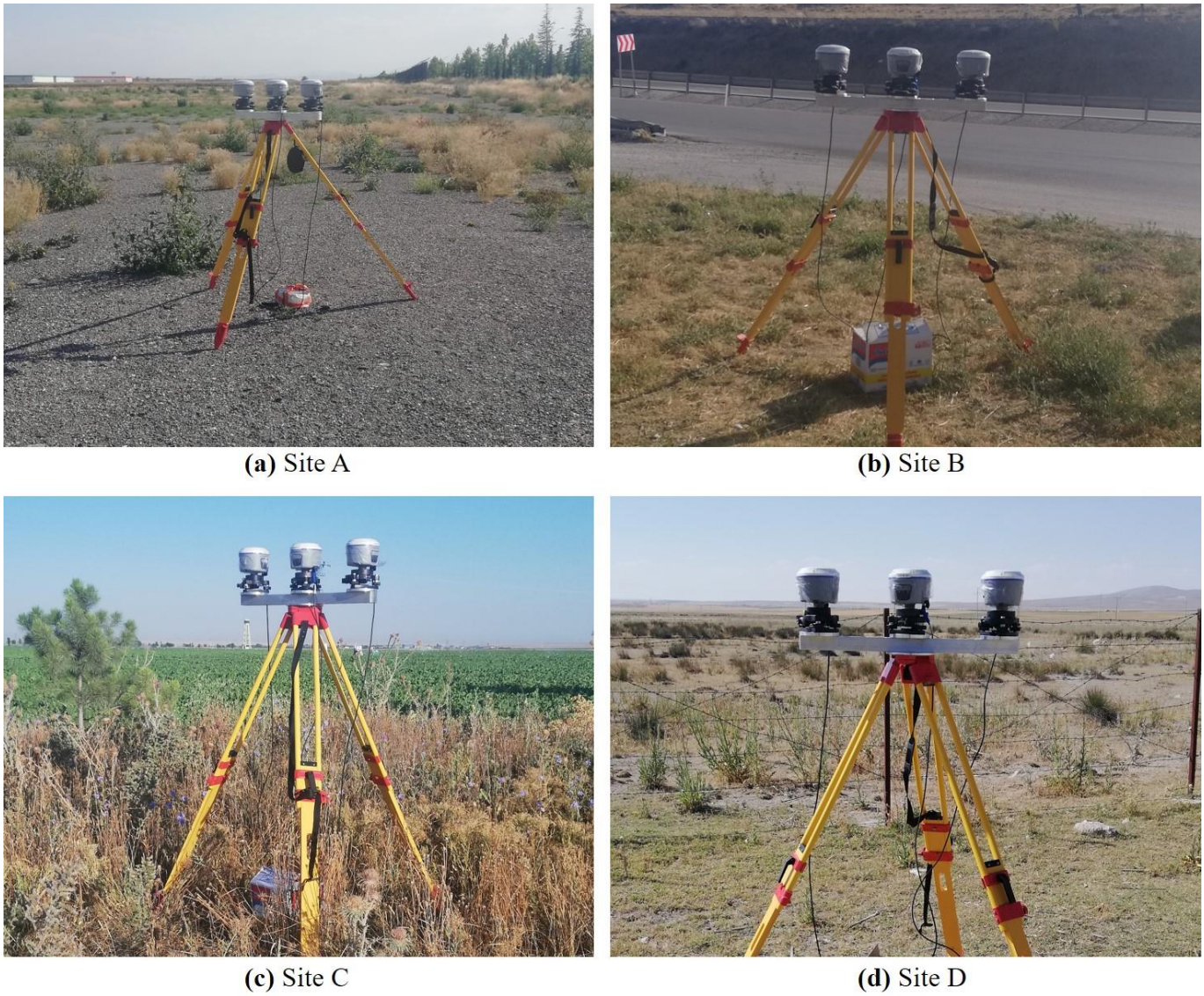

(a) Site A **(b)** Site B

(c) Site C **(d)** Site D

Figure 2. The rovers during the measurements

A minimum of 6, 9, and 18 satellites tracked in G, GR, and GREC combinations, respectively. Due to measurements conducted at similar times of the consecutive days, the average visible satellites are close to each other in different test sites.

When utilizing different satellite combinations, the position dilution of precision (PDOP) becomes essential. PDOP values denote the state of satellite geometry. To examine this, PDOP values with respect to each cut-off angle for each session are given in Figure 3-5.

As expected for all sessions, GREC has the best PDOP while G has the worst PDOP value. All configurations are ideal at the 10° cut-off angle option. Besides, a degradation occurred in the last quarter of measurements at Site-D. At the 20° cut-off angle option, GREC and GR configurations are about 1.5 and 2.0, respectively. Although G has higher PDOP, it is still at a good level. PDOP change in different sites is similar as they are performed at the approximately same time of day. At the 30° cut-off angle option, PDOP values are much bigger for all satellite configurations. Nevertheless, they are in a good range.

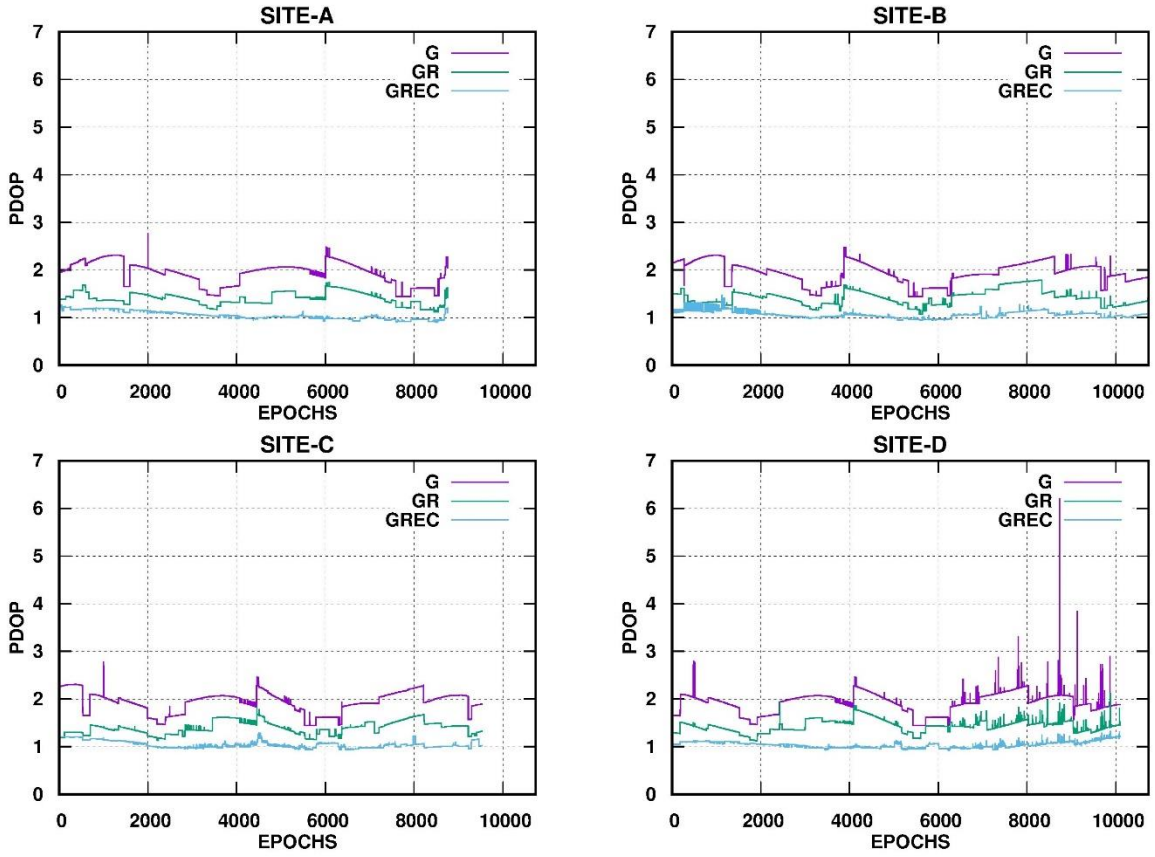

Figure 3. PDOP values for 10° cut-off angle option

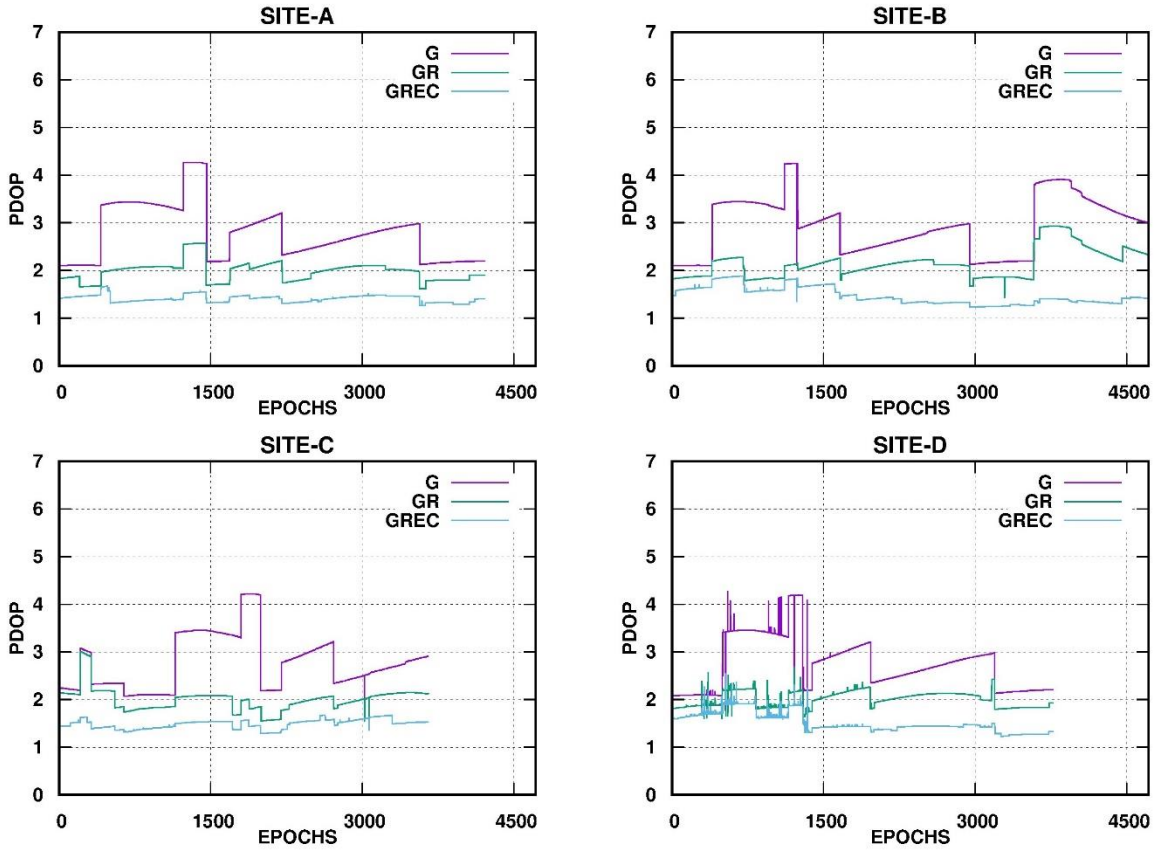

Figure 4. PDOP values for 20° cut-off angle option

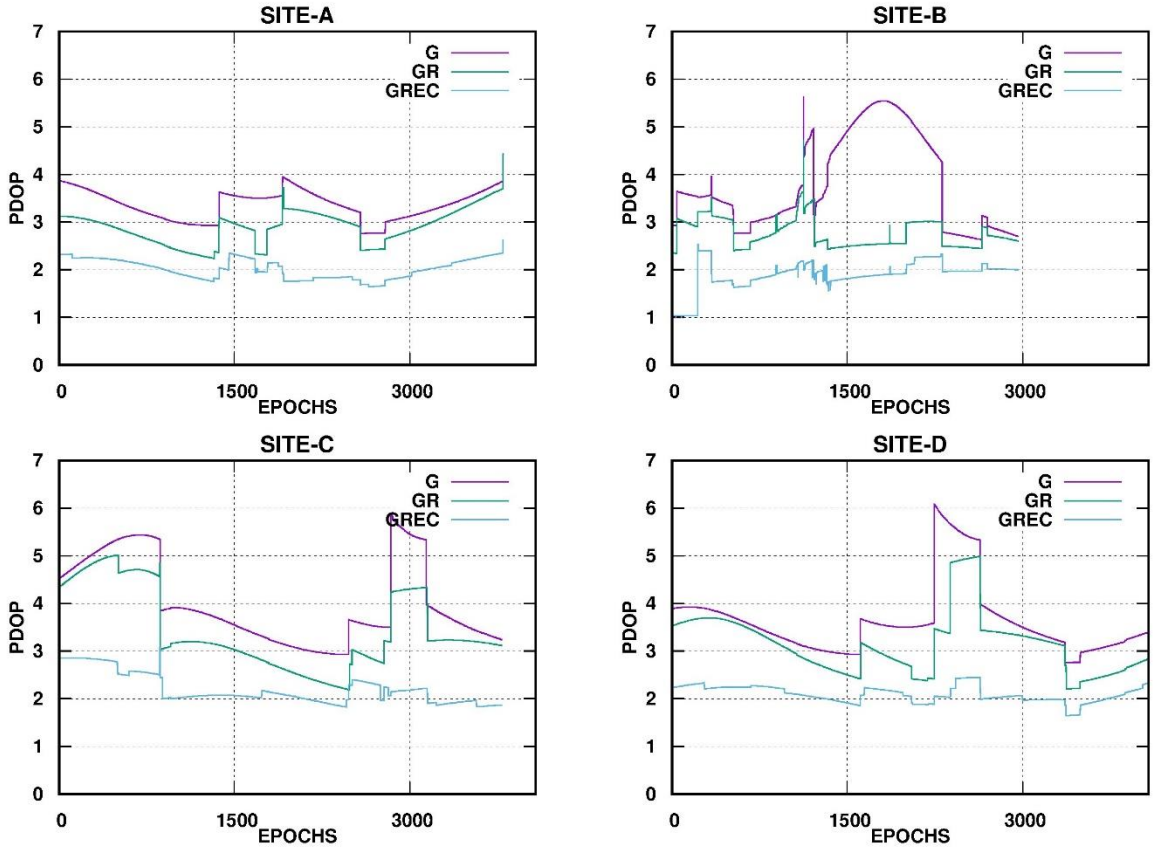

Figure 5. PDOP values for 30° cut-off angle option

3. RESULTS

In order to make a proper accuracy analysis, the reference coordinates of each rover were obtained by post-process relative method. For this purpose, a well-known scientific GNSS data processing software (GAMIT/GLOBK) was used (Herring et al. 2010). GAMIT/GLOBK is one of the scientific GNSS data processing software. Since the RTK measurements used in this study provide relative solutions using the NEU-CORS station, the ground truth coordinates of the rovers should be obtained in the same way to avoid any systematic bias. The static data of each session was processed in GAMIT/GLOBK software. A summary of processing parameters is provided in Table 3.

The percentages of fixed Wide-Lane (WL) and Narrow-Lane (NL) phase ambiguities were checked to examine the success of post-process positioning. Fixed WL and NL phase ambiguity percentages for all three rovers were nearly identical at the same test site. For simplicity, only the mean ambiguity fixing percentages of three rovers at each test site are given in Table 4.

Using these results as ground truth, Earth Centered Earth Fixed (ECEF) RTK coordinates were converted to topocentric system (north, east, up). Since ambiguity resolution is an important issue for RTK positioning, the ambiguity-fixed solution ratio of each session was assessed (Table 5).

Table 3. GAMIT/GLOBK processing parameters

Parameter	Strategy
GNSS System	GPS
Adjustment model	Stochastic Kalman filter
Weighting strategy	Phase and code data 1.0 cm/ 1.0 m, Weighting with elevation
Epoch interval	30 s
Elevation cut-off angle	10°
Satellite orbit and clock	IGS final products
Cycle-slip	Corrected
Receiver clock jump	Corrected
Ionosphere	Ionosphere-free combination and IGS IONEX file were used.
A Priori troposphere	GPT2 model (Lagler et al. 2013) were applied using tropospheric gradient
Wet tropospheric delay	Estimated as random-walk model (5x10-8 m2/s)
Tropospheric gradients	Estimated as random-walk model (5x10-8 m2/s)
Phase ambiguity	Wide-Lane and Narrow-Lane
Antenna phase offsets	PCO and PCV values from up-to-date IGS. atx were used.
Satellite DCB	CODE DCB file were used.

Table 4. WL and NL ambiguities for post-process

Site	WL	NL
A	100.0%	100.0%
B	100.0%	72.7%
C	100.0%	73.3%
D	100.0%	100.0%

Table 5. The percentage of ambiguity fixed solutions

Sites	Cut-off	G	GR	GREC
A	10°	99.9	100.0	93.3
	20°	100.0	100.0	100.0
	30°	87.5	100.0	100.0
B	10°	99.9	99.8	94.5
	20°	99.5	99.6	97.1
	30°	88.0	99.2	95.5
C	10°	100.0	99.7	98.9
	20°	100.0	100.0	96.7
	30°	99.8	100.0	92.3
D	10°	97.1	100.0	100.0
	20°	93.9	100.0	100.0
	30°	100.0	100.0	98.9

According to Table 5, the minimum ambiguity fixing ratio is 87.5% in the G-30° session at Site-A. Moreover, an outlier test was utilized using 10.0 cm threshold for north, east, and up components. Since there are not many float solutions, only ambiguity fixed results were taken into consideration. The outlier percentages for each session are given in Table 6.

As can be seen in Table 6, outlier percentages are almost similar for G, GR and GREC configurations. All results in the G-30° session at Site-C are above the outlier threshold. As depicted in Table 5, 99.8% of the ambiguities were fixed in the G-30° session at Site-C. Therefore, the reason for this may be wrong fixing of the integer ambiguities obtained from RTK measurements. This session was therefore excluded from subsequent analysis. Also, an alignment was performed between three different RTK solutions at each test site to keeping the RTK solutions from three rovers share the exactly same time.

Table 6. The outlier percentages

Sites	Cut-off	G (%)	GR (%)	GREC (%)
A	10°	0.16	0.05	0.09
	20°	5.95	9.17	4.34
	30°	0.08	0.11	0.03
B	10°	0.07	0.11	0.07
	20°	28.29	29.88	13.87
	30°	5.20	4.73	5.33
C	10°	2.40	0.28	0.23
	20°	7.95	5.30	18.86
	30°	100.0	8.78	21.38
D	10°	0.06	0.08	1.04
	20°	1.70	0.79	4.34
	30°	0.69	0.78	21.09

The standard deviation (std) values are examined to evaluate repeatability. The improvement percentage can be calculated simply as given in Equation 2.

$$std\ improvement(\%)_{GR} = 100 * \left(1 - \frac{std_{GR}}{std_{G}}\right) \quad (2)$$

where subscript G and GR indicate G and GR configurations, respectively. Besides GR, improvement for GREC can be calculated similarly. The contribution of GR and GREC configurations to the repeatability for each cut-off angle option is shown in Figure 6-8.

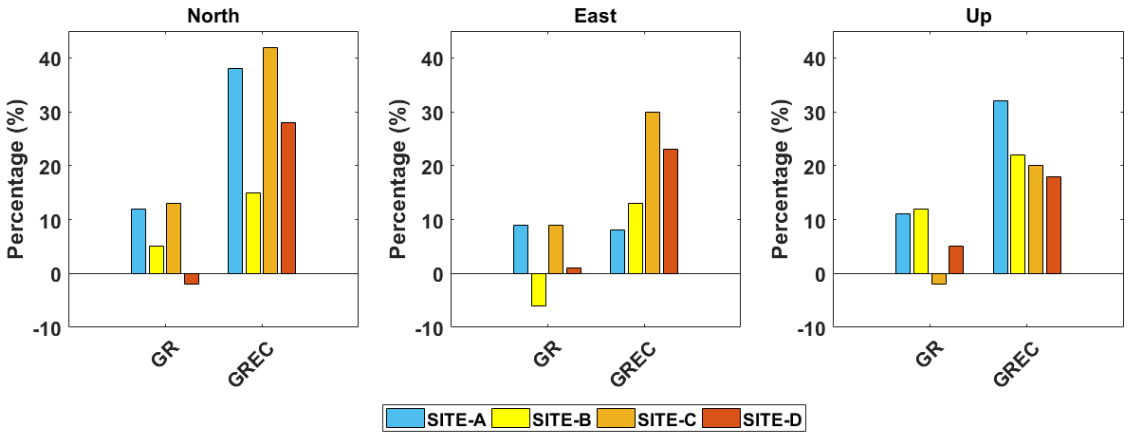

Figure 6. Repeatability improvements for 10° cut-off angle option

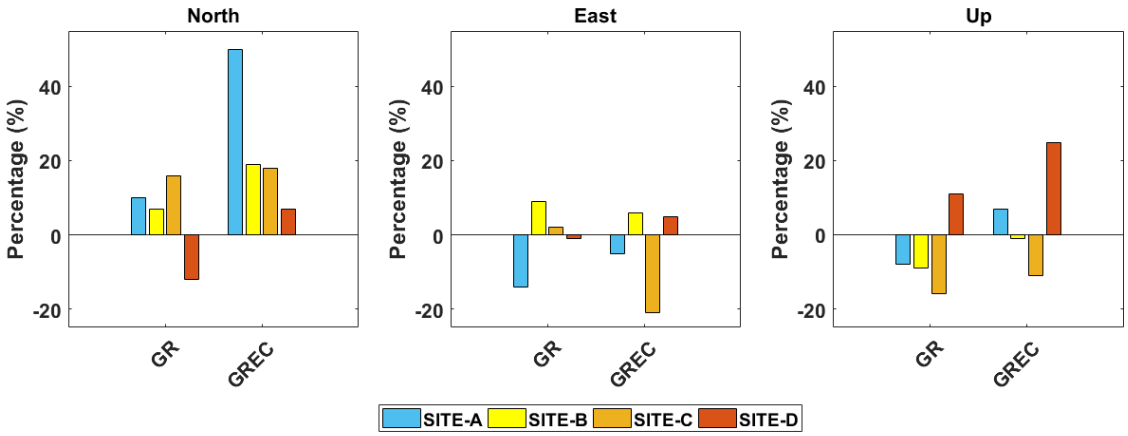

Figure 7. Repeatability improvements for 20° cut-off angle option

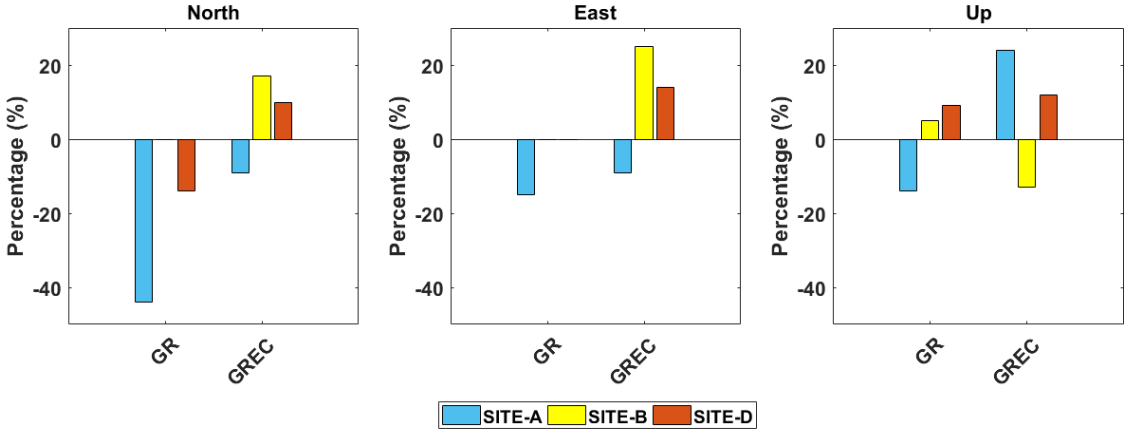

Figure 8. Repeatability improvements for 30° cut-off angle option

As can be seen in Figure 6-8, GR and GREC configurations clearly improve the repeatability in the north, east and up components for 10° cut-off angle option. Compared to GREC, the GR configuration has less effect in terms of std improvement. For 20° cut-off angle option, GR and GREC improve the repeatability in the north component. While GREC has the least improvement at Site-D, GR has a negative value. Particularly in high cut-off angle options, multi-GNSS combinations have a negative effect. For the 30° cut-off angle option, GR is bigger than -40% in north component. However, some bars do not appear in Figure 8 because their values are equal to zero. Negative values may be due to the measurement time. Because the first phase lasted 5-hour, while the second and third phases only lasted 2 hours. Odijk and Wanninger (2017) investigated the combined GPS+BDS long RTK (80 km). Accordingly, the precision reaches 2 cm for the horizontal component and 5 cm for the vertical component in almost 3 hours. The results in this study are consistent with those in Odijk and Wanninger (2017). Also, since the G-30° session of Site-C was removed from the statistical analysis, it is not given in Figure 8.

Table 7. Mean values for G, GR and GREC sessions

Sites	Cut-off	G			GR			GREC		
		N (cm)	E (cm)	U (cm)	N (cm)	E (cm)	U (cm)	N (cm)	E (cm)	U (cm)
A	10°	-0.62	-0.17	-0.72	-0.49	0.04	-2.13	-0.86	-0.02	-2.02
	20°	-1.71	-0.02	1.61	-0.74	-0.47	-1.38	-0.91	-0.14	-0.69
	30°	-0.47	-0.84	0.59	0.11	-0.99	0.19	-0.63	-0.86	1.33
B	10°	0.15	-0.33	-0.62	-0.31	-0.32	-2.44	-1.21	0.03	-0.01
	20°	0.32	-1.49	-1.71	0.45	-1.19	-3.40	-0.32	-0.90	0.48
	30°	-0.02	-0.02	-0.43	-0.18	0.06	-1.41	-1.05	0.37	-0.36
C	10°	-0.73	-0.45	4.00	-0.72	-0.50	2.25	-1.35	-0.61	3.38
	20°	-1.02	0.29	4.08	-0.77	-0.27	2.34	-1.52	-0.38	2.58
	30°	-	-	-	-1.20	1.08	-1.64	-0.58	0.29	-0.63
D	10°	-0.74	-0.25	-0.84	-0.74	-0.67	-0.18	0.12	-2.00	3.70
	20°	-0.34	0.06	1.43	-0.74	-0.29	1.60	0.49	-2.46	3.76
	30°	-0.51	-0.06	0.61	-0.90	-0.12	1.71	1.17	-2.01	6.00

In addition, mean values for each session were investigated (Table 7). Accordingly, the horizontal components vary between -1.71/0.32 cm, -1.20/1.08 cm, and -2.46/1.17 cm for G, GR, and GREC configurations, respectively. However, up components are in the range of -1.71/4.08 cm, -3.40/2.34 cm, and -2.02/6.00 cm for G, GR, and GREC configurations, respectively.

Furthermore, accuracy improvements were evaluated with the help of root mean square error (RMSe) values (Equation 3). The RMSe can be calculated as:

$$RMSe = \sqrt{\frac{\sum(x)^2}{n}} \quad (3)$$

where x denotes the topocentric coordinate component and n indicates the total number of measurements. RMSe values for each session was calculated using Equation 3. In Table 8, RMSe values for GPS-only solutions are given. As seen from Table 8, RMSe vary between 0.96/2.17 cm, 0.63/2.04 cm, and 2.40/4.94 cm for north, east, and up components, respectively.

Table 8. RMSe of GPS-only solutions

Sites	Cut-off	North (cm)	East (cm)	Up (cm)
A	10°	1.13	0.63	2.40
	20°	2.17	0.94	4.32
	30°	0.96	1.27	3.36
B	10°	1.02	1.13	2.54
	20°	1.33	2.04	3.66
	30°	1.13	1.10	3.85
C	10°	1.66	1.09	4.69
	20°	2.16	1.10	4.94
	30°	-	-	-
D	10°	1.59	0.97	2.74
	20°	1.29	1.23	3.91
	30°	1.11	0.89	2.73

A simple equation such as Equation 2 was used to assess the RMSe values as improvements. In Figures 9-11, accuracy improvements are given for each test site and elevation cut-off angle option.

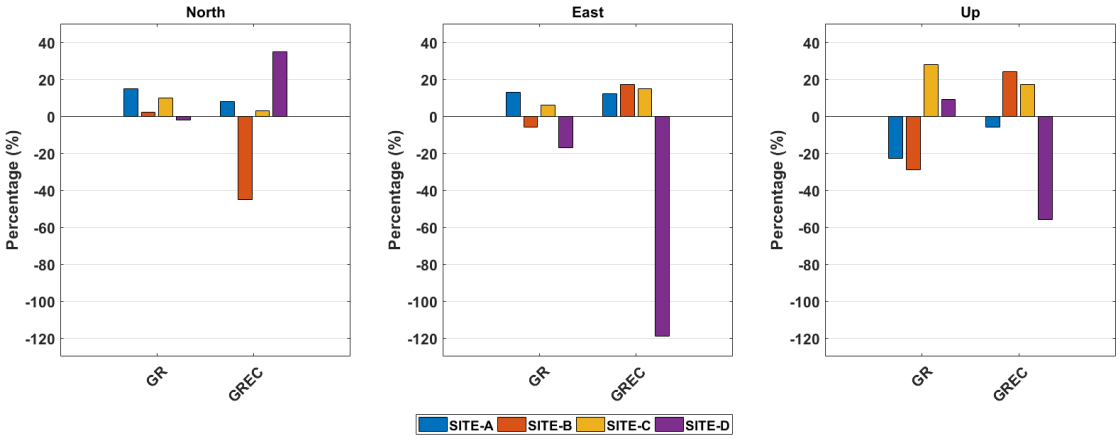

Figure 9. Accuracy improvements for 10° cut-off angle option

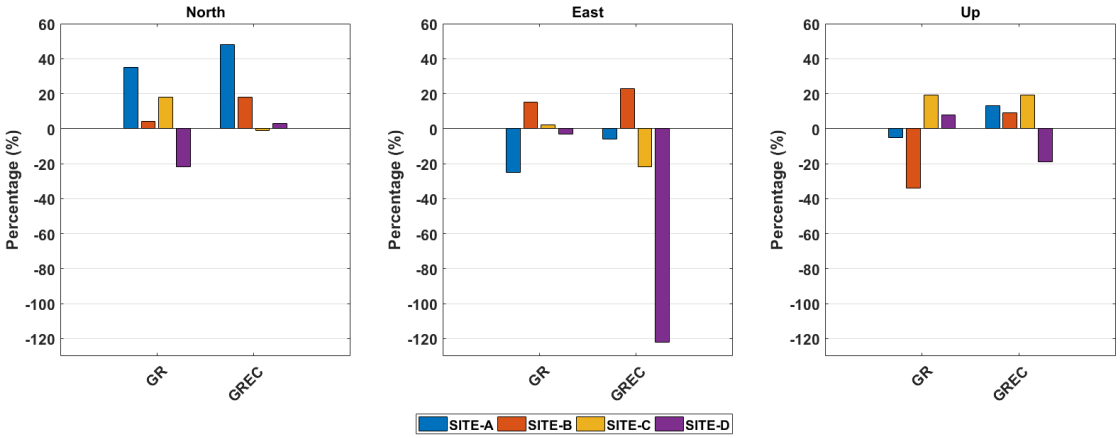

Figure 10. Accuracy improvements for 20° cut-off angle option

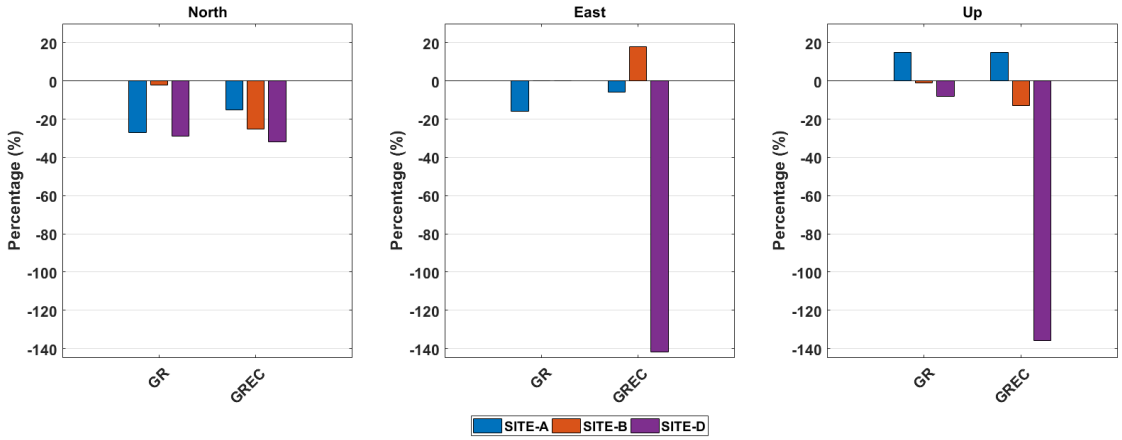

Figure 11. Accuracy improvements for 30° cut-off angle option

Both GR and GREC have improved the accuracy in Site-A at the low elevation cut-off angle. For Site-A, multi-GNSS were not increase at higher cut-off angles. For Site-C, multi-GNSS improved the accuracy. In general, GR and GREC degraded the accuracies at Site-D. The maximum improvement in the horizontal component is in the north component of Site-A.

The error distribution for each session and coordinate component were investigated for better comprehension of data. The error is defined as the RTK coordinate differences from the assumed real value obtained from the static processing. In order to represent error distribution, topocentric coordinates (north, east, and up) were used. For the sake of simplicity, only data belong to the first phase of Site-B is presented in this manuscript (Figure 12-14).

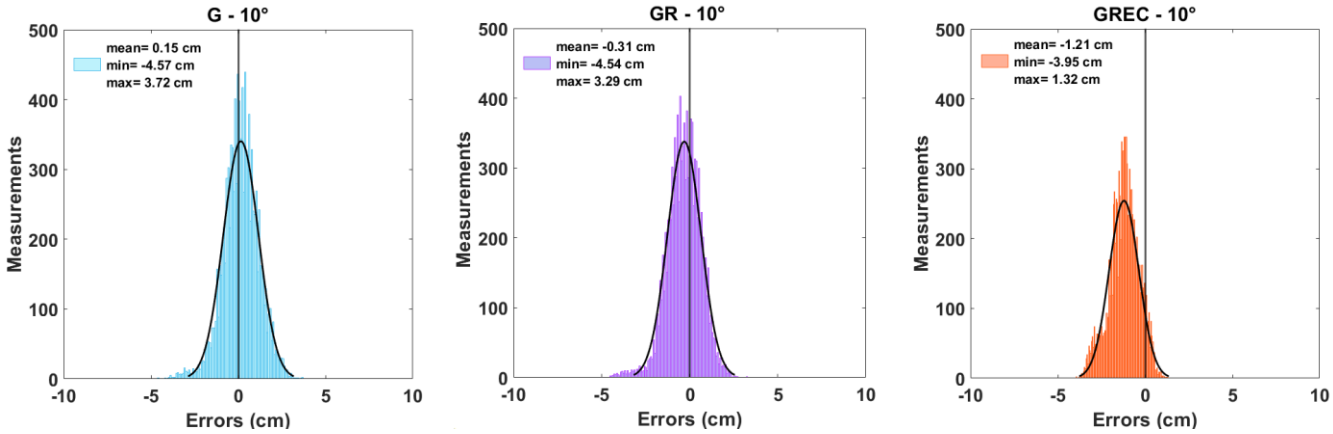

Figure 12. Error distribution of the north component for G, GR and GREC configurations (Site-B)

As seen in Figure 13-14, the error distributions for horizontal components are in the range of -5.0/4.0 cm. Whereas in the vertical component, errors can reach -10 cm (Figure 14). Moreover, it can be stated that the errors in all components are similar to the Gaussian distribution. For the north component, GPS-only solutions are better than multi-GNSS solutions. The solution of GREC is biased with a mean of -1.20 cm in the north component. Whereas GPS-only and GR solutions are similar, GREC provides the ideal solution in east and up components. For the up component, the solution of GR is biased with a mean of -2.44 cm. As a result, GR improved repeatability, but not accuracy since the solution is biased. The biased error distributions like this degrade the positioning accuracy. Therefore, multiple GNSS combinations do not always improve accuracy as can be seen from their error distributions (Figure 12).

For a more in-depth analysis, the atmospheric conditions were examined as they are crucial to real-time positioning. Mainly, the atmospheric effects in positioning with GNSS are examined by means of ionosphere and troposphere. GNSS signals are exposed to free electrons in the ionosphere layer of the atmosphere that disrupts the signal propagation. The density of electron content in the ionosphere is described as Total Electron Content (TEC). The major changes in TEC value indicate the ionospheric disturbance. Moreover, space weather condition indices can provide information about anomalies in the ionosphere. When there is an ionospheric storm, the indices exceed their limit values (Bothmer and Daglis 2007; Alcay and Gungor 2020). Therefore, in this study, geomagnetic storm (Kp), geomagnetic activity (Dst), and solar activity (F10.7) indices examined to check whether any ionospheric disturbance during the field tests (Figure 15). As a result, Kp, Dst, and F10.7 index values do not exceed limit values. Therefore, there is no ionospheric storm during field tests.

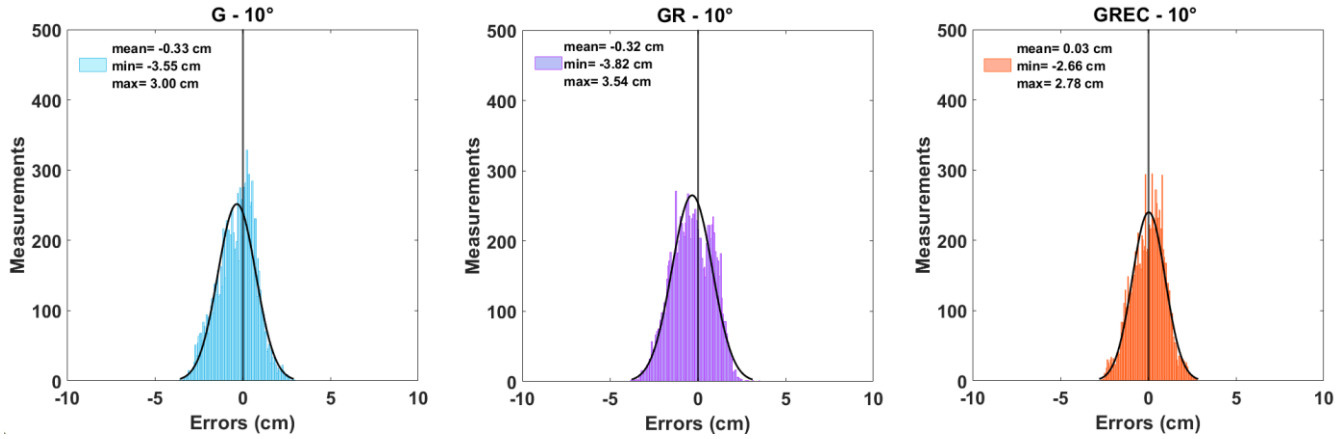

Figure 13. Error distribution of the east component for G, GR and GREC configurations (Site-B)

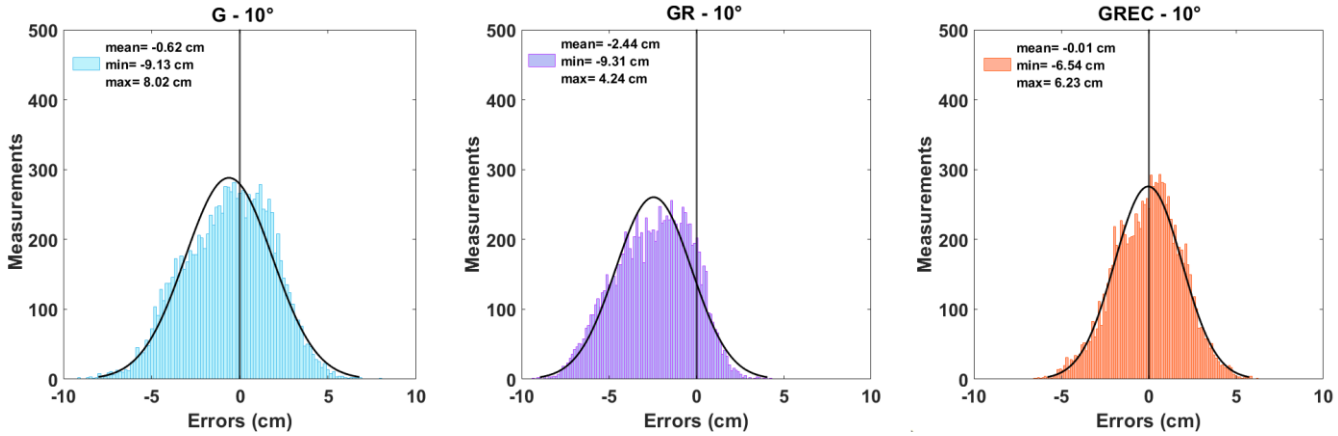

Figure 14. Error distribution of the up component for G, GR and GREC configurations (Site-B)

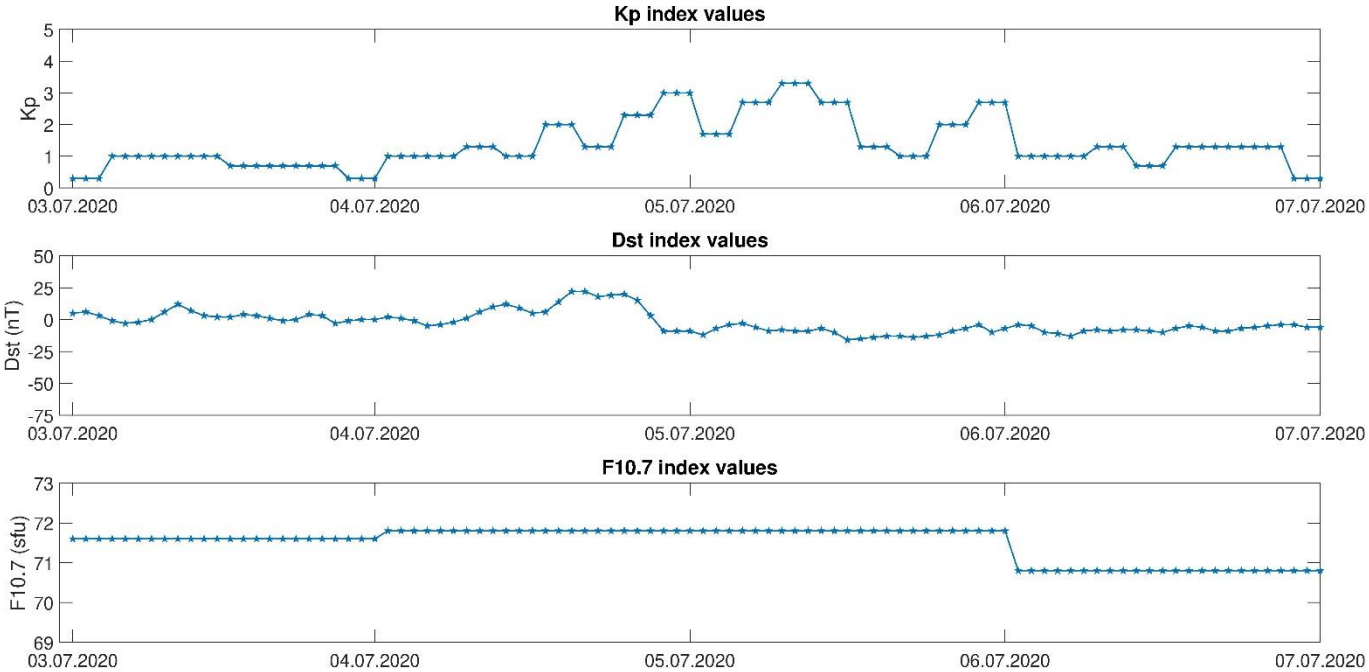

Figure 15. Kp, Dst and F10.7 index values during the field tests (https://omniweb.gsfc.nasa.gov/form/dx1.html)

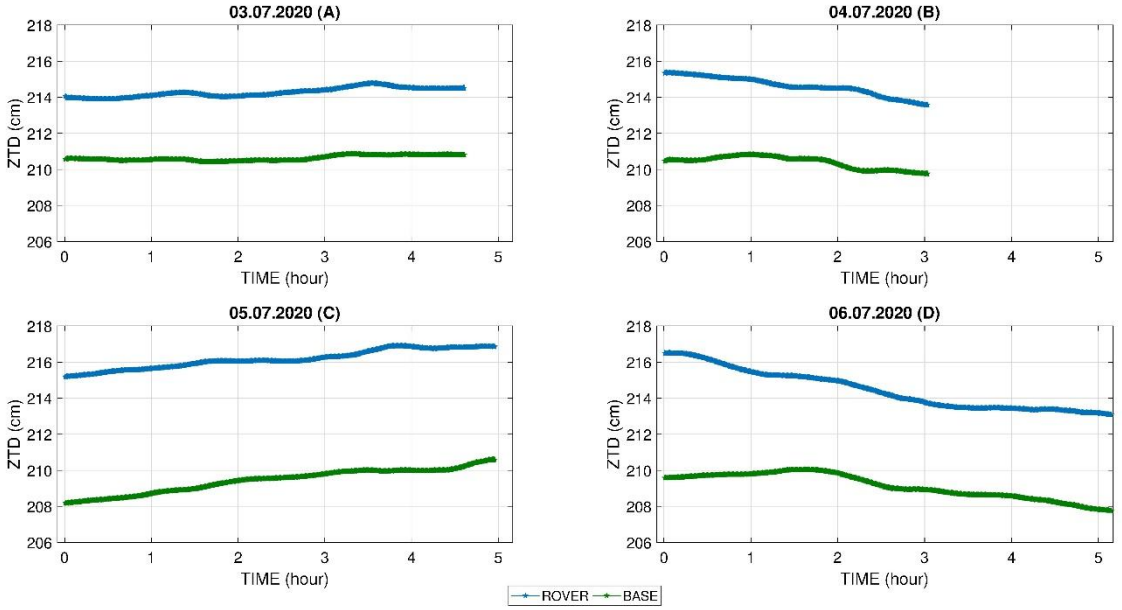

Figure 16. ZTD values at the first phase of measurements (https://webapp.geod.nrcan.gc.ca/geod/tools-outils/ppp.php)

Another subject related to GNSS signal path delay is the nonionized layer of the atmosphere so-called, troposphere. The tropospheric delay consists of hydrostatic and wet components. With the PPP method, coordinate components, ambiguities, receiver clock error, and tropospheric delay parameters are estimated (Hofmann-Wellenhof et al. 2007). For this study, tropospheric delays were obtained by using CSRS-PPP (The Canadian Spatial Reference System-PPP) online service. CSRS-PPP is a practical and robust online PPP post-processing service for estimating coordinate or troposphere (Mendez Astudillo et al. 2018). The CSRS-PPP provides tropospheric dry and wet components separately. The sum of dry and wet components is equal to ZTD (Zenith Total Delay). Since the static data recording was only performed in the first phase of measurements, only ZTD values in the first phase could be evaluated. As the troposphere condition was the same for different satellite configurations at the test sites, only data of GR was processed since the CSRS-PPP supports GPS and GLONASS satellite systems. Besides, the data of the base station was processed to distinguish the troposphere correlation between the base station and the rover. Figure 16 shows the ZTD values of base station and rovers for each measurement day. Also, the ZTD differences between base station and rover were examined. Accordingly, the maximum ZTD differences are computed as 3.97 cm, 4.88 cm, 7.07 cm, and 6.92 cm for the consecutive days (3-6 July 2020), respectively. These differences should be taken into consideration since they can defect the solutions. Moreover, the ZTD correlation coefficients between the base station and rovers were computed and given in Table 9.

Table 9. The ZTD correlation percentages

Sites	Date	Correlation (%)
A	03.07.2020	84.93
B	04.07.2020	81.20
C	05.07.2020	95.37
D	06.07.2020	87.15

As clearly seen from Table 9, troposphere highly correlated between the base station and rovers in all four sites. Furthermore, to better illustrate the high correlation, the RTK coordinate time series of G, GR and GREC configurations at 10° cut-off angle option is provided in Figure 17, as an example (Site-D). As can be seen from the up component in Figure 17, the G and GREC solutions show a similar trend with the ZTD difference.

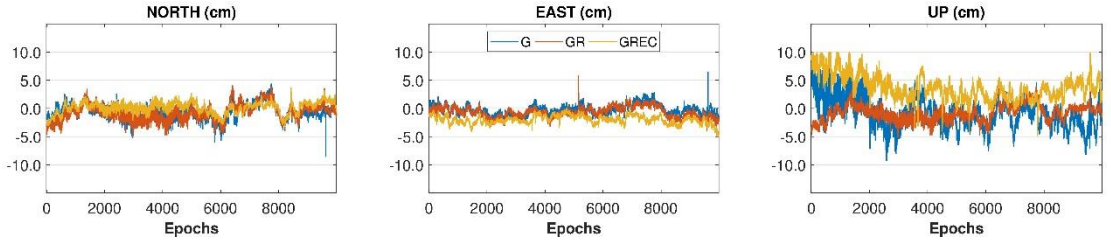

Figure 17. The coordinate time series for the day 06.07.2020 (Site-D)

4. CONCLUSION

In this study, the performance of the RTK method with different satellite combinations (G, GR and GREC) has been investigated comprehensively. For this purpose, a field test was conducted considering short and long-baseline lengths. Moreover, low and high satellite elevation cut-off angles were used to represent urban canyon and open sky conditions. The ground truth coordinates of rovers were obtained by post-process

relative method using the same base station as the reference. The results were evaluated considering atmospheric conditions, which is important for real time positioning.

When the results are analyzed, multi-GNSS combinations have an undeniable impact on repeatability. In terms of accuracy, the maximum RMSe of GPS-only solutions were 2.17 cm, 2.04 and 4.94 for north, east and up components, respectively. It can be concluded that single-base RTK can provide a few centimeters level of accuracy even for baseline distances up to ~80 km. Despite the fact that the number of satellites increases the RTK performance, in this study, the multi-GNSS combinations are not always improved the results. Even at high cut-off angle, GPS-only solutions are more accurate than at a very high cut-off angle. It can be concluded that, when the satellite geometry is good, GPS-only solutions are comparable with multi-GNSS solutions. However, baseline distance is an important issue for RTK measurements. From the results of this case study, it can be stated that the horizontal accuracy differences between short and long-baseline distances are sub-centimeter level. As well, the vertical accuracy differences are in a few centimeters level.

The changes in the troposphere and ionosphere layers were investigated in terms of atmospheric conditions. There was not any ionospheric storm during applications. When the troposphere is evaluated, in general, it is found that ZTD values are correlated between base station and rover. However, the maximum ZTD differences of the base-rover station achieve 7.07 cm. As the height difference increased the maximum ZTD difference is increased. Due to this reason, as well as the baseline distance, the height difference should be considered for a better comparison of multi-GNSS RTK measurements.

ACKNOWLEDMENT

This study was funded by Necmettin Erbakan University Scientific Research Projects (Project No: 201319004). We appreciate the technical team of CHC Turkey and Ufuk R. Ozbey for their support during this study. The authors also thank MIT for providing GAMIT/GLOBK software.

Author contribution

Omer Faruk Atiz: Methodology, Visualization, Editing; **Ceren Konukseven**: Methodology, Writing-Original draft preparation, Editing; **Salih Sermet Öğütcü**: Conceptualization, Writing-Original draft preparation; **Salih Alçay**: Conceptualization, Investigation, Writing-Reviewing

Conflicts of interest

The authors declare no conflicts of interest.

REFERENCES

Alçay S & Atiz Ö (2021). Farklı Yazılımlar Kullanılarak Gerçek Zamanlı Hassas Nokta Konum Belirleme (RT-PPP) Yönteminin Performansının İncelenmesi. Geomatik, 6 (1), 77-83. https://doi.org/10.29128/geomatik.687709.

Alcay S & Gungor M (2020). Investigation of ionospheric TEC anomalies caused by space weather conditions. Astrophysics and Space Science, 365(9), 1-15. https://doi.org/10.1007/s10509-020-03862-x.

Atiz O, Alcay S, Ogutcu S & Kalayci I (2020). Necmettin Erbakan University Continuously Operating Reference Station. Intercontinental Geoinformation Days (IGD), 44-47, Mersin, Turkey.

Baybura T, Tiryakioğlu İ, Uğur M A, Solak H İ & Şafak Ş (2019). Examining the accuracy of network RTK and long base RTK methods with repetitive measurements. Journal of Sensors, 2019. https://doi.org/10.1155/2019/3572605.

Bothmer V & Daglis I A (2007). Space weather: physics and effects. Springer Science & Business Media. ISBN 978-3-540-23907-9

Bramanto B, Gumilar I, Taufik M & Hermawan I M D (2019). Long-range Single Baseline RTK GNSS Positioning for Land Cadastral Survey Mapping. In E3S Web of Conferences (ISGNSS 2018), 94, 01022, Bali, Indonesia.

Castro-Arvizu J M, Medina D & Ziebold R (2020). Impact of Satellite Elevation Mask in GPS+ Galileo RTK Positioning. In Institute of Navigation International Technical Meeting 2020, 487-498, San Diego, California.

Dabove P & Di Pietra V (2019). Single-baseline RTK positioning using dual-frequency GNSS receivers inside smartphones. Sensors, 19(19), 4302. http://dx.doi.org/10.3390/s19194302.

Dabove P (2019). The usability of GNSS mass-market receivers for cadastral surveys considering RTK and NRTK techniques. Geodesy and Geodynamics, 10(4), 282-289. https://doi.org/10.1016/j.geog.2019.04.006.

Edwards S J, Clarke P J, Penna N T & Goebell S (2010). An examination of network RTK GPS services in Great Britain. Survey Review, 42(316), 107-121. https://doi.org/10.1179/003962610X12572516251529.

El-Mowafy A & Kubo N (2017). Integrity monitoring of vehicle positioning in urban environment using RTK-GNSS, IMU and speedometer. Measurement Science and Technology, 28(5), 055102. https://doi.org/10.1088/1361-6501/aa5c66.

Erenoglu R C (2017). A comprehensive evaluation of GNSS-and CORS-based positioning and terrestrial surveying for cadastral surveys. Survey Review, 49(352), 28-38. https://doi.org/10.1080/00396265.2015.1104093.

Herring T A, King R W & McClusky S C (2010). Introduction to GAMIT/GLOBK. Massachusetts Institute of Technology, Cambridge, Massachusetts.

Hofmann-Wellenhof B, Lichtenegger H & Wasle E (2007). GNSS–global navigation satellite systems: GPS, GLONASS, Galileo, and more. Springer Science & Business Media. ISBN 978-3-211-73012-6

Kim D & Langley R B (2008). Improving Long-Range RTK. GPS World.

Kouba J & Héroux P (2001). Precise point positioning using IGS orbit and clock products. GPS solutions, 5(2), 12-28. https://doi.org/10.1007/PL00012883.

Lagler K, Schindelegger M, Böhm J, Krásná H & Nilsson T (2013). GPT2: Empirical slant delay model for radio space geodetic techniques. Geophysical research letters, 40(6), 1069-1073. https://doi.org/10.1002/grl.50288.

Li G, Wu J, Zhao C & Tian Y (2017b). Double differencing within GNSS constellations. GPS Solutions, 21(3), 1161-1177. https://doi.org/10.1007/s10291-017-0599-4.

Li T, Zhang H, Niu X & Gao Z (2017a). Tightly-coupled integration of multi-GNSS single-frequency RTK and MEMS-IMU for enhanced positioning performance. Sensors, 17(11), 2462. http://dx.doi.org/10.3390/s17112462.

Li X, Lv H, Ma F, Li X, Liu J & Jiang Z (2019). GNSS RTK positioning augmented with large LEO constellation. Remote Sensing, 11(3), 228. https://doi.org/10.3390/rs11030228.

Luo X, Schaufler S, Branzanti M & Chen J (2020). Assessing the benefits of Galileo to high-precision GNSS positioning–RTK, PPP and post-processing. Advances in Space Research. https://doi.org/10.1016/j.asr.2020.08.022.

Mendez Astudillo J, Lau L, Tang Y T & Moore T (2018). Analysing the zenith tropospheric delay estimates in on-line precise point positioning (PPP) services and PPP software packages. Sensors, 18(2), 580. https://doi.org/10.3390/s18020580.

Mi X, Zhang B & Yuan Y (2019). Multi-GNSS inter-system biases: estimability analysis and impact on RTK positioning. GPS Solutions, 23(3), 81. https://doi.org/10.1007/s10291-019-0873-8.

Odijk D & Teunissen P J (2013). Characterization of between-receiver GPS-Galileo inter-system biases and their effect on mixed ambiguity resolution. GPS solutions. 17(4), 521-533. https://doi.org/10.1007/s10291-012-0298-0.

Odijk D & Wanninger L (2017). Differential Positioning. In: Teunissen P.J., Montenbruck O. (eds) Springer Handbook of Global Navigation Satellite Systems. Springer Handbooks. ISBN 978-3-319-42928-1

Odijk D, Verhagen S & Teunissen P J G (2012). Medium-distance GPS ambiguity resolution with controlled failure rate. In Geodesy for Planet Earth (pp. 745-751). Springer, Berlin, Heidelberg. https://doi.org/10.1007/978-3-642-20338-1_93.

Odolinski R, Teunissen P J G & Odijk D (2015a). Combined GPS+ BDS for short to long baseline RTK positioning. Measurement Science and Technology, 26(4), 045801. http://dx.doi.org/10.1088/0957-0233/26/4/045801.

Odolinski R, Teunissen P J G & Odijk D (2015b). Combined BDS, Galileo, QZSS and GPS Single-Frequency RTK. GPS Solutions, 19(1), 151-163. https://doi.org/10.1007/s10291-014-0376-6.

Ogutcu S & Kalayci I (2018). Accuracy and precision of network-based RTK techniques as a function of baseline distance and occupation time. Arabian Journal of Geosciences, 11(13), 354. https://doi.org/10.1007/s12517-018-3712-2.

Ogutcu S (2019). Temporal correlation length of network based RTK techniques. Measurement, 134, 539-547. https://doi.org/10.1016/j.measurement.2018.10.099.

Paziewski J & Wielgosz P (2017). Investigation of some selected strategies for multi-GNSS instantaneous RTK positioning. Advances in Space Research, 59(1), 12-23. https://doi.org/10.1016/j.asr.2016.08.034.

Shu B, Liu H, Xu L, Qian C, Gong X & An X (2018). Performance analysis of BDS medium-long baseline RTK positioning using an empirical troposphere model. Sensors, 18(4), 1199. https://doi.org/10.3390/s18041199.

Tian Y, Sui L, Xiao G, Zhao D & Tian Y (2019). Analysis of Galileo/BDS/GPS signals and RTK performance. GPS Solutions, 23(2), 37. https://doi.org/10.1007/s10291-019-0831-5.

Weber G, Dettmering D & Gebhard H (2005). Networked transport of RTCM via internet protocol (NTRIP). In A Window on the Future of Geodesy, 60-64, Berlin, Germany.

Wessel P, Luis J F, Uieda L, Scharroo R, Wobbe F, Smith W H F & Tian D (2019). The generic mapping tools version 6. Geochemistry, Geophysics, Geosystems, 20(11), 5556-5564. https://doi.org/10.1029/2019GC008515.

Wielgosz P, Kashani I & Grejner-Brzezinska D (2005). Analysis of long-range network RTK during a severe ionospheric storm. Journal of Geodesy, 79(9), 524-531. https://doi.org/10.1007/s00190-005-0003-y.

Yu J, Yan B, Meng X, Shao X & Ye H (2016). Measurement of bridge dynamic responses using network-based real-time kinematic GNSS technique. Journal of Surveying Engineering, 142(3), 04015013. http://dx.doi.org/10.1061/(ASCE)SU.1943-5428.0000167.

Zhang Y, Kubo N, Chen J, Chu F Y, Wang H & Wang J (2020). Contribution of QZSS with four satellites to multi-GNSS long baseline RTK. Journal of Spatial Science, 65(1), 41-60. https://doi.org/10.1080/14498596.2019.1646676.

Zumberge J F, Heflin M B, Jefferson D C, Watkins M M & Webb F H (1997). Precise point positioning for the efficient and robust analysis of GPS data from large networks. Journal of geophysical research: solid earth, 102(B3), 5005-5017. https://doi.org/10.1029/96JB03860.

International Journal of Engineering and Geosciences
https://dergipark.org.tr/en/pub/ijeg
e-ISSN 2548-0960

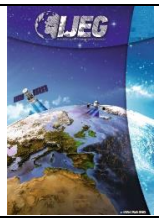

Investigation of the performance of different wavelet-based fusions of SAR and optical images using Sentinel-1 and Sentinel-2 datasets

Hüseyin Duysak [*1], **Enes Yigit** [2]

[1]*Karamanoglu Mehmetbey University, Engineering Faculty, Electrical Electronics Engineering, Karaman, Turkey*
[2]*Bursa Uludag University, Engineering Faculty, Electrical Electronics Engineering, Bursa, Turkey*

Keywords
Synthetic aperture radar (SAR)
Optical
Wavelet
Sentinel

ABSTRACT

In this study, the fusion of optical and synthetic aperture radar images with wavelet transform was investigated. Images are obtained from Sentinel-1 and sentinel-2 satellites. Images were decomposed by wavelet transform. The four main coefficients were obtained for different wavelet packages and up to ten decomposition levels. The coefficients were combined taking the maximum, minimum or mean. 1710 Fused images were obtained for all possible combinations in terms of different wavelet packets, decomposition levels and fusion rules. Fused images were evaluated according to the structural similarity index (SSI). It was seen that the missing regions in the optical images were improved in the fused images with the appropriate wavelet packets and highest SSI.

1. INTRODUCTION

Image fusion is the unification of different images. The fused image includes information from all images. Image fusion has a wide range of applications such as sensor networks, remote sensing and medical (James and Dasarathy, 2014; Khaleghi et al. 2013). On the other hand, multimodal image fusion is performed by using images of different sensors. Thus, more meaningful information than a single sensor can be obtained in the fused image. In remote sensing applications, the fusion of synthetic aperture radar (SAR) image and the optical image has become popular due to the specific properties of images. SAR is one of the most important imaging systems, since radar are independent of weather and environmental conditions such as dust, smoke and cloud. Therefore, SAR images are an important information source in the evaluation of hazardous situations such as earthquake, landslide and volcanic eruption. Technically, SAR systems electromagnetically illuminate earth surface and collects reflected signals from earth objects. The energy of the reflected signal depends on the moisture, shape, dielectric coefficient of the surface and sensor parameters such as frequency, polarization, observation angle. On the other hand, optical imaging system (OIS) is based on passive sensor and passive imaging systems need external source such as solar. Optical image (OI) is obtained by collecting a reflected solar energy from earth objects. Thus, OI depends on spectral resolution (infrared, visible or ultraviolet) and weather conditions. In terms of spectral characteristic, OI are categorized as panchromatic (PAN), multispectral (MS) and hyperspectral images (HS). PAN images are obtained using sensors with a frequency range covering from visible to a portion near-infrared of the spectrum. MS sensors provide MS images having different bands of spectrum. Thus, MS images are higher spectral resolution than PAN, but lower spatial resolution. The HS sensor generates the image by collecting signal from more bands of spectrum than MS. Therefore, hyperspectral images have more spectral information than MS and PAN, but their spatial resolutions are lower than MS and PAN images (Kulkarni and Rege 2020).

Optical-Optical and Optical-SAR image fusion types have each specific beneficial for practical applications. Optical-optical image fusion can be used to increase spectral resolution. Optical-SAR fusion can be used for better evaluation of surface features of the study area like

* **Corresponding Author**
*(huseyinduysak@kmu.edu.tr) ORCID ID 0000-0002-2748-0660
(enesyigit81@gmail.com) ORCID ID 0000-0002-0960-5335

Cite this article
Duysak H & Yigit E (2022). Investigation of the performance of different wavelet-based fusions of SAR and optical images using Sentinel-1 and Sentinel-2 datasets. International Journal of Engineering and Geosciences, 7(1), 81-90

Research Article / DOI: 10.26833/ijeg.882589 **Received: 18/02/2021; Accepted: 09/04/2021**

identifying Antarctic Ice features (Shah et al. 2019), plant species detection (Rajah et al. 2018).

SAR and optical systems are mounted on plane or satellite (Kulkarni and Rege 2020). Today, there are many satellites that actively provide SAR and optical images for academic research. One of them is sentinel. While the radar-based Sentinel-1 satellite captures SAR images, Sentinel-2 satellite is based on optical imaging and captures multispectral images. Images of Sentinel satellites are used in various applications such as agriculture (Veloso et al. 2017) and evaluation of natural disasters (Ghorbanzadeh et al. 2020).

For a valuable evaluation, it is important to combine as much data as possible from both image sources in the fusion process. In this way, missing data in SAR or optical images caused by some situations such as weather conditions, system noise, or smoke can be effectively completed. One of the basis of level fusion technique is pixel-level fusion (PLF). PLF is more appropriate in remote sensing applications due to less information loss than decision and feature level fusion techniques. However, PLF needs high computational process. In PLF, the fused image is obtained by combining pixel values of different images. Thus, before the fusion, some pre-processing techniques such as registration, denoising may be required, especially in multimodal medical image fusion (Aslan et al. 2019).

Image fusion can be performed by different methods such as Intensity Hue Saturation (IHS), Principal Component analysis (PCA), multiresolution techniques, sparse representations. One of the most popular method of multiresolution techniques is the wavelet transform (Kulkarni and Rege 2020). In this study, the SAR and optical images are fused using wavelet transform. Images were analysed by wavelet transform and fused according to maximum, minimum and mean methods based a fusion rule. This fusion rule is one of the traditional methods used in wavelet based fusion (Hemdan, 2021; Pajares and Manuel de la Cruz 2004). Fused images were obtained using different wavelet packages and decomposition levels. The similarity between fused image and original images is determined by using quality metrics with peak signal to noise ratio (PSNR), mean square error (MSE), structural similarity index (SSI), entropy (H) and feature similarity index (FSI).

The remainder of this work is organized as follows; in the second part includes the wavelet-based fusion, dataset and quality metrics. The results of the images given in the third part; the conclusions are summarized in the last part.

2. METHOD

2.1. Wavelet Transform Based Image Fusion

Wavelet transform is one of the most popular multiresolution analyse techniques in signal/ image processing applications such as noise removal and compression. Wavelet transform decomposes the image into low and high frequency components using wavelet packages. Four main coefficients are obtained as lower resolution approximation (LL), vertical (LH), horizontal (HL), and diagonal (HH) (Hemdan, 2021; Pajares and Manuel de la Cruz 2004). These coefficients of different images can be used to constitute a new coefficient by means of a fusion rule. Therefore, the fusion of images can be obtained with the new coefficient.

2.2. Fusion Rule

The different images are decomposed by applying the discrete wavelet transform (DWT). The combination of coefficients (LL, LH, HL, HH) is merged according to a fusion rule.

The one of the basic rules is to obtain new coefficients by taking the maximum, minimum or mean value of the coefficients, and then the fused image is obtained by taking inverse discrete wavelet transform (IDWT) (Pajares and Manuel de la Cruz 2004). The fusion rule is summarized in Fig. 1.

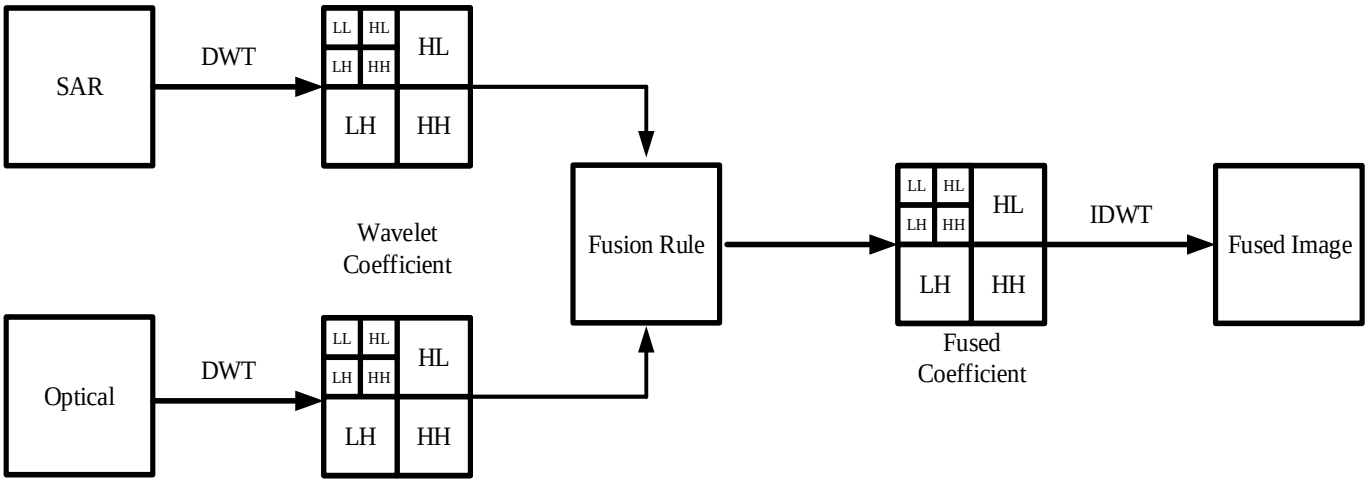

Figure 1. Fusion Rule Block Diagram

2.3. Quality Metrics

PSNR, SSI, H, FSI and MSE were used to evaluate the performance of the fused images. H with a higher value indicates that the images contain more information. The PSNR value indicates the dominance of the input image in the fused image. If the SSI and FSI are high, this indicates that there is much similarity between the source image and the fused image. Besides, as MSE

decreases, the similarity between the input and the fused images increases (Kulkarni and Rege 2020).

2.4. Dataset

In this study, optical and SAR images captured by Sentinel-1 and Sentinel-2 satellites were used. The location of the site in the images, which is a part of the city of Karaman, is indicated in the Table 1.

Table 1. Geo-coordinates of site

Latitude Bound		Longitudes Bound	
North	37.235	West	33.177
South	37.197	East	33.277

Three datasets were downloaded from Copernicus Open Access Hub. Information of datasets are given in Table 2. The images were obtained by processing the datasets in sentinel application platform (SNAP) software (Foumelis et al. 2018). The optical images were obtained by applying the procedure given in Fig. 2. Prior to the subset the data were resampled to generate the image with the same spatial resolution since Sentinel-2 bands have different spatial resolution of 10, 20 and 60 meters. In order to constitute the SAR image, procedure shown in Fig. 3 were applied in SNAP. After the subset, calibration was applied to create the SAR image with accurate backscattering data. Then, Lee filter (Yommy et al. 2015) was performed to remove speckle noise. In order to represent pixels of images with correct locations, range doppler terrain correction was used. Finally, colorization of SAR image were obtained using vertical-vertical (VV) and vertical-horizontal (VH) polarization data. Red(R), green(G) and blue(B) components of coloured SAR image are obtained as follows,

$$R = Amplitude\ of\ VV\ backscattering\ data\ in\ dB$$
$$G = Amplitude\ of\ VH\ backscattering\ data\ in\ dB$$
$$B = \frac{Amplitude\ of\ VH\ backscattering\ data\ in\ dB}{Amplitude\ of\ VV\ backscattering\ data\ in\ dB}$$

Two optical (OP-1 and OP-2) and SAR (SAR1) images are given in Fig. 4. Optical images have some missing regions arising from various factors like smoke, dust or fog. These regions are shown with red rectangles.

Table 2. Information of Datasets

Image Label	Satellite	Acquisition Date	Acquisition Modes	Polarization	Level
OP1	Sentinel-2	08.01.2021	-	-	L1C
OP2	Sentinel-2	01.01.2021	-	-	L2A
SAR1	Sentinel-1	25.01.2021	*Interferometric Wide* (IW)	VV, VH	L1

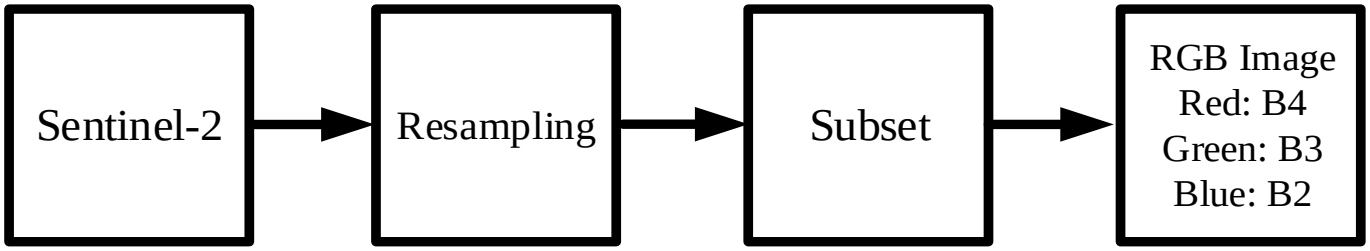

Figure 2. Sentinel-2 Data Processing

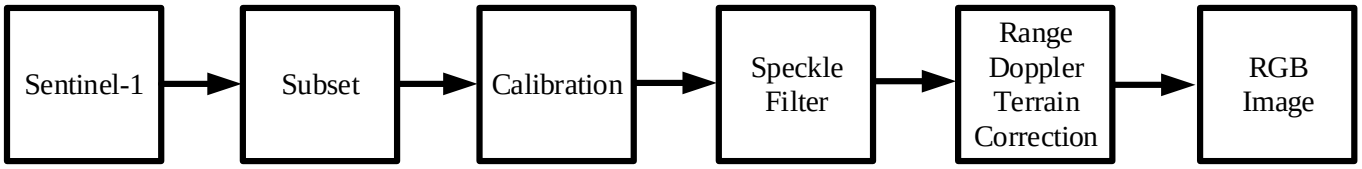

Figure 3. Sentinel-1 Data Processing

3. RESULTS

The Optical and SAR images in Fig. 4 were analysed by applying wavelet transform with different wavelet packages including Daubechies (db1, db2, db3), Coiflets (coif1, coif2, coif3), Symlets (sym1, sym2, sym3), Fejer-Korovkin filters (fk4, fk6, fk8), Discrete Meyer (dmey), Biorthogonal (bior1.1, bior1.3, bior1.5) and Reverse Biorthogonal (rbior1.1, rbior1.3, rbior1.5) (Pajares and Manuel de la Cruz 2004). Wavelet coefficients of OP1, OP2 and SAR1 images are shown for "db1" wavelet package with level 1 in Fig. 5.

The optical images were fused with each other and the SAR image. Besides, images were analysed for decomposition level from 1 to 10. The combination of coefficients was performed by applying nine fusion rules in Table 3.

A total of 1710 fused images with 9 fusion rules, 19 wavelet packets and 10 decomposition levels can be obtained for each fusion application. In this study, 1710 fused images were obtained for each fusion of OP1-OP2, OP1-SAR1 and OP2-SAR1 images. Fused images were evaluated using quality metrics. Missing regions in optical images were evaluated in terms of clearness.

(a)

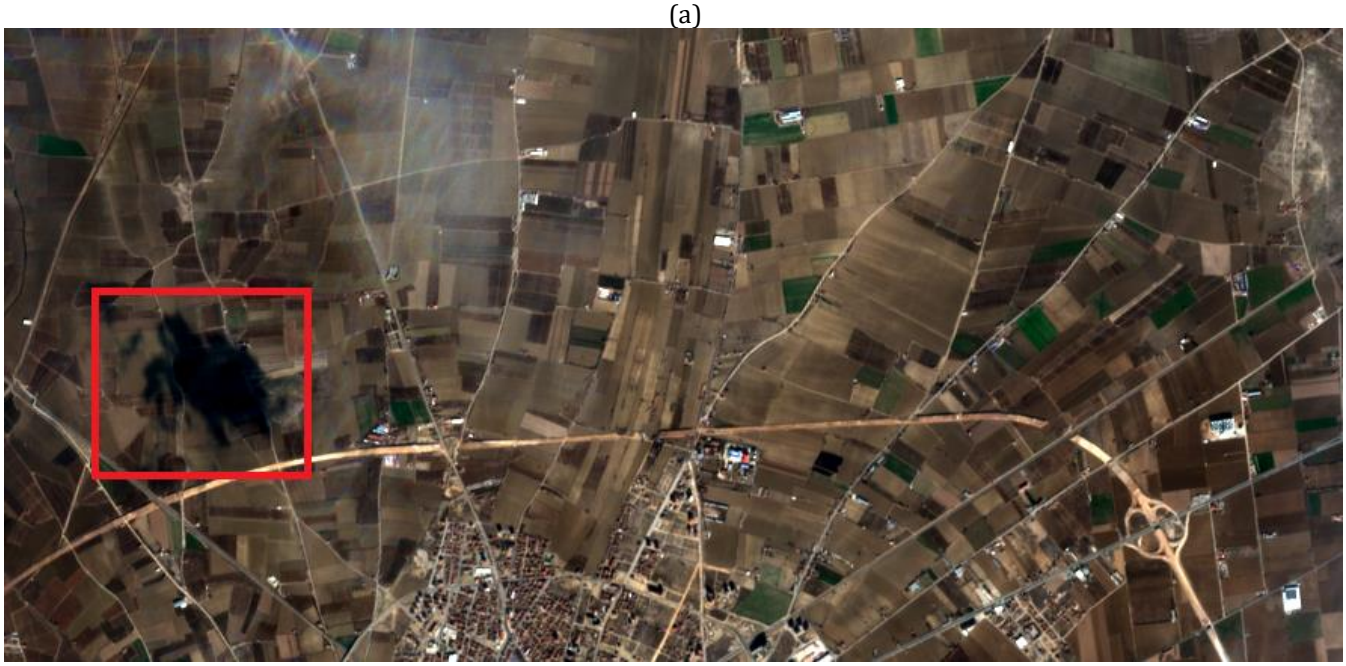

(b)

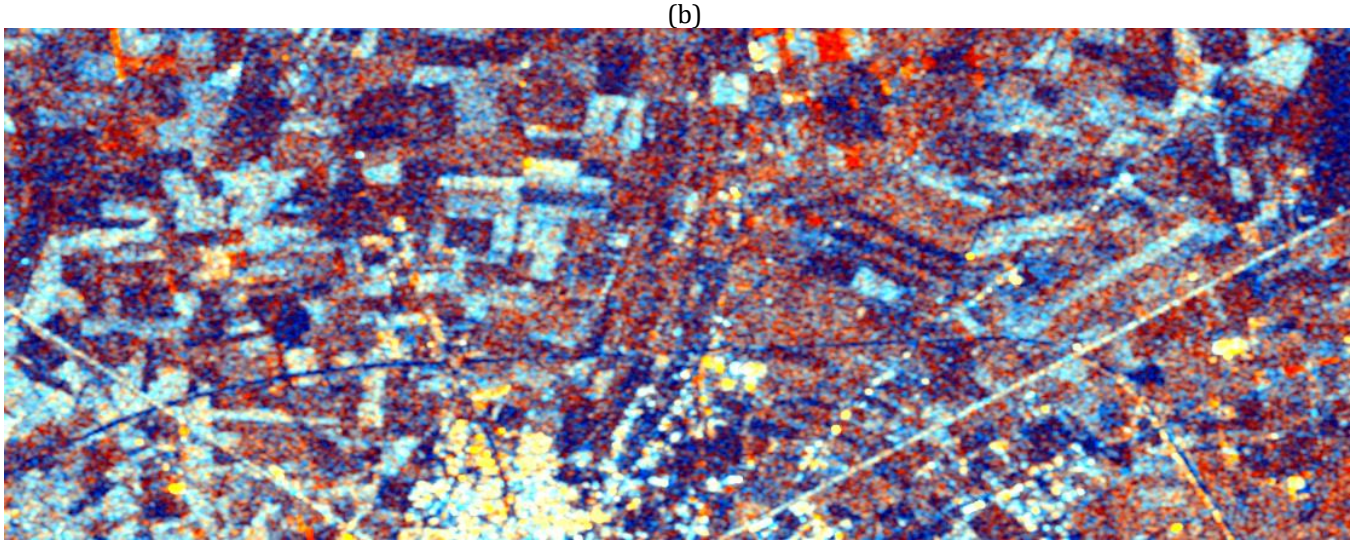

(c)

Figure 4. Sentinel 1 and Sentinel 2 dataset (a) OP1: Optical image from Sentinel-2 on 08 January 2021, (b) OP2: Optical image from Sentinel-2 on 01 January 2021 (c) SAR1: SAR RGB Image from Sentinel-1 IW- L1 ground range detected (GRD) on 25 January 2021

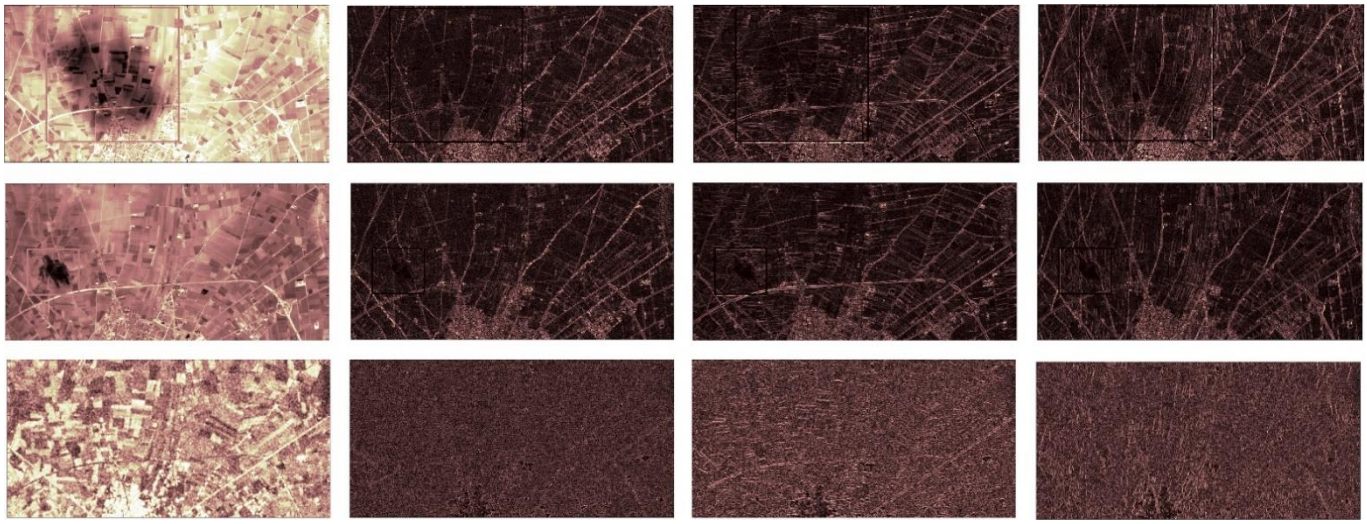

(a) (b) (c) (d)

Figure 5. Representation of wavelet coeficients of OP1, OP2 and SAR1 images for "db1" of level 1 (a) approximation (b) diagonal (c) horizontal (d) vertical

Table 3. Fusion rules used in combining the wavelet coefficients.

Approximation Coefficient.	Detail Coefficient
Max	Max
Max	Min
Max	Mean
Min	Min
Min	Max
Min	Mean
Mean	Mean
Mean	Max
Mean	Min

3.1. OP1-OP2 Image Fusion

In this section, fusion of optical images were evaluated. 1710 fused images were obtained using OP1 and OP2 images. Results are sorted by SSI values. The fusion parameters and metric values for the top 10 highest SSI values between the OP1 and the fused images are given in Table 4. The results for the 10 highest SSI values between OP2 and fused images are given in Table 5. The Fus1 and Fus11 fused images with the best SSI value in the Table 4-5 are given in Fig. 6 and Fig .7. SSI values of the Fus1 image with OP1 and OP2 images were respectively 0,86 and 0,56. Thus, the Fus1 image is more similar to the OP1 image. On other hand, SSI values of the Fus11 image and original images were calculated as 0,54 and 0,84. Unlike Fus1, the Fus11 is more similar to the OP2 image. However, the Fus1 is better than the Fus 11 in terms of clarity.

Figure *6.* The Fused image of OP1-OP2 according to the Fus1 parameters in Table 4

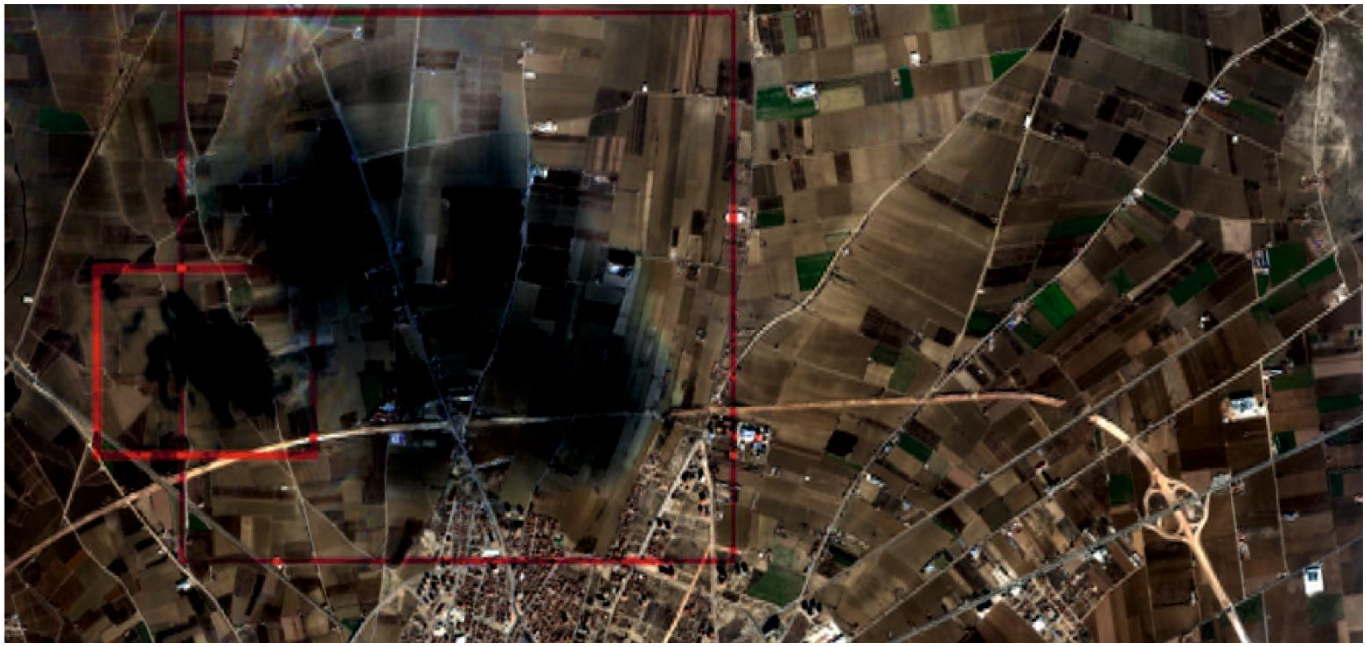

Figure 7. The Fused image of OP1-OP2 according to the Fus11 parameters in Table 5

Table 4. Fusion parameters and quality metrics of fusion of OP1 and OP2 images (selected by SSI of OP1)

Fused Image Label	Fusion Parameters				Quality Metrics								
			Fusion Rule		OP2					OP1			
	Level	Wavelet packet	Approx. Coef.	Detail Coef.	H	MSE	PSNR	SSI	FSI	MSE	PSNR	SSI	FSIM
Fus1	1	fk8	max	mean	7,69	6673,79	9,89	0,56	0,81	533,69	20,86	0,86	0,96
Fus2	8	rbio1.3	max	max	7,77	6754,43	9,83	0,48	0,81	264,03	23,91	0,86	0,94
Fus3	1	coif3	max	mean	7,68	6667,14	9,89	0,56	0,81	539,23	20,81	0,86	0,96
Fus4	1	fk6	max	mean	7,69	6668,70	9,89	0,56	0,81	534,70	20,85	0,86	0,96
Fus5	1	coif2	max	mean	7,68	6663,90	9,89	0,56	0,81	540,25	20,80	0,86	0,96
Fus6	1	dmey	max	mean	7,69	6672,21	9,89	0,56	0,81	536,99	20,83	0,86	0,96
Fus7	1	db3	max	mean	7,69	6667,97	9,89	0,56	0,81	534,60	20,85	0,86	0,96
Fus8	1	sym3	max	mean	7,69	6667,97	9,89	0,56	0,81	534,60	20,85	0,86	0,96
Fus9	1	fk8	max	max	7,69	6718,42	9,86	0,55	0,81	538,87	20,82	0,86	0,96
Fus10	1	rbio1.5	max	mean	7,69	6660,34	9,90	0,56	0,81	536,53	20,83	0,86	0,96

Table 5. Fusion parameters and quality metrics for fusion of OP1 and OP2 images (selected by SSI of OP2)

Fused Image Label	Fusion Parameters				Quality Metrics								
			Fusion Rule		OP2					OP1			
	Level	Wavelet packet	Approx. Coef.	Detail Coef.	H	MSE	PSNR	SSI	FSIM	MSE	PSNR	SSI	FSIM
Fus11	1	fk8	min	min	7,05	545,40	20,76	0,84	0,94	6755,03	9,83	0,54	0,81
Fus12	1	db3	min	min	7,04	546,46	20,76	0,84	0,94	6754,36	9,83	0,54	0,81
Fus13	1	sym3	min	min	7,04	546,46	20,76	0,84	0,94	6754,36	9,83	0,54	0,81
Fus14	1	fk8	min	mean	7,06	534,23	20,85	0,84	0,94	6688,65	9,88	0,57	0,81
Fus15	1	dmey	min	min	7,05	546,30	20,76	0,84	0,94	6753,48	9,84	0,54	0,81
Fus16	1	fk6	min	min	7,04	547,15	20,75	0,84	0,94	6753,36	9,84	0,54	0,81
Fus17	1	coif3	min	min	7,05	550,03	20,73	0,84	0,94	6749,97	9,84	0,54	0,81
Fus18	1	fk6	min	mean	7,06	535,25	20,85	0,84	0,94	6684,41	9,88	0,57	0,81
Fus19	1	db3	min	mean	7,06	535,14	20,85	0,84	0,94	6682,48	9,88	0,57	0,82
Fus20	1	sym3	min	mean	7,06	535,14	20,85	0,84	0,94	6682,48	9,88	0,57	0,82

3.2. OP1-SAR1 Image Fusion

In this section, the performance of the fusion of OP1 and SAR1 images are investigated. The fusion parameters and metric values with the highest similarity between the fused and SAR1 images are given in Table 6 for top ten results. Besides, the fusion parameters and metric values with the highest similarity between the fused and OP1 images are given in Table 7 for top ten results. Whereas the highest SSI value between SAR1 and fused images is 0,78, the highest SSI value between OP2 and fused images is 0,46. The fused images (Fus21 and Fus31) are shown in Fig. 8 and Fig. 9. As seen from the fused images, the missing regions in optical images were improved by SAR images.

Table 6. Fusion parameters and quality metrics for fusion of OP1 and SAR1 images (selected by SSI of SAR1)

Fused Image Label	Fusion Parameters				Quality Metrics								
	Level	Wavelet packet	Fusion Rule		OP1					SAR1			
			Approx. Coef.	Detail Coef.	H	MSE	PSNR	SSI	FSI	MSE	PSNR	SSI	FSI
Fus21	5	rbio1.3	mean	max	7,74	4234,11	11,86	0,23	0,66	2090,60	14,93	0,78	0,88
Fus22	4	rbio1.3	mean	max	7,74	3701,92	12,45	0,24	0,67	2156,31	14,79	0,78	0,86
Fus23	5	coif2	mean	max	7,75	4230,84	11,87	0,22	0,66	2109,38	14,89	0,78	0,88
Fus24	5	db3	mean	max	7,74	4254,31	11,84	0,22	0,66	2111,84	14,88	0,78	0,87
Fus25	5	sym3	mean	max	7,74	4254,31	11,84	0,22	0,66	2111,84	14,88	0,78	0,87
Fus26	5	coif1	mean	max	7,75	4285,21	11,81	0,22	0,66	2102,16	14,90	0,78	0,87
Fus27	5	fk6	mean	max	7,75	4263,14	11,83	0,22	0,66	2105,35	14,90	0,78	0,87
Fus28	4	coif2	mean	max	7,74	3715,68	12,43	0,23	0,67	2178,87	14,75	0,78	0,86
Fus29	4	rbio1.5	mean	max	7,73	3693,07	12,46	0,24	0,67	2178,97	14,75	0,77	0,86
Fus30	5	rbio1.5	mean	max	7,74	4252,96	11,84	0,22	0,66	2120,25	14,87	0,77	0,88

Table 7. Fusion parameters and quality metrics for fusion of OP1 and SAR1 images (selected by SSI of OP1)

Fused Image Label	Fusion Parameters				Quality Metrics								
	Level	Wavelet packet	Fusion Rule		OP1					SAR1			
			Approx. Coef.	Detail Coef.	H	MSE	PSNR	SSI	FSI	MSE	PSNR	SSI	FSI
Fus31	1	dmey	max	max	7,48	4290,36	11,81	0,46	0,76	4362,61	11,73	0,54	0,77
Fus32	1	rbio1.5	max	mean	7,51	4288,86	11,81	0,45	0,77	4256,68	11,84	0,55	0,78
Fus33	1	rbio1.5	max	max	7,49	4273,07	11,82	0,45	0,77	4309,69	11,79	0,55	0,78
Fus34	1	coif3	max	max	7,48	4299,69	11,80	0,45	0,76	4350,66	11,75	0,55	0,78
Fus35	1	rbio1.3	max	mean	7,51	4279,61	11,82	0,45	0,77	4241,61	11,86	0,56	0,78
Fus36	1	dmey	max	mean	7,49	4326,09	11,77	0,45	0,76	4298,56	11,80	0,55	0,78
Fus37	1	coif3	max	mean	7,49	4323,20	11,77	0,44	0,76	4291,77	11,80	0,55	0,78
Fus38	1	fk8	max	mean	7,49	4318,33	11,78	0,44	0,76	4290,36	11,81	0,55	0,78
Fus39	1	coif2	max	mean	7,49	4319,51	11,78	0,44	0,76	4285,66	11,81	0,55	0,78
Fus40	1	fk8	max	max	7,48	4298,62	11,80	0,44	0,76	4346,17	11,75	0,55	0,78

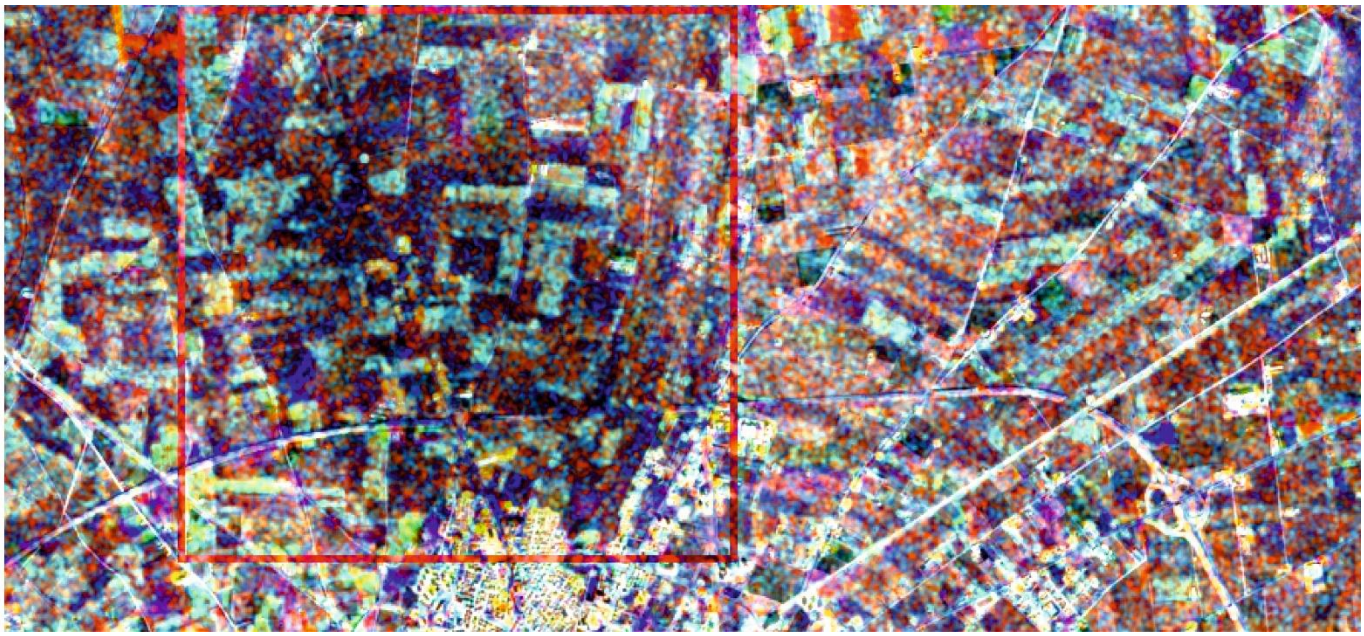

Figure 8. The Fused Image of OP1-SAR1 according to the Fus21 parameters in Table 6

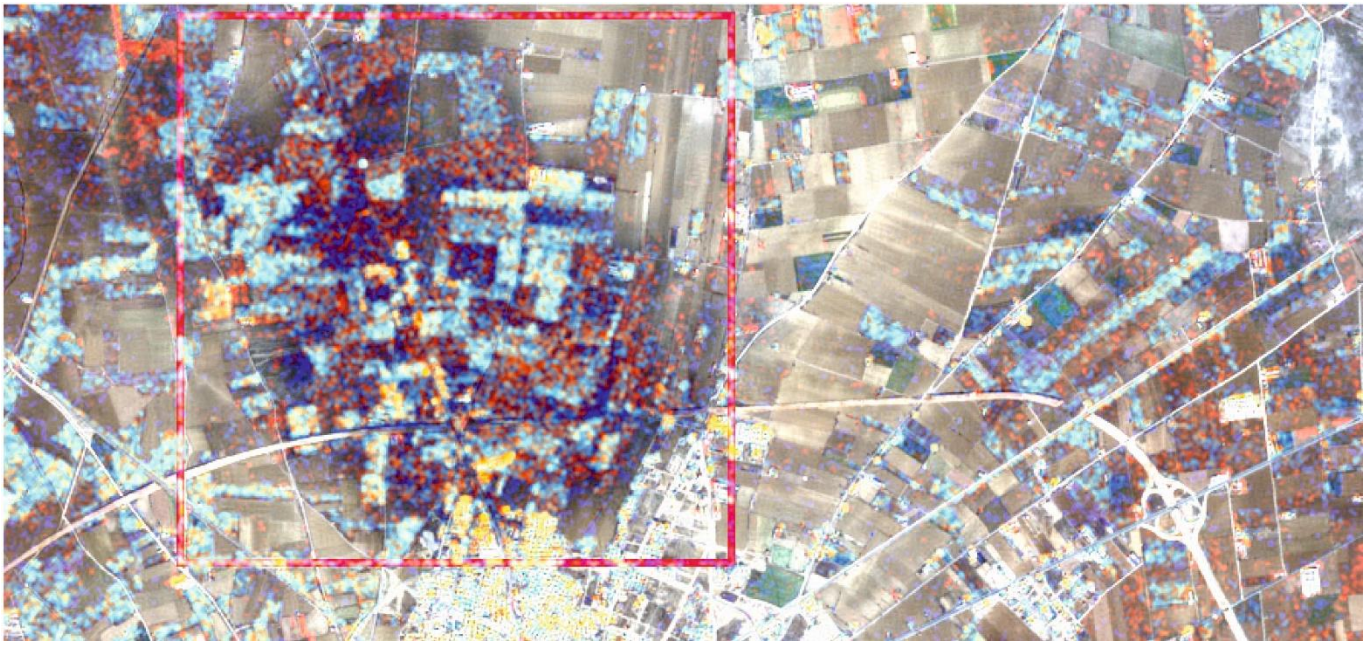

Figure 9. The Fused Image of OP1-SAR1 according to the Fus31 parameters in Table 7

3.3. OP2-SAR1 Image Fusion

In this section, the OP2 and SAR1 images were fused. The best results for ten fused images are given in Table 8 and Table 9. The highest SSI between fused and SAR1 images was obtained with " rbio1.3" wavelet packet as 0,91. The Fus41 image is indicated in Fig. 10. On the other hand, Fus51 image with highest SSI was obtained with "dmey" wavelet packet. SSI between Fus51 and OP2 images is 0,72 and Fus51 is shown in Fig. 11. As can be seen from Fig. 9, the missing regions in the optical images were improved by SAR image. However, the Fus51 includes still missing regions in Fig. 11.

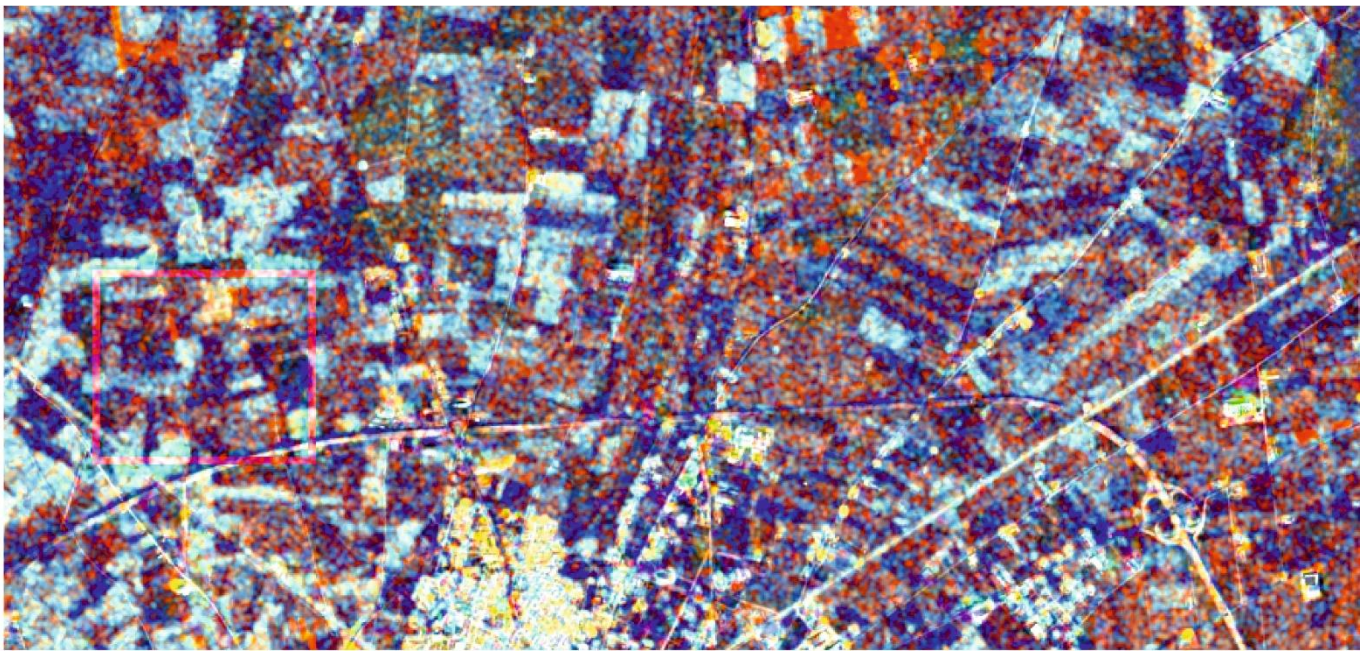

Figure 10. The Fused Image of OP2-SAR1 according to the Fus41 parameters in Table 8

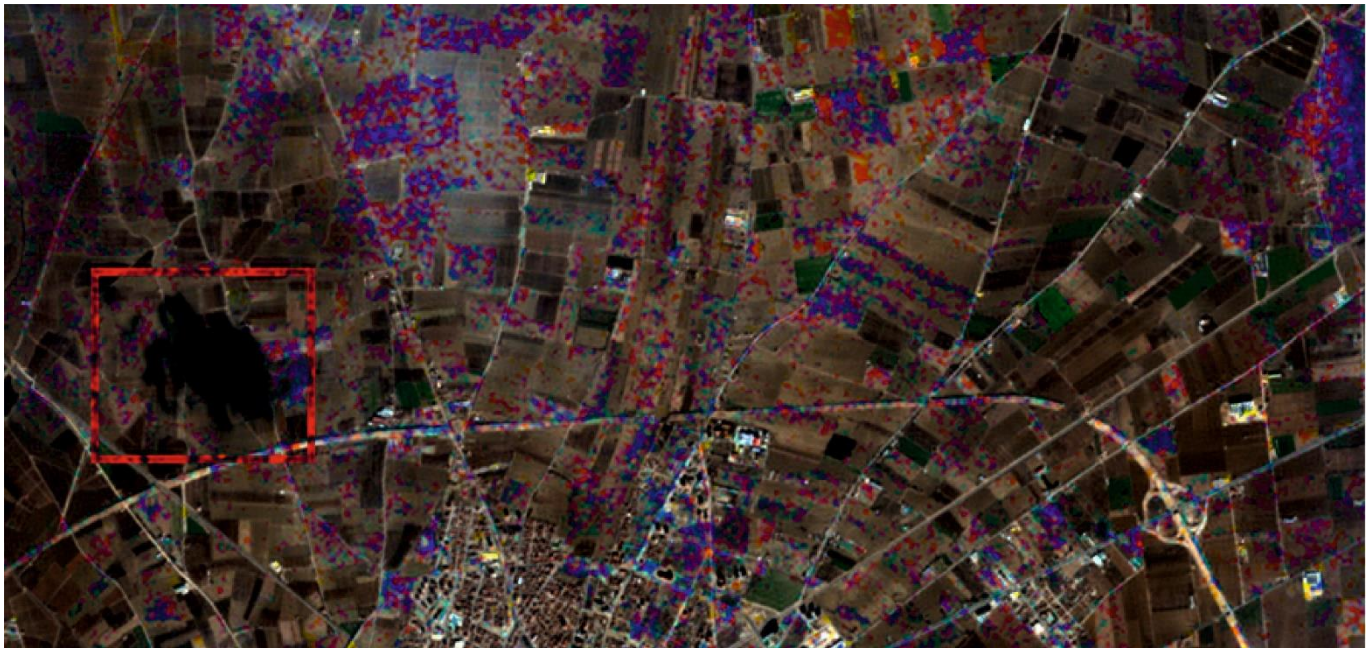

Figure 11. The Fused Image of OP2-SAR1 according to the Fus51 parameters in Table 8

Table 8. Fusion parameters and quality metrics for fusion of OP2 and SAR1 images (selected by SSI of SAR1)

Fused Image Label	Fusion Parameters				Quality Metrics								
	Level	Wavelet packet	Fusion Rule		OP2					SAR1			
			Approx. Coef.	Detail Coef.	H	MSE	PSNR	SSI	FSI	MSE	PSNR	SSI	FSI
Fus41	4	rbio1.3	max	max	7,80	7827,62	9,19	0,12	0,60	507,34	21,08	0,91	0,93
Fus42	3	rbio1.3	max	max	7,77	7877,23	9,17	0,12	0,60	500,55	21,14	0,91	0,93
Fus43	4	rbio1.5	max	max	7,80	7853,11	9,18	0,12	0,60	506,93	21,08	0,91	0,93
Fus44	3	rbio1.5	max	max	7,77	7896,71	9,16	0,12	0,60	501,51	21,13	0,91	0,93
Fus45	4	db2	max	max	7,80	7888,54	9,16	0,12	0,60	516,04	21,00	0,91	0,93
Fus46	4	sym2	max	max	7,80	7888,54	9,16	0,12	0,60	516,04	21,00	0,91	0,93
Fus47	5	coif1	max	max	7,81	7821,10	9,20	0,11	0,60	539,89	20,81	0,91	0,93
Fus48	3	db2	max	max	7,77	7933,52	9,14	0,12	0,60	519,02	20,98	0,91	0,93
Fus49	3	sym2	max	max	7,77	7933,52	9,14	0,12	0,60	519,02	20,98	0,91	0,93
Fus50	4	rbio1.3	max	max	7,80	7827,62	9,19	0,12	0,60	507,34	21,08	0,91	0,93

Table 9. Fusion parameters and quality metrics for fusion of OP2 and SAR1 images (selected by SSI of OP2)

Fused Image Label	Fusion Parameters				Quality Metrics								
	Level	Wavelet packet	Fusion Rule		OP2					SAR1			
			Approx. Coef.	Detail Coef.	H	MSE	PSNR	SSI	FSI	MSE	PSNR	SSI	FSI
Fus51	1	dmey	min	mean	6,92	580,25	20,49	0,72	0,85	7992,97	9,10	0,26	0,66
Fus52	1	rbio1.5	min	mean	6,93	565,55	20,61	0,72	0,85	7937,16	9,13	0,27	0,66
Fus53	1	rbio1.3	min	min	6,91	589,98	20,42	0,72	0,85	7975,33	9,11	0,24	0,66
Fus54	1	coif3	min	mean	6,92	581,79	20,48	0,72	0,85	7979,99	9,11	0,26	0,66
Fus55	1	rbio1.5	min	min	6,91	592,74	20,40	0,72	0,85	7975,44	9,11	0,25	0,66
Fus56	2	rbio1.3	min	min	6,88	563,32	20,62	0,71	0,85	7971,97	9,12	0,19	0,64
Fus57	3	rbio1.3	min	min	6,85	541,42	20,80	0,71	0,83	7989,92	9,11	0,12	0,60
Fus58	1	fk8	min	mean	6,92	583,83	20,47	0,71	0,85	7974,93	9,11	0,27	0,66
Fus59	1	rbio1.3	min	mean	6,93	567,64	20,59	0,71	0,85	7910,54	9,15	0,27	0,66
Fus60	1	db1	min	min	6,90	600,63	20,34	0,71	0,85	8002,30	9,10	0,23	0,66

4. CONCLUSION

In this study, wavelet-based fusion of optical-optical and optical-SAR images were investigated. Optical and SAR images were obtained from Sentinel-1 and Sentinel-2 satellites datasets. The four main wavelet coefficients of original images were obtained. The optical images were fused with optical and SAR images. Images were analysed for 19 different wavelet packets with up to 10 decomposition levels. The wavelet coefficients are combined by applying the fusion rule that includes the maximum, minimum and mean methods. Under these parameters' conditions, a total of 1710 fused images were obtained for each fusion application. Fused images were evaluated using 5 different metric criteria. In each fusion application, 20 fused images most similar to the original images were selected by SSI values. It was observed that the missing regions in the optical images

were improved in fused images. However, it was determined that the most effective wavelet-packets changes according to the change in the images to be fused. The most effective wavelet packets in 3 different fusions were found as “dmey”, “fk8” and “rbio1.3”. The results obtained in this article reveal that there are many parameters in the fusion process and thousands of combinations must be evaluated to obtain the most informative and clear image. However, in future studies, instead of evaluating all possible fused images, optimal fusion parameters can be obtained with natural inspired optimization algorithms.

Author contributions

Huseyin Duysak: Investigation, Data preparation and Image fusion, **Enes Yigit**: Evaluation of the images, Writing-Reviewing and Editing.

Conflicts of interest

The authors declare no conflicts of interest.

REFERENCES

Aslan M F, Durdu A & Sabanci K (2019). Fusion of CT and MR Liver Images by SURF-Based Registration. *International Journal of Intelligent Systems and Applications in Engineering*, *7*(4), SE-Research Article). doi:10.18201/ijisae.2019457233

Foumelis M, Blasco J M D, Desnos Y, Engdahl M, Fernandez D, Veci L, … Wong C (2018). *Esa Snap - Stamps Integrated Processing for Sentinel-1 Persistent Scatterer Interferometry*. In *IGARSS 2018 - 2018 IEEE International Geoscience and Remote Sensing Symposium*, 1364–1367. doi:10.1109/IGARSS.2018.8519545

Ghorbanzadeh O, Didehban K, Rasouli H, Kamran K V, Feizizadeh, B., & Blaschke, T. (2020). An application of sentinel-1, sentinel-2, and GNSS data for landslide susceptibility mapping. *ISPRS International Journal of Geo-Information*, *9*(10), 561.

Hemdan E E-D (2021). An efficient and robust watermarking approach based on single value decompression, multi-level DWT, and wavelet fusion with scrambled medical images. *Multimedia Tools and Applications*, *80*(2), 1749–1777. doi:10.1007/s11042-020-09769-7

James A P & Dasarathy B V (2014). Medical image fusion: A survey of the state of the art. *Information Fusion*, *19*, 4–19. doi:https://doi.org/10.1016/j.inffus.2013.12.002

Khaleghi B, Khamis A, Karray F O & Razavi S N (2013). Multisensor data fusion: A review of the state-of-the-art. *Information Fusion*, *14*(1), 28–44. doi:https://doi.org/10.1016/j.inffus.2011.08.001

Kulkarni S C & Rege P P (2020). Pixel level fusion techniques for SAR and optical images: A review. *Information Fusion*, *59*, 13–29. doi:https://doi.org/10.1016/j.inffus.2020.01.003

Pajares G & Manuel de la Cruz J (2004). A wavelet-based image fusion tutorial. *Pattern Recognition*, *37*(9), 1855–1872. doi:https://doi.org/10.1016/j.patcog.2004.03.010

Rajah P, Odindi J & Mutanga O (2018). Feature level image fusion of optical imagery and Synthetic Aperture Radar (SAR) for invasive alien plant species detection and mapping. *Remote Sensing Applications: Society and Environment*, *10*, 198–208. doi:https://doi.org/10.1016/j.rsase.2018.04.007

Shah E, Jayaprasad P & James M E (2019). Image fusion of SAR and optical images for identifying antarctic ice features. *Journal of the Indian Society of Remote Sensing*, *47*(12), 2113–2127.

Veloso A, Mermoz S, Bouvet A, Le Toan T, Planells M, Dejoux J-F & Ceschia E (2017). Understanding the temporal behavior of crops using Sentinel-1 and Sentinel-2-like data for agricultural applications. *Remote Sensing of Environment*, *199*, 415–426. doi:https://doi.org/10.1016/j.rse.2017.07.015

Yommy A S, Liu R & Wu A S (2015). *SAR Image Despeckling Using Refined Lee Filter*. In *2015 7th International Conference on Intelligent Human-Machine Systems and Cybernetics*, 2, 260–265. doi:10.1109/IHMSC.2015.236